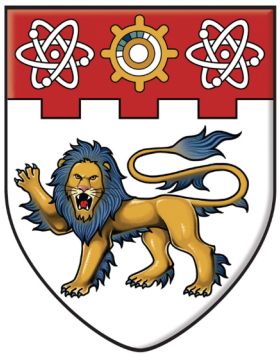

NANYANG TECHNOLOGICAL UNIVERSITY

AN ANALYSIS OF SOLID-STATE RECYCLING OF ALUMINUM ALLOY AA6061 FROM CONTROLLABLE HOT EXTRUSION PROCESSES

SHAZAREL SHAMSUDIN

School of Mechanical & Aerospace Engineering

A thesis submitted to the Nanyang Technological University
in partial fulfilment of the requirement for the degree of
Doctor of Philosophy

2018

ABSTRACT

Solid-state recycling of machining chip wastes via hot extrusion has nowadays been seen important to reduce energy consumption and greenhouse effect, perceived more important than the recycling by remelting. Characteristics of machining chips that are micro in size and large area-to-volume ratio in nature, melting can cause a massive molten metal vaporization leading to huge material losses. The hot extrusion process has long been recognised as the most outstanding direct recycling method which can result in much better material recovery. However, the high quality weld bonds among chips must be well developed during the process to ensure the mechanical performance of the recycled product is comparable to as-cast material. The optimum weld bond quality often relies on the selection of accurate process parameters to be combined with the appropriate die design. Nevertheless, the use of conventional approach of trial and error to complete the process parameter selection offers an unrealistic implementation, time consuming, and a costly process cycle. This conventional method was identified as the key shortcoming of the current solid-state recycling process.

This research provides an investigation into the optimum homogenisation condition for chip-based billet, a mathematical model development which allows the prediction of weld strength recycled materials and a proposed heat treatment for performance improvement. For homogenisation aspect, a series of hot extrusion experiments were performed at different settings of temperature (400 °C - 550 °C) and preheating time (1 - 6 hours). Each extrudate profile was then tested for its tensile strength performance. To further investigate the effect of temperature in homogenisation via damage evolution within the extrudate structure, a numerical simulation using a finite element method

was implemented. The normalized Cockcroft and Latham (C & L) fracture criterion was applied. Besides, a mathematical model for tensile bond strength prediction was developed using both theories of thin film bonding and diffusion. All related deformation variables for model calculation were numerically obtained via the finite element simulations, undertaken by the DEFORM 3D software. The model's validation was done by a series of tensile tests on gear and rectangular profiles, where the predicted strengths were compared with the strengths obtained experimentally. Finally, the heat treatment process was carried out at T6 condition for all samples.

For chip-based billet homogenisation, both experimental and numerical findings showed that the billet temperature must be kept higher than 400°C while for preheating time, minimum two hours was required to obtain a satisfactory tensile strength under the extrusion ratio of 11.22 or lower. The derived weld strength model was fairly accurate in predicting the tensile bond strength of extrudate. The average error resulting from the gear profile was 12 % while 23 % was calculated for the rectangular profile, both compared between the predicted and experimental results. The sources of error in the analysis were mainly contributed by the extreme state of strain-rate and deviations in the shear area estimation. The research shows that a great amount of heat or induced normal stress or shear stress was demanded to reduce the threshold strain of weld creation, thus promoting a sound weld bond. The greater magnitude of the normal stress (perpendicular to the extrudate surface) than the yield strength of material increases the real contact area of chips to result in a better cohesion and a delay in the contact time between die and billet enhances diffusion. Finally, the heat treated AA6061-T4 aluminium chips at T6 condition resulted in 105.66 HV, inferior just by ≈ 5 % hardness of as-received AA6061-T6, indicates that the mechanical properties of the direct recycled material can be successfully enhanced for practical applications.

ACKNOWLEDGEMENT

I would like to express my greatest gratitude and appreciation to my supervisor, Assoc. Prof. Dr. Zhong Zhaowei, and research collaborator Prof. Dr. Mohd Amri Lajis for their support, guidance, encouragement and effort throughout my research. I believe, without them, I would not be able to contribute in this research.

I would like to express my gratitude towards my family for the encouragement and kind help in the completion of this project. My beloved and supportive wife, Hasnah who always stood by my side to support me during hard times and lovely children who served as my inspiration to pursue this undertaking.

I would also acknowledge the help of Dr. Ahmed Syed Adnan, Dr. Mohd Faizal Mohideen Batcha, Dr. Periyasamy Manikandan and Mr. Shanmugasundaram Durairaj for their valuable support. I always seek support from them whenever I am in need. My sense of gratitude also conveyed to all other individuals, directly or indirectly, who have helped me out with their abilities throughout this venture.

TABLE OF CONTENTS

LIST OF TABLES

LIST OF FIGURES

LIST OF ABBREVIATIONS

Al_2O_3	Alumina / Aluminium oxide
ANOVA	Analysis of variant
BMA	Bulk mechanical alloying
C & L	Cockcroft and Latham
DOE	Design of Experiment
DSR	Differential speed rolling
ECAP	Equal channel angular pressing tool
ED	Extrusion direction
ER	Extrusion ratio
FE	Finite element
GHG	Greenhouse gas
LOM	Light Optical Microscopy
PCG	Periphery course grain
RSM	Response Surface Methodology
SEM-EDS	Scanning Electron Microscope-Energy Dispersive Spectroscopy
SPD	Severe plastic deformation
UTS	Ultimate tensile strength
WQI	Welding Quality Index
XRD	X-Ray Diffraction
YS	Yield strength

LIST OF SYMBOLS

Q_d	Activation energy for diffusion
Y	Aluminium flow stress
k	Aluminium shear flow stress
θ	Angle of force component in Y direction
A_s	Area of contact between the substrate aluminium
A_{ex}	Area of exposed substrate aluminium
A_{shear}	Area of shear generated on billet, near to die entrance
ψ	Asperity inclination angle
e	Average crack width
F_y	Component of force in direction parallel to shear area (Y direction)
D	Diffusion coefficient
ε	Engineering strain
TS_{exp}	Experimental tensile strength
A_c	Fraction of area in contact
η	Fraction of surface oxidized by the entrapped air
ν	Fraction of the final contact area without a protective oxide layer
R	Gas constant
λ	Length of oxide fragments
σ_{eff}	Local effective Von Mises stress
σ_m	Maximum tensile stress

A_n	Nominal area
σ_0	Nominal strength of the bulk aluminium
σ_n	Normal contact stress
p_{ex}	Pressure required to micro-extrude the substrate aluminium through the cracks
T	Room temperature
τ_{app}	Shear stress
r	Square root of asperity height of chips
TS_{rd}	Tensile bond strength recovery due to diffusion mechanism
R_{TS}	Tensile bond strength recovery rate
σ_{oxide}	Tensile strength of oxide fragments
t_c	Thickness of oxide fragments
t	Time in (sec)
R_y	Total force in Y direction
L_o	Unstretched length

CHAPTER 1 : INTRODUCTION

1.1 Background

The emergence of aluminium is relatively new among other metals, dating back to 19th century, its pure form was successfully extracted by Danish chemist Hans-Christian in 1825. After so many years, the cost-effective technique of aluminium production was then invented in 1889 and mostly utilizing Bayer and Hall-Herout concepts of aluminium refinement [1]. Over the years, the aluminum industry witnessed contributions to the substantial economy of more than 30 countries all over the world. Approximately 45 million tonnes of semi-fabricated aluminum products are produced annually and 14 million tonnes from recycled aluminum [2]. The beginning industries report about 780 million tonnes of primary aluminum have been produced and since then, nearly 400 million tonnes of the metal is still in use that will eventually be available for the recycling [3-5].

Possessing favorable characteristics such as lightweight, high strength, easily deformability, good conductivity and excellent corrosion resistance, aluminium demand will continue to survive well in future. Aluminium in the nature, in which its alloys can be tailor-made to meet the expressed needs, allows improvement and performance of aluminium related products to be continuously upgraded. Potential beneficiaries of this metal are well recognised in transportation, packaging, food and beverage containers, energy transmission, air conditioning, construction and some other related sectors.

Due to increasingly high demand of this material, it is necessary to have an efficient virgin ore extraction from its primary resources that must reduce energy consumption and be friendly to the environment. These entirely fact-driven reasons motivated society throughout the world to adopt the principle of recycling philosophy and energy-saving related operations. Also, recycling becomes increasingly important to industry to meet the goals of cost reduction, preserving limited resources, and minimization in landfill utilization. Although recycling by remelting can unceasingly be exercised on aluminium, some serious negative impacts arose. These include high-energy consumption, high cost and a large number of operation [6] compared to solid-state recycling by plastic working.

In the case of aluminum chips recycling, the thin elongated and spiral shapes made conventional recycling by remelting unfavourable due to a significant metal loss. The low density of the compacted chips enhances losses through oxidation. There are further losses on each stage of subsequent processing leading to ultimately no more than 54% of the metal recovered during conventional recycling by remelting [7]. A significant evidence can be seen in Figure 1-1which illustrates the proportion of metal yield during conventional recycling of aluminum turnings.

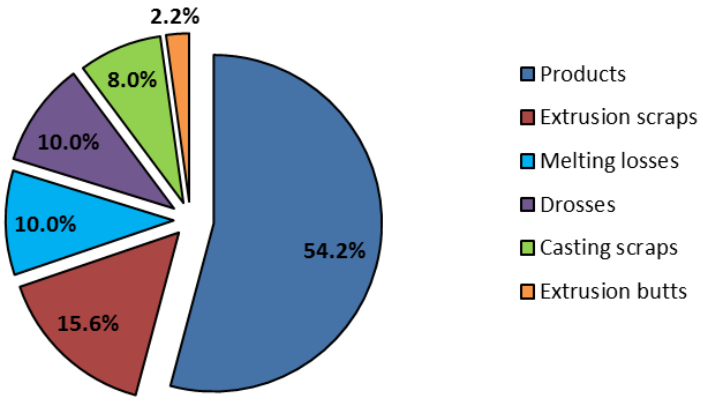

Figure 1-1: Proportion of metal yield during conventional recycling of aluminum chips [6]

The solid-state recycling (also called direct recycling) implementation on aluminium chips clearly has its specific advantages, such as fewer recycling steps, higher recovery efficiency, fewer new scraps and higher recovery of tensile strength [6, 8]. This novel recycling technique can result in much better metal yield than the conventional way and the material will not undergo high energy remelting operation. A significant number of researchers [9] recognized that the amount of plastic work induced in the hot extrusion was outstanding compared to other techniques. The capability of imparting an excessive plastic strain onto the consolidated chips made it the compelling recycling technique available today.

The production of chip-based finished or semi-finished goods in direct aluminium recycling are subjected to various factors that control their quality such as the chip constituents, chip morphology, types of reinforced materials, purity of chips, compaction strategy, heat treatment, types of plastic working, and die design. Various

process factors and advancement in recent direct recycling techniques contribute to the enhancement of the mechanical properties of extrudates. It is beneficial to discuss and characterize numerous factors affecting the quality of directly recycled chips to ensure any applicable advantages can be fully utilized. Hitherto the challenges in realising the technological feasibility of the solid-state aluminum recycling are still being debated, in spite of its numerous advantages.

1.2 Problem Statement

A worldwide global warming led to the increasingly demand for recyclable materials, energy saving processes and a reduced carbon dioxide emissions process in all aspects of manufacturing as well as in the area of transportation. Due to fundamental operation that requires high energy for conventional recycling, an alternative technique of recycling in the solid-state is proposed. Recycling in the solid-state incorporates low energy consumption and cost in its implementation. This emerging technique is most appropriate for chip recycling due to their elongated spiral shape and micro size. Their surface area-to-volume ratio is relatively large and not effective to recycle through remelting in light of the fact that the melts can be easily vaporized at high temperature.

The main principle in the solid-state recycling is to establish the weld bond. Welding occurs in the solid-state if appropriate parameters of temperature, stress and strain are present. Incomplete weld bonding between chips lead to the formation of unwanted defects such as cracks, delamination and peeled off of chip-based extruded profiles, saw blade tears and warping defects as obtained by previous researchers and depicted in

Figure 1-2. These kinds of damages which result in a progressive degradation of the metal can cause failure to the chip-based extrudates in subsequent forming processes.

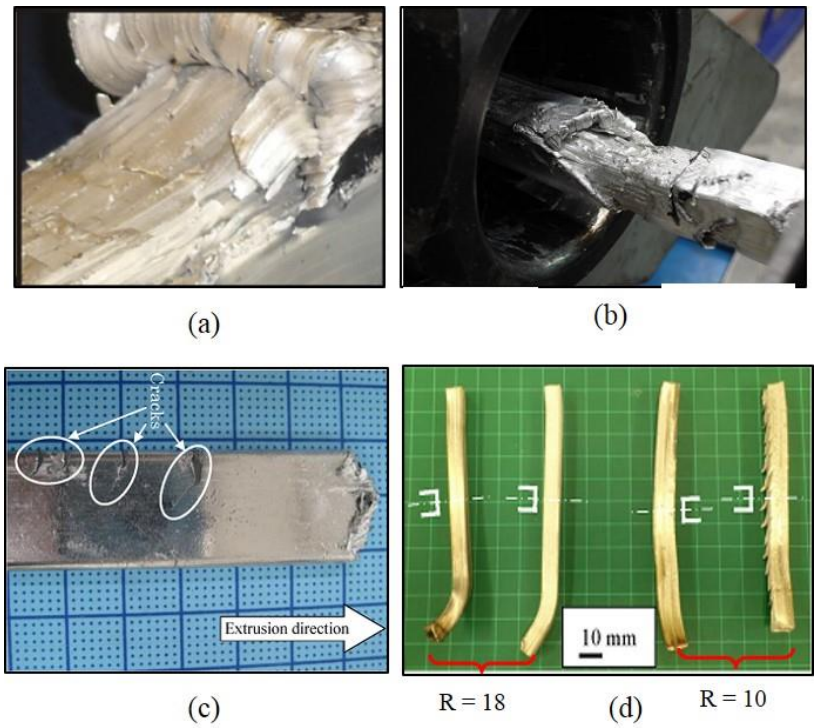

Figure 1-2: (a) Delaminated chip-based profile [10], (b) peeled off profile [11], (c) crack formation on extruded bar [12], (d) saw blade tears and warping defects [13]

Nowadays, the computer simulation of forming processes contributes to a significant enhancement for the understanding and prediction of metal behaviour. With this sophistication, the defects within the chip extrudates can be avoided or reduced by introducing a structured finite element simulation. In order to control the chip extrusion process and to obtain good final extrudate properties prior to the actual extrusion, prediction of the crack evolution and weld quality in the hot extrusion of recycled chips should be carried out in advance.

In direct recycling, the utilization of complex die geometry with low extrusion ratio in hot extrusion should be able to impart sufficient amount of pressure and strain onto the chip-based extrudates to guarantee that a sound bonding among individual chips is established. The chip-based extrudates from recycled chips should possess high quality of longitudinal and transverse welds to take up high load when put in practical use. To obtain a good metallurgical bonding between chips, it needs a combination of die design and operating conditions that can break the oxide layers covering the chips efficiently and distributing them into the billet structure homogeneously.

As of now, the current practice to produce chip-based extrudates involves a trial and error method to select the die and process parameters. However, the chip-based recycled products are relatively more complicated to process and therefore the existing skills or experience may not be sufficient. Figure 1-3 shows uneven distributions of tensile strength over the side and bottom structure of the extruded c-channel from aluminium chips. Cutting out the part sections for tensile test every time after the extrusion has been carried out will be uneconomic and time-consuming. Furthermore, there are major differences in the strength levels between the side part and back part as can be observed. This can be attributed to the poor quality of the weld presence within the extruded profile. Variations in the induced-strain were among the reasons for this drawback. Degradation in the mechanical strength of the recycled materials is a sign of imperfection bonding among the individual pieces of swarf. A number of experimental trials to determine the best combination of extrusion ratio that directly reflected by the die geometry and processing parameters lead to time and money wastage. Therefore, to

achieve the highest possible tensile strength recovery in direct chip recycling becomes the ultimate aim.

In this study, a systematic approach of finite element simulation coupled with an appropriate damage model is proposed to predict damage evolution within the chip-based extrudates when subjected to varying temperatures for extrusion at relatively low extrusion ratio. On the other hand, the weld quality among chips will be predicted via the tensile bond strength model. The model is developed on the basis of existing shear strength model deduced from the previous researchers. Although the damage criterion and weld quality prediction might give only a rough estimation, an insight it can provide to the process planner from traditionally trial and error practice is significantly important which will lead to huge savings in time, money and materials.

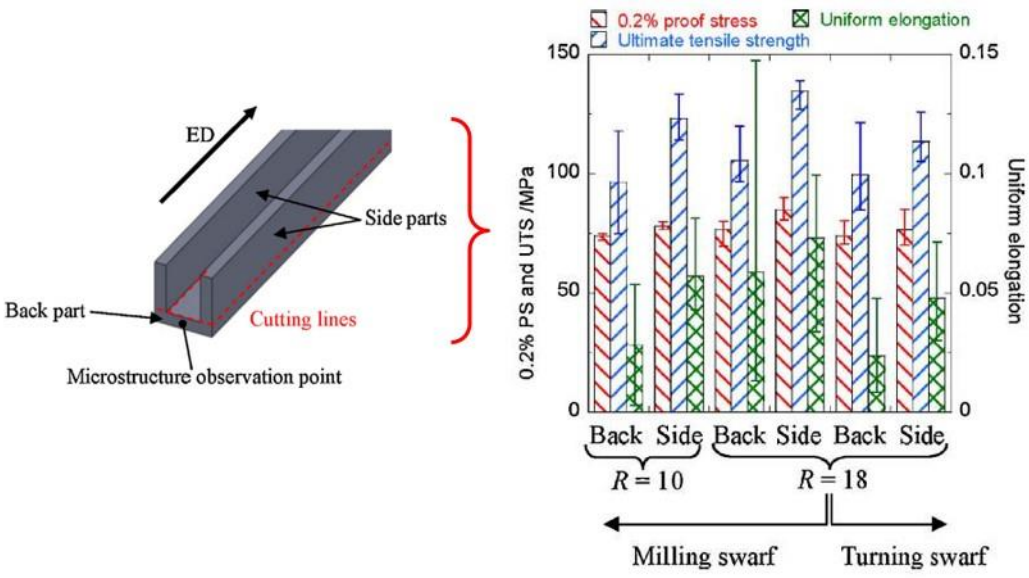

Figure 1-3: Tensile strength of extruded c-channel for samples taken from side and back parts of the recycled material [13]

1.3 Research Motivation

In recent years, recycling in the solid-state, often associated with the low energy process, became a subject of interest to many researchers, in particularly regarding the strength recoverability of the chip-based recycled product. Distinct phases when implementing the hot extrusion process in solid-state recycling may need to predict the conditions within the deforming billets. These phases could lead to crack emergence and low strength recovery as a result of the poor weld formability among chips. To ensure the formed weld bonds are satisfying, the strength recovery on the chip-based recycled material should be reached as close as possible to the as-cast material.

Since the advancement of numerical simulation nowadays can help the designer to develop more reliable extrusion process, an accurate knowledge of the local state variables of deformation can be obtained for further analysis. The relevant advantages of numerical simulation thus allow foreseeing the weld strength and damage evolution of complex-shaped products when varying the processing parameters (pressure, temperature and chip conditions).

Optimising the effects of die design and processing parameters on the weld strength of chip-based extrudates in early stage becomes important and this could prevent much more expensive reworks of upgrading the extrudates quality at the later stage. Understanding the influence of deformation conditions on the resulting strength is an interesting way for a systematic process where optimum extrudate quality can be ensured. Besides, it could also convince the potential of hot extrusion in the field of

direct recycling to realize its technological feasibility towards the industrial implementation.

1.4 Research Objectives

The objectives of the current research are outlined as follows:

1) to investigate the mechanical properties and damage evolution of chip-based extrudates subjected to distinct preheating time and temperatures;

2) to investigate the influence of chip's surface topography over the weld strength of directly recycled aluminium chips;

3) to establish an analytical model for predicting the weld strength of complex-shaped extruded profiles from aluminium chips by incorporating thin film theory and diffusion theory;

4) to carry out heat treatment at T6 condition on the extruded profiles produced through the die of complex geometry.

1.5 Research Scope

The scope of this research includes the following:

1) The damage evolution within the extrudate structure that is subjected to distinct preheating temperatures will be predicted numerically using DEFORM^{TM} 3D finite

element software and the normalized Cockcroft and Latham (C & L) fracture criterion is selected to calculate the damage. The effects of preheating time are assessed through the mechanical properties and microstructure examination.

2) The mathematical model to predict the weld strength is established by integrating tensile bond strength model (adapted from previous researchers) and diffusion-strengthening model. The tensile bond strength model is developed on the basis of thin film bonding theory while the diffusion-strengthening model is derived from diffusion theory of Fick's second law and an Arrhenius relationship. All the corresponding deformation variables for the weld strength computation will be retrieved from results of finite element simulation, undertaken by DEFORM 3D software. The model is validated through a series of tensile strength tests on various profiles at different temperatures and extrusion ratios (ER).
3) The extrusion process is carried out via a rectangular die geometry and two dies of spur gear geometry with the corresponding extrusion ratios of 11.22, 4.86 and 2.16 respectively. Feasibility study for the extrusion of chip-based billet through low and extremely low extrusion ratios is tested for the gear geometry with 4.86 and 2.16 ERs. The gear geometry represents as a complex-shaped of extruded profile. All samples for the tensile test are prepared according to ASTM E 8M-40 standards.
4) The hot forging operation is used to produce samples for several experiments: (1) chip's topography effects on the resulting weld strength, and (2) to obtain a correlation between process time and strength recovery. All samples will follow ASTM E 8M-40 standards, sub-size tensile sample, 25 mm in gage length with 6 mm width for the reduced section and an approximately 6 mm thickness.

5) The heat treatment at T6 condition covers the solution heat treatment, quenching and artificial aging with the varying aging time.
6) The chips are produced by high speed milling of aluminium AA6061 series blocks and extrusion is carried out by a conventional 300 tonne extrusion press. The chip-based billets are prepared by a cold press of 50 tonne capacity.
7) The microstructure investigations merely focused on the microstructure evolution of the extrudate, fracture surface of the tensile sample, chip boundary size, weld line of fragmented oxides and phase presence on the heat treated extrudates. All the corresponding samples are examined with the Light Optical Microscopy (LOM), Scanning Electron Microscope with Energy Dispersive Spectroscopy (SEM-EDS), and X-Ray Diffraction (XRD) equipment.

CHAPTER 2 : LITERATURE REVIEW

2.1 Introduction

This chapter presents a comprehensive review of past and current research work in solid-state recycling mainly for aluminum and partly focuses on magnesium material. The review provides an insight of several important aspects in the solid-state recycling development which demonstrates how different factors and advancement in the techniques reflect the property enhancement of the extruded profiles. It is essential to determine various factors which might influence the success of solid-state recycling implementation. The key techniques in direct recycling to be covered here are mainly focused on the hot extrusion and powder metallurgy, while other methods will be discussed in the dedicated section. In sum, the review covers the effects of chip preparation method, reinforcing phase and mixture of different metal alloys, die geometry design, the influence of processing parameters, and the performance of miscellaneous techniques available in the direct recycling. A proper control on the enumerated aspects will determine the quality of the chip-based extrudate. The analytical modelling and simulation work in extrusion related processes and weld strength prediction are also reviewed to provide some basic fundamentals in analytical model development and finite element analysis. Finally, concluding remarks highlight the linkage between the arising issues to the current research work.

2.2 Overview of Aluminum Recycling

In general, solid-state recycling is a process of recovering metal chips through direct conversion by means of plastic deformation into final product without melting. The solid-state recycling method can result in much better metal yield than the conventional recycling. Common course associated with direct recycling of aluminum chips through hot extrusion are comminuting the metal chips, cleaning, drying, cold compaction, and finally hot extrusion followed by cutting to the desired length. The method varies depending on the processing route. Powder metallurgy approach and plastic deformation (e.g.: extrusion, rolling, conform, direct forging, and etc.) or combination between them are also possible as illustrated in Figure 2-1. Currently, metals that can be directly recycled include magnesium, iron, copper, aluminium, titanium and certain cast irons as reported. The difference between conventional recycling with solid-state recycling is shown in Figure 2-2.

Increasing volume of vehicles production for transportation nowadays causes high contribution of greenhouse gas (GHG) emissions influencing air quality and contributing to global warming. The GHG emissions contributed by transport sector represents about 19% of total contribution as shown in Figure 2-3 and this number is considered significant. The metals such as aluminium, magnesium, titanium, and beryllium alloys are practical and entirely useful to accomplish the lightweight strategies in transportation. As far as economical aspect is concerned, the aluminium and magnesium are more preferable to the automotive industry, and are always employed when there is a demand in terms of strength-to-lightweight strategy. Both of

these materials demonstrate good potential in reducing the weight of vehicles which bring direct impact to fuel consumption and global warming.

Production of aluminium from primary resources needs 31.1 GJ/ton aluminium to reduce it from alumina whereby aluminium by secondary production consumes energy about 10 GJ/ton of the material, making up about 5-10 % of the energy in the primary aluminium output [14, 15]. The trend appears to increase in the subsequent years. In 2030, a recycling rate of 50% aluminium is expected [16]. A rising in energy consumption for remelting consequently releasing more carbon footprint in atmosphere affects climate change. Although there have been several successful efforts to improve the energy efficiency of melting furnaces since the 1980s, nevertheless the energy consumption for secondary aluminium production can still go up to 20 GJ/ton depending on the condition of aluminium scrap, production facilities and processes [17, 18].

In the case of aluminium chips, the conventional recycling method was unfavourable due to significant metal loss. The thin spiral shape and a large surface area of chip-to-volume ratio result in substantial losses during melting because the melts can be easily vaporized at high temperature. There are further losses during casting counted to about 8%. Later, during the processing of aluminium ingots, there are losses amounting to about 18%. Therefore, ultimately no more than 54% of the metal is recovered [7]. Approximately 45% losses were found in the form of casting scraps, melting losses, drosses, extrusion scraps and butt thus support findings in [7]. Due to these reasons, an alternative approach has been suggested to embrace direct recycling of aluminium waste in the form of chips into semi-finished or finished products through the plastic

deformation, which was first patented by Stern in 1945 [19].

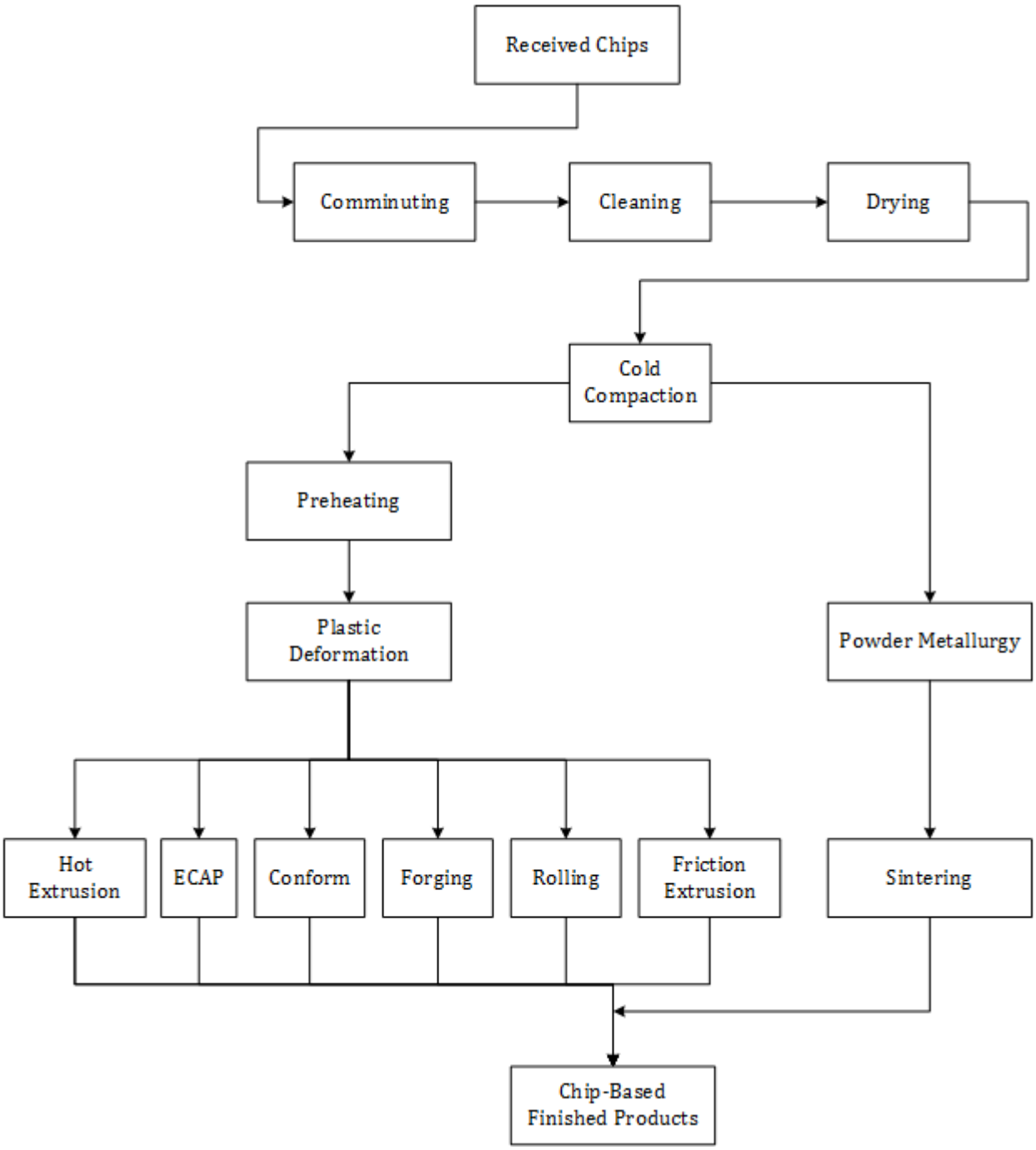

Figure 2-1: Flow chart of multiple solid-state recycling techniques through plastic deformation and powder metallurgy approach

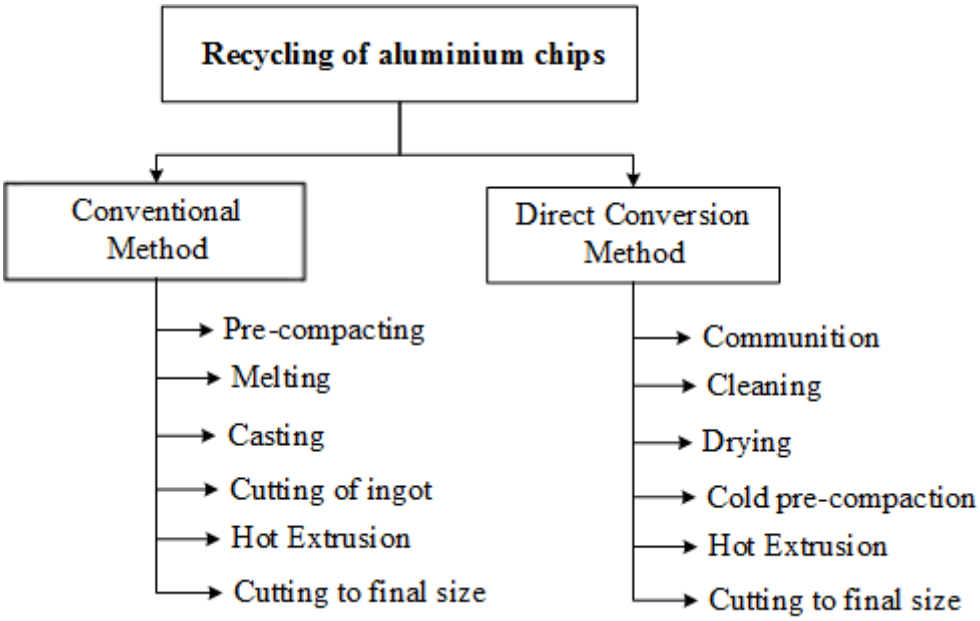

Figure 2-2: Differences between recycling by direct conversion and conventional method [20]

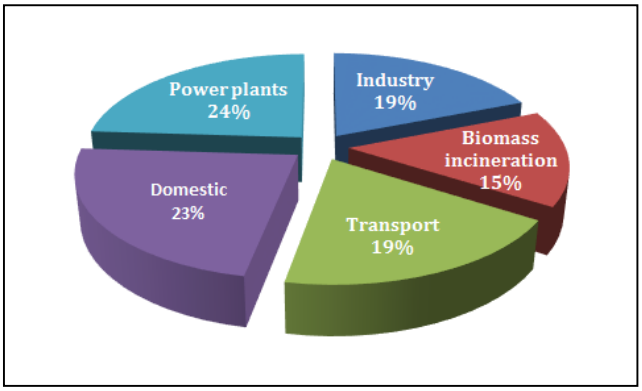

Figure 2-3: The percentage contribution of different sectors to GHG emissions [21]

The benefits of the solid-state recycling of aluminium and its alloys are perceived important by researchers as it could reduce costs on environmental protection and saving the earth by reducing carbon footprint during the extraction of aluminium from

its ores and secondary processes. Direct conversion of aluminium deploys only 5% of the total energy needed for conventional recycling [8]. Compared with conventional recycling, the direct conversion of aluminium scrap into a compact metal may result in 40% material, 26–31% energy and 16–60% labor savings [22]. Therefore, the overall cost of the aluminium production can be reduced by the direct recycling method.

2.3 Experimental Studies of Solid-state Recycling of Aluminium

A large amount of work has been done to optimise the quality of the extruded profiles through the solid-state recycling. It is found that several factors could have possibly influenced the quality of chip-based finished products. The factors can be classified into three main categories: (1) material-based parameters (e.g.: chip constituents, including types of chip, reinforced materials, and their morphology), (2) process-based parameters (e.g.: methods of chip cleaning, compaction strategy (cold/hot, force applied, and compaction layer), heat treatment and types of the plastic deformation method including the process parameters), and (3) geometry-based parameter (e.g.: die design that determines the level of strain and pressure induced to control the inter-chip bonding). All factors with their category are summarised in Figure 2-4. The historical developments pertaining to the experimental study of aluminum and its alloys under the solid-state recycling with the detailed aspects of study are chronologically tabulated in Table 2-1.

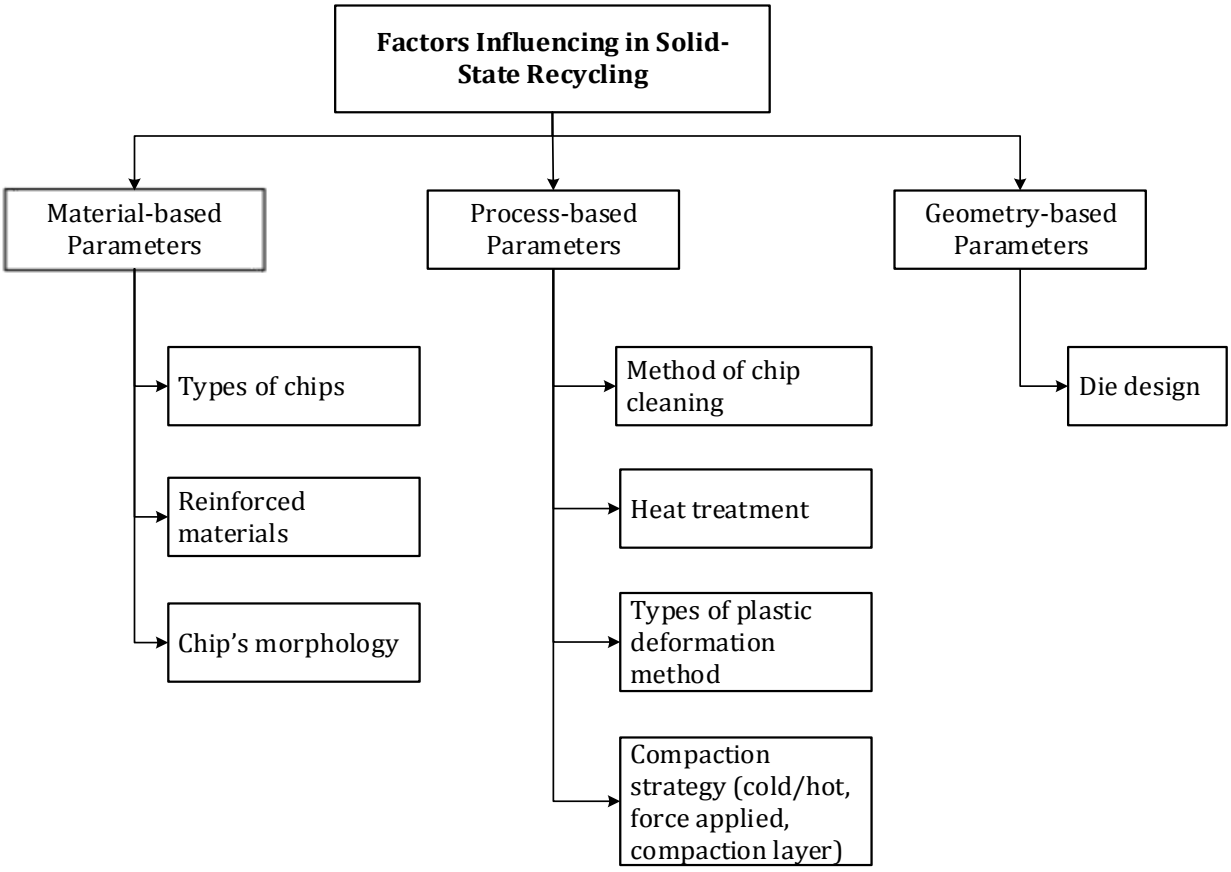

Figure 2-4: Factors influencing the solid-state recycling of aluminium chips, according to each category

2.3.1 Effects of Chips and Billet Preparation

In direct recycling, the quality of chip-based finished products processed by plastic deformation is significantly affected by the way chips are prepared for consolidation at the pre-processing stage. Several factors have been identified to influence the final quality of the chip-based recycled product during the chip preparation; the amount of pressure for cold compaction, duration of cold pressing, a method of chip cleaning, chips softening, types of chips and their morphology.

In normal practice prior to hot extrusion, the chips need to undergo pre-compaction to form a billet of a cylindrical shape. Fogagnolo et al. [23] reported that the quality difference between the recycled material by cold and hot pressed chips was insignificant. But, an increase in the pressing pressure or pressing time during pre-compaction produces higher degrees of consolidation. On the other hand, Tekkaya [20] studied the impact of cold compaction of chips acquired from two different operations of turning and milling. Although the chips were plastically deformed during the compaction, no cohesion was developed and their primary bonding was caused by the chips interlocking mechanism. The billets produced are structurally unstable by this mechanism. Direct powder metallurgy method was also attempted in the direct recycling of aluminium [24]. Heat and a low pressure were used on granulated aluminium to soften the particles and reduce the springback effect. The results showed that the method was inferior by 9-12% in green density, 2-13% in compressive strength, and 18-29% in Brinell hardness as compared to the sintered part using the commercial aluminium powder pressed at 360 MPa.

As reported in ref. [14], 1050 aluminium alloy in the form of pin was mixed with 6060 aluminium alloy chips successfully. Findings revealed that no optical difference can be seen between the extruded profiles and as-cast billet microstructures. In addition, Tekkaya et al. [20] also investigated the properties, yield behavior, microstructure and drilling behavior of the extrudates processed by the direct hot extrusion. The re-use chips of aluminium AA-6060 alloy derived from milling and turning operations with different sizes and shapes were used. The mechanical properties of the seam welds

surrounding the chips are nearly as good as the properties of the base material. The yield strength (YS) of the extruded chips is comparable to solid billet extrudates.

The purity and cleanliness of the chips are among the main factors identified influencing the bond quality in hot extrusion. As impurities can reduce the bond quality, the hot tearing in all chip-based profiles could be encountered as a result in poor chip cleaning [25]. Degreasing in the chip's cleaning pre-processing can be carried out either by the chemical or thermal means. It was strongly recommended to use acid and/or hydroxide for removing surface oxides after a thermal decoating process and to anneal the chips prior to proceeding with plastic deformation [24, 26]. The cleaned and annealed chips exhibited higher green density compared to chips without undergoing both processes [24] because these steps can reduce oxide content, impurities and soften the chips to obtain a dense billet [27]. Practically, segregation of different aluminium alloys according to their families is very much encouraged to achieve a high-quality weld bond during the deformation processes [28].

2.3.2 Effects of Reinforcing Phase and Mixture of Different Aluminum Alloys

Addition of reinforced materials to consolidate the chips has brought noticeable benefits in terms of mechanical and physical properties. In the case of composites with the reinforcing phases introduced, the amount, form and size of these phases are crucial elements to the final product. The reinforced phases functioned to restrict the free movement of dislocations and increase the yield and the tensile strength, but often a trade-off of porosity that could reduce these properties as well [29]. Some researchers

had devoted invaluable efforts to develop materials for bearings from recycled aluminium chips [30-32]. The bearing composites were conventionally produced from powders that derived from the aluminium chips and added with silicon, silicon-carbide and graphite [33]. Due to the potential of re-using the recycled aluminium chips for bearing composites, the production method is described and discussed here.

Fabrication of composites from Al, AlCu4-alloy and AlMg2-alloy granulated chips with different amounts of tungsten powder addition (≈ 80 mesh size) was proposed [8, 34]. The composites with low porosity, good diffusion bonds and relative density of exceeding 98% were obtained with the tungsten powder. The heat treatments on Al and AlCu4 base composites increase the strength however, the ductility is decreased slightly. Direct conversion of the granulated aluminium chips and its alloys ($AlMg_2$ and $AlCu_4$) into finished products through the hot extrusion process were clearly reported previously [7, 22, 35]. The reinforcing phases introduced were aluminium oxide, tungsten, carbon, ferro-chromium and aluminium bronze comminuted chips. The findings reveal that the relative densities of the composites after the hot extrusion are almost identical (over 98%) as those solid materials made by aluminium powder with the reinforced phase additions. The tungsten powder addition combined with aluminium oxides had improved the strength and hardness properties. According to Fogagnolo et al. [23], the oxide content when introducing Al_2O_3 hardening phase in recycled aluminium chips led to the higher ultimate tensile strength (UTS) of the developed composite when compared with the original composite.

While carbon addition results in discontinuities of the composite structure, thus impair the strength and the plastic properties of the composite. For ferro-chromium

composites, a smaller fraction of the granulated chips led to better mechanical properties due to uniform distribution of the ferro-chromium phase in the aluminium matrix. The effect of different presintering medium neither in the air, nor vacuum was found negligible. Good tribological properties were obtained in composites added with the comminuted aluminium-bronze chips. Gronostajski et al. [22] reported that the strength and plastic properties of all developed composites meeting the requirements for bearing materials.

Other bearing materials with good mechanical properties were obtained successfully without intervening metallurgical process through the granulated composites of CuAl8, CuAl12Fe4Ni4 and CuAl14Fe4Ni4 [9, 29, 36]. The mixtures were subjected to cold compacting, preheating, hot extrusion and heat treatment. The results from XRD revealed that due to reciprocal diffusion of copper and aluminium that took place, very hard phases were created which improved tribological properties [29, 36]. Gronostajski et al. [9] observed a very small effect on the wear intensity when different types of reinforcing phase (CuAl12Fe4Ni4 and CuAl14Fe4Ni4) were used. The poor interface bonding between aluminium matrix and reinforced materials led to the slightly poor performance in mechanical properties and the wear can be easily accelerated on the bearing composites. All bearing composites developed by researchers previously [9, 29, 36] experienced low diffusion bonding after the hot extrusion. As a countermeasure, a heat treatment process was applied which led to improvement in diffusion among bearing composites, and subsequently enhanced tribological properties, hardness, tensile and compressive strength of the respective composites.

The possibility of mixing multiple chips from AA6060, AA6082 and AA7075 was investigated by Schikorra et al. [37] and joining was established successfully among the alloys. As a trade-off strength increased of the mixed alloys, surface defect tends to emerge and this needs proper selection of extrusion parameters to avoid the unwanted defect. The possibility of adding SiC particles into the distinct chip geometry of aluminium 6060 alloy chips was tested by Tekkaya et al. [20] and the trials failed because the particles caused destruction in many spots of the extruded profiles, the surface was rough and the results from tensile tests revealed a reduction in flow stress, which reduced the strength.

Sherafat et al. [38, 39] discussed the possibility of adding aluminium powder to 7075 aluminium chips in direct recycling process to investigate the effects of powder content and extrusion temperature in mechanical properties of the developed composites. Significant conclusions can be drawn: (1) increasing the Al powder content caused decreasing in the density, ductility and a reduction in formability of the consolidated mixture while the tensile and compressive strength are increased, (2) increasing the weight percentage of 7075 aluminium chips caused the strength to increase and the ductility is decreased, (3) increase in extrusion temperature led to increase in the relative density, tensile strength and ductility while hardness of the samples is reduced, and (4) at constant extrusion temperature, increasing Al powder content causes the strength decrease and ductility increase, but the hardness remained unaffected.

In conclusion, alloying elements either from recyclable wastes or original forms can be mixed or sometimes alloyed with the aluminium chips as reinforced particles to strengthen the composites. The cold compaction and hot extrusion can produce high

bonding quality of aluminium-based bearing composites. The heat treatment that carried out after extrusion will improve tribological and mechanical properties by promoting diffusion bonding and formation of new hard phases. High quality bearing composites can be realized by removing the oxide film covering the aluminium chips and achievable if the intense chip shearing and compressive deformation are introduced. Sintering with high temperature promotes better atomic diffusions that can help to reduce porosities in aluminium-based composites.

2.3.3 Effects of Die Geometry

Die geometry plays an important role and determines the bond quality between chips' interface in an extrusion die. A proper die design will lead to deformation route that guarantees sufficient billet densification, chip bonding and the evolution of a desired microstructure [7]. The use of a complex hot extrusion die will improve quality of the chip-based finished extrudates produced [40]. Some existing dies such as a porthole die and an integrated equal channel angular pressing tool (ECAP) capable of inducing huge pressure and strain which can cause significant chip consolidation. Figure 2-5 shows multiple dies with different level of induced strain capability employed in the solid-state recycling of aluminium chips.

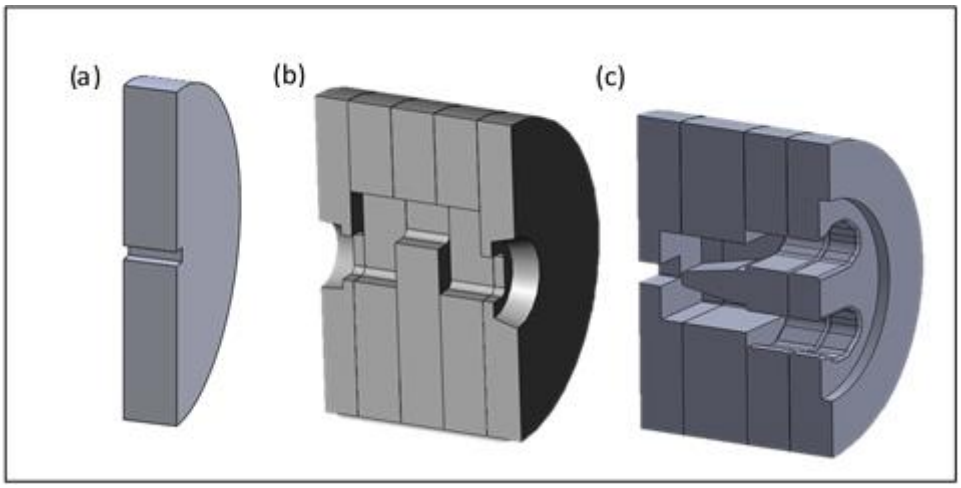

Figure 2-5: Multiple types of dies used in solid-state recycling via extrusion: (a) flat-face die, (b) iECAP die [11], and (c) porthole die [11, 41].

Several extruded profiles were produced by a modified four turn integrated equal channel angular pressing die (iECAP die) and a porthole die with AA6060 aluminium chips as reported [11]. The results indicate that no visible voids on the profiles from the both dies. The chip-based billets extruded through the iECAP showed superior hardness and tensile strength than the cast billets extruded from the flat-face die. The performance of the flat-face and porthole dies in direct recycling of AA6060 chips were also compared [41]. By employing the porthole die, the chip welding and the ductility are 80% higher than that obtained by the flat-face die. Meanwhile, for the microhardness and the yield strength, the porthole die performed worse than its rival. The microstructure of the sample extruded by the porthole die exhibited equiaxed grains and counted almost twice that of the grain size revealed by the flat-face die sample before the heat treatment.

The effects of different routes of chip consolidation and die design over mechanical

properties have been a matter of study by Misiolek et al. [10]. The AA6060 aluminium alloy chips were compacted into billets with three distinct techniques called traditional compaction in one stroke, multi-layer compaction and front-pad, method adapted from powder extrusion. The techniques were coupled with the use of three types of extrusion dies: (1) the flat-face die (R=8.6, v=1mm/s), (2) the modified porthole die (R = 8.6, v = 1mm/s), and (3) the ECAP die (R = 8.6 & v = 1 mm/s; R = 8.6 & v = 6 mm/s; R = 34 & 1 mm/s). The multi-layer compaction results in better density chip-based billets and at a low extrusion ratio (ER) of R = 8.6; the combination of cold compaction and hot extrusion via flat-face die does not guarantee sufficient chip bonding. The use of porthole and ECAP dies results in sufficient chip bonding and better ductility compared to as-cast billet extrudate. The mechanical properties, in particularly relating to tensile strength, did not change much between multi-layer and single-layer compaction. However, higher ram speed or ER for the ECAP die led to a slight decrease in strength and ductility of the extrudates due to the high temperature setting.

The iECAP die was again employed to investigate the influence of the deformation route on the quality of the chip-based finished parts [40, 42]. The chip consolidations have been carried out by using the hot and cold extrusion methods. The hot extrusion process helped to establish bonding of the pure metal by removing the oxide layer that often covered the chips, while the cold extrusion was carried out to produce the chip-based finished goods. Fabricated preforms were used in backward extrusion to produce cans and in forward extrusion to produce shafts. Tensile tests revealed superior mechanical properties of chips extruded through the iECAP die compared to those of chips extruded through the flat-face die. The backward can extrusion of chip-based

extrudates fabricated with the iECAP die resulted in defect-free cans for all investigated wall thicknesses, while the cans obtained from flat-face die processed chips showed cracks within the walls. Shafts without visible internal defects could be produced by forward rod extrusion of previously hot extruded chips, regardless of the hot extrusion die design.

The possibility of using c-channels die in solid-state recycling of aluminium alloy machining swarf by hot extrusion was also attempted [13]. The machining swart from a cast Al–Si alloy ingot was successfully extruded through the equilateral c-channels at 600K, under ERs of 10 and 18. At a low ER of 10, an insufficient plastic strain was generated in some regions to cause the presence of coarse residual voids and cracks. Instead, applying an ER 18 resulted in the straight profile without warping, voids disappearing, and the gained density was comparable to that of the original ingot.

To sum up, the mechanical properties of the extruded profiles can be improved by optimizing the die design for extrusion. For the porthole die, the distribution of homogeneous oxide layers, dynamic recrystallization, high heat and high shear force experienced by the chips were the main reasons of the great chip consolidation. While for the ECAP die, excellent mechanical properties of the extruded profiles were principally due to the fine uniform grains in all microstructure. Some disadvantages of using the ECAP die can be seen from the aspects of very high extrusion pressure required for every cycle, multiple die sections led to difficulty for assembly, length of the workpiece was limited and more material to be discarded in the die.

2.3.4 Miscellaneous Methods in Direct Recycling Technique

Certain extruded profiles in direct recycling of chips through the hot extrusion might experience some voids due to insufficient plastic strain, apparent grain boundary existence which reduce diffusion bonds, poor in density, inferior in strength and reduced ductility for subsequent processing. All these limitations have enabled researchers to combine the hot extrusion with other processes such as ECAP, rolling, conform extrusion, friction extrusion and forging to induce more pressure and plastic strain. Discussion on the advantages of each combined process is presented below and some fundamental ideas of the process are illustrated in Figure 2-6.

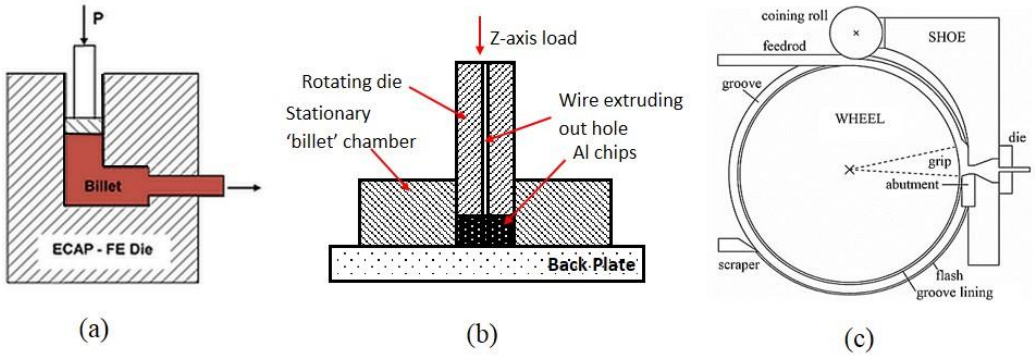

Figure 2-6: (a) Two-dimensional schematic view of the ECAP–FE die [43], (b) Friction extrusion setup [44], (c) A schematic view of continuous extrusion process (Conform) [45]

2.3.4.1 Extrusion and Rolling Method

Suzuki et al. [46] proposed a method for aluminium chip recycling by hot extrusion and hot rolling with T6 heat treatment. Hot rolling was performed in two conditions: normal and differential speed rolling (DSR). The tensile strength of the recycled materials obtained after 580K was slightly superior to non-recycled material (NR). In strength

and elongation, the DSR method outperformed the normal-based rolling. The smaller grain diameters obtained by recycled materials had increased ductility for subsequent forming processes. The possibility of recycling Al–Si alloy machining swarf (AC4CH) using cold extrusion and a subsequent cold rolling process was also tested [12]. The samples obtained were straight without warping, no grain boundaries were observed probably due to severe cold working and the recycled materials had gained better strengths than the original AC4CH ingot. Allwood et al. [47] investigated recycling of aluminium 1050A-H14 scrap by compaction, flat-rolling and forwards extrusion, all are performed separately. The findings show bonding in chips will increase with the increase of the extrusion ratio, while lubricant applied does not show a significant reduction in ram force. An extrusion ratio above 4, coupled with 20° die angle, was found necessary to achieve sound chips bonding. The deformed sheet metal was unstable with extensive edge cracking and a little bonding occurred.

2.3.4.2 Equal Channel Angular Pressing (ECAP) Method

Technique of severe plastic deformation (SPD) such as equal channel angular pressing die (ECAP) can also be incorporated in solid-state recycling. ECAP is a manifestation of SPD technique. It was reported by SPD, microstructure and texture of magnesium and aluminium alloy bars exhibited an excellent combination of strength and ductility. The gained mechanical properties can be attributed to the synergy of fine-grained microstructure and favorable texture promoting basal slip [48, 49]. Other than that, consolidation of Al–SiC powder to extruded profiles was successful by another

emerging SPD technique called forward extrusion-equal channel angular pressing (FE-ECAP) which resulted in higher hardness, strength and ductility than that of the FE extruded profiles for the same alloy composition due to accumulated strain and dense part in FE-ECAP [50]. In ECAP, the grain size refinement due to dynamic recrystallization and shear deformation in the die, as well as uniform dispersion of oxide contaminant during hot pressing, were the main reasons for enhancement of mechanical and physical properties in the ECAPed recycled material [51, 52].

In direct aluminium conversion, the ECAP method was performed as an alternative approach on the automotive aluminium scraps [25, 26]. The effects of heat and chemical cleaning methods on the chips were also studied. The sample was heated up to high temperature and acetone medium was used for chemical cleaning. The hot tearing took place on all sample surfaces neither deformation at l pass nor 3 passes. No metallic bonding was also observed in particles subjected to merely cold compaction. At high temperature of 450°C, even at one deformation pass, a full dense solid bar was successfully produced. Using thermal methods, the lubricant and acetone on aluminium turning scraps can be easily decomposed at temperatures around 290°C.

2.3.4.3 Continuous Extrusion Process (Conform)

Recycling viability of aluminium trimmings through a conform process directly into extruded products has been tested [6]. Aluminium in granule form was directly extruded in these trials. The process successfully produced wire, rod, bars, solid shapes and tubes

from the trimmings. The mechanical properties of the extruded products are very similar to the properties of products obtained by billet extrusion.

2.3.4.4 Friction Extrusion

Another variant in solid-state recycling is friction stir welding (FSW). This method involves joining and microstructure modification of the part with no heat for melting and casting required. Tang et al. [44] mixed AA2050 and AA2195 aluminium chips and used FSW to produce wire under varying conditions. The quality of the extruded wire was mainly depended on the extrusion temperature and die rotational speed. The results show the cracks encountered on the wire if using too high or too low in die rotational speed. The high temperature which is proportional to speed led to equiaxed and recrystallized grains in FSW. The ductility of the defect-free wire produced was demonstrated by the absence of cracking in 5T bend tests.

2.3.4.5 Forging

Bulk mechanical alloying (BMA) through cyclic cold compaction and cold extrusion followed by hot forging in the solid-state recycling of magnesium chips (AZ91D) and aluminium-silicon alloy were reported [53, 54]. After BMA, for AZ91D material, the final process was followed by single hot forging while for aluminium-silicon, the compact was subjected to warm-pressing and warm powder forging until near-net shaped before final sinter-forging. The relative density of about 80% was obtained in

both cases during BMA. Increasing the cyclic load in BMA will cause fine Si-particles distributed uniformly. High BMA cycle causes Fe additive particles to progressively dissolute into the Al matrix led to hardening. The relative density of each forged sample obtained is more than 99 % for AZ91D alloy. The hardness of the BMAed AZ91D alloy materials after hot forging increase with increasing the BMA cycles and the UTS of the direct hot forged parts are superior to that of as-cast AZ91D alloy. Longest process cycle is disadvantages for this approach to be implemented in the direct recycling of aluminium chips.

Yusuf and Lajis et al. [55, 56] have eliminated the two intermediate steps of cold-compaction and pre-heating in hot forging in direct aluminium recycling and response surface methodology (RSM) was used to obtain the best setting resulting in optimal UTS. The ANOVA results in RSM conclude that the chip size has more significant effect than temperature. This can be related to the small amount of oxide content on the smaller chips. The temperature plays a significant role in chip bonding by solid diffusions. The maximum UTS obtained was 174.78 MPa, about 53.3% from UTS of as-received material at operating temperature and pressure of 520˚C and 70 MPa, respectively. A linear correlation between temperature and UTS can be observed in Figure 2-7. At high temperature, atoms of solid solution diffuse to form small precipitates and acting as a barrier to prevent dislocations, thus enhancing the strength of the hot forged chips.

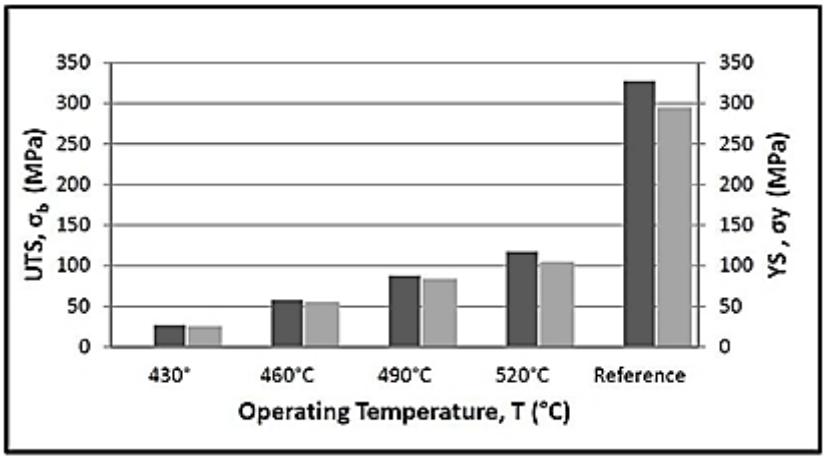

Figure 2-7: UTS and YS values at varying operating temperatures in hot forging [55]

2.3.5 Effects of Processing Parameters

The effects of chip characteristics, extrusion conditions, as well as types of reinforced materials, on the extruded profiles are very important [20, 57]. For a good bonding of granulated chips, a large plastic deformation was needed. Previous researchers [22, 34] concluded that factors contribute to weld quality in the soli-state recycling of aluminium chips can be summarised in Figure 2-8. The process parameters used, as reported in the direct aluminium chips recycling, are tabulated in Table 2-2.

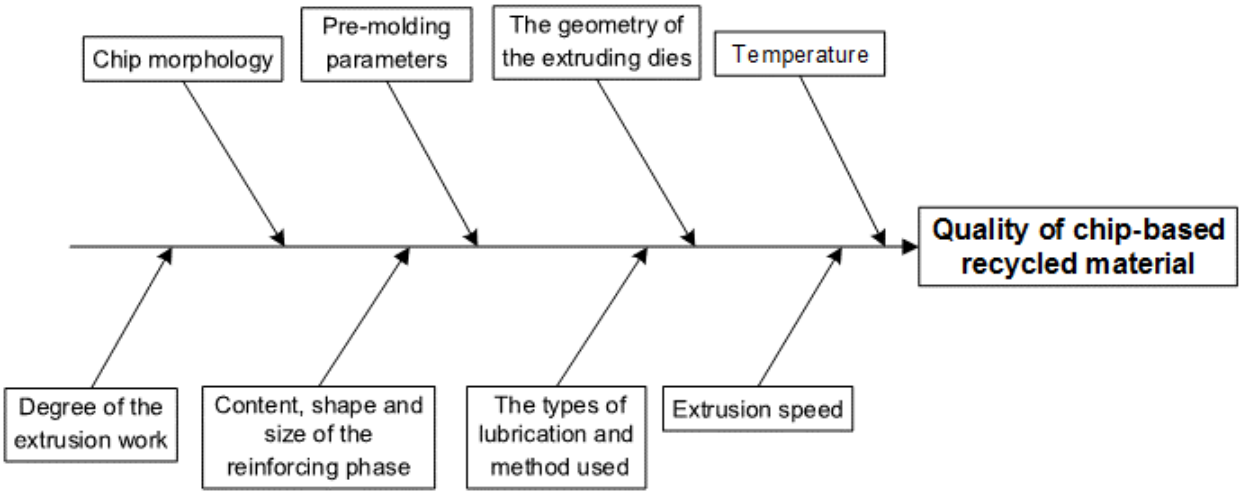

Figure 2-8: Process parameters influence on quality of the chip-based recycled material

2.3.5.1 Effects of Temperature and Extrusion Speed

Gronostajski et al. [34] elaborate that the good diffusion bonds and very low porosity of extruded composites are obtainable at high extrusion temperature. The combination of high heat and low extrusion speed enables the matrix material to flow plastically into the pores and voids, and thus allows longer inter-particle diffusions. Chips from alloy exhibits excellent tensile strength when consolidated at a significant high temperature, and at the same time contributed to poor grain refinement [58]. The high deformation temperature promotes particle precipitation and realize interfacial bonding between chips. Jahedi et al. [59] commented that performing the extrusion process at high ram speeds leads to a drastic change in the space between particle chains at the surface of the samples. Particles at the center location of the extruded part would not receive the effect of the friction from the surface. By increasing ram speed, the particles move collectively in larger distances, therefore shortening the diffusion. By increasing the

ram speed during the forward extrusion, the reinforcements rearranged according to the forces acting on them. This produces an oriented microstructure along the extrusion direction (ED). An acceptable compromise between the stress concentration and the strain and stress fields can be achieved to obtain higher mechanical properties and it is normally initiated at the ram speed ≤ 2 mm/s.

2.3.5.2 Effects of Die Geometry and Extrusion Ratio

The use of appropriate die geometry combined with the right extrusion parameters could produce good quality of extrudates from the recycled chips. Fine grain size and good bonding are closely related to ER. The significant high ER will largely extent the dynamic recrystallization to guarantee grain refinement. It also contributes to higher UTS and elongation attainment. This is due to the thin oxidize layers on the scraps, completely broken into small pieces by high compressive and shear forces which stimulate the individual chip bonding [60]. Guley et al. [61] in their study found that through the flat-face die, an ER of 10 did not guarantee a sufficient chip bonding. While at higher ER, the extruded profiles were found to gain superior strength and ductility. The profiles, extruded with 68:1 ER are superior in strength (21%) and ductility (15%) compared to the profiles extruded with 34:1 ER by the flat-face die. They subsequently confirmed that by the porthole die, at ER ≈ 10, the profiles strength was equivalent to the profiles extruded by the flat-face die at ER ≈ 68 and in ductility, the porthole die did better. Later, a study by Fogagnolo et al. [23] led to findings in lower ER (ER = 6.25); hot press and hot extrusion were needed to obtain good consolidated chips. It

was recommended that an ER above 4 with an aspect ratio larger than 1:3.8 and at least 50% extension strain were necessary to achieve significant bonding on the chips-based billet in cold extrusion [12, 47]. Meanwhile, Tekkaya et al. [20] show that the influence of chip morphology on the tensile properties is negligible when the porthole dies with the ER $\geq$ 30 are used.

2.3.5.3 Effects of Chip Morphology, Pre-molding and Lubrication Method

The geometry of the chips is an important factor in the chip compaction strategy to achieve uniform density in pre-compaction [41]. Samuel [24] commented that cold compaction pressure does affect the billet quality. At a given compacting pressure of 300 MPa, cleaned and annealed powder achieves the highest strength and hardness as compared with those without cleaning and annealing. Good lubrication improves the uniform deformation; at once, chip's bonding is not hindered and also during the consolidating phase [29]. In terms of chip types, the material recycled from turning swarf exhibited insufficient bonding among the individual pieces of the swarf, as compared to that recycled by the milling swarf under the same conditions [13]. Many voids, cracks and also apparent chip boundaries resulted in turning swarf. Wu et al. [62] demonstrated recycling of AZ31B magnesium alloy chips of different sizes by hot extrusion. The authors show that almost all recycled samples exhibit higher strength than the reference samples due to grain refinement strengthening and also found that the grain size, oxide amount, and density of the billet influenced elongation of the recycled materials.

The size fraction of chips plays a crucial factor to control oxides' contamination level. The oxygen concentration is proportional to the total surface area of the recycled samples. The total surface-area-to-volume ratio should be given more attention as it influence was severe than the chips appearance. The oxide contamination is less likely to affect strength, but can cause low elongation to failure at elevated temperatures [49]. At room temperature, the oxide contamination had a little negative effect on the mechanical properties and likewise less likely to influence the recrystallization. On the other hand, other findings suggested that the oxide contaminant has a detrimental effect on the plasticity behaviour of the recycled aluminium chips. Thus, a sufficient control on the contamination level should be primarily observed in the solid-state recycling. A further increment in the fractional reduction of chips has a minimum effect on the overall mass wear and friction coefficient to the recycled chips based composites [36].

Table 2-1: Summary of experimental study of direct recycling of aluminum and its alloys

Author /s	**Year**	**Material**	**Direct recycling method**	**Key experimental aspects**
[19]	1945	Al and Al alloys (grade-N/A)	• Extrusion, pressing, rolling and similar mechanical pressure operations	• Patented method for converting aluminium and aluminium alloy scrap and waste directly into finished items by mechanical methods.
[6]	1991	Al (grade-N/A)	• Conform process	• Performed recycling of aluminium trimmings by conform process directly into extruded products.
[8]	1996	Al (grade-N/A), AlCu4	• Hot extrusion + tungsten powder addition	• Fabricated composites from Al and AlCu4 chips with addition of different tungsten powder amount by

				hot extrusion and investigated the effects of heat treatment by means of aging at 170°C and solution treatment at 510°C for 1 hour on yield strength and hardness.
[34]	1998	Al (grade-N/A), W-powder, AlMg2-alloy	• Hot extrusion + small addition of tungsten powder of 80 mesh	• Studied the effects of small addition of tungsten powder of 80 mesh in production of composites Al and AlMg2-alloy granulated chips (sized < 4 mm) by hot extrusion.
[7, 9, 22, 35]	2000/ 1999/ 2001	Al (grade-N/A), AlMg2, AlCu4, Al_2O_3, W, C, Fe-Cr, CuAl	• Compaction + sintering + hot extrusion processes with hardening phase	• Developed the direct conversion of granulated aluminium and its alloy's chips (AlMg2 and AlCu4) into finished products through compaction, sintering and hot extrusion processes. The reinforcing phases used were aluminium oxide, tungsten, carbon, ferro-chromium and aluminium bronze comminuted chips.
[63, 64]	2000/ 2006	Al (grade-N/A), CuAl	• Cold compaction + hot extrusion	• Developed bearing composites through cold compaction and hot extrusion. The comminuted aluminium chips were used as matrix, while aluminium-bronze chips with 8%, 12% and 13% Al content were used as reinforcement particles.
[53, 54]	2002	AZ91D	• Cyclic cold compaction + extrusion followed by hot forging	• Used bulk mechanical alloying (BMA) through cyclic cold compaction and cold extrusion followed by hot forging in solid-state recycling of magnesium chips (AZ91D) and aluminium-silicon alloy.

[23]	2003	AA6061, Al_2O_3	• Hot extrusion without comminution step	• Employed direct recycling aluminium alloy chips reinforced with Al_2O_3 by cold/hot pressing without milling step followed by hot extrusion.
[24]	2003	Al alloy (grade-N/A)	• Direct powder metallurgy method	• Recycled aluminium scrap by a direct technique of powder metallurgy method.
[65]	2003	AA2014	• Hot extrusion	• Direct conversion of granulated Al-2014 scrap alloy with Al_2O_3 Saffil fiber addition into final products.
[49]	2004	AA5083	• Hot extrusion + hot rolling + blow forming	• Studied the tensile properties and blow forming characteristics of 5083 Al alloy recycled by the solid-state recycling.
[57]	2005	AA6061	• Hot extrusion	• Studied the influences of chips characteristics and extrusion conditions on the properties of a 6061 aluminium alloy.
[47]	2005	1050A-H14 sheet	• Compaction + flat-rolling + hot extrusion	• Performed recycling of aluminium scrap by compaction + flat-rolling (39%, 45%, 52% and 58% reduction) and compaction + forwards extrusion separately.
[29, 36]	2006	Al (grade-N/A), CuAl8	• Hot extrusion + hot rolling with T6 heat treatment	• Fabricated bearing material derived from aluminium and CuAl8 aluminium bronze composites using two fractions aluminium chips: below 2mm and 2-4mm. The mixtures were subjected to cold compacting, hot extrusion and heat treatment.
[46]	2007	AA6061	• Compaction + hot extrusion	• Performed recycling of cutting chips 6061

				aluminium alloy by hot extrusion and hot rolling with T6 heat treatment.
[37]	2008	AA6060, AA6082, AA7075	• ECAP	• Investigated the recycling of AA6060, AA6082 and AA7075 aluminium chips and their mixtures through compaction and hot extrusion.
[25, 26, 28]	2009/ 2010	AA6060	• ECAP	• Implemented technique of equal channel angular pressing (ECAP) in direct recycling of automotive aluminium scrap. The effectiveness of degreasing methods over aluminium alloy of AA6060 turnings also investigated.
[20]	2009	AA6060, SiC	• Hot extrusion	• Investigated the effects of chip sizes and shapes on the mechanical properties, microstructure and cutting behavior of extrudates by direct hot extrusion of aluminium AA6060 alloy chips with/without SiC particles addition.
[66]	2009	AA6082	▪ Hot extrusion	• Attempted to produce aluminium matrix composite by direct conversion of 6082 Al alloy machining chips mixed with fly ash.
[38, 39]	2009/ 2010	Al7075, Al powder	▪ Hot extrusion	• Fabrication of two phase material of Al7075 alloys chips with addition of air-atomized commercially pure Al powder.
[44]	2010	AA2050, AA2195	▪ Friction stir welding	• Recycled AA2050 and AA2195 aluminium chips by compaction and friction stir welding.

[14]	2010	AA1050, AA6060	▪ Hot extrusion	▪ Mixed 1050 aluminium alloy in the pins forms with 6060 aluminium alloy chips resulting from a turning operation, cold compacted into billets and hot extruded at 500°C.
[60]	2010	AZ91D	▪ Cold extrusion + cold rolling	▪ Investigated the effects of extrusion ratio on hot extrusion of recycled AZ91D magnesium alloy scraps.
[67]	2010	AA7075, Cu3Zn2, Cu	▪ Hot extrusion + cold rolling	▪ Recycled waste from brass wire in electric discharge machine and adding pure copper chips to AA7075 aluminium alloy.
[12]	2011	AC4CH	▪ Cold extrusion + cold rolling	▪ Tested the possibility of recycling Al–Si alloy machining swarf (AC4CH) by cold extrusion and a subsequent cold rolling process.
[61]	2011	AA6060	• Extrusion with flat-face die and porthole die	▪ Investigated the effect of the extrusion ratio (ER) and material flow by flat-face die and porthole die on the mechanical properties of solid-state recycled aluminium from 6060 aluminium chips by hot extrusion.
[11]	2012	AA6060	▪ Hot extrusion with flat-face die, the modified porthole die and ECAP die	• Succeeded to produce profiles extruded from aluminium AA6060 chips through a modified four turn equal channel angular pressing tool (iECAP die). The performance was compared with porthole die and flat-face die.
[10]	2012	AA6060	▪ Hot extrusion with a flat-face and porthole die	▪ Studied the effects of different routes of AA6060 chips consolidation and die

				design over mechanical properties. The three types of extrusion dies used were the flat-face die, the modified porthole die and ECAP die.
[68]	2013	AISI 1040, AlMg1Si-Cu	▪ Cold compaction + sintering under pure nitrogen atmosphere	▪ Mixed and blended the steel chips of AISI 1040 reinforced material in AlMg1SiCu aluminium chips matrix.
[41]	2013	AA6060	• Hot extrusion	▪ Extruded AA6060 chips through a flat-face and a porthole die to produce solid rectangular profiles.
[55, 56]	2013	AA6061-T6	• Direct hot forging	▪ Carried out direct hot forging on AA6061-T6 chips and eliminated the cold-compact and pre-heating steps. The RSM was used to optimize the process.
[40, 42]	2014/ 2015	AA6060	• Hot extrusion + cold extrusion	▪ Fabricated finished products in the form of cans and shafts through the chip-based billets produced by the iECAP die in the hot extrusion.
[13]	2015	Al–Si	• Hot extrusion through an equilateral c-channels	▪ Tested the possibility of using c-channels die in solid-state recycling of Al–Si alloy machining swarf by hot extrusion.

Table 2-2: Summary of applied key process parameters in direct recycling of aluminium chips

Key processing parameters		Researcher (s)
A: Billet Temperature (°C)	PT[a](400, 2hrs)	[42]
	PT(450, 20min)	[60]
	PT(450, 2-30min)	[53]
	PT(500, 50min)	[23]
	PT(500, 2hrs)	[35, 41]
	PT(500 / 550)	[20] / [10]
	PT(550, 15min)	[22]
	PT(550, 3hrs)	[61]
	PT(550, 6hrs)	[11, 14, 37]
	ST[b](550, 2hrs)	[7]
	ST(650, 2hrs)	[68]
B: Forming Temperature (°C)	ET[c](300)	[69]
	ET(350)	[51, 62, 69]
	ET(300-500)	[38]
	ET(400)	[58, 62, 69-72]
	ET(450)	[10, 11, 14, 20, 37, 40, 41, 61]
	ET(500)	[8, 22, 23, 34, 64]
	ET(520)	[63]
	ET(550)	[7, 11, 22]
	ECAPT[d](300-350)	[38]
	ECAPT(450)	[26]
	FT[e](430, 460, 490 & 520)	[55]
C: Compaction Force	400 kN	[61]
	25 MPa	[47]
	625 MPa	[25]
	400 MPa	[63, 64]

	500 kN	[10]
	650 & 700 MPa	[23]
	210 MPa	[8, 22, 34]
	60 kN	[14, 20, 37]
	303 MPa	[12]
	200 & 360 MPa	[24]
D: Extrusion Ratio	6:1 & 4:1	[12]
	2:1 & 4:1	[47]
	68:1 & 10:1	[61]
	34:1	[10, 41, 61]
	11:1 & 40:1	[60]
	8.7:1	[11]
	8.6:1	[10, 11]
	6.25:1	[22, 23]
	25:1	[23, 60]
	34.2:1	[14, 20]
E: Extrusion Speed (mm/s)	1 mm/s	[10, 11, 14, 20, 37, 41]
	2 mm/s	[12]
	6 mm/s	[10]
	10 mm/s	[7, 11, 12, 14]
	20 mm/s	[61]
F: Type of Lubricant	Graphite	[23, 50]
	Zinc stearate with graphite	[35, 64, 68, 73]
	MoS2	[13, 40, 47, 74]
	Stearic acid	[53]
G: Reinforced Material	Tungsten	[8, 22, 34]
	Graphite	[22]
	Aluminium bronze	[22]
	Ferro-chromium	[7]
	SiC	[20, 50]

	Alumina	[23]
	Copper	[67]
H: Heat Treatment	Annealing	[12, 36, 40, 49, 64, 73]
	Annealing (1h, 300°C)	[12]
	Chips annealing (60-110 min, 490-505°C)	[24]
	Quenching at 40°C	[24]
	Annealing (7hrs, 545°C)	[64]
	Artificial aging (15h, 160°C)	[44]
	Aging (0.5-128h, 225°C)	[44]
I: Die Angle	20° & 45°	[47]
	30°	[12]

Note: [a]PT (preheating temperature), [b]ST (sintering temperature), [c]ET (extrusion temperature), [d]ECAPT (ECAP temperature), [e]FT (forging temperature)

2.4 Numerical Simulation Studies

In metal forming, numerical analyses mainly based on finite element method represent a beneficial way for die and process optimization. The numerical simulation allows the local state variables concerning material temperature, strain, strain-rate, pressure and stress to be properly calculated through step-by-step basis. The finite element simulation can assist in predicting the weld strength within the extruded structures with the development of an appropriate analytical model. This will lead to mechanical properties and welding characteristics of the chip-based extruded profiles optimised. Reviewed articles applying the commercial finite element software in solid-state

recycling investigations are chronologically summarized in Table 2-3 with discussion followed.

Table 2-3: Summary of modeling and numerical simulation work in direct recycling of aluminium and its alloys.

Author/s	Year	Software utilized	Key aspects
Chiba et al. [12]	2011	DYNA3D explicit	▪ Established correlation between strain distribution and Vickers hardness in the plane perpendicular to the extrusion direction (ED) in solid-state recycling of aluminium alloy swarf using cold extrusion through the DYNA3D explicit nonlinear finite element code.
Guley et al. [41]	2013	DEFORM 3D^{TM} through Lagrangian approach	▪ Studied the chip welding phenomena through the porthole and conventional flat-face dies and established the welding quality index (WQI) through finite element method.
Haase et al. [40]	2015	Altair HyperXtrude	▪ Carried out numerical analysis to quantify the strain and pressure affecting chips during hot extrusion through the flat-face and iECAP dies.
Chiba et al. [13]	2015	DEFORM-3D^{TM}	▪ Analyzed the extrusion-induced strain distribution on c-channels die numerically through finite element code.

Finite element simulation was used by Chiba et al. [12] to correlate strain distribution and Vickers hardness in the plane perpendicular to the extrusion direction (ED) for the extruded bar in solid-state recycling of aluminum alloy swarf using cold extrusion. The aspect ratio and ER for the die applied was 1:1.8 and 4, respectively. The results in Figure 2-9 show an acceptable agreement between the equivalent strain distributions obtained through the simulation with regards to the Vickers hardness. The trend shows that the hardness is superior towards the outermost surfaces given by the graph whereby the equivalent strain value mostly exceeds 4 at the external surfaces.

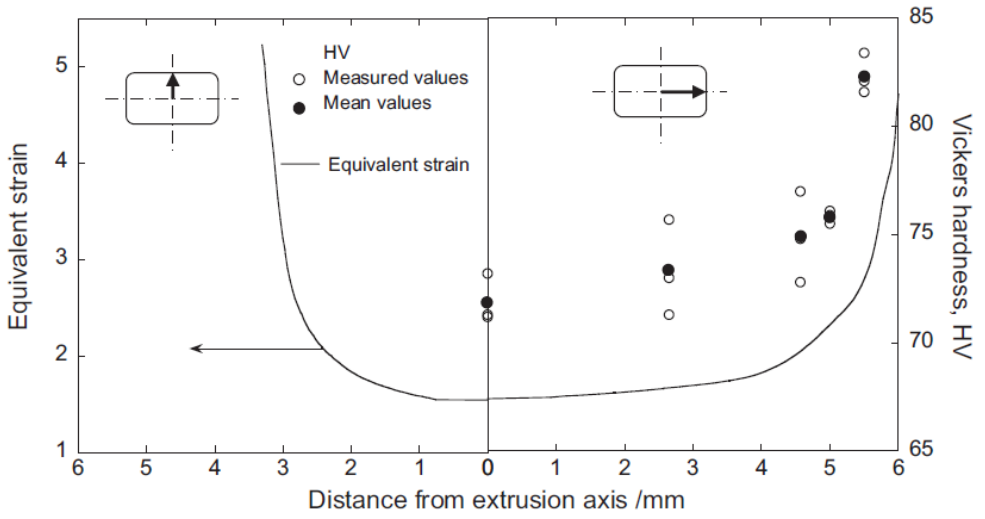

Figure 2-9: Spatial variations in equivalent strain and Vickers hardness in sample extruded for R = 4 and the 1:1.8 aspect ratio [12]

Haase and Tekkaya [40] carried out numerical analysis to quantify the strain and pressure affecting the chips during hot extrusion through the flat-face and iECAP dies. The strain analyses revealed that the iECAP die imposes a higher amount of strain compared to the flat-face into the processed material as given in Figure 2-10 (a) – (b). In addition, the effect of cross sections on the amount of strain imposed on the processed material through the flat-face die is found negligible as shown in Figure 2-10 (c). The same amount of strain was imposed on the material for both flat-face die with the cylindrical and rectangular shapes. It helped the author to reduce the experimental trials by excluding the influence of different cross-sectional geometries of the flat-face and iECAP dies on the mechanical properties investigated.

The extrusion-induced strain distribution on c-channels die was analysed numerically by Chiba and Yoshimura [13] in their recent work on solid-state recycling. The

simulation results reveal that both c-channels die with ER equal to 10 and 18 produced a non-uniform strain distribution over the cross section with the corners experiencing the highest strain as shown in Figure 2-11. Overall, more strain was found concentrated on the side parts rather than on the back part, which in turn, can cause higher strength and ductility obtainable on the side parts during the tensile test. Furthermore, performing extrusion at a higher ER can improve the bonding quality among individual machining swarf consequently result in higher mechanical strength and elongation of the extrudate.

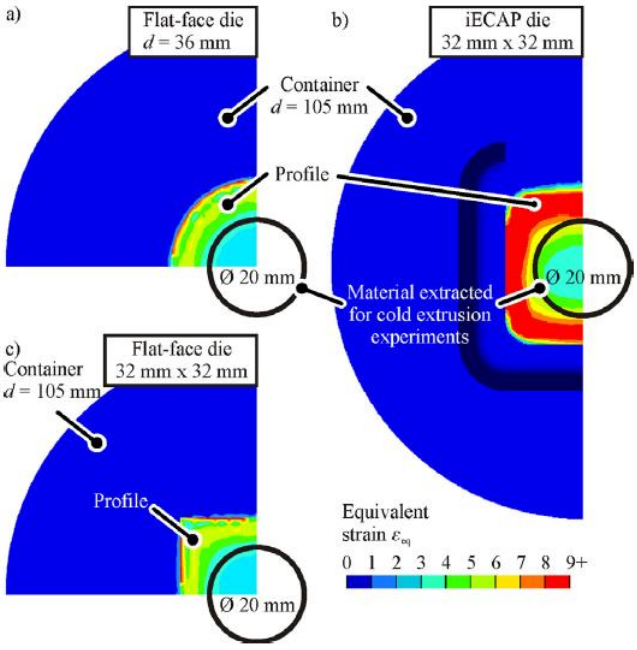

Figure 2-10: Strain distribution over the profile cross section for different hot extrusion dies. (a) Flat-face die, (b) iECAP die, (c) a flat-face die leading to a rectangular cross section [40]

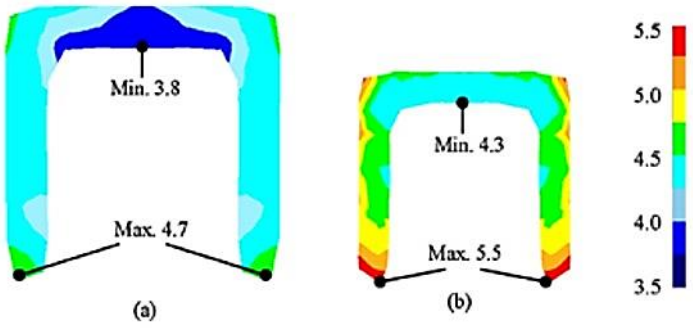

Figure 2-11: Spatial distribution of equivalent strain in samples extruded at (a) R=10 and (b) R = 18 [13]

The conditions of solid-state welding during extrusions were successfully studied by Güley et al. [41]. The authors investigated the chip welding phenomena through the porthole and conventional flat-face dies. The pressure-time-flow criterion as proposed by Donati and Tomesani [75] was used to determine the welding quality in the simulation. The results in Figure 2-12 show the effective strain is counted almost two times higher for the porthole die than the flat-face die at the die exit as observed. The results in Figure 2-13 show that the welding quality index (WQI) is higher on the outer regions compared to the core of the recycled profile and the trend is found to be similar to the effective strain values as given in Figure 2-12. The porthole die reveals WQI to be almost 70% higher than the flat-face die. In general, the use of porthole die can reach WQI of above 2.0 while for flat-face only 1.2 is achievable. This explains on the increase in ductility of any extrusions through the porthole die.

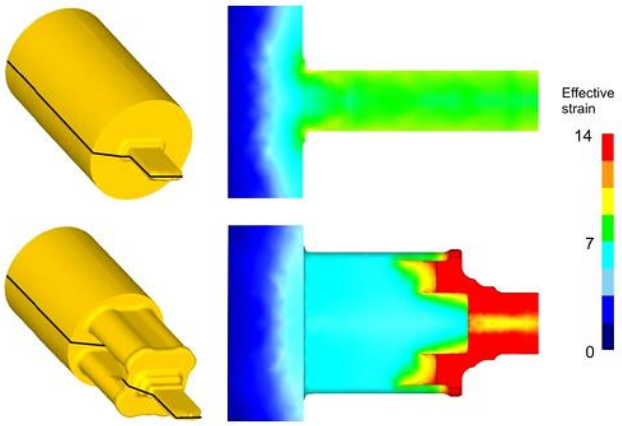

Figure 2-12: Effective strain values for the aluminum extrusion through flat-face (above) and porthole die (below) at the middle axis of the extrudate

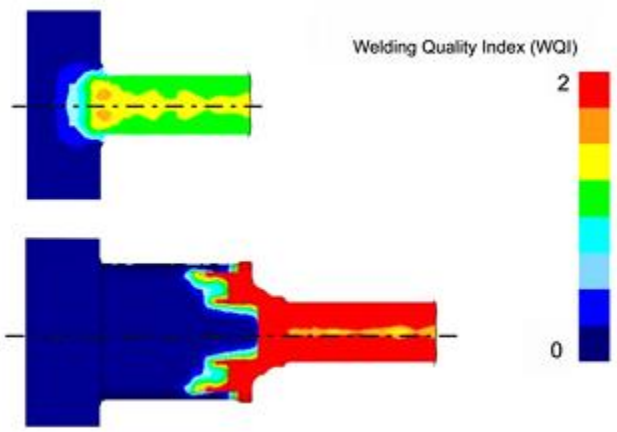

Figure 2-13: Welding quality index (WQI) as applied to extrusion of aluminum chips through the flat-face and porthole dies

2.5 Analytical Modelling Studies

The analytical models may become a powerful tool to get a fast predictive results for a given phenomenon if incorporated with a relevant theoretical considerations. This section reviews the analytical models used to predict the weld strength of solid-state

bonding of metals. The models are summarized from previous work of other researchers mainly focused on bond strength of accumulative roll bonding (ARB), porthole die extrusion (PDE) and flat rolling in different deformation conditions. Several deformation parameters which are important to grant creation of a weld bond between metal interfaces have been revealed through the reviews and listed as follows: normal contact stress, operating temperature, strain-rate, shear stress and the longitudinal strain at the bonding interface. The summary and critics about the existing models used to predict the weld strength are given in Table 2-4.

Table 2-4: Summary of weld strength models

Author /s	Year	Process	Weld Strength Model	Remarks
Bay [76]	1983	Accumulative roll bonding	$\left(\frac{\sigma_b}{\sigma_0}\right) = (1-\psi^2)\, R_f\, \frac{\sigma_b - p_{ex}}{\sigma_0} + \psi^2\, \frac{R_f - R'}{1-R'}\, \frac{\sigma_n}{\sigma_0}$ where, σ_b = resulting strength, σ_0 = normal strength of aluminium, σ_n = normal contact stress, p_{ex} = micro-extrusion pressure needed to force substrate material through the cracks in the cover layer, ψ = a fraction of aluminium surfaces that consist of an oxide film, R' = threshold rolling reduction needed for initial welding and R_f = actual rolling reduction: $R_f = 1 - \frac{initial\ thickness}{final\ thickness}$	▪The model was validated by the plane strain compression tests on aluminium interfaces and the results are much dispersed, however the general trend following the theoretical results was observed. ▪The hot rolling was not considered and the model assumed that the aluminium sheets can be modelled as perfectly flat surfaces. ▪Nevertheless, in reality the surface topography will generate localized shear stresses and

				air also can be entrapped between the two surfaces as rolling progressed. ▪Since oxide film will form within milliseconds upon exposure to the air, the oxidized layer formed on the exposed metal will reduce its strength.
Plata and Piwnik [77]	2000	Porthole die extrusion	Pressure − time criterion = $\int \left(\frac{\sigma_n}{k}\right) dt > C3$ Where, σ_n = normal contact stress experienced on the bonding plane and k = material yield stress in shear. Bonding is assumed to occur when the integral exceeds a critical value, C.	▪It is found that prediction of a reduction in bonding quality for a decrease in die leg angle is incorrect using this model when compared with experimental results from Valberg, 2002 [78]. ▪The effect of strain was ignored (varied by changing the extrusion ratio). ▪The model suggests that the diffusion plays an active role in bonding even though at high strain-rate process.
Ceretti et al. [79]	2009	Flat rolling and porthole die extrusion	$Criterion = \int \left(\frac{\sigma_n}{k}\right) dt > C3$	▪The model can predict the effect of chamber height on the weld quality, but no actual test

			$W_{lim} = 4.9063e^{-0.0017T}\ for\ T \geq 320\ ℃$ * Pivnik and Plata criterion [77] was used to predict weld quality in PDE and implemented with deduced temperature dependency welding limit (W_{lim}). Good agreement has been obtained when validated through flat rolling tests at rolling ratio of 44.4% and a working temperature of 320 °C.	was conducted to validate the welding limit in PDE.
Cooper et al., [80]	2014	Flat rolling	$Shear\ strength, \tau_b = \frac{1}{\sqrt{3}}\left(\frac{0.8}{Y}\sqrt{{\sigma_n}^2 + 3(\tau_{app})^2}\right)_{\leq} \times \upsilon_{\geq 0} \times \left(0.8\frac{\sigma_n - p_{ex}}{Y}\right)_{\leq 1} \times \sigma_0$ where, σ_n = normal contact stress, τ_{app} = nominal shear stress, Y = aluminium flow stress, υ = fraction of the final contact area that is exposed aluminium without a protective oxide layer, p_{ex} = pressure required to micro-extrude the substrate aluminium through the cracks, and σ_0 = strength of the cold bulk aluminium.	▪The model correctly predicts the bond strengths for temperatures 298 °K, 373 °K and 423 °K but underestimates bond strength at higher temperature (473 °K). ▪The model excluded weld bond strengthening mechanism due to diffusion phenomenon.

2.6 Damage and Fracture Prediction in Extrusion Process

Prediction of damage formation allows the influence of several deformation parameters be studied thoroughly and the quality of extruded profile can be foreseen in advance. Figure 2-14 illustrates the evolution of damage process: (1) crack initiation, (2) further growth of crack which creates cavities, (3) coalescence of cavities and (4) final rupture and failure. Often a mathematical function was used to model the failure phenomenon which is assumed to represent the physical behavior of the material and occurs when the function reaches a critical value C. The fracture functions can be written in the following form [81]:

$$If \int_0^{\varepsilon_R} f(\sigma, \varepsilon_{eq}) d\varepsilon_{eq} - C_c < 0, \text{ when there is no failure} \qquad (2\text{-}1)$$

$$If \int_0^{\varepsilon_R} f(\sigma, \varepsilon_{eq}) d\varepsilon_{eq} - C_c \geq 0, \text{ when the failure occurs.} \qquad (2\text{-}2)$$

In the above expressions, ε_R is the strain at rupture, ε_{eq} is the equivalent plastic strain defined by means of the total plastic part deformation.

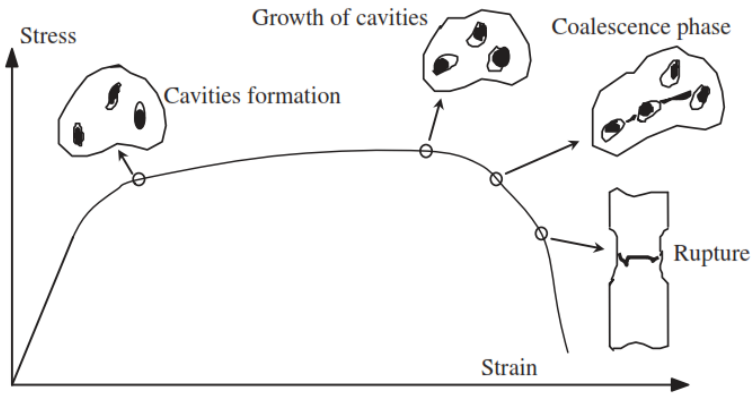

Figure 2-14: Mechanisms of damage leading to rupture [81].

Hambli et al. [82] developed a mathematical model that allows identification of any critical values when its satisfied the fracture criteria at the crack initiation. Methods of an inverse technique of circular blanking experiments were realised by incorporating the finite element calibration model. The critical values of the fracture criteria were derived by minimizing the difference between the punch penetrations prior to rupture values (U_R) obtained by the blanking experiment and deduced from the finite element simulation as shown in Figure 2-15.

In experiments performed by Hambli et al. [82], the fracture criteria were computed at the point where cracks initiated within the sample for a punch penetration of about 32% of the sheet thickness. When the fracture threshold is satisfied within an element, the element fractures and cracks occur. The crack initiation is assumed to occur at any point in the mesh when the fracture criteria reaches its critical value, Cc. Crack propagation in a finite element mesh can be simulated by four possible methods that are element splitting, nodes separation, element deletion and decreasing of stiffness finite element.

The critical values of different fracture criteria predicted by the proposed identification technique are reported in Table 2-5.

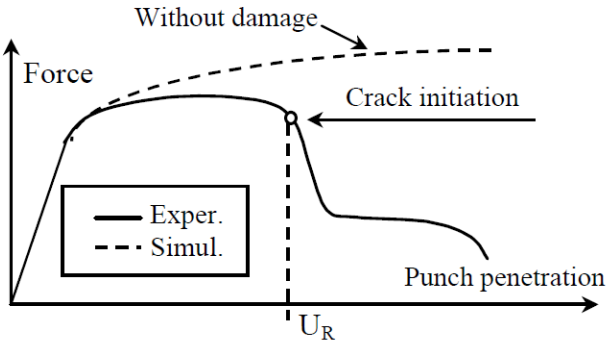

Figure 2-15: Illustration of the difference between the predicted and the experimental force–penetration curves [82]

Table 2-5: Critical values of the fracture criteria predicted by simulation [82]

Fracture criteria	**Damage Model**	**Critical value**	**Validity of the criteria**
Rice and Tracey [83]	$\int_0^{\varepsilon_R} exp(1.5\,\frac{\sigma_H}{\sigma_{eq}})d\varepsilon_{eq} - C1 = 0$	*C1* = 1.6	Good
Freudenthal [84]	$\int_0^{\varepsilon_R} \sigma_{eq}\, d\varepsilon_{eq} - C2 = 0$	*C2 = 4260*	Good
Cockroft and Latham [85]	$\int_0^{\varepsilon_R} \frac{\Omega}{\sigma_{eq}} d\varepsilon_{eq} - C3 = 0$	*C3 = 0.455*	Good
Brozzo [86]	$\int_0^{\varepsilon_R} \frac{2}{3}(\frac{\Omega}{\Omega - \sigma_H})\, d\varepsilon_{eq} - C4 = 0$	*C4 = 1.85*	Bad
Ghosh [87]	$\left(\frac{\sigma_I - \sigma_{III}}{2}\right)\sigma_H - C5 = 0$	*C5 = 3.25*	Bad
Norris [84]	$\int_0^{\varepsilon_R} (\frac{1}{1 - c\sigma_H})d\varepsilon_{eq} - C6 = 0$	*C6 = 1.165*	Bad
Atkins [88, 89]	$\int_0^{\varepsilon_R} (\frac{1 + 1/2L}{1 - c\sigma_H})\, d\varepsilon_{eq} - C7 = 0$	*C7 = 1.72*	Good

Oyane [90]	$\int_0^{\varepsilon_R} (1 + A\,\frac{\sigma_H}{\sigma_{eq}}) d\varepsilon_{eq} - C8 = 0$	*C8 = 2.455*	Good
Ayada [91]	$\int_0^{\varepsilon_R} (\frac{\sigma_H}{\sigma_{eq}}) d\varepsilon_{eq} - C9 = 0$	*C9 = 0.52*	Good
Plastic strain [82]	$\varepsilon_{eq} - C10 = 0$	*C10 = 4.2*	Good

2.7 Theories of Metallic Bond Formation

In solid metals, the bond is formed by the attraction of positive-ion core and electron cloud that move freely in a large extent of space [92]. The primary inter-atomic and secondary van der Waals forces are the main sources of attraction between the atoms. Both forces are negligible when two atoms are set apart in a large distance. However, when the intimate contact of less than 10 atomic spacings is achieved in the condition where metallic radius of aluminium atoms is taken as 0.143 nm, the attractive inter-atomic force will form a joint, the crystal mismatch causing a non-cohesive grain boundary [93]. To ensure such close contact can be achieved, the surface must be free or contains lesser amount of any oxides film or contaminants. The van der Waals as a secondary attraction force act over greater distances than the inter-atomic forces. Therefore, the van der Waals force always be present over the wide area of the crystal structure to form a weak bond whereby the inter-atomic forces effectively act at the area of intimate contact within the asperity tips. On top of that, Inglesfeld (1976) reveals that the bond is created due to inter-atomic forces when intimate contact of clean metal interfaces are established and this proved that the ratio of inter-atomic to van der Waals forces across an interface are typically very large.

The characteristics of solid-state welding processes are well explained by the film theory and energy barrier theory. The film theory is consistent with the above theory of forces, dictating that when any clean metal surfaces are brought into intimate contact, the weld will be created and that the existence of different degree of oxide layers and contaminants explains the varying propensity of metals to weld in the solid-state [94]. Findings by Conrad and Rice [95] supports this theory and agreed that the weld strength of fractured metal area in close contact that takes place in a vacuum is quite equivalent to the load applied, implying that the bond has been established. In the condition where surface films presence, bonding requires that, (a) breaking up the surface films to expose the virgin substrate metal and, (b) normal stress to be applied between close contact of the substrate metal. The surface films may include contaminants and adsorbed water vapour, as well as the surface oxide [96]. All the contaminants and water vapour can be vanished away or reduced by using chemical surface treatments [57] or heating the surface to a certain temperature [6]. High purity and cleanliness of the chips can drastically improve the bond quality as suggested by Samuel et al. [24] in their research findings.

The energy barrier mechanism has addressed two theories: the ‘mismatch of the crystal lattice’ and ‘recrystallisation’ theories [80]. The energy barrier theory suggests that there will be no resulting weld if any clean surfaces are merely brought into contact. According to the theory, an existing energy barrier must be overcome before welding can occur [97, 98]. Parks [98] states that recrystallisation which led to grain growth in metal removes the film barrier while Erdmann-Jesnitzer and Kazakov [94, 97] suggest that it is interdiffusion between the intimate contact surface that is responsible in the

bond formation other than plastic deformation. The theory of misorientation of the crystals lattice at the contact surface proposed by Semenov [97] deduces that certain distortion of the crystal lattice of the metals must present to create bond, implying that the existence of the localized energy barrier must be overcome. However, the Conrad and Rice [95] proves the creation of bond is possible without deformation ('energy-free' bonding) provided that a clean mating interface is established during the process. In view of any energy barriers that is associated with the plastic deformation in state of the art of cold welding research by Zhang and Bay [99], they postulate that an establishment of intimate contact between the surfaces is deemed necessary to fracture the surface films instead of distorting the crystal lattice. However, Pendrous et al. [100] stated that no recrystallization occurs during solid bonding at low temperature.

2.8 Summary of Literature Review

This chapter has covered review of a wide area of research topics from the work of previous researchers who devoted their efforts to thoroughly investigate the phenomena and mechanical performance of the directly recycled materials from multiple sources. An overview of the experimental investigations on direct recycling of chip is categorized according to various factors that control its quality. Subsequently, related work employing finite element method to quantify the deformation-induced variables and to establish their correlations with physical, mechanical and weld strength performance are gathered and reviewed. A summary of previous analytical models developed to predict the weld strength/quality is also compiled and discussed. As a

result of the review, it is worthwhile to use Deform 3D/Implicit FE platform to model the extrusion process of complex-shaped extruded profile from aluminium chips to achieve the utmost computational setup and accuracy. Some issues and research gaps that can be deduced from this comprehensive literature study conducted are discussed as follows:

2.8.1 Issue in Solid-state Recycling Research

Some issues that can be further explored through this comprehensive review are addressed as follows:

- Although one of the advantages of recycling in the solid-state can be noticed from its reduction of using the intensive energy for remelting, prolong preheating chip-based billet at high temperature to establish a sufficient weld bond will continue to waste the energy. A literature survey shows there is no specific study carried out to investigate the minimum preheating time for billet's homogenization and minimum temperature that should be applied for extrusion in relatively low extrusion ratio which can result in an acceptable chip-based extrudate quality.
- On top of that, the applicable damage models in Deform 3D finite element software can be quickly utilized with appropriate damage criterion to predict the effect of temperature on damage evolution of the extrudate structure for quick screening of weld bond quality.
- Since the die design affects mainly the amount of induced-plastic work onto the chip-based extrudate, extrusion with complex-shaped die geometry at low extrusion

ratio needs a proper study. Extruding at extremely low extrusion ratio of aluminium chips is also rarely reported in the literature review. Minimum threshold values of strain, normal force and shear force must be obtained in any die geometry to break the oxide layers efficiently.

- The derived model by Cooper and Allwood [80] to predict bond shear strength in a nominal room temperature can be further extended to predict the weld quality in complex-shaped extruded profile from recycled aluminium chips and later can be validated through tensile test. When considering extrusion of chip-based billet, attention should be given to the critical aspect of the resulting weld quality between chip interfaces. The weld quality of chips can be collectively represented by the resulting ultimate tensile strength/tensile strength. Since the weld strength is very sensitive to temperature [80], the effect of diffusion in strengthening the weld bond will be incorporated in the proposed model. All corresponding deformation parameters for calculating the predicted tensile strength will be taken care by Deform 3D FE software through simulation work.

2.8.2 Research Gap Analysis

MAIN ISSUE	GAP ANALYSIS	ACTION PLAN	METHODOLOGY
	What is the current problem could be solved/investigated in direct recycling of aluminium chips?	**What actions can be taken to close the gaps?**	**Possible research methodology to cater the addressed issue**
To obtain minimum time and temperature in homogenization of chip-based billet that	• What is the minimum possible preheating time?	• Decide several time domain and temperature range for preheating	• Conduct a series of hot extrusion experiments at (1, 2, 3, and 6) hour/s preheating time, (400,

can yield a satisfactory strength for energy-savings purpose	• What is the minimum possible temperature for preheating? • How to quickly inspect the acceptable weld quality of chip-based billet?	according to literature review. • Run the experiments to find the suitable homogenization condition. • Use damage evolution on extrudate structure to quickly examine the weld quality.	450, 500 and 550) °C preheating temperature and run tensile test. • Run finite element (FE) simulation using Cockroft and Latham fracture criterion to quantify the damage level.
Effect of surface topography on weld strength	• How severe the effect of surface topography by means of asperity height on the propensity of oxide layer formation? • Why the general model of bonds strength prediction developed by Cooper et al. [80] includes the effect of entrapped air within the asperity tips? • Why with a presence of large amount of the entrapped air within the asperity height causes poor weld bonds and reduced strength of solid-state recycled aluminium? • How severe the influence of surface topography in affecting the bond strength compared to temperature and pressure?	• The hot closed-die forging can be proposed to clarify this phenomenon. • This process imparts hydrostatic stress normal to the surface of chips. With a constant pressure and varied asperity height (surface roughness), the severity of oxidation corresponding to each surface condition can be clearly identified and clarified.	• The effect of chip's surface topography, pressure and temperature on the weld strength can be analysed by the hot forging and a dog-bone shaped closed die can be employed. • Chips with three different surface roughness levels can be selected. • Temperatures at (400, 450, and 500) °C while pressures at (20, 30, and 40) tonnes can be selected.
Development of Analytical Modelling of Weld Strength Prediction	• What is the possibility to extrude chip-based billet through a complex-shaped die geometry at extremely low extrusion ratio? • How to predict the weld strength of solid-state recycled aluminium chips	• Develop a tensile bond strength model to predict the weld bonds quality of the solid-state recycled aluminium chips. • Test the accuracy of tensile bond strength model by extrusion via the	• The tensile bond strength model includes both the tensile bond strength recovery due to diffusion mechanism and plastic deformation. • The diffusion-strengthening model can be derived through the combination of

	through the hot extrusion process? • How to correctly combine the deformation parameters with the extrusion ratio (reflected directly by the die design) that can result in an optimum weld strength recovery with the least trial?	complex die geometry. • Run the finite element simulation to retrieve the state variables of deformation.	diffusion theory of Fick's second law and an Arrhenius relationship. While the tensile bond strength model can be developed through the theory of thin film bonding.
Heat treatment for mechanical properties improvement	• How to improve the strength and hardness of the chip-based gear extruded at extremely low ER? • What is the possibility to enhance the mechanical properties of chip-based extrudate from the bulk aluminium AA6061-T4 (used as raw material) via the heat treatment to reach to AA6061-T6 condition after the hot extrusion?	• Perform the heat treatment to all selected gears at T6 condition (solution heat treatment, rapid quenching, and artificial aging)	• The extruded gears can be cut and ground to the length of 10 mm. • Solution heat treatment on each sample can be done by heating at 530°C for 120 minutes before rapidly quenched into cold water at 100˚C/s (quenching rate). • The effect of distinct artificial aging time can be investigated to examine its influences in heat treatment.

CHAPTER 3 : RESEARCH METHODOLOGY

This chapter broadly describes the experimental procedures and finite element setup implemented in the analysis of solid-state aluminium recycling. Details of the experimental setup are covered in Section 3.1 which includes die development, chips and billet preparations, hot extrusion setup, hot forging setup and experimental design in hot forging experiment. The procedures for mechanical and physical properties tests on the respective samples are presented in Sections 3.2 and 3.3 while Section 3.4 briefly describes about methods and standards followed in the analysis of microstructure. Procedures of FE simulation in damage evolution prediction and assumptions made in formulating the weld strength model are covered in Section 3.5. The deduced weld strength model will be validated through a series of tensile strength tests on the profiles extruded via the rectangular and gear die geometries. Several tests are also carried out to evaluate the mechanical and physical properties enhancement of the chip-based extrudates.

3.1 Experimental Setup

3.1.1 Development of Dies

Two types of die were designed and fabricated for hot extrusion of chip-based billet: (a) A flat-face die with rectangular geometry and (b) A flat-face die with spur gear geometry and two module sizes were employed. Details of the dimensions are given in Table 3-1 while Figure 3-1 shows dies with the corresponding geometry. The

rectangular die was used in the heating homogenisation analysis, to validate the damage evolution of the extrudate structures and to test accuracy of the deduced weld strength model. The gear die geometry was used to investigate the possibility of extrusion for the complex aluminium profiles with low and extremely low extrusion ratio and also used to validate the derived weld strength model on the chip-based extruded gears. The details drawing are given in Appendices A, B and C.

The spur gear geometry was selected because the gear teeth is straight and it is parallel to the axis of the wheel, thus possible to be produced by the extrusion process by pushing the bar/billet through the die opening. Since the material is experienced compression stress, the outside area is work hardened. It is more economical to slice a segment off an extruded gear than to cut an individual gear through machine. The product of gears from recycled materials have a large variety of applications that could be used in switch apparatus, clocks movement mechanism, watches, small motors, certain machines, mechanical toys and other related parts to machinery of all kinds. Instead, the gear product can also be hardened by any carburizing, induction hardening and solution heat treatment methods [101].

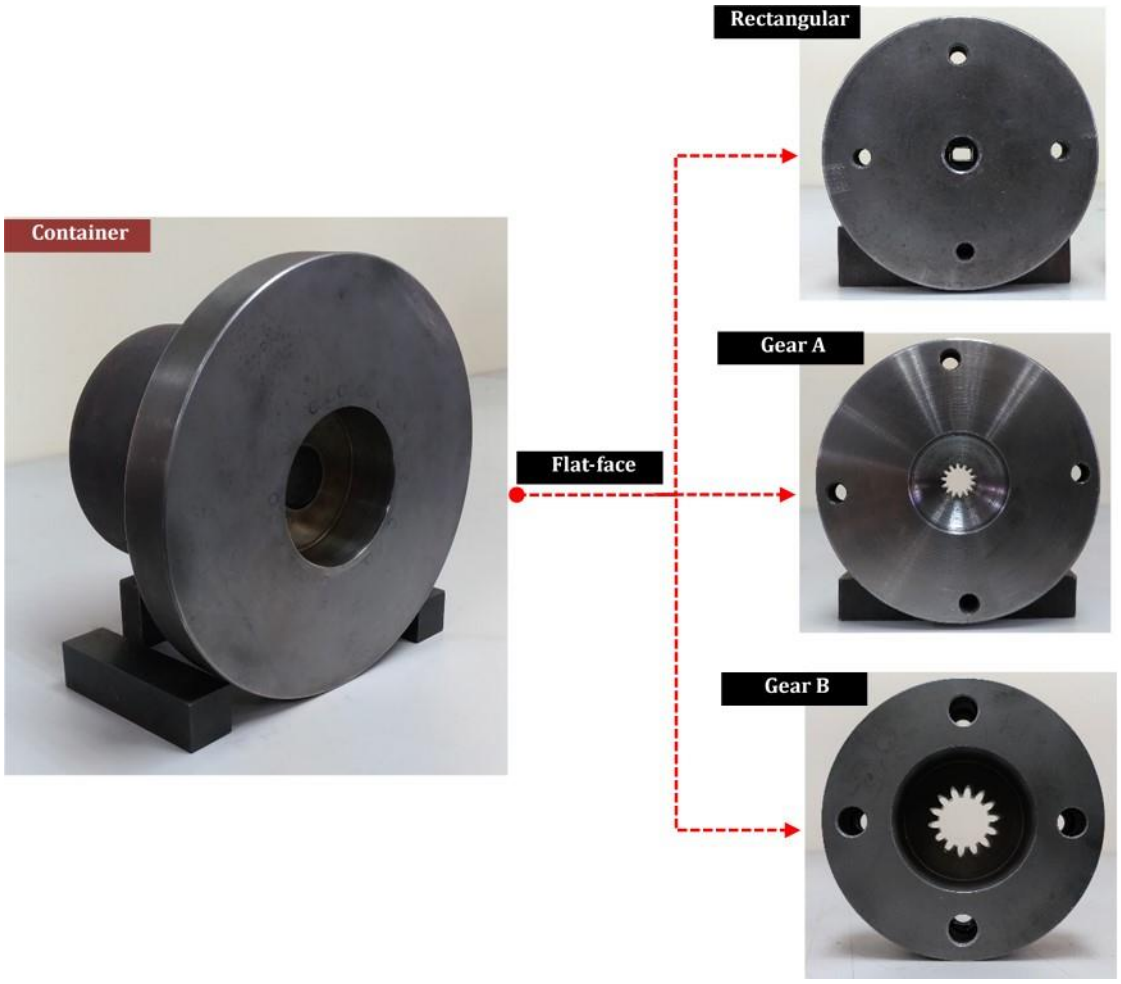

Figure 3-1: Design of die geometries for hot extrusion of chips

Table 3-1: Die and extrusion parameters

Parameter	**Die Type**		
	Flat-face		
Die notation	R	G_A	G_B
Geometry	Rectangular	Spur gear	Spur gear
Cross sectional area, A (mm^2)	63.00 (6.3 x 10)	145.43	327.88
Bearing length, l (mm)	27	24	11.4
Billet diameter, $Ø$ (mm)		30	
Extrusion ratio, ER	11.22	4.86	2.16
Extrusion speed, v (mm/s)	1.0 - 4.4	4.4	4.4
Container temp., T_C (°C)		300	
Die temp., T_D (°C)		300	
Preheating temp., T_P (°C)		400-550	
Preheat duration, t (hour/s)		1-6	
Die material		H13 heat treated tool steel	

3.1.2 Preparation of Chips and Billet

The material selected for the study was aluminium AA6061 from different grades of O, T4 and T6, where its applications had been broadly found in the automotive industry. Examination of the chemical compositions of the received materials was carried out to confirm their originality using SEM machine with EDS as shown in Figure 3-2. The chemical composition and mechanical properties of the aluminium alloy used in this study are summarized in Table 3-2 and Table 3-3.

Figure 3-2: SEM machine with EDS (Model: JSM 6380 La)

Table 3-2: Chemical compositions of AA6061 [102]

Element (%)	**Ti**	**Si**	**Mn**	**Mg**	**Cu**	**Cr**	**Zn**	**Fe**	**Others**	**Al**
AA6061	0.09	0.65	0.04	1.00	0.23	0.07	0.07	0.03	0.15	Bal.

Table 3-3: Mechanical properties of as-received AA6061-T0, AA6061-T4 and AA6061-T6 [102]

Mechanical Properties	**Aluminium Type**		
	AA6061-T0	AA6061-T4	AA6061-T6
Tensile Strength (MPa)	150	230	319
Yield Strength (MPa)	110	130	292
Shear Strength (MPa)	84	170	210
Elongation (%)	19	18	13
Brinell Hardness (HB)	30	65	95
Density (g/cm^3)		2.70	

* All values in measured under T = 25ºC

To mimic waste produced from the machining process, the chips were prepared by comminuting aluminium block AA6061 through the high-speed milling. The milling-type of chip was selected because it has a thinner shape which subsequently resulted in better deformability [13]. The chips were machined in a controlled manner to result in chips that only contained an average length less than 4 mm as recommended [22]. Morphology and size of the chip particles were examined by a Tool Makers measuring microscope equipped with digital Nikon MM-60 camera, and are shown in Table 3-4. The chips obtained by face milling were curled up and are discontinuous. Estimation method was used to compute total surface area of the machined chips taking into assumption that the produced chips followed a cubical shape. The following equation is deployed for the chip's surface area estimation [72]:

$$S = \frac{2(lw + wt + tl)}{lwt} \tag{3-1}$$

where S is the total surface area per unit volume, l is the chip length, w is the chip width and t is the chip thickness. The obtained chip morphology was though appropriate for solid-state recycling due to its constant shape, small in size and in a homogenous form.

The aluminium chips produced by machining should not contain any impurities and dirt such as coolant and lubricant because all those could alter their chemical composition and subsequently impair diffusion bonding among chips during the solid-state recycling. Therefore, the chips were degreased with acetone inside an ultrasonic bath for 10 minutes. Cleaning of the chips from impurities followed ASTM G131-96 [103], the standard practice applicable for cleaning materials by the ultrasonic techniques.

The cleaned machining chips were then placed in a cylindrical container and compacted at room temperature by a cold press to form billets of 30 mm diameter and height approximately from 80 mm to 90 mm. Each compaction step was stopped when a maximum force of 30 tonnes was reached. After removing the punch, the resulting free volume inside cylindrical die was filled with additional chips and the compaction was resumed until a billet with the prescribed size was completely obtained. The sequence of the chips pre-processing is depicted in Figure 3-3.

Table 3-4: Characteristics of milling-chip type and chip-based billet appearance after compaction

Chip appearance	Chip-based billet	Chip Characteristics		
		Type	Geometry	Size (mm)
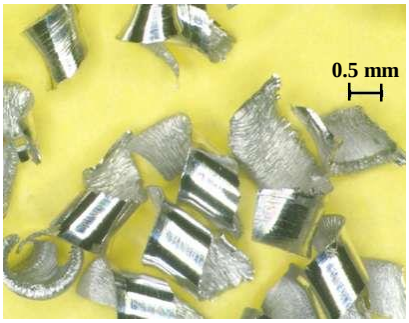	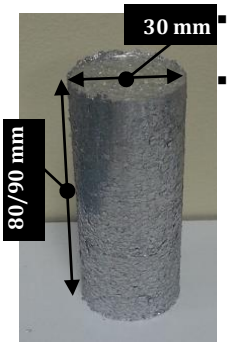	▪ Milling-chips ▪ Machining parameters: ▪ Cutting speed, (mm/min) = 1100 ▪ Feed, f (mm/tooth) = 0.05 ▪ Depth of Cut, (mm) = 0.04	Length (*l*) Width (*w*) Thickness (*t*) Surface area	≈ 3.10-3.20 ≈ 1.097 ≈ 0.091 ≈ 24.43

Figure 3-3: Pre-processing of chips before extrusion

3.1.3 Hot Extrusion Process

In pre-processing step, each billet was annealed to an assigned temperature for several hours before the extrusion process. This step is mandatory to prevent cracks on the extrudates and to minimise the extrusion force [13]. Hot extrusion of the chip-based billets was carried out on a hydraulic extrusion press, having a maximum extrusion force of 300 tonnes as shown in Figure 3-4. The ram speed was set at 1-5 mm/s and the container temperature was set at 300 ^{o}C. The maximum temperature setting was limited to 550 ^{o}C because heating the billet above 550 ^{o}C led to hot cracks in the surface of the extrudates, while the ram speed was set to within 1-5 mm/s to prevent an inhomogeneous material flow due to the stick-slip effect resulting in chatter marks on the profile surface at a higher speed [14]. The heat was generated using a ceramic heater installed around the container and the temperature can be independently controlled at the extrusion press itself. A small amount of graphite-based lubricant was applied over the inner surface of the die's bearing land at every cycle of extrusion in order to prevent an increase in extrusion load as a result of excessive friction [13]. The extrusion

parameters including for chip annealing/preheating employed correspond to the experimental aims and objectives.

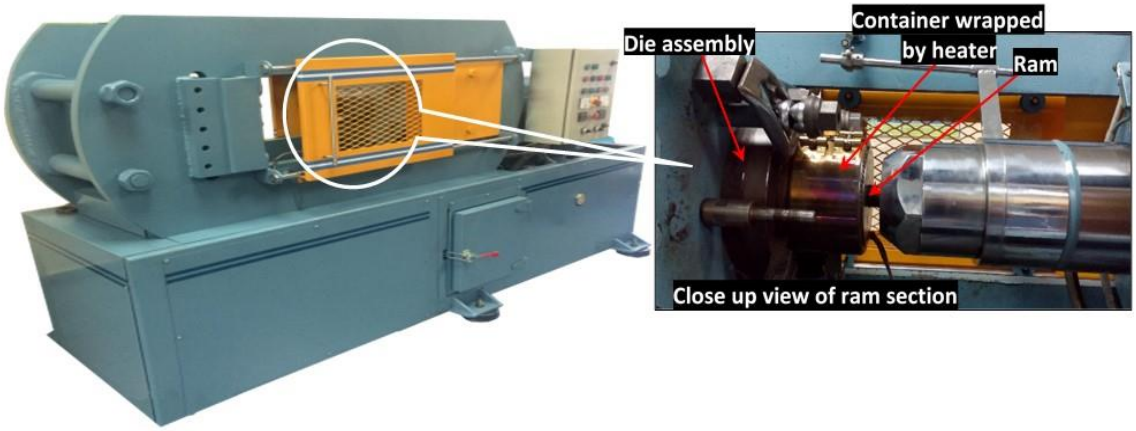

Figure 3-4: 300 tonne hydraulic extrusion press machine

3.1.4 Hot Forging

The hot forging experiments are carried out to investigate the effects of chip's surface asperity height (surface topography) on the propensity of oxide layer formation. On top of that, a mathematical model for tensile strength recovery due to diffusion mechanisms as an extension to the previously developed tensile bond strength model can be established via this method. To establish the weld strength model which influenced by other than the deformation variables, factors such as surface topography and area of chips are necessary to be investigated. The decision can be made to either include or exclude the effect from the model terms. These aims can be accomplished by the hot forging experiment. Since the hot forging process mostly applied load perpendicular to the surface of the chips, the effect of shear stress on breaking the oxide layers that normally encountered in extrusion can be excluded. Therefore, the hot forging

operation represents a process of imparting normal/hydrostatic stress onto the chips and the strength recovery is assumed to occur solely by the diffusion mechanisms. The forging process acts as a plane-strain experiment where movement of chips were constrained in xy-plane during compression. This was done by performing the hot forging test, analogous to closed-die forging assuming that very minimum tensile stress stretching the forged material merely on z-plane. Thus, the consolidation of chips was assumed to be mainly by the diffusion mechanisms.

In hot forging operation, the chips were prepared according to the method briefed in Section 3.1.2. Prior to forging, the cleaned chips were placed in a dog-bone shaped closed die and compacted in room temperature by a cold press to 10 tonnes to produce green parts and to ensure all weighted chips filling up the die evenly. Each sample produced followed the ASTM-E8 M standards, sub-size tensile sample, 25 mm in gage length with 6 mm width for reduced section and an approximately 6 mm thickness. The die and its assembly are shown in Figure 3-5. Each compaction step was stopped when a maximum force of 10 tonnes was reached, and it was repeated for several times until a sample with the prescribed thickness was completely secured. With the assigned sample dimensions, 12 g chips were required for every experimental run. Finally, the hot forging was carried out on each sample through the hot press machine with varying holding time. Then, the tensile test was carried out on each sample according to the procedure briefed in Section 3.2. Details of the experimental setup and process flow are shown in Figure 3-6.

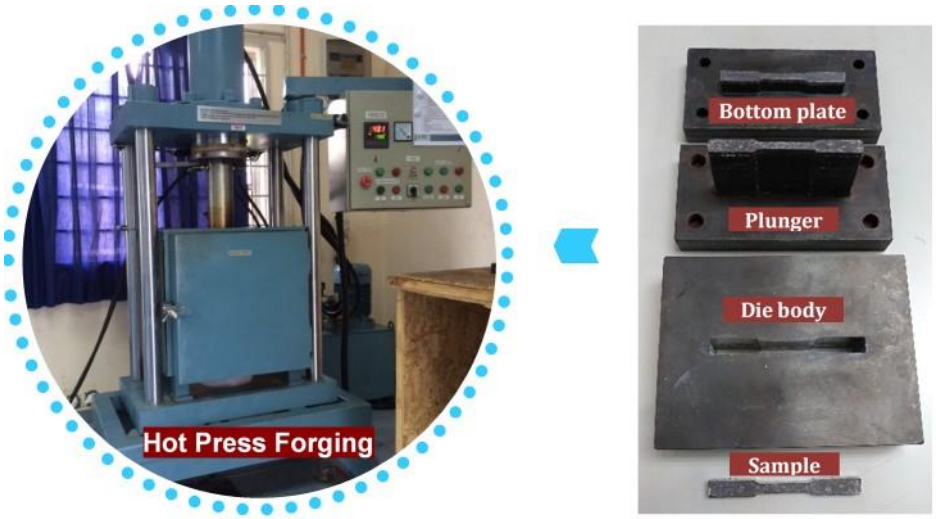

Figure 3-5: Hot press forging machine and dog-bone shaped die

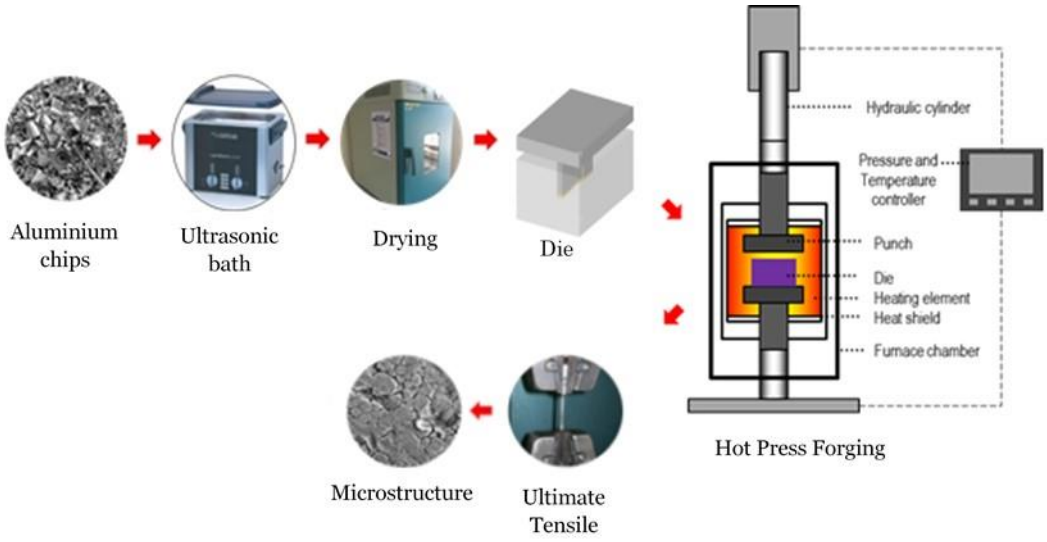

Figure 3-6: Schematic diagram of hot forging press and overall process flow

3.1.5 Experimental Design

Design of Experiment (DOE) provides an effective statistical tool that may assist to draw an accurate conclusion on the effects of each factor and their interactions over the response of interest (output) in experiments conducted. The DOE is also very helpful in discovering the key variables influencing the quality characteristics and the variables can be ranked according to their degree of importance. In order to analyse the effect of chip's surface topography over the weld strength through the hot forging experiment, the 2^k factorial design was chosen. The 2^k factorial design is the most common technique used in DOE and very much helpful in screening the important factors of the experiment. With time and fund constraints during the entire study, the 2^k factorial design was given a priority.

The effect of chip's surface topography was investigated together with the factors of temperature and pressure. For surface topography variables, three different chip sizes were used (small, medium and large) with distinct measured surface roughness values, operating temperatures were set at 400 ^oC, 450 ^oC, 500 ^oC and pressures were set at 20, 30, 40 tonnes respectively. ANOVA is very essential in 2^k design to come up with a structured analysis of results. In this study, Minitab 16 has been used to assist the ANOVA calculations and graph plotting. The effective ANOVA process has five major steps:

- Calculating the sum of squares (*SS*).
- Determining the degrees of freedom (*DOF*).
- Calculating the mean squares (*MS*).

- Determining the test ratio F_0.
- Drawing conclusions from the results.

Prior to carrying out ANOVA for the remaining significant factors, the effects of all single factors and their interactions can be determined by the following procedures [104]:

1. *Sum of square factor (SS)* is calculated using the following formula,

$$SS = \frac{C^2}{N} \tag{3-2}$$

where N is the total samples number taken during the experiment, and C is known as the *Contrast.* In order to calculate C, the (+) and (-) table for the experiment must be constructed.

2. *Sum of square total (SS_{tot})* is calculated using the following formula:

$$SS_{Tot} = \sum_{i=1}^{a}\sum_{j=1}^{b}\sum_{k=1}^{c}\sum_{l=1}^{d}\sum_{m=1}^{n} y_{ijklm} - \frac{y^2}{abcdn} \tag{3-3}$$

3. While *Sum of square error (SS_E)* is calculated as below:

$$SS_E = SS_T - SS_A - SS_B - SS_{AB} - \cdots - SS_{ABCD} \tag{3-4}$$

4. *Degree of freedom (DOF)* for different terms such as *A*, *B*, *AB* and so on including DOF for total and DOF for error are calculated based on the following formulas:

$$DOF_A = A - 1 \quad (3\text{-}7)$$

$$DOF_{Total} = N - 1 \quad (3\text{-}5)$$

$$DOF_{Error} = 2^k(n-1) \quad (3\text{-}6)$$

5. The *Mean Square* (*MS)* of the measurements is obtained using:

$$MS = \frac{SS}{DOF} \quad (3\text{-}8)$$

6. The F_0 test ratio is obtained using both *MS* for each factor as well as MS_E. The following formula is used:

$$F_{0x} = \frac{MS_x}{MS_E} \quad (3\text{-}9)$$

where x=*A, B, AB*... and so on.

7. In order to be able to draw any conclusion from this test, the control limit, F_{α,v_1,v_2}must be obtained, where:

$v_1 = DOF$ of the numerator of the F_0 ratio

$v_2 = DOF_E$

α =The probability of a Type I error

The F_0 test can be accomplished by referring to table *F* distribution. Then, this value should be compared to all the F_{0x} values that have been calculated. If $F_{0x} > F_{\alpha,v_1,v_2}$, the factor *x* is said to have a significant effect on the process.

In some experimental design cases, it is necessary to know whether the 2^k design is sufficient to model the response function as the function could be a linear or nonlinear. If a nonlinear function exists, then more factor levels must be considered and further analysis can be carried out through the Response Surface Method (RSM). The experimenter may have a choice of replicating the corner or "cube" points in a 2^k factorial, or placing replicate runs at the design center as shown in Figure 3-7.

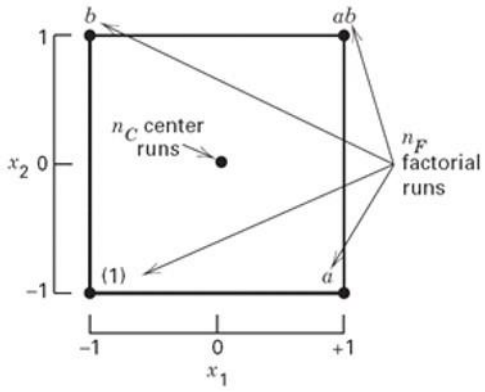

Figure 3-7: A 2^k design with center points

The related formulas used to analyze the ANOVA for curvature analysis are shown as follows [104]:

1. Sum of square curvature:

$$SS_{Pure\ Quad} = \frac{n_F n_C\ (\bar{y}_F - \bar{y}_C)^2}{n_F\ +\ n_C} \qquad (3\text{-}10)$$

where, $n_f = 2^k n$, number of observations in the ordinary factorial design, n_c = number of observations at the center point, $\bar{y}_c$ = the average of the n_c observations in the center point, $\bar{y}_F$ = the average of the n_f observations in the ordinary factorial design

2. Mean square error:

$$MS_E = s^2 = \sigma^2 = \frac{\sum_{i=1}^{n_c}(\bar{y}_i - \bar{y}_c)^2}{n_c - 1} \quad (3\text{-}11)$$

3. Test ratio F_o:

$$F_o = \frac{MS_{curvature}}{MS_E} = \frac{\frac{SS_{curvature}}{DOF}}{MS_E} \quad (3\text{-}12)$$

3.2 Mechanical Properties Test

The mechanical properties of the respective samples were investigated in terms of yield strength, tensile strength, elongation, and hardness. Each mechanical characteristic is measured for three times and the average value was reported. Following are the procedures for each test:

(i) Tensile test

Tensile tests were performed with an initial strain-rate of 2.5×10^{-3} s^{-1} at room temperature on a Testometric™ M500 100kN tensile test machine for both samples

produced by hot extrusion and hot forging. For hot extrusion process, the tensile test samples were fabricated parallel to extrusion direction (ED) according to ASTM-E8 M sub-size [105] as shown in Table 3-5 with a 25 mm gage length and reduced section width of 6 mm and pulled to failure. The strain was measured using a crosshead movement because the failure was frequently encountered at the area beyond the extensometer limit.

(ii) Hardness test

Vickers hardness tests were carried out at an applied load between 0.9807 N to 2.942 N and a holding time of 10 s at room temperature using a Vickers Hardness tester (Shimadzu HMV-2TE) in accordance with DIN EN ISO 6507-1:2005 standards. The microhardness test was performed by forcing a square-based pyramidal diamond indenter having a face angles of 136º for about 10 s. Then, the measurements were repeated at several locations for repeatability.

Table 3-5: Specification details of tensile test sample [105]

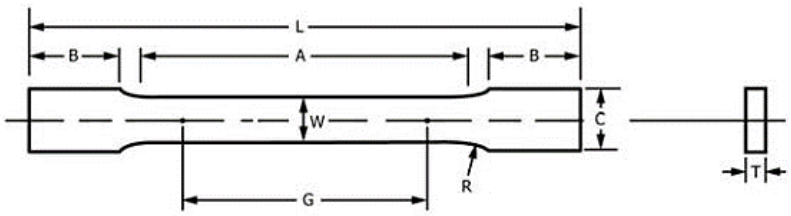

Dimensions	Sub-size Specimen (mm)
	6
G – Gage length	25.0 ± 0.1
W – Width	6.0 ± 0.1
T – Thickness	Maximum 6
R – Radius of fillet	6
L – Overall Length	100
A – Length of reduced section	32
B – Length of grip section	30
C – Width of grip section	10

3.3 Physical Properties Test

Density meter using Archimedes' water immersion principle (in distilled water) was used to carry out the density measurement of as cast-based billets, chip-based billets and extrudates. The density is measured according to the Eq. 3-13. The measured density of as-cast billet and chip-based billet are given in Table 3-6.

$$Density = \frac{A}{|B|} \times density\ of\ distilled\ water \tag{3-13}$$

where,

A = weight of sample on air

$|B|$ = weight of sample in liquid

Table 3-6: Density of as-cast billet and chip-based billet

Sample	Temp. (^{o}C)	Density of distilled water (g/cm^3)	Weight on air (g)	Weight in liquid (g)	Average density (g/cm^3)
As-received AA6061-T6	24.9	0.99704	2.6284	-0.9864	2.6600
Chip-based billet	27.4	0.99651	1.7554	-0.7031	2.4879

3.4 Analysis of Microstructure

Microstructures of all extrudates and as-cast aluminum material were characterised and analysed with the techniques of Light Optical Microscopy (LOM), Scanning Electron Microscope with Energy Dispersive Spectroscopy (SEM-EDS), and X-Ray Diffraction (XRD). The samples taken for microstructure examination were machined from the specified area as shown in Figure 3-8.

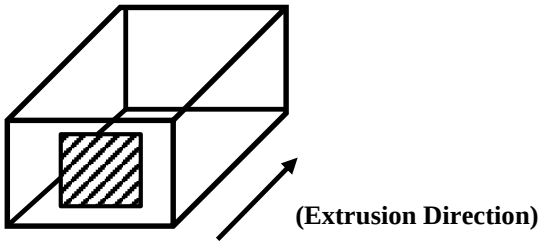

Figure 3-8: Location of samples taken from extrudates for microstructure analysis

The samples for microstructure investigation through LOM were mechanically ground using SiC paper of grits 240, 600 and 1200 (for 180 s each in wet condition) and

polished for 600 s with colloidal silica. The polished samples were electrolytically etched using Barker's reagent with a voltage of U= 12V dc for 120s. This procedure permits the grain structure to be observed under the crossed polarised illumination and the interference colours revealed allows inspection of physical and chemical inhomogeneities. The average grain size was measured using the linear intercept method in accordance with ASTM E112-13 standards [106] and the test pattern for intercept counting is shown in Figure 3-9.

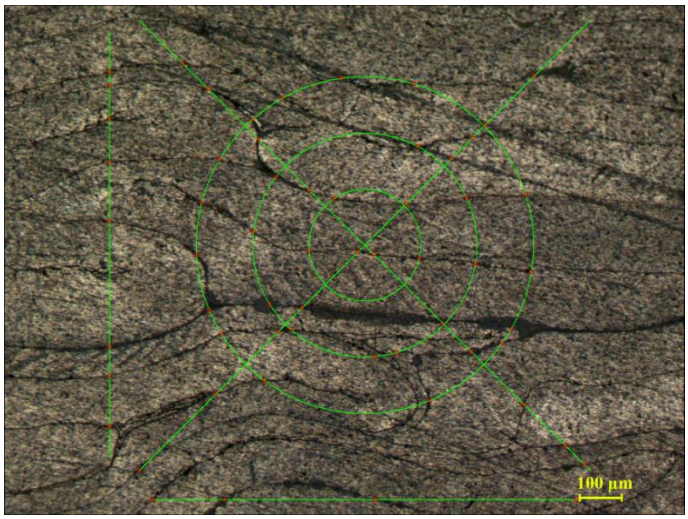

Figure 3-9: Test pattern for intercept counting of sample

Fracture surface of the extruded profiles and billets butt discarded from the extrusion process were examined using a Scanning Electron Microscope (SEM). While the elements content on the as-cast material extrudates and chip-based extrudates were examined by SEM-EDS. The XRD technique was utilised to identify the phase changes in the non-heat treated and heat treated chip-based extrudates produced by the hot extrusion. Analyses obtained from the microstructure examinations were further extended for evaluating and comparing the effects of several factors on the mechanical

and physical properties when varying preheating time and temperature during chips consolidation, die geometry design, operating temperature and extrusion ratio.

3.5 Modelling and Simulation of Extrusion Process

Numerical and experimental validation represents key tools for the optimization of the hot extrusion process with different die geometry and process variables, hence providing different information about the process reliability. FE simulation was used in this study to investigate the effects of preheating temperature on the extrudate quality by predicting damage evolution for billets subjected to different extrusion temperatures, and validated experimentally. The weld strength prediction on the extruded profiles at development stage was accomplished by computing the developed weld strength model in which the deformation variables were retrieved from the results of FE simulation on each physical extrusion process. The mechanical/physical properties of the extrudates were also associated with the amount of stress and strain induced during the FE simulations. Flow chart of the overall procedures in damage evolution prediction and weld strength modelling is shown in Figure 3-10. General FE simulation setup for extrusion process is given in Table 3-7.

Table 3-7: General setup of 3D FE simulation in extrusion process

Parameter Setting	**Component/Part**			
	Billet	**Ram**	**Container**	**Die**
Material	AA6061	H-13 tool steel	H-13 tool steel	H-13 tool steel
Temperature (°C)	400-550	27	300	300
Object type	Plastic	Rigid	Rigid	Rigid
Ram speed (mm/s)	NA	4.4	NA	NA
Number of elements	150000	NA	50000	50000

Primary die displacement (mm)	NA	95	NA	NA
Type	Lagrangian incremental			
Number of simulation steps	100			
Remeshing method	Average of neighbors			
Convergence error limit (velocity)	0.005			
Convergence error limit (force)	0.05			
Solver	Conjugate gradient			
Convection coefficient (N/sec/mm/C)	Constant 0.02			
Heat transfer coefficient (W/m^2)	3000			
Flow stress model	Sellars-Tegart (1972)			

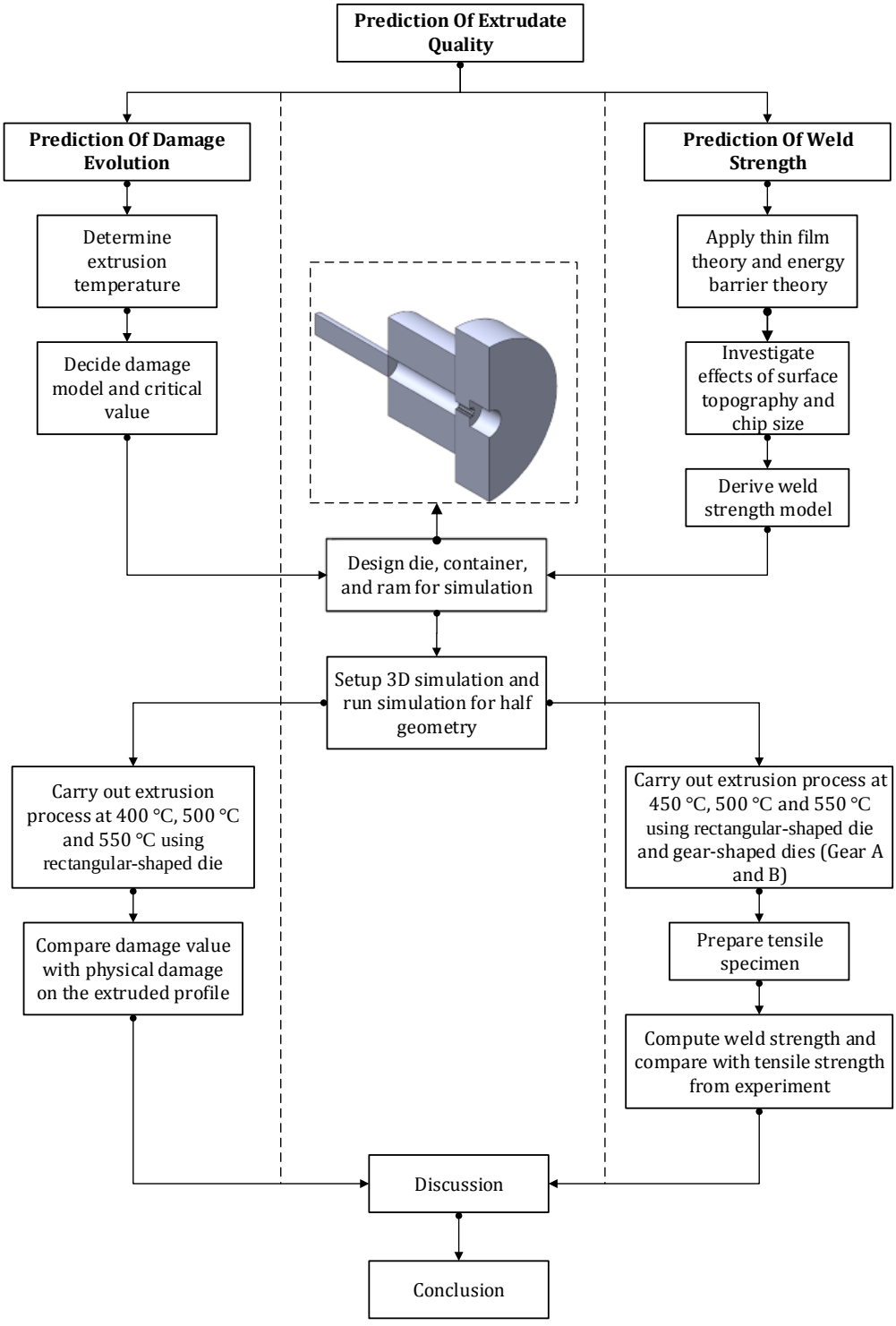

Figure 3-10: Process flow of simulation work in damage prediction and validation process on the developed tensile bond strength model

3.5.1 Finite Element Simulation on Damage Evolution

This section reports the methodology of simulation work for hot extrusion through the flat-face die at different process conditions. Numerical analyses by means of finite element method represent a beneficial way for process optimization. Numerical simulations allow local state variables concerning material temperature, strain, strain-rate, pressure and stress to be manipulated in several damage models for optimizing the extrudate quality in metal forming. The effect of temperature in hot extrusion can be studied from a numerical point of view, through the damage prediction. This study was employed DEFORM^{TM} 3D, one of the most utilized commercial FEM codes for bulk metal forming analysis. Several process parameters such as the amount of pressure, strain, strain-rate, normal contact stress and shear stress are critical to bonding quality among individual chips. All these parameters have been identified responsible for breaking the oxides enveloping the individual chips to enable bonding of the pure metal [36].

The use of a crack damage criterion allows prediction of the surface damage within the chip-based extrudates during hot extrusion. This can ensure that the hot extrusion could produce defect-free chip-based products since development stage. The damage evolution within the chip-based extrudate may affect service life and quality of the finished goods under loading conditions. The crack initiation is assumed to occur when the critical damage value is satisfied within an element and the element fractures. In this work, the normalized Cockcroft and Latham (C & L) fracture criterion was applied to predict the fracture risk within the extruded profile. Similar fracture criterion was used previously [107, 108], and they found that the normalized C & L fracture criterion

was the most accurate in which the cross section in tension test obtained during the experiment agreed with the simulation results. The maximum damage value obtained (max damage value) and the value corresponding to the critical damage of the material (critical damage value) can successfully predict the ductility of the arrow-shaped cracks resulting from molding damage. The maximum value of the damage and destruction is attained when the material is deformed under the maximum tensile stress condition [107]. The following damage criterion was used to predict the initiation and growth of a spherical void of radius R in the case of chip extrusion.

$$C = \int_0^{\bar{\varepsilon}_f} \frac{\sigma_{max}}{\bar{\sigma}} d\bar{\varepsilon} \tag{3-14}$$

where C is the damage index, σ_{max} is maximum tensile stress, $\bar{\varepsilon}_f$ is fracture strain and $\bar{\varepsilon}$ is effective strain. The critical fracture criterion value at rupture, Cc for the aluminum AA6061 is taken from reference [107] because the value was found valid for other aluminium materials according to the authors. The stress-strain relationship of plastic behaviour was derived from Deform 3D library and ref. [109] for temperature range 260-550 °C. The parameter setting assigned for 3D finite element simulations is tabulated in Table 3-8.

Table 3-8: Parameter setting for 3D finite element analysis of damage prediction in extrusion process

Parameter	Value/Type
Billet material	AA6061-T6
Ram, container, & die materials	H-13 tool steel (set as rigid body)
Element type	3D Tetrahedral, 1 point integration
Billet temperature	400°C, 500°C, 550°C
Tools temperature	300°C
Heat transfer coefficient	5 (N/sec/mm/°C)
Ram speed	1.0 mm/s
Friction (billet/container)	Shear type, $\mu = 0.95$ (Adhesion was considered between billet and container since no lubricant was applied)
Friction coefficient (bearing)	Shear type, $\mu = 0.85$ (Minimum lubricant was applied at entrance of bearing land)
Flow stress model	Sellars & Tegart $\sigma_Y = f(\varepsilon, \dot{\varepsilon}, T)$
Fracture criterion	Normalized Cockroft & Latham (Critical value, Dc = 0.455)

3.5.2 Modelling of Weld Strength

Modelling of weld strength was based on the following assumptions:

- A close contact between two chip's surfaces is established by combination of normal stress and shear stress.
- Strain developed during extrusion stretches the materials and the oxide remains unchanged along the interface until the metal is exposed.
- Entrapped air oxidizes some of the exposed metal; however, due to existence of high pressure and temperature, the clean metal will still develop bonding due to diffusion mechanisms although chip contact time with bearing land is limited as proved by the hot press forging.

- The minimum strength recovery after hot extrusion is equal to minimum strength of AA6061 base metal at room temperature once clean metal surfaces are within atomic distances.
- The model presented in the following sub-sections considers plane-strain deformation and a perfectly plastic material.
- The equivalent amount of strain, flow stress, normal contact stress and shear stress affecting the material during the hot extrusion process, all are calculated by the FE software.
- The effect of diffusion mechanisms is considered by adding the diffusion-strengthening model (developed through the hot forging experiment with varying temperature and holding time at constant pressure) with the existing weld strength model.
- The material behaviour was modelled using an inverse hyperbolic sine function as shown in Eq. (3-15) with parameters fitted to stress/strain curve as obtained through the Deform 3D library and ref. [109]. The relationship models plasticity behaviour linking the flow stress with temperature, strain and strain-rate is given as follows:

$$\sigma = f\ (\varepsilon, \dot{\varepsilon}, T) \tag{3-15}$$

3.6 Concluding Remarks

The methodology of using the experimental, mathematical derivation and finite element simulation approaches in this research endeavor is to provide a comprehensive investigation for the study of solid-state recycling via the controllable hot extrusion processes on aluminum alloy AA6061. These approaches enable not only the effects of various factors in plastic deformation process to investigate the solid-state recyclability of aluminium machining chips, but also allows the prediction of strength recovery of the extruded profiles and damage evolution within the extrudate structure when subjected to various operating regimes, chip morphology and die design combination. Summary of the overall research methodology is graphically illustrated in Figure 3-11 and followed by a brief explanation below:

(i) Investigation on homogenization aspect of chip-based billet

Heating for homogenization is very important to allow sufficient amount of heat absorbed and retained by the chip-based billet to facilitate the weld bonds formation. There are no any specific studies devoted to investigate the minimum preheating temperature and preheating time in homogenization treatment that used to further minimise the energy consumption in solid-state recycling, as summarised in Table 2-2. The homogenization related variables were selected without a concrete justification by the numerous researchers. Therefore, the homogenisation treatments at 400 ^{o}C, 450 ^{o}C 500 ^{o}C, and 550 ^{o}C preheating temperature and 1, 2, 3, and 6 hours preheating time are investigated. This is important to analyse their effects towards the distribution of intermetallic particles, microstructure evolution, changes in constituent of particle phases,

and static and dynamic recrystallisations that can lead to a satisfactory extrudate quality. In this set of experiments, the samples are extruded after preheated at the designated conditions as shown in Table 4-2. Finally, the samples are cut and sent for tensile strength evaluations.

(ii) Study of Surface Topography Effect on Weld Strength

Since if the entrapped air within the asperity height of aluminium surfaces presence largely, it may influence the oxide layer formation that can cause poor weld bonds and reduce strength of the solid-state recycled material. An approximately 2.9 nm oxide layer thickness can inhibit bonding [80]. The chips produced in machining contain a different degree of surface irregularity level. Therefore, the effect of surface topography in particularly asperity height to entrap air and oxidize at the chip interfaces needs further clarifications. The hot forging test, analogous to closed-die forging is proposed to undertake this task. This is a controlled forging operation, and it is assumed that the chips flow in xy-plane is constrained and the chips are stretched merely on z-plane due to normal pressure. The normal pressure acts perpendicularly to the surface of chips and the asperities height is expected to collapse, subsequently the surface topography effect towards the bonding propensity can be clearly examined. The deduced findings could provide some fundamentals underlying on the severity level of oxidation effect to the strength recovery of chips. The methodology is further described in Chapter 5.

(iii) Development of Analytical Modelling of Weld Strength

This work covers development of the analytical model to predict tensile bond strength recovery of chip-based extrudates, processed through various die geometries and operating regimes. The effect of diffusion mechanism is included in the new proposed model. A series of hot forging experiments are conducted to develop a diffusion-strengthening model. The finite element simulations are performed to enable the state variables (normal stress, shear stress, strain, etc.) to be retrieved. Then, the state variables are fed to the final model to predict the tensile bond strength recovery. A series of hot extrusion experiments with rectangular and gear geometry dies are carried out to validate the proposed model of tensile bond strength prediction for its accuracy checking. The results of validation are presented in Chapter 6.

(iv) Heat treatment for mechanical properties improvement

Generally, the chip-based products or composites developed through the solid-state recycling experienced low strength compared to the as-cast material. Since this study deploys two dies in gear form, with ERs of 2.16 and 4.68, the extrusion process is considered performed at extremely low ER. The chip-based gear profile extruded at low ER is difficult to get rid of voids, oxide layers, and often experienced poor mechanical properties. To overcome these drawbacks, post-processing of heat treatment for whole gear is recommended and presented

in Chapter 7. The heat treatment process can enhance the metallic materials to the desirable properties. Besides, a complete cycle of direct recycling which begins from the hot extrusion (to crush the oxides layer and actuating diffusion processes) and followed by the heat treatment (to create hard phases) can be implemented successfully, thereby the final product of gear can be made ready for practical application.

Figure 3-11: Flowchart of summary of research methodology

CHAPTER 4 : EFFECTS OF PREHEATING TIME AND TEMPERATURE

This chapter discusses the results of experimental and simulation work pertaining to effects of preheating time and temperature in hot extrusion of direct recycling aluminum AA6061. The threshold values of minimum preheating time and minimum temperature for billet's homogenization that can yield an acceptable extrudate quality will be obtained through this experiment and the results will then be used to guide for setting of upcoming experiments. The experimental work begins with compaction of chips, preheating of billet, and finally extrusion at different billet's temperature through a flat-face die. Extrudates with varying quality have been successfully produced in these trials. Subsequently, the results of pressure, strain and temperature from finite element simulation are presented to correlate with the extrudate quality after the hot extrusion process.

4.1 Experimental Procedure

The procedures for chip preparation including comminution, morphology and size, cleaning method and billet preparation all are briefed in Section 3.1.2. The aluminium AA6061-T6 grade was used for this experiment and the mechanical properties are given in Table 3-3. To observe the influences of temperature and preheating time, the billets were extruded through the designated conditions as shown in Table 4-1. The procedure of hot extrusion was clearly described in Section 3.1.3. The ranges of temperatures and

preheating durations selected were between 400 °C -550 °C and 1-6 hours, respectively. Samples with the corresponding designated heating conditions for extrusion are shown in Table 4-2.

Table 4-1: Parameters setting of hot extrusion process in direct recycling

Parameter	Value/Type
Extrusion die	Flat-face (rectangular)
Extrusion ratio, R	11.22
Billet, Ø (mm)	30
Extrudate size (mm)	6.3 x 10.0
Extrusion speed (mm/s)	1
Container temp. (^oC)	300
Die temp. (^oC)	300
Preheating temp. (^oC)	400, 500, 550
Preheating duration (hour/s)	1, 2, 3 and 6

Table 4-2: Samples' designation for different preheating conditions

Sample Designation	Preheating Temperature (^oC)	Preheating Time (hour/s)
S_1	400	1
S_2	400	2
S_3	400	3
S_4	500	1
S_5	500	2
S_6	500	6
S_7	550	3
S_8	As-received	

4.2 Results and Discussion of Tensile Tests

The mechanical properties of the extrudates were investigated by tensile tests. A series of experimental trials have been carried out through distinct billet temperatures and preheating durations and the results are presented and discussed here. In order to analyse the effect of the temperature variable on chip consolidation, the tensile test samples were fabricated parallel to the extrusion direction according to ASTM-E8 M sub-size [110]. The tensile strength results shown in Figure 4-1 are so sensitive to temperature and exhibit an increasing trend when the temperature is kept in range of 400°C to 550°C. As can be seen from Figure 4-1, Sample 7 that was preheated to 550°C shows the highest tensile strength with 98% relative strength attainment as compared to the as-received material. Nevertheless, the ductility revealed is slightly lower than those extruded at 500°C. The relative tensile strength (UTS) attainment in (%) was measured by comparing the tensile strength of samples with as-received aluminum AA6061 as given in Table 4-3. It is found that increasing the billet's temperature prior to extrusion facilitates the chip welding and has directly impacted the material strength. The optimum ductility can be obtained when the temperature of extrusion is maintained at 500°C.

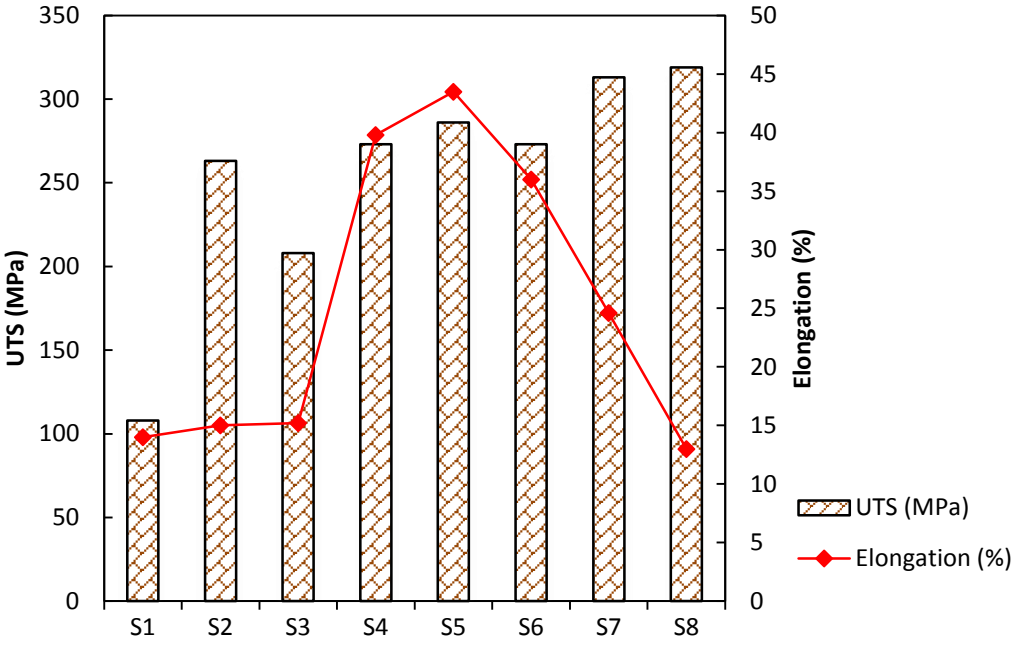

Figure 4-1: Mechanical properties of samples extruded under different process conditions

Table 4-3: Results of tensile tests for all samples

Sample designation	UTS (MPa)	Relative UTS attainment in (%)	Elongation at break (mm)	Elongation (%)
S_1	108	34	3.500	3.500/25x100 = 14.0
S_2	263	82	3.772	3.772/25x100 = 15.0
S_3	208	65	3.800	3.800/25x100 = 15.2
S_4	273	86	9.953	9.953/25x100 = 39.8
S_5	286	90	10.881	10.881/25x100 = 43.5
S_6	273	86	9.000	9.000/25x100 = 36.0
S_7	313	98	6.159	6.159/25x100 = 24.6
S_8 (reference)	319	-	-	13

Higher ductility of the extruded profiles can be attributed to the increased chips flow in all directions and homogenous distribution of the oxide particles. The maximum ductility on Sample 5 with 43.5% elongation was superior to as-received material with only 13%. Prolongation of the preheating time to 6 hours at 500°C results in less influence on the sample's strength and ductility. Increasing temperature to 550°C solely improves the tensile strength, but not the ductility, and similar results were found from Wu and Lela [62, 111]. Furthermore, the worst performance in terms of strength and ductility can be observed in all samples extruded at 400°C with the worst spotted on Sample 1 (S_1), preheated for 1 hour. This could be attributed to the poor welding towards inner regions of all samples due to the restricted atomic diffusion. The results inferred that the extrusion process at a low billet temperature could not consolidate materials efficiently, similar previous observations by Lela and Sherafat [38, 111].

In the case of temperature influence, the strength of the extruded profile is greatly determined by the individual bonding quality of chips including the grain growth strengthening and the diffusion mechanism. The differences in strength and ductility between samples can be related to the differences in observed microstructure. The chip-based billets extruded at higher temperatures would result in more fine equiaxed grains which led to the higher uniform elongation and better tensile strength [38, 40, 112]. The high extrusion temperature combined with a low extrusion speed applied for an instance at samples 4 and 5 have resulted in the matrix aluminium to flow plastically, filling up the pores and voids to promote prolongation of inter-particle diffusions, contributing to stronger bonding between individual chips [34, 113]. The efficiency of the diffusion relies between the amounts of virgin aluminium fraction with those covered by the

oxide layers. The heat applied on the chips reduced the strength and increased the ductility. The localized shear strain increases proportionally with the ductility and therefore more oxide layers are broken down to expose more virgin aluminium. The bonding is significantly enhanced when more virgin aluminium in the compression state. Although the temperature has a significant effect, longer preheating time is deemed unnecessary in recycling by the hot extrusion which against the Gronostajski [9] suggestion for 6 hours duration.

The appearance of samples after tensile tests is given in Figures 4-2 and 4-3. As can be seen in Figure 4-3, sample S_5 exhibited a ductile failure mode with a smooth surface. The samples extruded through 400°C temperature, for an instance depicted in Figure 4-2 (a), shows rough, large cracks, and surface peel-off can be easily encountered within their structures. The failure took place nearby the grip section of the samples, mostly due to the brittle rupture failure. The failure incident was frequently encountered at the weakest point caused by the sudden change in force equilibrium within the reduced section of sample. The occurrence was due to the imperfect bonding amongst the individual chips which directly impacted the mechanical strength of the extrudates at applied billet temperature of 400°C. Applying an extrusion ratio of 11.22 by incorporating a low temperature in this study, it was unable to strengthen the chips. As reported by Guley [61], an extrusion ratio (ER) of 10 applied on the flat-face die did not guarantee sufficient chip bonding unless different dies with the capability to induce high stresses and strains have been replaced and operated at high billet temperatures.

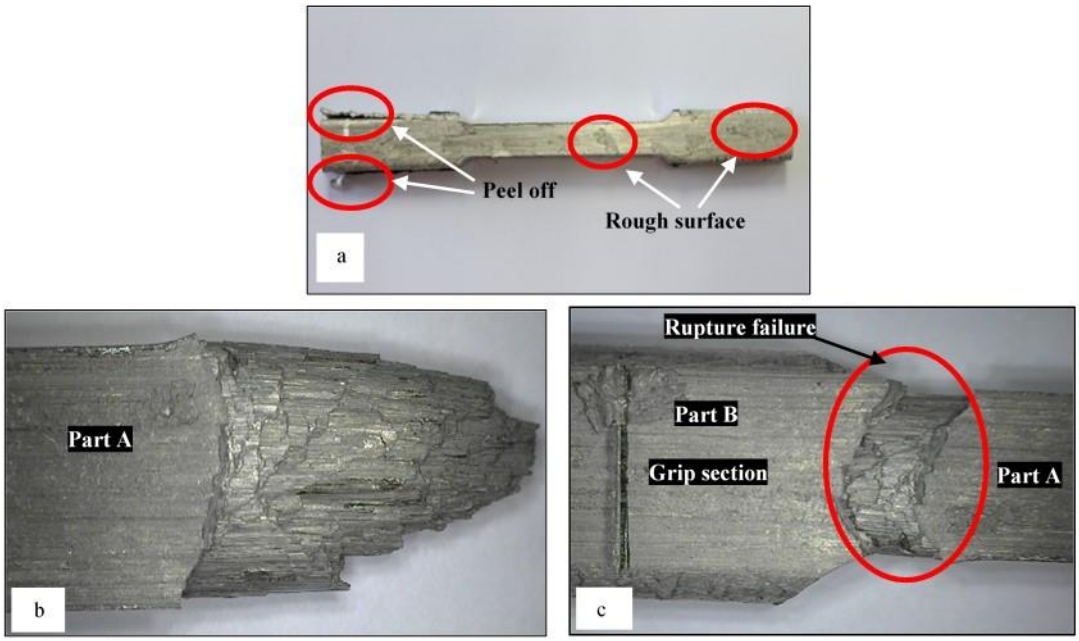

Figure 4-2: Surface defects of samples after extruded at 400°C pre-heated for 2 hours (S_2): (a) Severe damages on tensile profile, (b) Internal brittle rupture failure took place in the sample and (c) Failure occurred at the area of the grip section

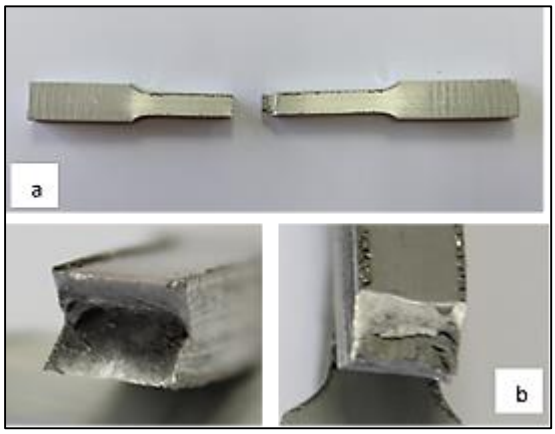

Figure 4-3: Surface appearance of tensile sample of sample 5 (S_5): (a) Smooth surface of tensile profile, (b) Cup-and-cone shape at the fracture area

Fracture surfaces of the recycled samples at low temperatures exhibited ridges instead of equiaxed dimples as shown in Figure 4-4. This showed that the fracture failure was the main mechanism encountered in this sample. In this circumstances, the brittle fracture has propagated through the inter-granular manner caused by embrittlement of the chip boundary region as a result of the detrimental segregated chips existence during the diffusion stage. The other samples extruded at the 500 °C and 550 °C with varying preheating time as given in Figures 4-5 and 4-6 show appearance of dimples and cleavage planes, revealing that the recycled samples might have mixed fracture mechanism consisting of microvoid and cleavage fracture [62]. Also, the samples in Figure 4-5 (S_5) shows grain boundary cracks while the sample in Figure 4-6 (S_7) reveals microcracks at the fracture surfaces. Conical equiaxed dimples and no microcracks were observed at the fracture surface of the reference sample as shown in Figure 4-7, indicating the ductile mode failure.

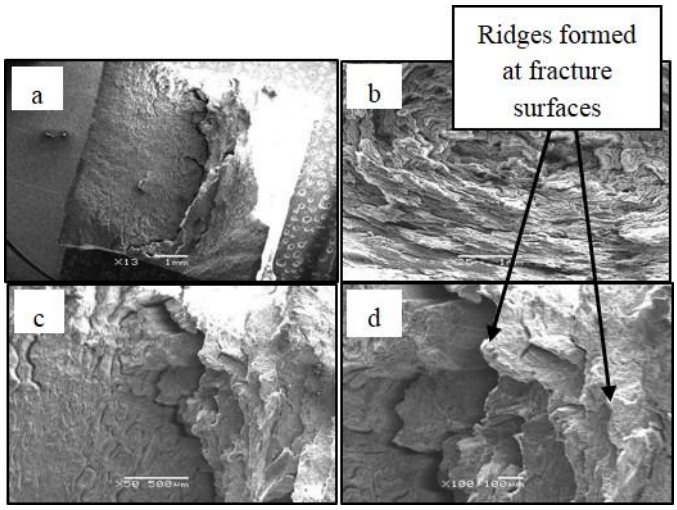

Figure 4-4: SEM micrographs showing the fracture surface of the tensile sample (billet temperature = 400°C, preheating time = 2 hours) extruded via flat-face die (S_2): (a) a broad view of brittle fracture surface; (b) the lamellar topography on fracture surface, 25x, (c) observed ridges emanated from the center, 50x and (d) 100x

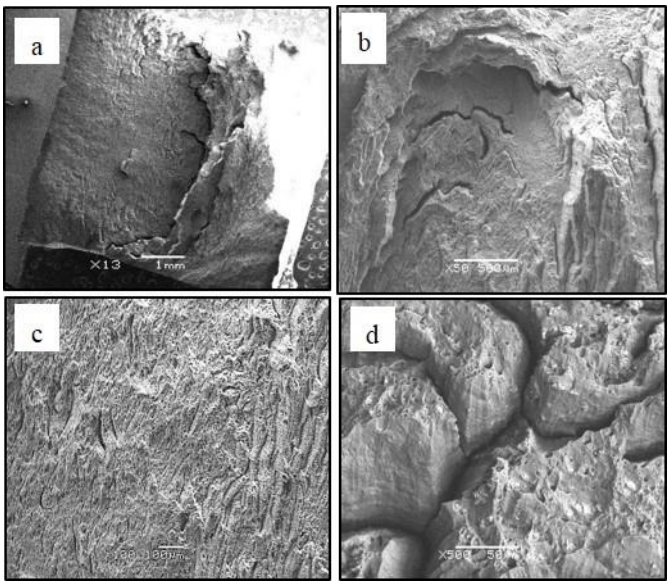

Figure 4-5: SEM micrographs showing the fracture surface of the tensile sample for billet heated at 500°C for 2 hours, extruded through the flat-face die (S_5): (a) an overview of the fracture surface; (b) the tears and cracks topography on the fracture surface, 50x, (c) 100x and (d) cracks of chips boundary on the outer fracture surface, 500x

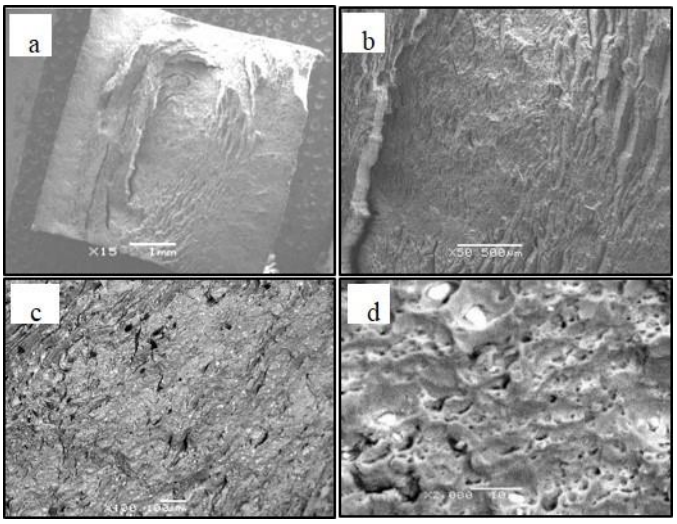

Figure 4-6: SEM micrographs showing the fracture surface of the tensile sample (billet temperature = 550°C, preheating time = 3 hours) extruded via flat-face die (S_7): (a) an overview of the fracture surface; (b) the small tears and cracks topography on the fracture surface, 50x, (c) 100x and, (d) fine equiaxed dimples, 2000x

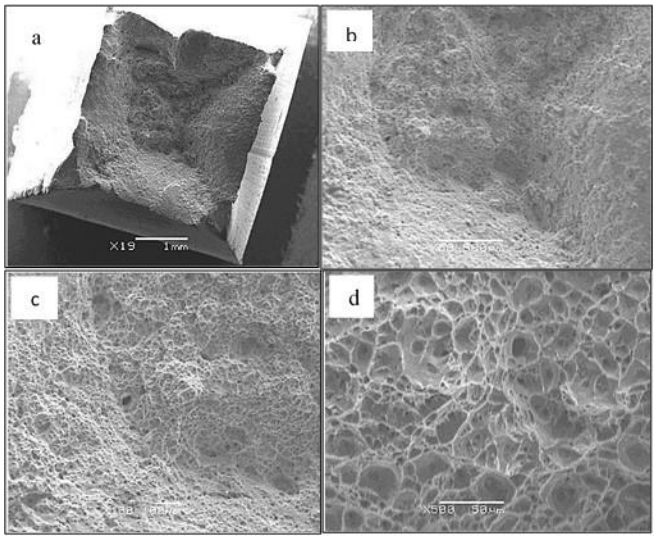

Figure 4-7: SEM micrographs showing the fracture surface of the reference sample (as-received), (billet temperature = 550°C, preheating time = 3 hours) extruded via flat-face die: (a) an overview of the fracture surface; (b) the fine topography on the fracture surface, 50x, (c) conical equiaxed dimples observed, 100x (d) 500x

4.3 Results and Analysis of Microhardness

Microhardness tests were carried out at an applied load of 0.9807 N and a holding time of 10s at the room temperature, following DIN EN ISO 6507-1:2005 standards. Different points were considered to observe the uniformity of the weld region during the microhardness measurement as indicated by the top legend in Figure 4-8 (a). The microhardness values presented here are taken as an average of three surface measurements (top, center and bottom), on the transverse direction of the extruded samples. Even though the effect of measurement location on the microhardness was relatively small, the trend could be used to explain the hardness distribution throughout the sample's cross-section to relate with the welding mechanism dominated in each sample. By considering the effect of temperature and preheating time, the material

recycled at a lower extrusion temperature is found to be harder than recycled at a high temperature. As can be seen in Figure 4-8 (a), Sample 2 reveals the highest hardness which corresponds to its low ductility behaviour as shown in Figure 4-1. The materials with high hardness would normally have high yield strength, but in return experienced a lack of plasticity behaviour [41]. At high temperatures between 500-550°C, most samples can be sufficiently consolidated, nevertheless they tend to exhibit a low hardness. The analysis of results also revealed that the hardness of samples is less likely to be influenced by the high extrusion temperature. This could be due to the fact that the measured regions full with the grains of enlarged size when operated at high temperatures.

The hardness of samples heated at a constant temperature (e.g.: 500°C) is noticeably insensitive to the duration of preheating prior to extrusion. The effect of temperature seems to be more obvious on the material hardness rather than the preheating duration (for billet homogenization). Extruding chip-based billets at lower temperatures is found to induce high amount of normal stress and shear strain at the region adjacent to the die wall to form a hard skin on extrudates as shown in Figure 4-9 (a). The thickness was varied by varying the preheating time as observed on the other samples. On the hard skin layer, the plastic flow of the chips is restricted to a relatively small zone beneath the indenter resulting in higher hardness. As can be observed in Figure 4-9 (a), chip welding is poor on the layers towards the center region of the extrudate's cross-section. The poor bonding on the inner region of samples at low extrusion temperatures causes the chip flow retarded. The sensitivity of the hardness over temperature rather than the preheating time could be due to the atomic diffusion, the main principle of the chip

bonding which was significantly influenced by the amount of heat applied. Also, the results of the microhardness measurements showed no significant difference between hardness at the seam weld and regions away from the seam as seen in Figure 4-8 (b), similarly obtained by Guley, 2013 [41]. The hardness will increase when a low temperature is used during preheating of billet while prolongation in preheating time for homogenization has caused no improvement in hardness. Kondoh [53] also commented that by prolonging thermal explosion in preheating of forged AZ91D alloys, the micro-hardness of the forged AZ91D alloys tend to decrease.

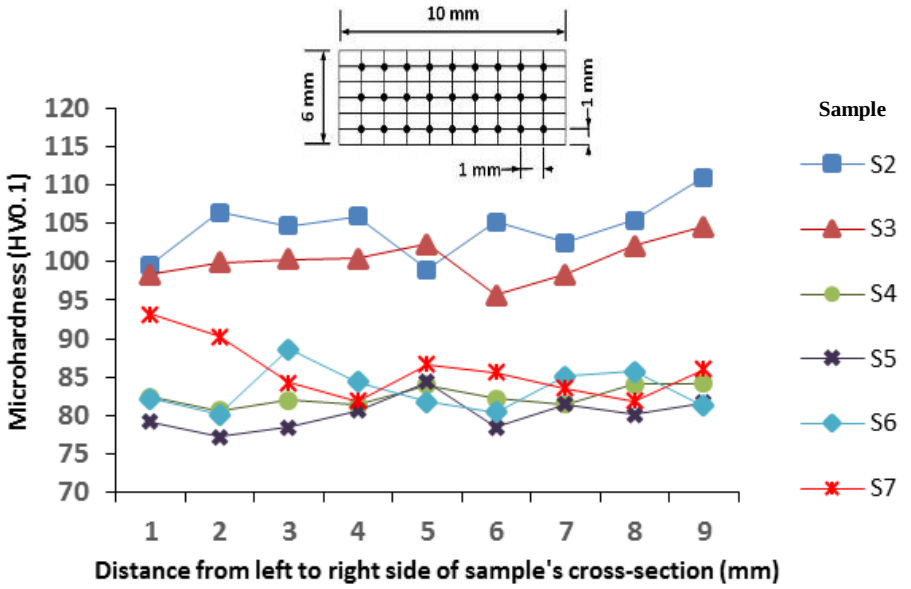

(a)

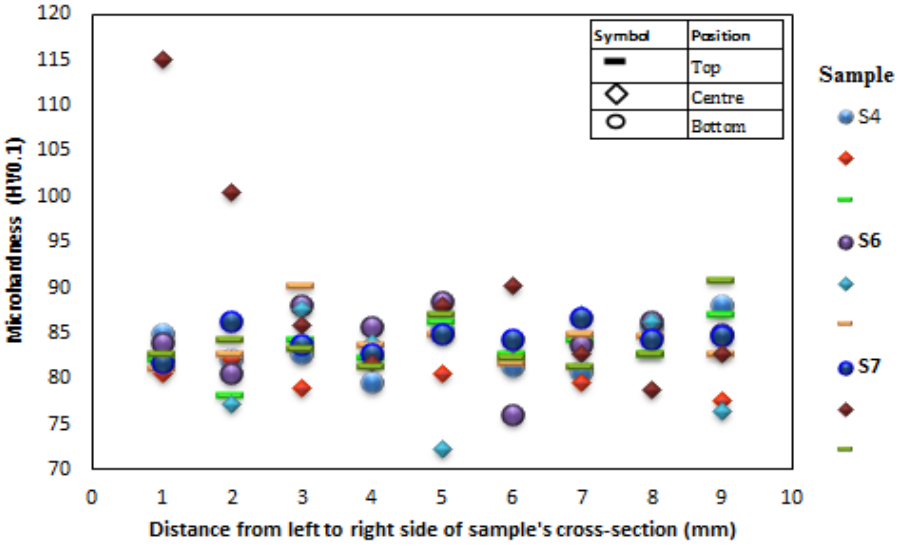

(b)

Figure 4-8: Microhardness values (a) measured as an average at three different planes on the sample's cross-section along the transverse extrusion direction, (b) measured at three different planes on the selected samples

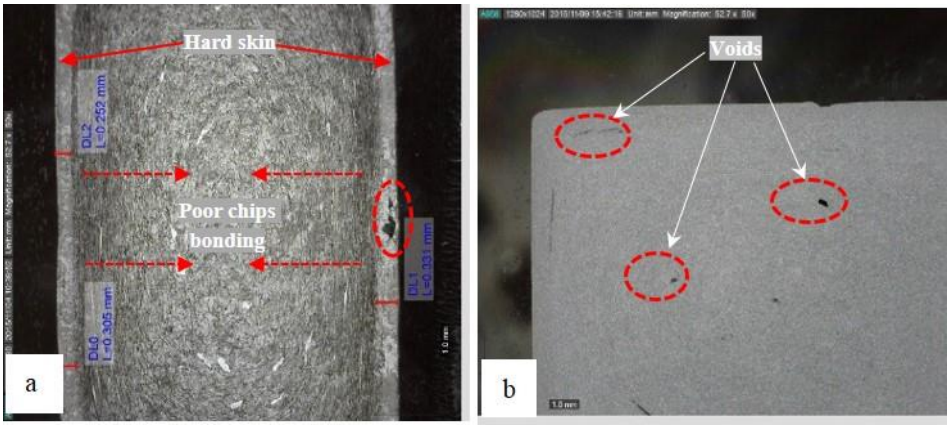

Figure 4-9: Optical micrographs showing the cross-section of the extruded profiles in the transverse extrusion direction (50x magnification): (a) Preheated at 400°C for 2 hrs (S_2), (b) Preheated at 500°C for 1 hr (S_4)

4.4 Results and Discussion of Density

Density balance using Archimedes' water immersion principle (in distilled water) was used to carry out density measurement of as-received and extruded profiles. As described above, three temperature settings were used in the preheating step to produce samples of a rectangular cross-section. The samples were cut to approximately 1 mm length at the transverse direction for density measurement. The results shown in Figure 4-10 contain error bars which represent the standard error of measurement. Each measured density noticeably lies within the small error range regardless of the operating temperatures. This shows that the measurement of density has high repeatability and accuracy. The density of the samples extruded at different preheating temperatures and times shows reduced in trend with a dramatic drop from 400°C to 550°C as shown in Figure 4-10. Samples 4, 5, and 6 are found being equal in relative density of 0.98 to as-cast material. The drastic decrease in density indicates that the extrudates are still containing some voids. The drastic decrease in density after preheating just over 500°C indeed envisions the emergence of voids in each sample's structure. Samples extruded at 400°C exhibited denser profiles than those extruded at higher temperatures. The relative densities obtained were in range of 1-1.02, exceeding that of the as-received material.

The fracture surface of each tensile specimen was inspected at the macroscopic level. A huge region of dense chips can be easily observed across the surface, however, a lot of chips exhibit poor bonding as shown in Figure 4-4. A large stress generated at a lower temperature range eliminates the voids, but the weld bonds of chips are still insufficiently developed. At higher extrusion temperatures, the strength recovery of

samples was substantially higher than the samples with low temperatures, nevertheless, they are particularly susceptible to low density characteristic. This could be due to the remaining residual voids and cracks existence on the respective samples as shown in Figure 4-9 (b).

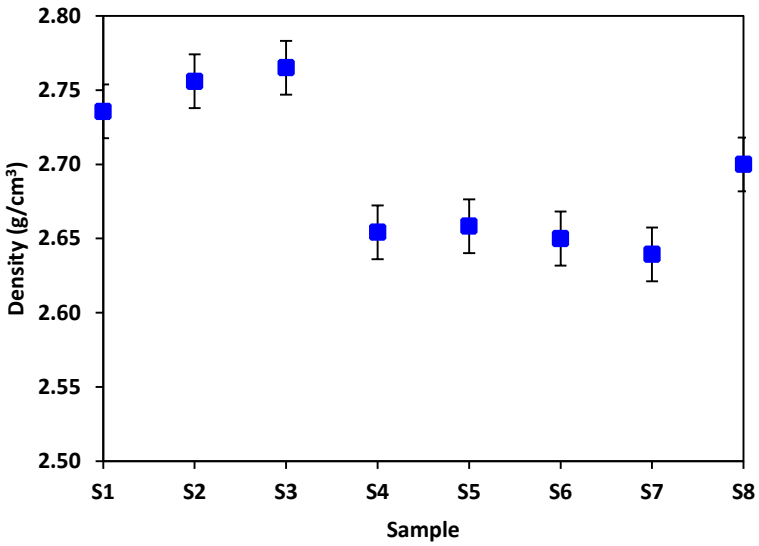

Figure 4-10: Measured density of samples

4.5 Analysis of Microstructure

The samples for microstructure investigation through optical microscope (LOM) were mechanically ground using SiC papers of grits 240, 600, and 1200 for 180 s each in wet condition and polished for 600 s with colloidal silica. Then, the polished samples were electrolytically etched using Barker's reagent with voltage setting of U = 12 V dc for 120 s. This would reveal the grain size and grain boundary under the crossed polarized illumination to allow inspection of physical and chemical inhomogeneities. The average grain size was measured using the linear intercept method in accordance with ASTM E112-13 (2014) standards [11]. The analyses were focusing on the evaluation

and comparison of the microstructures evolution when varying the billet temperature, and preheating time. Although all the samples were subjected to microstructure investigation, just a few selected images are presented in the following discussions.

As can be seen from the optical images shown in Figure 4-11 (a), the sample extruded at the temperature setting of 400°C exhibited relatively small chip boundaries and grain sizes. No visible cracks or voids can be observed in the extruded profiles. On the other hand, the hot extruded materials at high temperatures with different homogenization times from the identical chips as depicted in Figure 4-11 (b), (c) and (d) are free from any observable cracks on the selected areas. The initial form of chips were transformed into the non-uniform unrecognized shapes. Smooth boundary lines and no discontinuity have been observed on the chip interfaces, but the grain size is slightly larger within the grain boundary regions compared to samples pre-heated at 400°C. The corresponding optical images in samples pre-heated at 500 °C and 550 °C reveal that the samples contained a very dense microstructure and the existence of voids were very difficult to be observed. It was also found that the dimension of periphery course grain (PCG) zone increases with increasing preheating temperature for homogenization. This finding can be related with Haase's [11] work where he found the dimension of the PCG zone increases for every die set with increasing temperature. It is strongly supported by the results of grain size measurement as shown in Table 4-4.

(a) Temperature: 400° C, Duration: 1 hour (S_1)

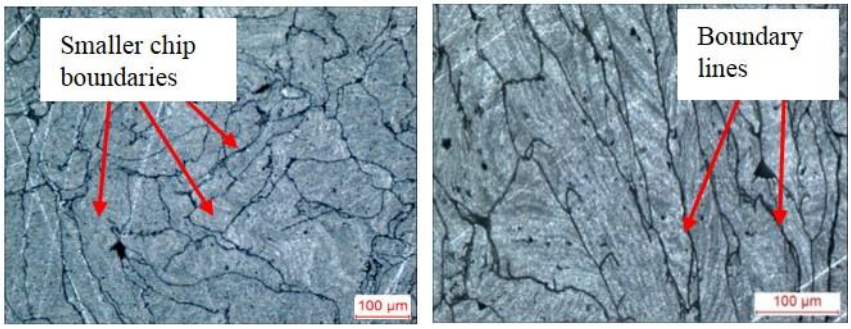

100x 200x

(b) Temperature: 500° C, Duration: 1 hour (S_4)

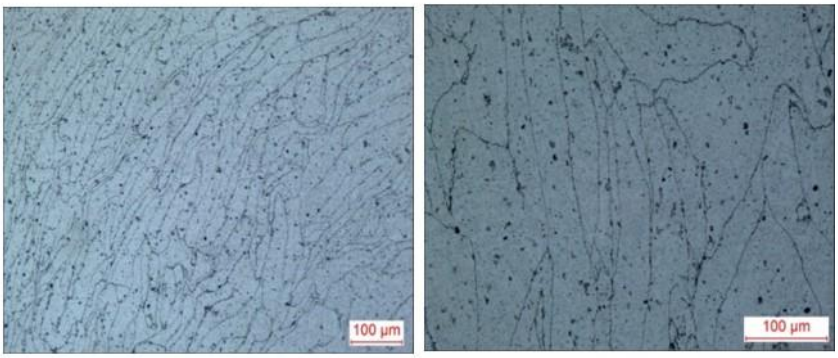

100x 200x

(c) Temperature: 500° C, Duration: 2 hours (S_5)

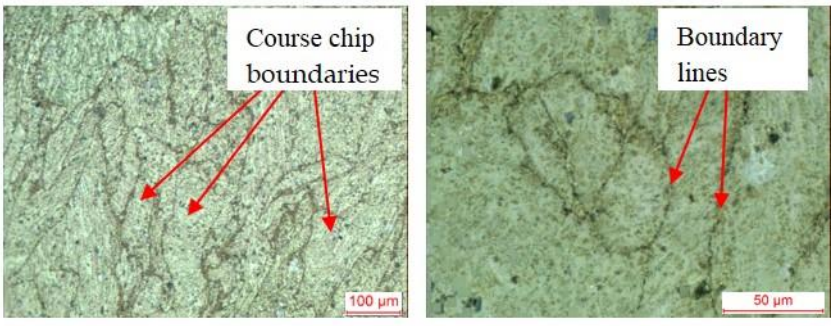

100x 500x

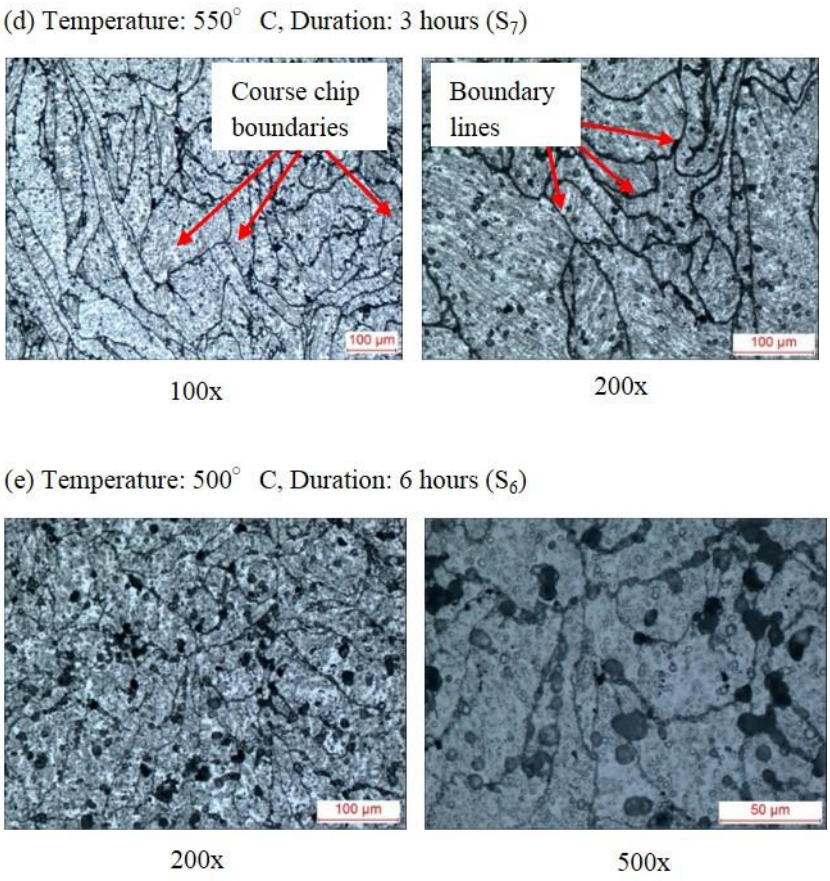

Figure 4-11: Optical micrograph of the samples extruded from the chip-based billets at different temperatures and homogenization times: (a) 400°C: 1 hrs (S_1), (b) 500°C: 1 hrs (S_4), (c) 500°C: 2 hrs (S_5), (d) 500°C: 6 hrs (S_6), and (e) 550°C: 3 hrs (S_7)

Table 4-4: Results of grain size measurement

Sample	Preheating condition	G No.	Average Dia. (μm)
S_1	400°C: 1hr	7.59	25.94
S_2	400°C: 2hrs	7.73	24.77
S_3	400°C: 3hrs	7.32	28.54
S_4	500°C: 1hr	7.25	29.25
S_5	500°C: 2hrs	6.42	43.76
S_6	500C: 6hrs	4.73	69.50
S_7	550C: 3hrs	5.76	49.32

4.6 Finite Element Simulation of Temperature Effect

This section presents results of simulation of hot extrusion through the flat-face die at different process conditions. The selected parameter setting for the 3D finite element simulations is described in Section 3.5.1. The accuracy of simulations was checked and details are presented in Section 6.7.5 and the tooling setup for the simulation work is presented in Figure 6-8 (Section 6.7.5).

4.6.1 Temperature Effect of Damage Evolution

Figures 4-12 and 4-13 show the distribution of normalized Cockroft and Latham damage evolution within the extrudate structures, simulated at 400°C and 500°C preheating temperature. The damage here can be interpreted as surface cracks, surface peel-off and rough surface appearance or combination between them. From the results Figure 4-13, it can be seen that the maximum damage occurs on the billet extruded at

400°C. This is in line with the experimental observations where severe defects were obviously encountered at the surface of the extruded profile as shown in Figure 4-15. The damage for billet pre-heated at 500°C is almost negligible as shown in Figure 4-14 and the simulation results in Figure 4-12 support this finding. The damage value observed is considerably lower than that of the billet extruded at 400°C. The trend provided by the simulation results is very useful to predict the extrudates quality when new operating regimes or dies were to be tested.

Results in Figure 4-13 show that the normalized Cockroft and Latham damage criterion applied was capable of predicting the frequency of surface cracks emergence fairly to the experimental results as indicated by Spots 1 and 2. By comparing the location where the surface crack emerged, the simulation results provide a satisfied trends with the experimental results as shown in Figure 4-15. The cracks on the extrudate appear when the damage value exceeds a critical value of Dc.

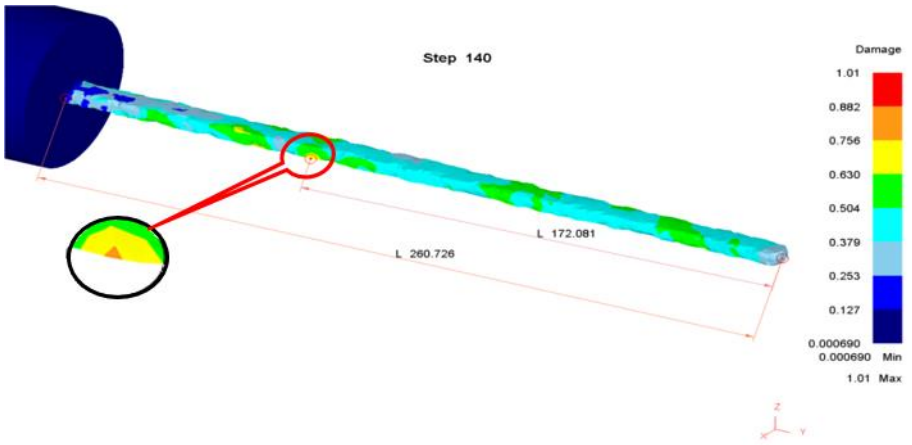

Figure 4-12: Damage value when hot extruded at 500°C billet temperature (All dimensions in mm)

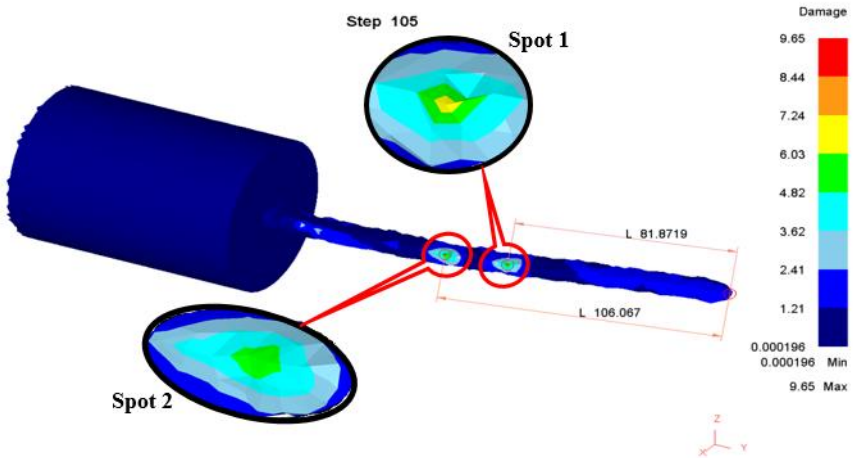

Figure 4-13: Predicted surface damage in hot extrusion at 400°C (All dimensions in mm)

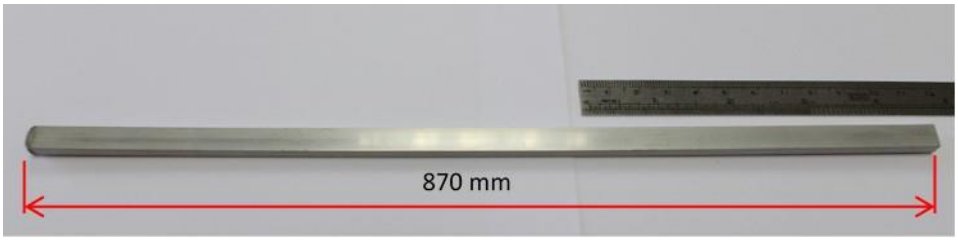

Figure 4-14: Superior quality of extrudate obtained at 500°C

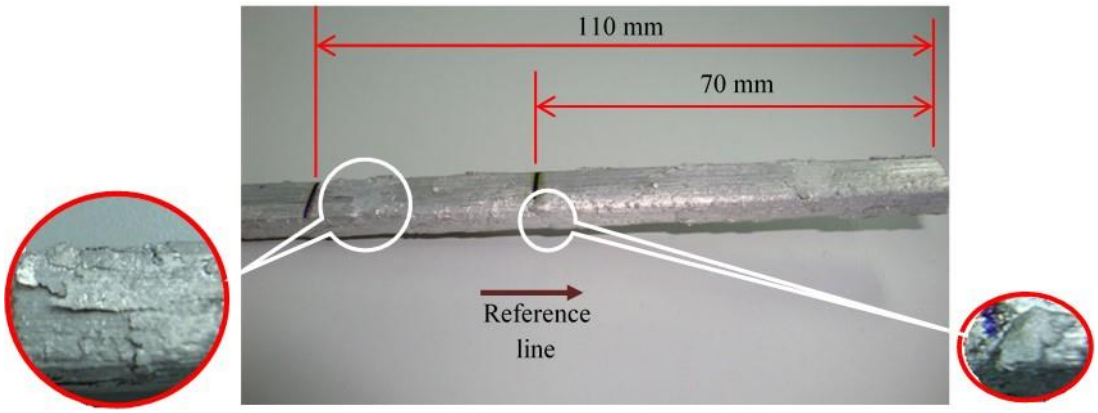

Figure 4-15: Surface cracks and peel-off appear after extrusion at 400 °C

The damage values at the predicted spots are higher than the other areas. The sample extruded at 400°C also exhibited warping at the center: bending upwards to the right side throughout the length of the sample. This can be seen in Figure 4-17 from the top and front views. The simulation results in Figure 4-16 indicate that the shape of the warpage extrudate can also be predicted fairly by the damage criterion via finite element simulations. To sum up, the surface damage on the chip-based extrudate has to be prevented, and possibly can be controlled by setting the temperature at high level. On the other hand, the external appearance of the extruded profiles can be used to attribute to the bonding strength of the individual chips.

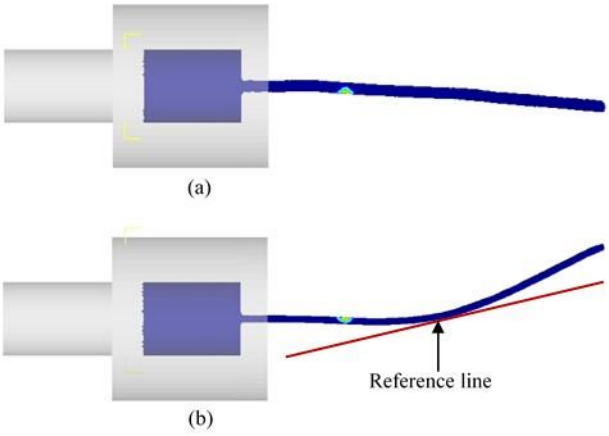

Figure 4-16: Warping on extrudate, predicted by finite element simulations, extruded at 400°C billet temperature (a) top view, (b) front view

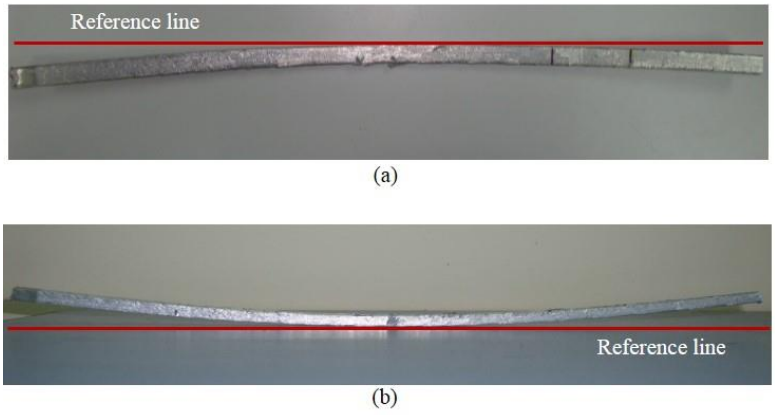

Figure 4-17: Warping encountered on the extrudate (billet temperature = 400°C) (a) top view, (b) front view

4.7 Concluding Remarks

In conclusion, it is found that the billet temperature and preheating duration resulted in a significant effect on the mechanical properties of chip-based extrudates. The highest ductility and tensile strength obtained were 43.5% (on sample S_5) and 98% (on sample S_7), respectively. The presence of high strain as the billet temperature increases in the hot extrusion process enhances the diffusivity among virgin chips. The observed scenario was supported by both results from experiment and numerical simulation. The experimental results show that higher mechanical strength and ductility of the extrudates are possible at 500°C while results from numerical simulation proved that the damage-free extrudates can be realized at higher temperatures. An efficient heating of the chip-based billet improves the inter-particle chips diffusion substantially.

In addition, if the preheating is extended to slightly longer, complete homogenisation on a chip-based billet can be achieved. Furthermore, a significant force can be also reduced at higher extrusion temperatures which can lead to energy-savings. Therefore, a sufficient homogenisation that can result in an extrudate with a structurally stable in the case of extrusion ratio is equal or below than 11.22 can be possibly obtained at a temperature is greater than 400°C and minimum preheating time of 2 hours. The frequency of cracks emergence and warpage formation on the extrudate structures are fairly well predicted by the numerical simulations, implying that the damage criterion applied (normalized Cockroft and Latham) yields an acceptable agreement between the numerical and experimental results. Monitoring the crack emergence and warping on the chip-based extrudate beforehand is a useful way to optimise and reduce the cost of experimental trials and quality issues before a physical die is built. The minimum

preheat temperature and time should be maintained at the recommend settings to achieve an acceptable condition of the intended extrudate quality. Therefore, the above enumerated parameter setting of preheat temperature and time should be followed for setting of the upcoming experiments in Chapters 5 and 6 to ensure a desired extrudate quality can been obtained.

CHAPTER 5 : SURFACE TOPOGRAPHY EFFECT ON WELD STRENGTH

This chapter presents the effect of chip morphology, in particular, relating to chip topography and surface area on the weld strength of aluminium chips in solid-state recycling. The influences of these factors were compared with the influence of temperature and pressure. Full factorial experimental design with center point analysis was adopted to rank the factor effects. A total of 11 runs were conducted with 3 factors and 3 center points. The chips of AA6061 were cold compacted at 10 tonnes, subsequently hot forged through a dog bone shape-die at different operating regimes. The elastic and plastic behaviours and ultimate tensile strength of the hot-pressed samples were analyzed and compared.

In solid-state recycling, chip morphology-related parameters such as size fraction, surface topography, and geometry are important factors in resulting final bond strength. The size fraction of chips plays a crucial factor to control oxide contaminants while the oxygen concentration is known proportional to the total surface area of chip. Recent work by Cooper [80] in developing a general model for bonds strength on aluminium cold welding, has included the effect of entrapped air within the asperity tips of aluminium surface on the bonds strength. A chip interface with the presence of a large amount of the entrapped air within the asperity height influences the severity of oxide layer formation. It causes poor weld bond and strength of solid-state recycled aluminium. If the thickness of the oxidize layers reached to 2.9 nm depth (ten

aluminium atom spacings), this would prevent inter-atomic forces creating a bond [93]. Since that 2.9 nm thick oxidized layer can inhibit bonding, a study on the relationship between asperity height and propensity of the surface to oxidize in direct chip recycling becomes important and needs further investigations.

Since there are no specific experimental studies reporting the influence of chip's surface roughness on the weld strength, study on this aspect is hoped to clarify the correlation between the weld strength and surface topography in solid-state recycling of chips. Analysing deforming parameters together with chip morphology can provide an insight into which factors are very crucial to mechanical performance of the recycled chips and the results can be further used in the development of mathematical model for tensile bond strength prediction.

5.1 Experimental Setup

Direct hot forging was the principal operation of the experiment. Method of preparing the chips is briefed in Section 3.1.2. The aluminium blocks were machined with a different parameter setting to produce three different chip morphologies as shown in Table 5-1. The size of each chip type was examined by a tool makers measuring microscope equipped with a digital Nikon MM-60 camera, while the roughness measurement was carried out by a Confocal Imaging Profiler. The total surface area of chip was estimated using Eq. (3-1) in Section 3.1.2. The corresponding geometry of the chips with their surface topography is presented in Figure 5-2.

In order to analyse the effect of chip's surface topography on the weld strength, three different chip sizes were used: small, medium and large with distinct surface roughness values measured by the Confocal Imaging Profiler and represented by the roughness average as shown in Table 5-1. Surface roughness most commonly refers to the variations in the height of the surface relative to a reference plane as shown in Figure 5-1. It is measured either along a single line profile or along a set of parallel line profiles. In this study, the arithmetic mean of the absolute values of vertical deviation from the mean line through the profile, (*Ra*) was applied. This *Ra* is an official standard in most industrialized countries and can be calculated using Eqs. (5-1) and (5-2) [114]. By using *Ra*, an estimation of the entrapped air volume in a single 'valley' (per unit depth) becomes possible.

$$R_a = CLA = AA = \frac{1}{L}\int_0^L |z - m|\, dx \tag{5-1}$$

$$m = \frac{1}{L}\int_0^L z\, dx \tag{5-2}$$

where, z is profile height, m is mean line and L is the sampling length of the profile (profile length).

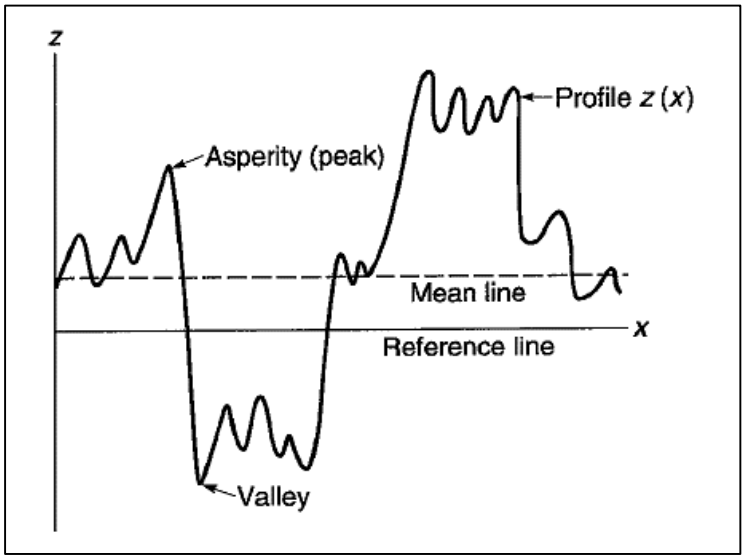

Figure 5-1: Schematic of a surface profile z (x) [114]

The operating temperatures were set at 400 ^{o}C, 450 ^{o}C, 500 ^{o}C while pressures were set at 20, 30, 40 tonnes, respectively. The importance of incorporating all three parameters was inspired by the fact that each has a significant contribution to the strength recovery of the solid-state recycled chips. The parameters will be ranked according to their effect score in factorial design analysis. All experiments were carried out according to the experimental plan as described in the next sub-topic. Detailed procedure describing the method of hot forging experiment is presented in Section 3.1.4. The tensile test of each sample was carried out according to the procedure briefed in Section 3.2.

Table 5-1: Morphology of milling chips used in the experiment

Chip notation	**Type of chip**	**Chip morphology**		
		Roughness average (µm)	**Geometry size (mm)** *l* x *w* x *t*	**Surface area (mm^2)**
S	Small	2.301	≈ 3.100 x 1.097 x 0.091	24.43
M	Medium	3.558	≈ 5.418 x 2.520 x 0.083	25.26
L	Large	2.850	≈ 5.228 x 4.0423 x 0.147	14.48

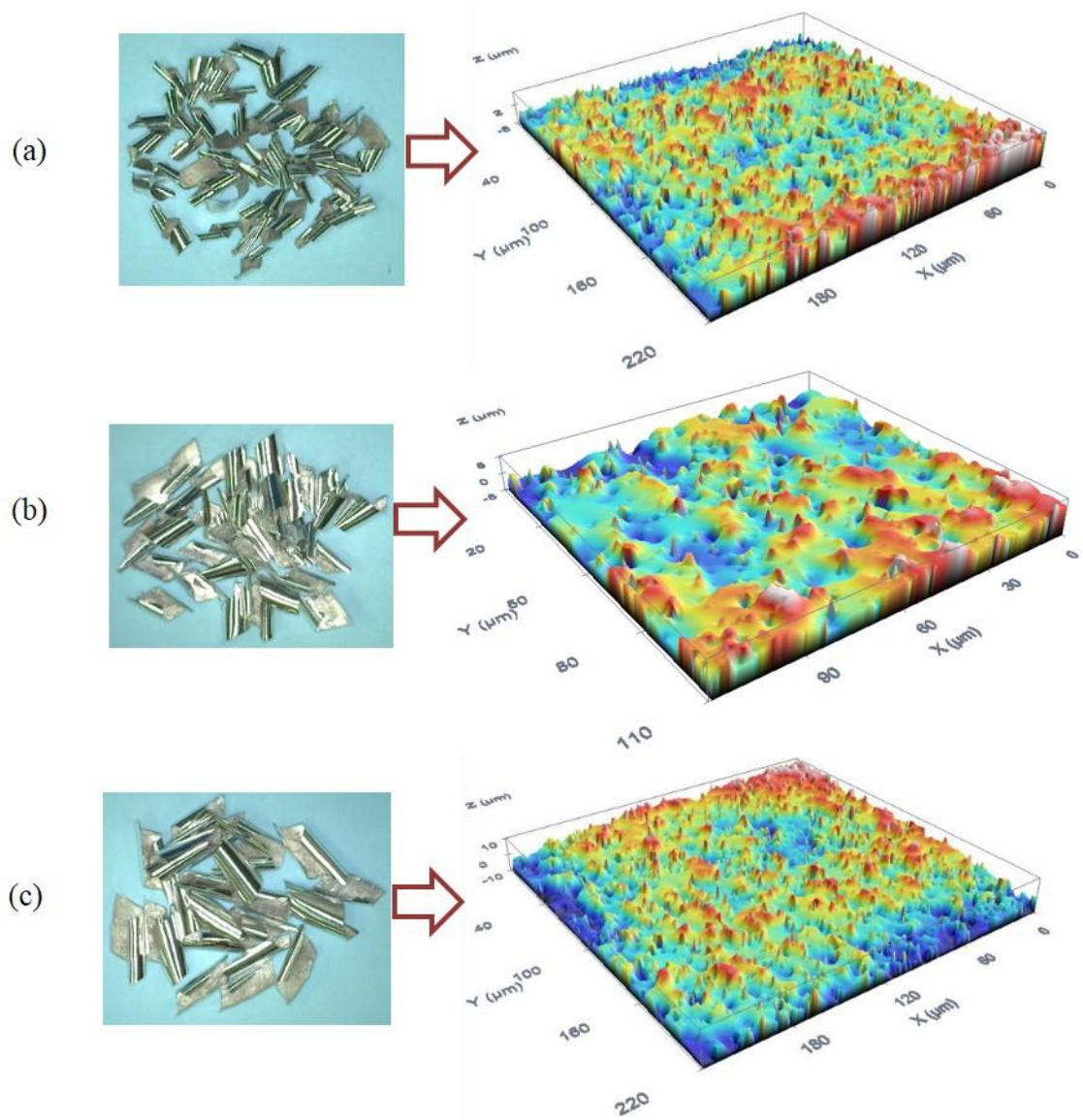

Figure 5-2: Geometry and measured surface topography of chips: (a) Small size, (b) Medium size and (c) Large size

5.2 Experimental Design

Experimental runs based on the 2^3 full factorial design were performed to study the effects of three process parameters previously identified. Three center points were included in the design to test the curvature effect of the model and the interactions among parameters were also considered. The design scheme is listed in Table 5-2. Only single run was implemented in each corner and a total of 11 runs were involved. Details of the experimental run are given in Table 5-3. The parameter of roughness average was remained in uncoded form to simplify the analysis. Response in this study was tensile strength of the fabricated samples. Analysis of variance (ANOVA) was applied to rank the main effects and to analyze the interactions among the input parameters. The DOE results can suggest an insight into further experimental direction for process optimization.

Table 5-2: Design scheme of process parameters and their levels

Factor symbol	**Parameter**	**Levels**		
		Low (−1)	Center (0)	High (+1)
T	Temperature, (°C)	450	500	550
P	Pressure, (Bar)	20	30	40
Ra	Roughness average, (μm)	2.301 (S)	2.850 (L)	3.558 (M)

5.3 Results and Discussions

A total of eleven runs were carried out according to the full factorial design with three center points. The overall results of the experiments are presented in Table 5-3. To complete one experiment, it took nearly 4 hours from setup. Due to limited time and resources, a single replicate of a 2^k design was utilized in this experiment. For one replicate design, no any internal estimate of error can be calculated. Therefore, all high-order interactions are neglected. Then, the mean squares of the omitted factors are combined to estimate the error. Realising the obvious risk of fitting a model to noise when conducting an experiment that has only one run at each test combination, the variability test of response was conducted on the center runs [104]. Using Eq. (5-3), the calculated standard deviation is 16 and the resulting R^2 is 0.0006. The calculated standard deviation and R^2 are small, thus the results are acceptable. The trend shows that whenever high temperature and high pressure are set, the resulting strengths improved considerably regardless of the root mean square value of the asperity height (roughness average). The discussions are broken into two parts for assisting the clarifications on ANOVA of the DOE and the stress-strain relationship of each sample.

$$S^2 = \frac{\sum_{i=1}^{n} (y_i - \bar{y})^2}{n - 1} \qquad (5\text{-}3)$$

where, y_i is individual observation, $\bar{y}$ is average and n is number of observation.

5.3.1 Analysis of ANOVA Results

The final ANOVA table for tensile strength after removing insignificant factor is given in Table 5-4. Formulas, as given in Section 3.1.5, are used to calculate the ANOVA. As identified by the ANOVA analysis, the significant terms connected with tensile strength recovery in direct hot forging of aluminium AA6061 are temperature, interactions of temperature-pressure, temperature-roughness average, and temperature-pressure-roughness average, all indicated by $p < 0.05$. The preliminary ANOVA results of the first screening resulted in interaction of pressure-roughness average, which was insignificant, and this made it excluded for further analysis. According to the main effect values as given in Table 5-5, the most influential factors towards the strength attainment is temperature and followed by the interaction between temperature and pressure.

Majority of samples pressed at the lowest temperature showed low strength regardless of the pressure levels utilized. The chips are significantly strengthened with the presence of high temperature. High amount of heat helps to increase the plasticity of the material which subsequently enhanced the consolidation. Added to this, it promotes particle precipitation and higher diffusion rate which realizes excellent interfacial bonding among chips that in turn reduces voids as well [34, 38, 58]. The pressure also contributes to better chip consolidation [23]. The factors influencing the strength of the hot pressed chips can be ranked as shown in Table 5-5, determined by considering the main effect values of the corresponding factors.

Table 5-3: Results of tensile strength of each experimental run

Sample Designation	Std. Run	Input Variables						
		Coded Value			Uncoded Value			
		T	*P*	*Ra*	Temp. (°C)	Press. (Bar)	Roughness ave. (μm)	Tensile Strength, *TS* (MPa)
SO1	1	-1	-1	-1	400	20	-1	3.72
SO2	2	1	-1	-1	500	20	-1	138.98
SO3	3	-1	1	-1	400	40	-1	22.51
SO4	4	1	1	-1	500	40	-1	158.40
SO5	5	-1	-1	1	400	20	1	104.30
SO6	6	1	-1	1	500	20	1	76.02
SO7	7	-1	1	1	400	40	1	13.62
SO8	8	1	1	1	500	40	1	181.00
SO9	9	0	0	0	450	30	0	121.32
SO10	10	0	0	0	450	30	0	93.86
SO11	11	0	0	0	450	30	0	122.08

Table 5-4: ANOVA results of tensile strength (after backward elimination)

Source	Sum of squares	Degrees of freedom	Mean square	*f*-Value	P-value
T	21038.1	1	21038.1	107.25	0.002
P	344.7	1	344.7	1.76	0.277
Ra	329.3	1	329.3	1.68	0.286
T*P	4816.2	1	4816.2	24.55	0.016
T*Ra	2179.7	1	2179.7	11.11	0.045
T*P*Ra	4754.6	1	4754.6	24.24	0.016
Curvature	1374.7	1	1374.7	7.01	0.077
Error	588.5	3	196.2		
Lack-of-Fit	71.5	1	71.5	0.28	0.652
Total	35425.8	10			

Standard deviation = 14.0055
R^2 = 0.9834
R^2 adjusted = 0.9446
Predicted R^2 = 0.8381
Predicted residual error of sum of squares (PRESS) = 5736.75

Table 5-5: Influencial factors ranked according to main effect values

Factor	Effect Score	Ranking
T	102.56	1
P	13.13	5
Ra	12.83	6
T*P	49.07	2
T*Ra	-33.01	4
T*P*Ra	48.76	3

In DOE analysis, it is important to check the measurement error so that the effects of the nuisance factors are not included in the analysis. This can be realized by checking the normality of the observed data. The data must be normally distributed, independence with zero mean value and constant variance to ensure F_o ratio follows an F distribution [104]. The residual plot of normal probability as given in Figure 5-3 (a) indicates that the model meets the assumptions of the analysis where majority points follow a straight line while residual plots versus fits show randomly scattered about zero and no obvious pattern can be observed. The normal probability plot also shows that the strength data are scattered closely to the straight line (reference) and noticeably only one point lies slightly far away from the central data. However, it is assumed that the errors are normal.

The main effects plot shown in Figure 5-3 (b) clearly demonstrates that all center points are quite close to the lines connected average tensile strength from low to high setting of all parameters. The same trend can be also observed in the interaction plot as shown in Figure 5-3 (c). It tells that the final model formulated is appropriate for the observed data. On the other hand, the curvature effect is insignificant on the response and also confirmed by the ANOVA results in Table 5-4, where $p > 0.05$ for the curvature term. Therefore, a linear model is satisfactory to fit all the data. The findings could suggest

that the merely effect of surface roughness factor on strength improvement is negligible if there is an adequate presence of pressure and temperature. In fact, by applying a pressure without incorporated by an adequate amount of heat may cause strengthening of the chips with rougher surface becomes less effective.

Theoretically, when the intimate contact of less than 10 atomic spacings is taken place on the interface of the adjacent chips (the metallic radius of aluminium atoms being 0.143 nm), the inter-atomic force attracts the atoms to form a joint [93]. In contrast, a large asperity height between the chips reduced the inter-atomic forces. Also, any adjacent chips that contained any film of oxide layers or impurities would considerably hinder the further bonding of chips. Although the bonding may be contributed by the Vander Waals forces, the ratio of inter-atomic to van der Waals forces across an interface is typically very large, implying that the bonding is a result of interatomic forces when a close contact is established between clean metal surfaces [115].

The theory above explains why the interaction of temperature-pressure is more important than the interaction of temperature-pressure-roughness average, and is ranked second. Under high pressure and temperature with reduced oxide layers, a good diffusion bonding between particles can be obtained [22]. The role of temperature is to reduce the strength and to increase the ductility of chips. The localized shear strain increases proportionally with the ductility causing more oxide layers breaking down, thus exposing more virgin aluminium. When the normal pressure was applied perpendicularly to the chip's surfaces in the hot press forging die, the asperities collapse due to large plastic deformation, and consequently lead to significant decrease in distance of asperity height. As long as the distance between the interface tips of asperity

height can be reduced to less than 10 atomic spacings by the normal stress, metals will be welded in the solid-state.

The findings above supported by the results of grain size measurement and optical micrograph of the selected samples as shown in Figure 5-4. The measured grain size resulting from two different applied conditions is reported as: (i) 127.48 μm (Sample SO4 with 500 °C, 40 bar, and lowest roughness value of 2.301 μm), and (ii) 192.96 μm (SO7 with 400 °C, 40 bar, and highest roughness value of 3.558 μm). It is found that lower interface tips of asperity height is closely related to the small grain size as shown in Figure 5-4. Both grains exhibit different thickness size as examined via the LOM, under the similar magnification. The resulting tensile strength of the sample SO4 consolidated at higher temperature is 158.40 MPa, 144.78 MPa superior to that of sample SO7 (revealed thicker grain size). Therefore, the samples with the smaller grain size and consolidated at high temperature are of importance in the solid-state recycled aluminium. The smaller grain size principally promotes more virgin aluminium to exceed the threshold stretching for deformation. Therefore, the chip weld bonds are enhanced considerably by the inter-atomic force, grain growth strengthening (increased cohesion) and diffusion mechanism (intensified inter-atomic force).

Besides, the factor of chip's roughness became significant whenever it is combined with the temperature. As can be seen in Figure 5-3 (c), when the temperature kept at high setting (500 °C) with chips of the lowest roughness being used (correspond to small chip type), the tensile strength reached to maximum. Nevertheless, the resulting strength between high to low roughness chips does not change much as long as the temperature is kept at high setting. If consideration is solely to be made on chip

morphology influence, chips with the lowest surface area (correspond to large chip size) result in the highest tensile strength as indicated in Figure 5-3 (b), graph mean of TS versus Ra. However, the chip morphology effects as observed are to be more obvious towards ductility than that of tensile strength according to some researchers [13, 49, 116]. Although the size fraction of chips is a crucial factor to control the oxide contamination level, with the existence of high temperature and normal stress (500 °C and 40 tonnes), its effect becomes negligible. The regression model derived from the ANOVA results explains a concrete relationship between the independent variables (significant terms) and the response of tensile strength. The values of R^2-adjusted and R^2-predicted obtained are over 90% and 80% respectively. The lack-of-fit term is non-significant, indicated by $p > 0.05$, and therefore the model is considered to be statistically significant. The final regression equation is given as follows:

$$TS = 87.32 + 51.28\ Temp. + 6.56\ Press. + 6.42\ Ra + 24.54\ Temp.*Press. - 16.51\ Temp.*Ra + 24.38 Temp.*Press.*Ra + 25.10\ Ct\ Pt \quad (5\text{-}4)$$

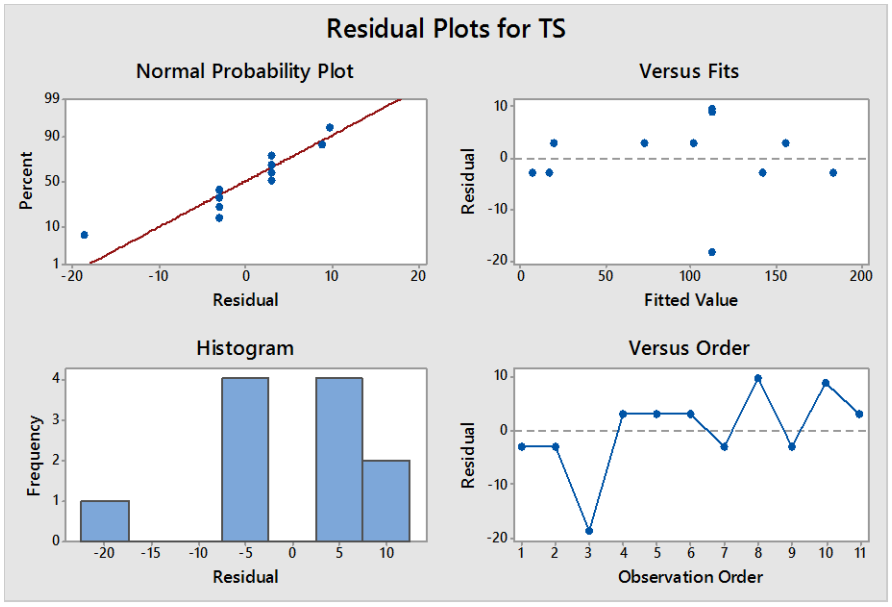

(a)

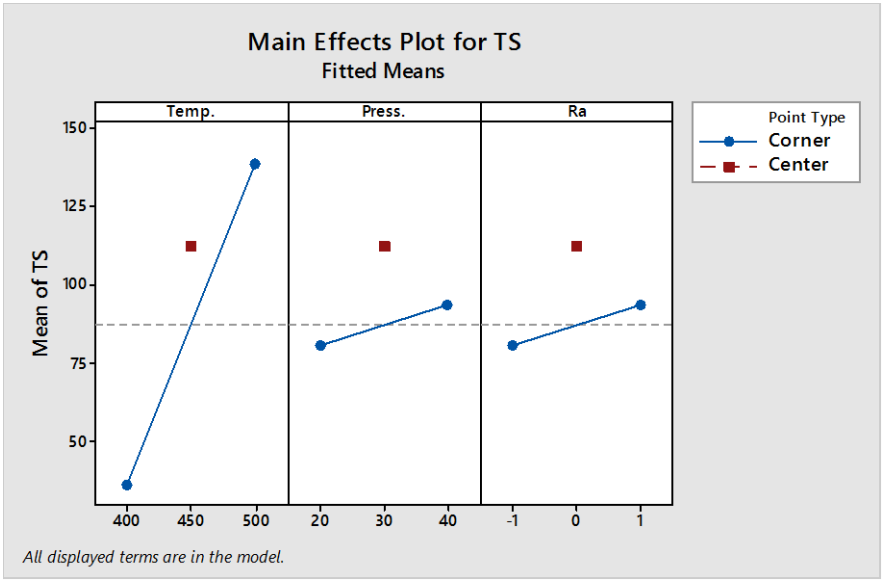

(b)

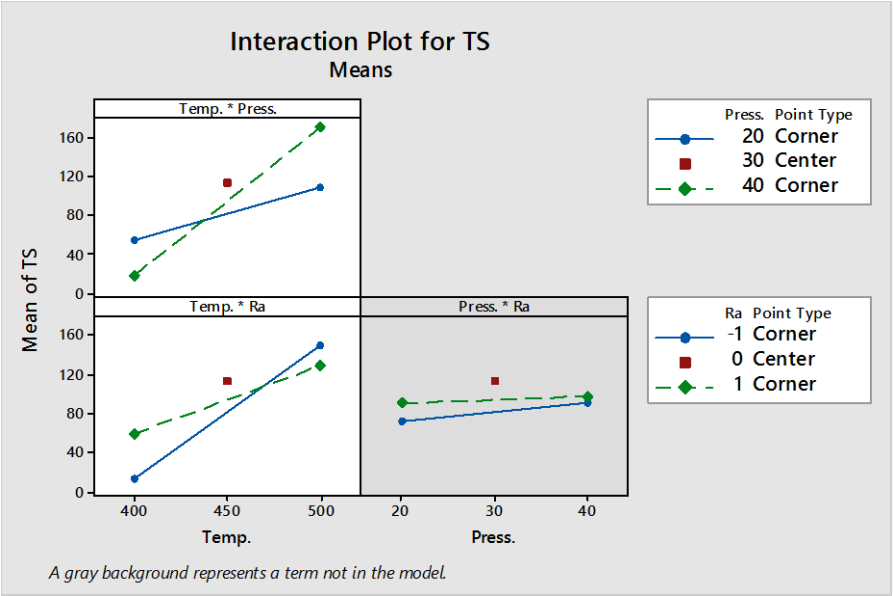

(c)

Figure 5-3: Results of full factorial analysis with curvature test: (a) Normal probability plot of residual, (b) Main effects plot of tensile strength and, (c) Interaction plot of factors

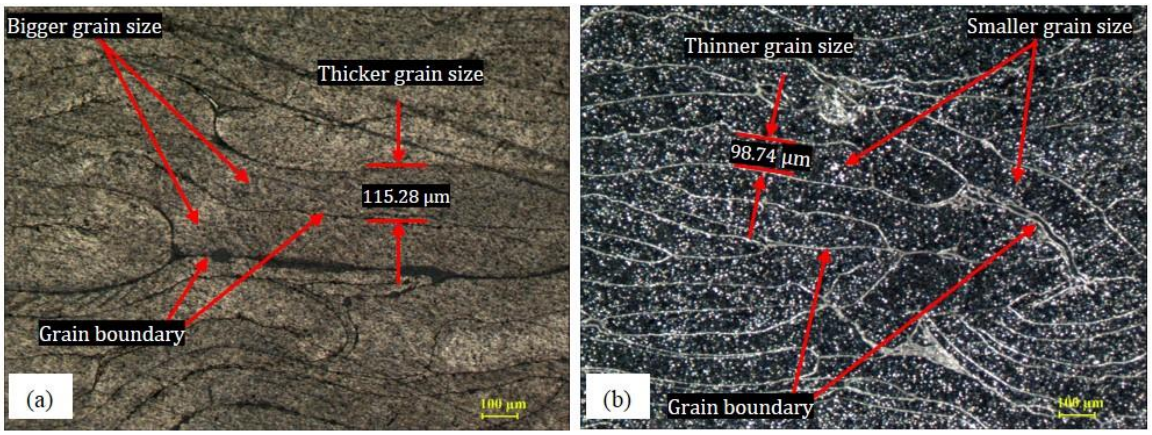

Figure 5-4: Optical micrographs of the measured grain size: (a) Sample SO7 and, (b) Sample SO4

5.3.2 Analysis of Stress-Strain Relationship

Figure 5-5 shows plot of true stress-strain for each sample. The graphs are plotted according to the sample designation shown in Table 5-3. Referring to Figure 5-5 (a), the samples pressed at 500°C (labelled as SO2, SO4, and SO8) demonstrate a ductile-like material. The corresponding samples exhibit a greater plastic region before failure. It is followed by samples SO9, SO10 and SO11, pressed at 450°C, anyhow they demonstrate a slightly lower ductility than the previous samples. Most of the samples that behave ductile-like behaviour failed within the gage length as shown in Figure 5-5 (b) and vice versa to the too brittle samples like SO1, SO3 and SO7. With the setting combination of high pressure and temperature, the tensile strength and ductility are outperformed. On the other hand, samples that pressed at lower temperature exhibit a brittle-like behaviour as observed. This is shown by the lacking plasticity and the samples failed instantaneously after they reach the ultimate tensile strength.

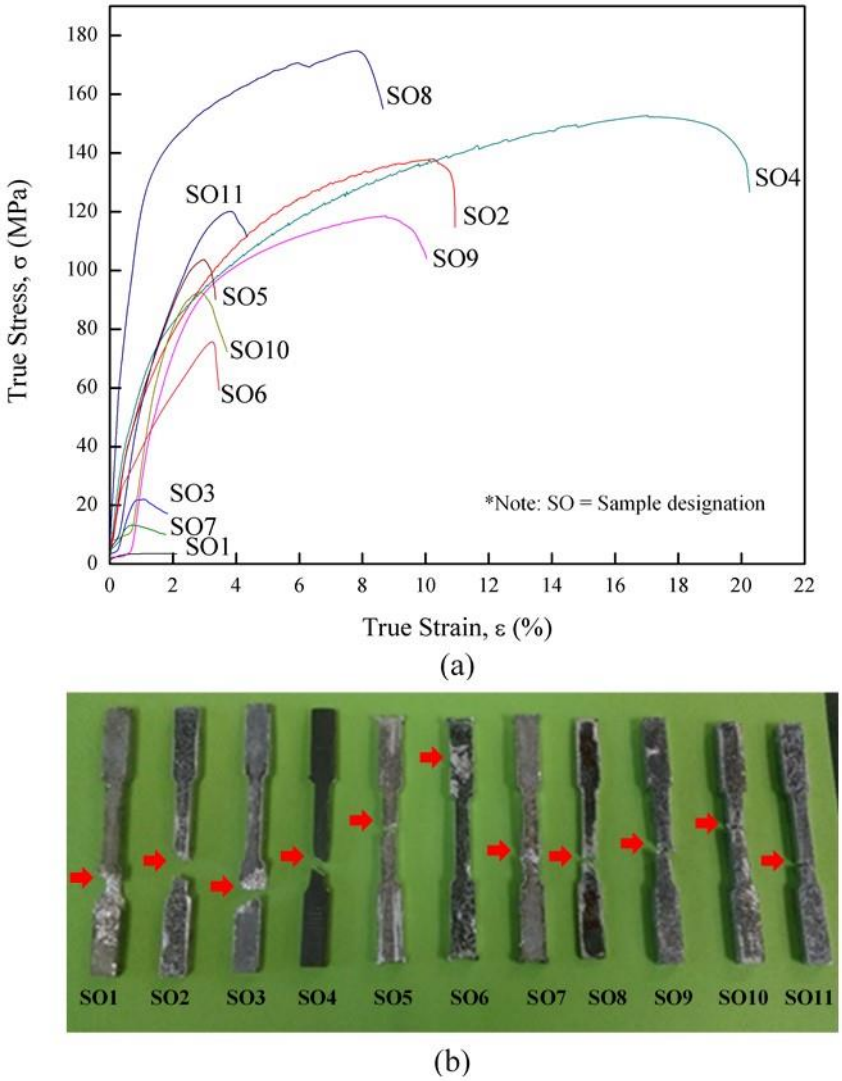

Figure 5-5: (a) True stress vs. true strain of tensile samples, (b) Failure points of each sample after tensile test

5.4 Summary

This study elucidates the influence of surface topography on the weld strength of the hot pressed chips in direct recycling of aluminium. The ANOVA results demonstrate that the factor of temperature is dominant, resulting in excellent weld strength. It is followed by the combination of temperature and pressure. The factor of surface topography manifested by the roughness value does not really affect the weld strength of the hot pressed chips as long as sufficient heat and pressure are retained. It is found that by merely applying the pressure without the presence of heat on the rougher chip surfaces, the weld bonds formation could be too weak to sustain. To conclude, heat and normal stress are required to continuously stretch the chips, exceeding the threshold stretch deformation which will finally promote welding in the solid state. Also, chips with clean and smooth surfaces help to enhance the bond strength of the chips.

CHAPTER 6 : ANALYTICAL MODELLING OF WELD STRENGTH

This chapter covers analytical modelling of tensile bond strength built on the basis of Cooper and Allwood [80] work and an improvement has been made by adding the effect of diffusion mechanisms on a proposed new model. Next, the relevant experimental works are clearly described to evaluate the model's accuracy. Finite element simulations were performed to retrieve the state variables (e.g.: normal stress, shear stress, strain, etc.), which is very unlikely to be obtained during physical deformation. The retrieved state variables are then fed to the final model to predict the tensile bond strength. The accuracy of the tensile bond strength prediction on a complex extruded profile is critical to meet the required process reliability. The investigations are carried out solely for the effects of deformation variables towards a weld quality rather than focusing on material variables.

6.1 Fundamental Understanding of Developed Model

Several assumptions are proposed for the model. The initial close contact between two chip surfaces is established by combination of normal stress and shear stress. Strain developed continues to stretch the material, breaking the remaining interfacial oxide fractions to expose the virgin metal. Entrapped air oxidizes some of the exposed metal; however, due to existence of high pressure and temperature, the clean metal will still develop bonding due to diffusion mechanism although contact time of chips with die is

limited as proved by the hot press forging experiments. The minimum strength recovered after the hot extrusion of aluminium AA6061 is equivalent to nominal strength of the base metal (AA6061- O) at room temperature once the clean metal surfaces are within the atomic distances. The developed model considers plane-strain deformation and a perfectly plastic material. The equivalent magnitude of strain, strain-rate, normal contact stress and shear stress affecting the material during the hot extrusion process, all are calculated by the FE model and simulations. The effect of diffusion mechanism in strength recovery is considered by adding the existing weld strength model with diffusion-strengthening model (developed through the hot forging experiment with constant pressure and varied temperature). The material behaviour was modelled using an inverse hyperbolic sine function (with parameters fitted to stress/strain data obtained through Deform 3D library and previous work [109]). The flow stress of material during deformation is governed by the plasticity behaviour model which linked the flow stress with temperature, strain and strain-rate.

6.2 Close Contact Approximation Between Surfaces

Initial contact between chips is only established on the asperity tips when both surfaces are pressed together. A fraction of area in contact (A_c) from the nominal area (A_n) equivalent to the normal contact stress (σ_n) divided by the aluminium flow stress (Y), deduced through the force equilibrium between two surfaces analysis. Conrad and Rice [95] suggest that the true contact area is approximately 80% of the above ratio. Therefore, the fraction of true contact area with nominal area between interfaces is

represented by 80% of the normal stress divided by the flow stress, according to Eq. (6-1).

$$A_C = 0.8 \frac{\sigma_n}{Y} A_n \tag{6-1}$$

where if $A_c > A_n$ then set $A_c = A_n$. The percentage above is acknowledged as an approximation and its accuracy could be further improved by thorough modelling and experimentation on the surface contact.

Continuous development of shear stress (τ_{app}) before the die entrance in addition to a built normal contact stress in the die results in a local effective von Mises stress (σ_{eff}) according to Eq. (6-2).

$$\left(\sigma_{eff}\right)^2 = \left(\frac{\sigma_n A_n}{A_c}\right)^2 + 3\left(\frac{\tau_{app} A_n}{A_c}\right)^2 \tag{6-2}$$

To maintain local equilibrium of ($\sigma_{eff} = Y$), the area of surface in contact must increase to:

$$A_c = \frac{0.8 A_n}{Y} \sqrt{{\sigma_n}^2 + 3\left(\tau_{app}\right)^2} \tag{6-3}$$

where if $Ac > An$, set $Ac = An$. Note that the 80% scale factor has been applied. The flow stress (Y) here depends on the strain, strain-rate and temperature [117].

The initial contact is created between the oxide films. When the temperatures below 1000 ˚C or with the presence of air, no bonding initiated according to Nicholas [118] in his research about ceramic-ceramic and ceramic-metal bonding. It is known that aluminium and its oxide are insoluble [93], therefore no diffusion will take place between the oxide films to create a weld. Bonding only occurs when the interface is stretched laterally, exposing the aluminium substrate.

6.3 Initial Stretching of the Interface and Oxidation by Entrapped Air

There is a threshold stretching deformation to exceed at the interface before which welding will occur. As the aluminium oxide is too brittle, it possesses a failure strain of less than 1% as suggested (given tensile strength of 260 MPa and Young's modulus of 350 GPa). As expected from its brittleness, the reduction of threshold for weld creation in aluminium that performed in a vacuum is less than 1% as found by Sherwood and Milner [119]. This work proposed the resulting observable threshold strains in atmospheric conditions as a result of entrapped air oxidizing pure aluminium (area of absence from oxide films) at low strains. The existence of any aluminium exposed at higher strains in an inert atmosphere can only be realized when all the entrapped oxygen has chemically bonded to this aluminium. Hence, an estimation of oxygen content by means of its volume is required in order to quantify the fraction of the oxidized surface due to the entrapped air.

Actual contact geometry of between two surfaces of chips is complex. For simplification, the surface contact is assumed to have an imaginary rough contour,

represented by a triangular topography rather than a flat surface as recommended by O'Callaghan and Probert [120]. Roughness contains root mean square of the asperity heights (r) and the asperity inclination angle (ψ). It can be assumed that the equivalent surface roughness has a root mean square asperity height, r_{eq} of $\sqrt{2r}$ and asperity inclination angle, ψ_{eq} of $\sqrt{2\psi}$ respectively [120].

With the simplified geometry, the entrapped air volume that would prevent the inter-atomic forces to create a weld bond can be estimated (for 1 m^2 aluminium surface, approximately 1.7×10^{-4} moles of oxygen (O_2) are required to oxidize of 2.9 nm surface depth which is equivalent to ten aluminium atom spacings). The volume and temperature determine the amount of air entrapped, O_2 in moles. Therefore, the fraction of surface to be oxidized by the entrapped air,(η) is given in Eq. (6-4) where T is the process temperature (in Kelvin). (See Appendix D for details of derivation),

$$\eta = 50{,}000 \times r_{eq} \times \cos\left(\psi_{eq}\right) \times \frac{298}{T} \tag{6-4}$$

Value of η is calculated by substituting r, ψ and T as given in Table 6-6.

Thus, the fraction of the exposed final contact area (absence from protective oxide layers) is given by v in Eq. (6-5) (Figure 6-1 shows the unsimplified form of this equation).

$$v = \frac{\varepsilon - \eta}{1 + \varepsilon} \tag{6-5}$$

where if the $v < 0$, set = 0 and ε = engineering strain parallel to the interface (typical value equal to 1). To keep the final model simple, the engineering strain is used instead of logarithmic strain.

The area of exposed substrate aluminium (A_{ex}) is, therefore, given by Eq. (6-6)

$$A_{ex} = vA_c \tag{6-6}$$

where A_c is given by Eq. (6-3).

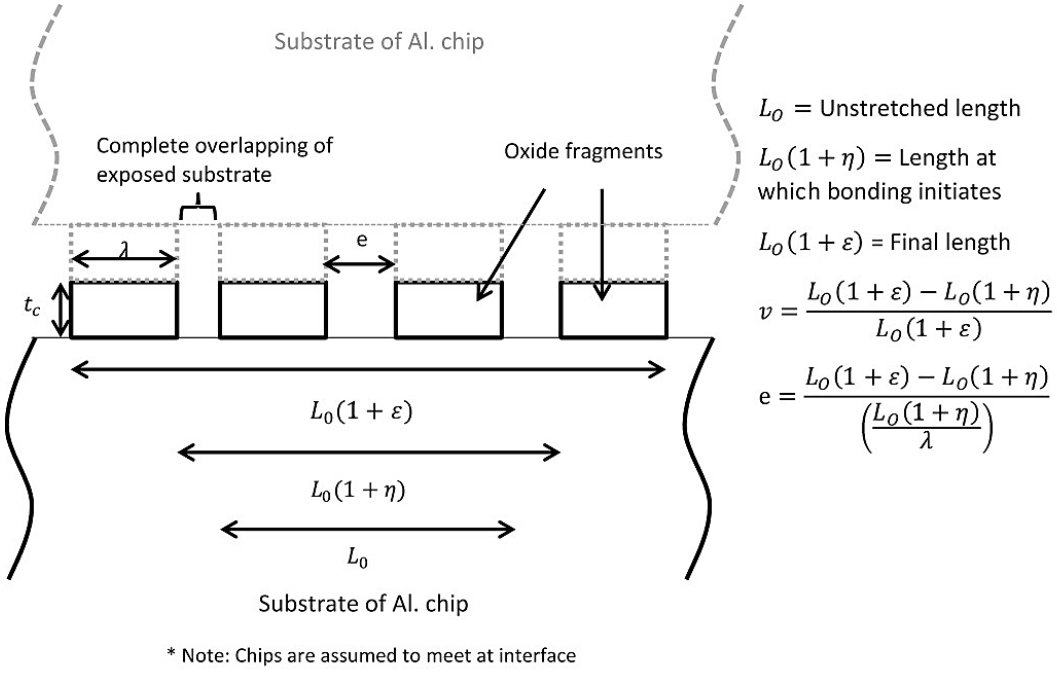

Figure 6-1: Surface of chips with an original length of *L*o stretched to length *L*o (*1* + ε) (adapted from [80])

6.4 Prolong Stretching of The Chip's Interface

Both sides of the exposed aluminium interface must be overlapping in order for bonding to occur. Analyses of force equilibrium on oxide fragments (refer to Appendix E) show that when the adjacent oxide layers break-up together, the fragments experienced a greater maximum tensile stress. It is assumed that the exposed aluminium substrate at the coalesced interface on one side is always adjacent to substrate aluminium exposed on the other side and both are completely overlapped, as shown in Figure 6-1.

$$\frac{\lambda}{t_c} = \frac{2\sigma_{oxide}}{k} \tag{6-7}$$

where, t_c and λ are thickness and length of the oxide fragments as defined in Figure 6-1, k is the aluminium shear flow stress and σ_{oxide} is the failure stress of aluminium oxide. Eq. (6-7) implies that the length of the oxide fragments increases for thicker oxide layers and for weaker substrate aluminium alloy.

When a shear stress, τ_{app} is present at the interface, the aspect ratio increases to

$$\left(\frac{\lambda}{t_c}\right)_{shear} = \frac{2\sigma_{oxide}}{k} \times \left(1 - \frac{{\tau_{app}}^2}{k^2}\right)^{-1} \tag{6-8}$$

With the presence of higher interfacial shear stresses, the length of oxide fragments keeps further increasing. Derivations of Eqs. (6-7) and (6-8) are detailed out in Appendix E. An oxide fragment aspect ratio of approximately 14 ($\lambda \approx 140$ nm) is obtained by substituting typical AA6061-O parameters into Eq. (6-7) ($\sigma_{oxide} \approx 260$ MPa,

$k \approx 37$ MPa, $t_c \approx 10$ nm). It is comparable to an aspect ratio of up to 13 as found by Barlow et al. [121] in analysis of the internal surfaces of roll bonded AA1050 foil via a transmission electron microscopy (TEM). Due to the close agreement between the calculated and observed aspect ratios, the methodology used to model the fracture of the oxide layers is concluded valid. Thus, the crack width can be calculated by dividing the area of exposed aluminium with the number of cracks. The number of cracks is equal to the length of stretched surface area at which bonding is initiated divided by the length of the oxide fragments and expressed as follows:

$$\frac{L_0(1+\eta)}{\lambda} \tag{6-9}$$

Hence an average crack width, e can be obtained by dividing the final length of exposed aluminium area by the number of cracks (Eq. (6-9)) and given by Eq. (6-10) (Figure 6-1 shows the unsimplified form of this equation).

$$e = \frac{\lambda(\varepsilon - \eta)}{1+\eta} \tag{6-10}$$

The value of e can be calculated by substituting the values of ε, η and λ as given in Table 6-6. Now the pressure necessary to micro-extrude the substrate aluminium within the cracks can be computed after considering with the crack width. There are a number of ways to do that by either slip-line field or finite element analysis, as summarised in Hill [122]. Here, a slab analysis as outlined by Hosford and Caddel [117] is adopted for simplicity. The analysis assumed plane-strain and square dies (dead zone angle $\approx 90^\circ$). The pressure required to micro-extrude the substrate aluminium through the cracks is given by p_{ex} in Eq. (6-11).

$$p_{ex} = Y \ln\left(\frac{\lambda + e}{e}\right) + \left(\frac{Y t_c}{e}\right) \quad (6\text{-}11)$$

where Y = flow stress of the extruded profile (MPa) and varied with the temperature changes. It is assumed that the substrates are forces together when there is a magnitude difference between the nominal normal contact stress (σ_n) and p_{ex}, resulting in an area of contact between the substrate aluminium (A_s) as follows:

$$A_s = 0.8\frac{\sigma_n - p_{ex}}{Y} A_{ex} \quad (6\text{-}12)$$

where if $A_s > A_{ex}$, set $A_s = A_{ex}$. A_{ex} is given by Eq. (6-6).

6.5 The Diffusion-Strengthening Model

Diffusion plays an important role in solid-state bonding as advocated by Plata & Piwnik [77] and Donati & Tomesani [75] in their pressure-time criterion which suggests that a sufficient time must be allowed for bonding to occur. The film theory suggests that the important effects of process duration and temperature only on the flow stress will be insufficient (equating to the propensity of the substrates to be micro-extruded through oxide layer cracks) [80]. Many postulated that at higher temperatures and longer time, diffusion dominated to cause an increase in lattice dislocations and recrystallization nucleation that finally improved the bond strength [69, 80, 123]. Also, the mechanical and deformation behavior in materials is controlled by a diffusion mechanism at higher temperatures [124].

In order to study the strengthening effect due to diffusion mechanism on consolidated chips subjected to different temperature and time, a set of closed-die hot forging

experiments were conducted as shown in Table 6-1. Each row of the table represents a matrix of tests, where an experiment was conducted for each combination of temperature, holding time and hydraulic pressure. Experiments in Set A was carried out to determine the effect of increasing the process time (holding time) on the weld strength and to establish the correlation between them. In experiment for Sets B-D, the tests were conducted at different process temperatures over a set of constant process times. Differences in process time that are expected to result in a varying bond strength recovery are necessary to be studied. Sets B-D experiments were conducted solely at higher temperatures to establish relationship between the strength recovery rate and temperature. The reason why the hot forging experiments at low temperature and pressure settings are excluded is due, to some extent, to the fact that the formation of weld bonds at this conditions are very poor as discussed in Sections 4.2 and 5.3, respectively. At higher temperatures, the chances to obtain high bond strength are very high. Details of the closed-die hot forging experiments are briefed in Section 3.1.4 while the tensile test procedure is described in Section 3.2 (i).

Table 6-1: Closed-die forging experiments conducted

Set	**Temperature (°C)**	**Holding time (sec)**	**Tensile Strength (MPa)**
A	500 °C	[5, 15, 30, 45, 60]	[83.621, 88.037, 90.096, 93.820, 96.389]
B	[400 °C, 430 °C, 480 °C, 530 °C]	3600	[11.720, 14.952, 48.036, 215.191]
C	[400 °C, 430 °C, 480 °C, 530 °C]	5400	[13.620, 16.726, 71.187, 218.418]
D	[400 °C, 430 °C, 480 °C, 530 °C]	7200	[22.510, 27.862, 87.518, 226.965]

**The pressure was set to 30 tonnes in all experiments*

6.5.1 Experimental Results

The results of the tensile strength in closed-die hot forging experiments, subjected to distinct process temperatures and times, are presented in Table 6-1. In these experiments, the strength recovery ranges from 4% to 72% as of as-received parent metal strength of 319 MPa (AA6061-T6). The influence of increasing process time at constant temperature is shown in Figure 6-2 (a). The general trend exhibits that the resulting bond strengths are stronger with the prolonged holding time. Eventhough the applied holding time is relatively slow and quick, the strength recovery improved linearly over the short period of time. Overall, the strength is recovered from as low as 26 % from the parent metal strength for 5 seconds holding time to a maximum of 30 % for 60 seconds holding time. The reason for varying the holding time at low range is to determine the effect of time increment in small intervals towards the tensile strength recovery. It is analysed in order to mimic the real phenomenon of rapid chip consolidations in the die's bearing land during the hot extrusion process. This enables the developed diffusion-strengthening model be accurately applied in the hot extrusion process.

The results in Sets B-D experiments are normal pressure-included effect in chip's consolidation. To exclude the effect of pressure, the tensile strength obtained at 400 °C was used as reference and all other strengths that gained in the subsequent temperatures were deducted with this reference and the data is tabulated in Table 6-2. Hence temperature increment relative to 400 °C was used, and it can be said that the strength increase was mainly due to temperature. Then, the data was used to plot Figure 6-2 (b) – (d). As can be seen in Figure 6-2 (b) – (d), the bond strength recovery in solid-state

weld is considerably influenced by the process temperature, and it is consistent with the results obtained in Section 5.3. Besides, the regression analysis with 95% confidence interval is done to fit the experimental data. An increased in R^2 from 99 % to 100 % indicates that the important variation seen in the tensile bond strength recovery is determined to a great extent by the factor of temperature. The tensile bond strength recoveries show an exponential growth over the temperature range and more rapidly at higher degree of temperature.

Table 6-2: Tensile bond strength recovery due to temperature effect

Set	**Temperature (K)**	**Holding time (sec)**	**Tensile Bond Strength Recovery, *TSr* (MPa)**
B	[273*, 303, 353, 403]	[3600]	[0, 3.232, 36.316, 203.471]
C	[273*, 303, 353, 403]	[5400]	[0, 3.106, 57.567, 204.798]
D	[273*, 303, 353, 403]	[7200]	[0, 5.352, 65.008, 204.455]

**Strength recovery at 400 °C (set as 273 K) was used as reference to compensate the effect of normal pressure on chip's consolidation*

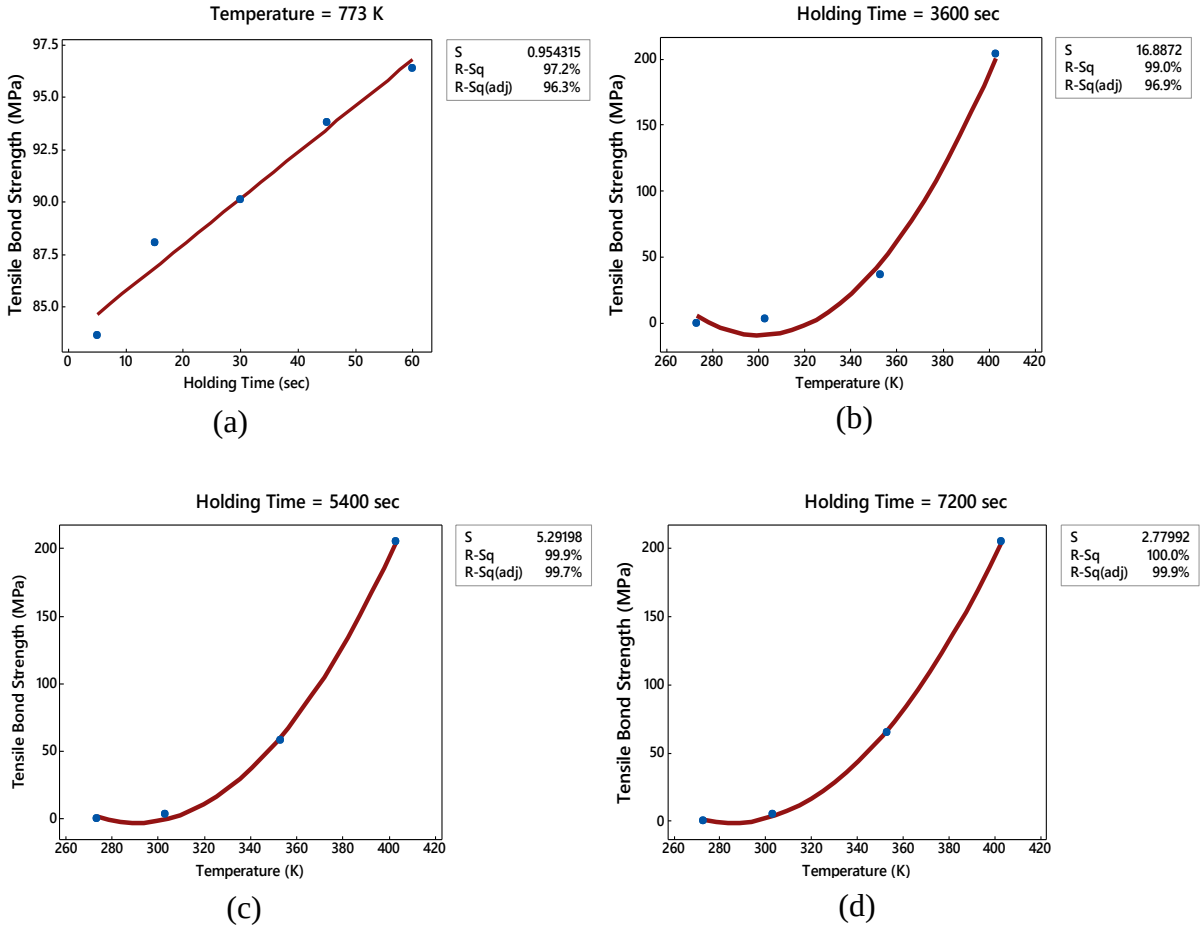

Figure 6-2: (a) Tensile bond strength in solid-state weld as a function of holding time; Tensile bond strength recovery due to temperature effect in solid-state weld at a holding time of (b) 3600 sec, (c) 5400 sec, (d) 7200 sec

6.5.2 Diffusion-Strengthening Model Development

The findings suggest that the temperature has a most profound influence on the bond strength recovery and to a lesser degree by the process time. In this section, an attempt is made to develop a diffusion-strengthening model in order to include the diffusion effect in tensile bond strength recovery. The model is subsequently integrated with the tensile bond strength model, developed by the work of Cooper and Allwood [80] and

the final model will be used to predict the total tensile bond strength recovery on the chip-based billet consolidated by the hot extrusion

In diffusion, typical distance that is travelled by the atomic species can be modelled through the Fick's second law as given by Eq. (6-13) [125, 126].

$$x \propto \sqrt{Dt} \tag{6-13}$$

where x is the characteristic diffusion distance in (m), D is diffusion coefficient in (m^2/s) and t is time in (sec). The most important part in diffusion is the ability of atoms to move through a short distance collectively in a shorter period of time, causing atoms to contain as much at their normal lattice positions within the chip interfaces and ready to move further with higher temperatures and pressures [93]. It can be postulated that the further atoms travelled across the chip's boundary, the weld creation becomes stronger. This can be supported from the results in Figure 6-3 (a) where the relationship between tensile bond strength and square-root of process time (holding time) is directly proportional and R^2 revealed 98.7 % indicates that about 98.7 % variations exist in the tensile bond strength, and this can be explained by the square-root of process time. The R^2 of 97.2 % from results in Figure 6-2 (a) improved to 98.7 % as shown in results in Figure 6-3 (a). This shows that the relationship between the tensile bond strength recovery and time can be best described by the Eq. (6-13) above. Thus, the tensile bond strength recovery in the solid-state recycling is assumed to have a linear relationship with diffusion distance and can be expressed as:

$$TS_{\mathrm{rd}} \propto x \propto \sqrt{R_{TS} \times t} \tag{6-15}$$

$$TS_{rd} = \delta \sqrt{R_{TS} \times t} \tag{6-15}$$

where TS_{rd} is the tensile bond strength recovery due to diffusion mechanisms in (MPa), R_{TS} is the tensile bond strength recovery rate in (MPa/s), t is time in (sec) and δ is the constant. The tensile bond strength recovery rate (R_{TS}) (its derivation is described below) is replaced instead of D to describe the relationship of tensile bond strength recovery with process time. Since R_{TS} is a diffusion-controlled parameter, therefore Eq. (6-15) is concluded valid.

The diffusion coefficient (D) is a measure of the mobility of the diffusing species (in this case aluminium atoms), and is given by Eq. (6-16).

$$D = A \exp\left(\frac{-Q_{\mathrm{d}}}{RT}\right) \tag{6-17}$$

where A is the a temperature-independent preexponential (m^2/s), Q_d is the activation energy for diffusion (J/mol), R is the gas constant (8.31 J/mol-K) and T is the absolute temperature (K). This is an Arrhenius type relationship and D increases exponentially over the temperature. The results in Figure 6-2 (b) – (d) consistently show that the tensile bond strength recovery is increased exponentially over the temperature range. Therefore, this study applies an Arrhenius relationship to describe the tensile bond strength recovery rate and can be written as follows:

$$\mathrm{R_{TS}} = A \exp\left(\frac{-\mathrm{Q_d}}{\mathrm{RT}}\right) \tag{6-18}$$

where R_{TS} is the tensile bond strength recovery rate (MPa/s), A is the temperature-independent preexponential in (MPa/s) and the other parameters are remained as in Eq. (6-16). New plots of tensile bond strength recovery rate against absolute temperature, as shown in Figure 6-3 (b) – (d), persistently show the Arrhenius relationship type. The tensile bond strength recovery rate was obtained by dividing the tensile bond strength recovery with the holding time of each experimental run in Sets B-D (Table 6-2). To further confirm that the tensile bond strength recovery rate followed the Arrhenius relationship, natural logarithm of the tensile bond strength recovery rate is plotted against the inverse of the process temperature, and its mathematical expression is given in Eq. (6-18).

$$\ln R_{TS} = \ln A - \frac{Q_d}{R}\left(\frac{1}{T}\right) \tag{6-18}$$

Figure 6-4 (a) - (c) show the plots of the tensile bond strength in natural logarithm against the inverse of the process temperature at different holding time. The plots show linear trends and the coefficient of determination, R^2 values of 98% - 100%. This indicates that the majority of the variation distributions in the tensile bond strength recovery rate are around the mean value. Therefore, the model fits very well to the data. The plots strongly suggest that the relationship between tensile bond recovery rate and temperature can be modelled as a diffusion-controlled process due to the consistency of the plots shown in Figure 6-4 (a) – (c) despite the fact that one data point at reference temperature (400 °C) was removed from each plots.

Thus, the general model of the tensile bond strength recovery rate can be written as follows:

$$R_{TS} = 12131.177 \exp\left(\frac{-40.818\ x\ 10^3}{RT}\right) \quad (6\text{-}19)$$

where A and Q_d are taken as an average of three data as given in Table 6-3.

From Eq. (6-15), the diffusion-strengthening model due to diffusion mechanisms can be written as follows:

$$TS_{rd} = 0.4939708 \sqrt{R_{TS} \times t} \quad (6\text{-}20)$$

where TS_{rd} is the tensile bond strength recovery due to diffusion mechanisms and t is the process time. Constant δ is obtained through the plot of TSr against $\sqrt{t}$ from Figure 6-3 (a) and tensile strength recovery at 5 seconds was used as a reference to exclude the effect of normal pressure. Data of tensile bond strength recovery calculated from Eq. (6-20) for $0 < t \leq 60$ (seconds) is replotted and the graph is shown in Figure 6-4 (d). The findings are consistent with the plot in Figure 6-3 (a) where the tensile bond strength recovery due to diffusion mechanisms is directly proportional with the square-root of process time. Figure 6-5 presents the experimental and predicted tensile strength recovery as a function of square root process time of hot press forging operation. The results show that Eq. (6-20) can accurately predict the resulting experimental tensile strengths. Hence, the developed model provides an accurate prediction over the observed trends of the strength recovered due to diffusion mechanism.

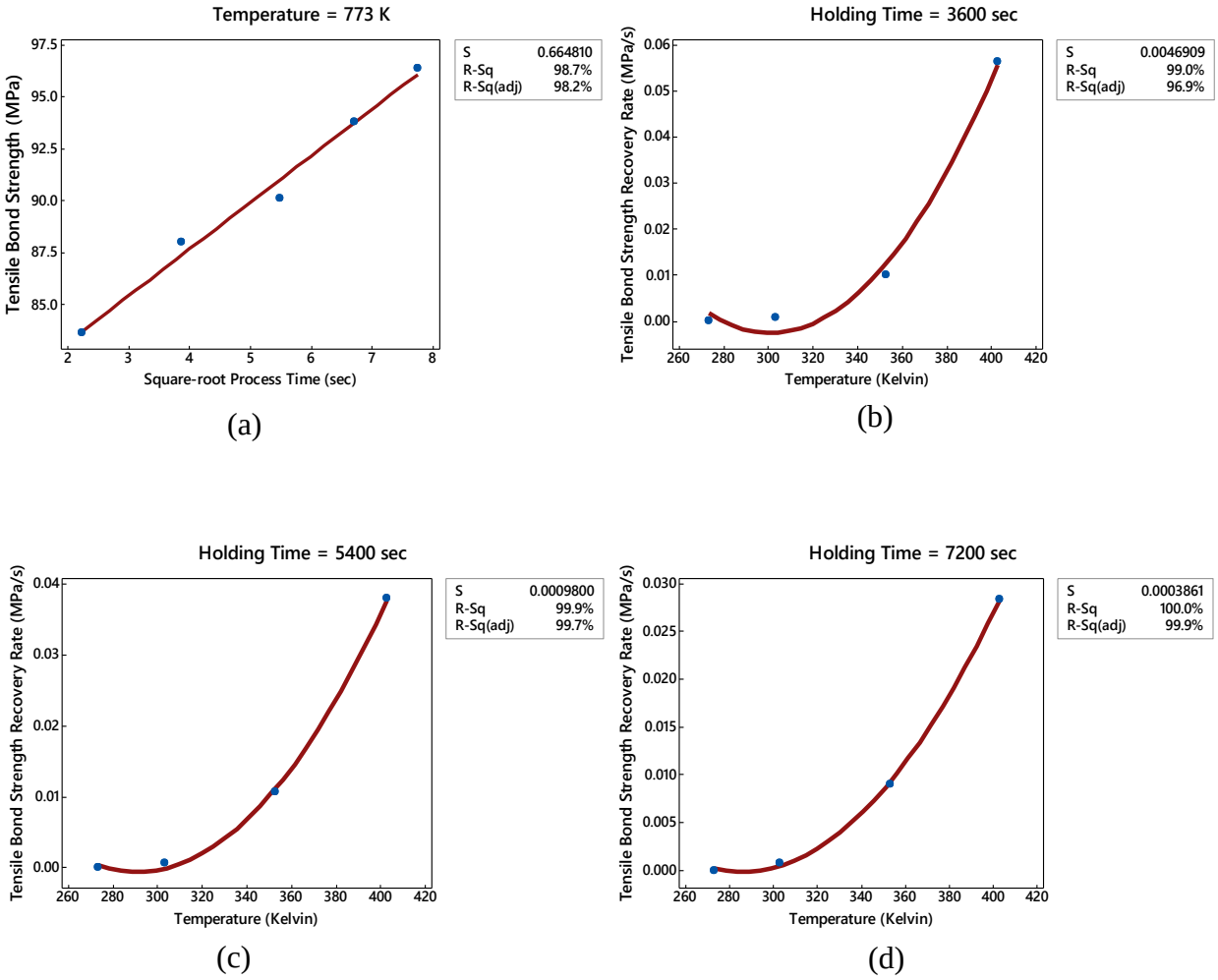

Figure 6-3: (a) Data from Figure 6-2 (a) is used to plot tensile bond strength against square root of the holding time for temperature 773K; Tensile bond strength recovery rate due to temperature different in solid-state weld at a holding time of (b) 3600 sec, (c) 5400 sec, (d) 7200 sec

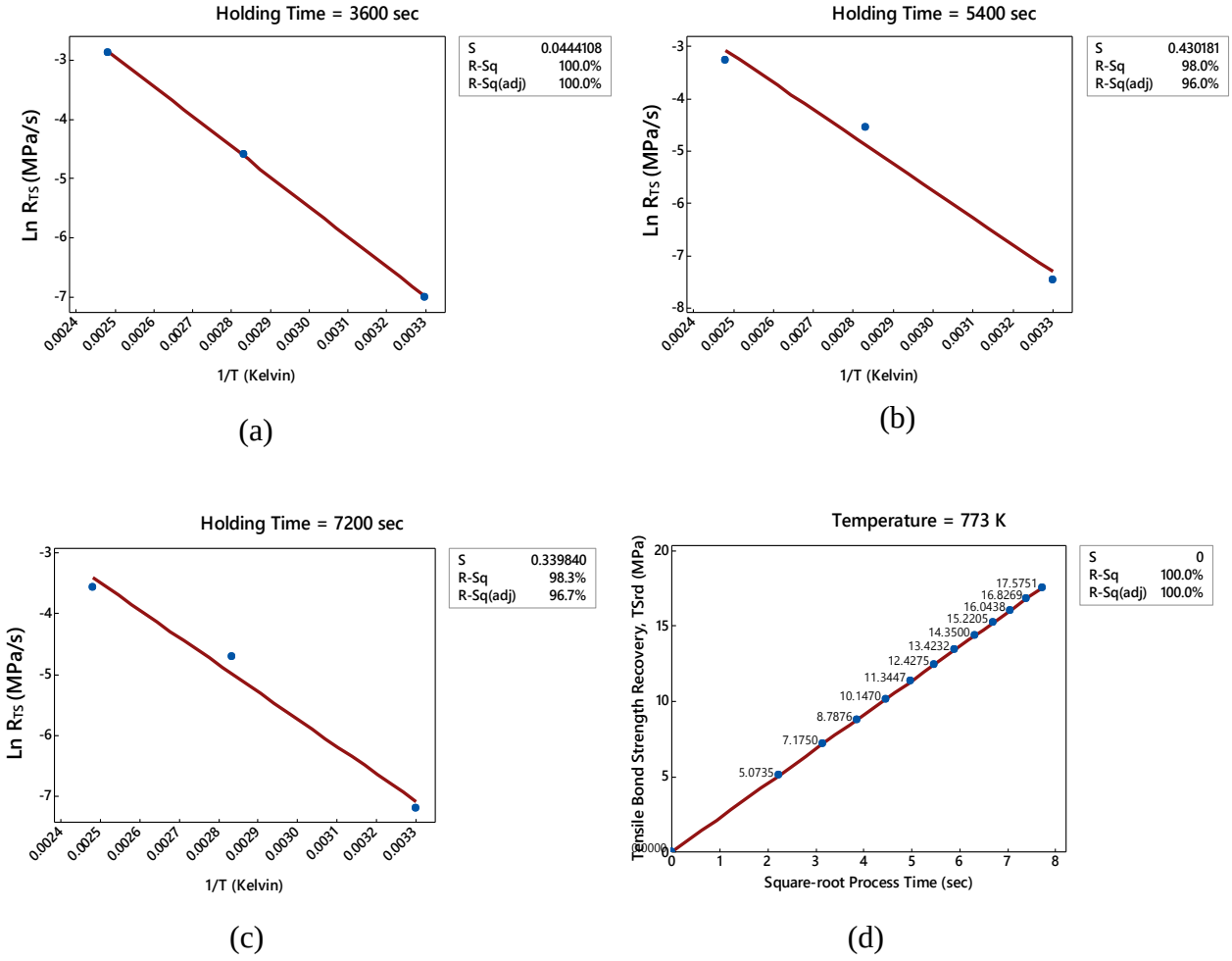

Figure 6-4: Data from Figure 6-3 (b)-(d) used to plot the natural logarithm of the tensile bond strength rate against the inverse of the process temperature at different holding time of (a) 3600 seconds, (b) 5400 seconds and (c) 7200 seconds; (d) Tensile bond strength recovery as a function of square-root of process time

Table 6-3: Constants of A and Q_d obtained from the plots in Figure 6-4 (a) - (c)

Holding Time (sec)	**Linear model**	**Q_d (kJ/mol)**	**A (MPa/s)**
3600	R_{TS} = 9.715 - 5065 (1/T)	42.090	16564.216
5400	R_{TS} = 9.770 - 5175 (1/T)	43.004	17500.767
7200	R_{TS} = 7.753 - 4496 (1/T)	37.361	2328.548

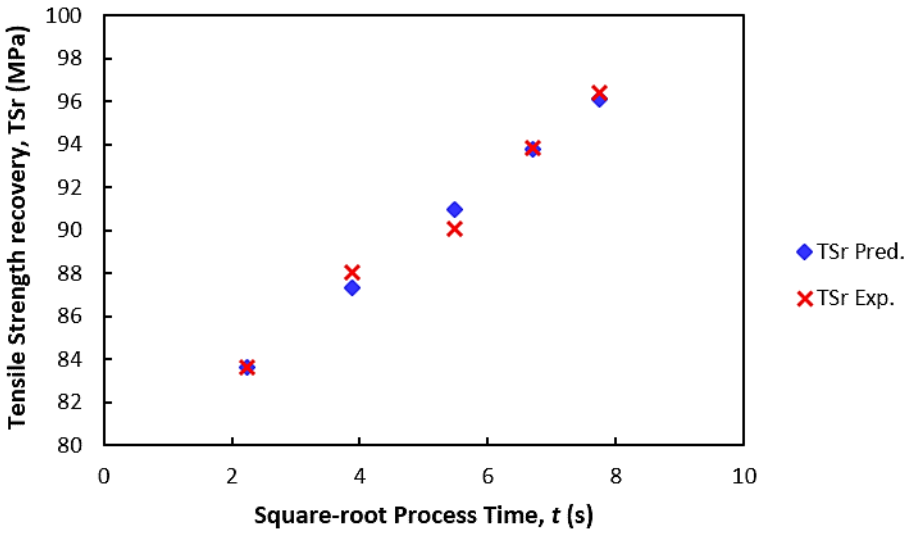

Figure 6-5: Tensile strength recovery between the experimental and predicted data

6.6 Final Weld Strength Model

The components deduced for the model are combined as given below to provide an estimate of the final weld strength. The area of contact between clean chip surfaces (A_s) is assumed to bond with each other and the minimum strength recovered was assumed to be equivalent with the nominal strength of the bulk aluminium (σ_0), AA6061- O (130 MPa). Force equilibrium implies Eq. (6-21).

$$\sigma_{TS}A_n = \left(\frac{0.8A_n}{Y}\sqrt{{\sigma_n}^2 + 3\left(\tau_{app}\right)^2}\right)_{\leq A_n} \times v_{\geq 0} \times \left(0.8\frac{\sigma_n - p_{ex}}{Y}\right)_{\leq 1} \times \sigma_0 \qquad (6\text{-}21)$$

where σ_{TS} is the final tensile bond strength, p_{ex} is given by Eq. (6-11), v is given by Eq. (6-5), and TS_{rd} is given in Eq. (6-20).

Therefore, the deduced model predicts a nominal room temperature tensile bond strength, σ_{TS}, as given in Eq. (6-22).

$$\sigma_{TS} = \left(\frac{0.8}{Y}\sqrt{{\sigma_n}^2 + 3\left(\tau_{app}\right)^2}\right)_{\leq A_n} \times v_{\geq 0} \times \left(0.8\frac{\sigma_n - p_{ex}}{Y}\right)_{\leq 1} \times \sigma_0 + TS_{rd} \qquad (6\text{-}22)$$

The tensile bond strength recovery on the consolidated chips through hot extrusion will be investigated by varying the process temperature. The effect of each deformation parameter on the tensile strength recovery when higher temperature setting was used can be explained as follows:

- A higher temperature increases strain which leads to the enlargement of exposed area and oxide crack width, thus increase the v and decrease the p_{ex} respectively.
- The strain-rate increment increases the flow stress of the metal, increasing both Y and p_{ex}. With an increase in Y, more metal flows entering the die opening area causing normal contact stress, σ_n to increase.
- An increment in deformation temperature will decrease the threshold strain (η) and flow stress of the aluminium. Reducing threshold strain will increase v, and a reduction in flow stress of aluminium decreases both Y and p_{ex}.
- A higher temperature generates a larger shear plane and expands the shearing area in the region of die entrance, thus increases shear stress, τ_{app} and increases the oxide crack width, decreasing p_{ex}.

6.7 Methodology for Evaluating the New Tensile Bond Strength Model

Evaluating the newly developed model requires the weld strength that was obtained under various process temperatures be compared with the weld strengths predicted by the model. Section 6.7.2 elaborates the physical hot extrusion experiments performed to acquire bonds of aluminium chips recycled without melting, and also describes tests conducted to evaluate the strength of the welded chips. To apply the model for predicting the weld strength, it is essential to fully understand the role of each deforming variable in the physical experiments. Since retrieval of some variables are impossible to be made during the physical experiments, finite element (FE) software was used to assist the analysis. Details of FE simulation procedures are presented in Section 6.7.5. The full range of physical and simulated experiments is described in Section 6.7.4.

6.7.1 Experimental Work

In hot extrusion of direct chips recycling, the welding occurs at chips' interface as a result of the normal stress, shear stress and atomic diffusions. The normal stress generates a massive compressive strain perpendicular to the surface of chips inside the die bearing while the shear stress is responsible of breaking the oxide layers in the direction of extrusion in which the shear force acts parallel to the shear area/plane. Diffusion is responsible to create a strong bond by exchanging atoms between chip interfaces and by creating a "bridge" between two mating surfaces through an excessive grain growth. Despite many deformation parameters being variables in this process,

they are strongly dependent on each other. Unlike experimental setup by Cooper and Allwood [80], the interfacial forces causing an expansion of interface strain between chips in this experiment are assumed induced by the shear force. The generated shear force acts parallel along the shear area of the billet, adjacent to the die entrance while the normal contact force acts perpendicular to the surface of chip-based billet.

6.7.2 Hot Extrusion of Rectangular and Spur Gear Profiles

Each compacted billet from chips was annealed for two hours prior to each extrusion. The machine used was described in Section 3.1.3. The ram speed was set to 4.4 mm/s and the container temperature was set to 300 ^{o}C. Two types of extrudate geometry were used to validate the model accuracy known as rectangular and spur gear. Details of the die characteristics are given in Section 3.1.1. There are two different ratios for gear geometry, 4.86 and 2.16 and the smaller ratio was used to test the possibility of extruding complex geometry part with extremely low extrusion ratio. Since that the extrusion speed was fixed, the normal contact stress, shear stress, strain and strain-rate were dependent on the temperature changes, extrusion ratio and shape complexity (reflect to back flow). The diffusion mechanisms were mainly influenced by the extrusion temperature (corresponding to billet's temperature) and chips' contact time with die. As the temperatures of container and die must be maintained around 300°C, a thermocouple was used to measure and provide the temperature feedback. This is done to reduce the heat transfer of billet upon contact with the container and die during the experiment. The desired temperature is maintained by a temperature controller.

6.7.3 Experimental Plan

A series of tests were conducted to evaluate the accuracy of the newly developed model and to assist understanding on the effects of temperature, extrusion ratio and geometry over the resulting weld strength. A list of the experiments covered in this study is presented in Table 6-4. Each row of the table represents a matrix of experiments in which an experiment was conducted for each combination of temperature, die geometry and extrusion ratio. Each experiment with a successful result was repeated for three times and compared with the predicted strength value.

Table 6-4: Experimental tests conducted on each die geometry

Set	Temperature (°C)	Geometry	Sample Notation	Bearing Length (mm)	Extrusion Speed (mm/s)	Extrusion Ratio
A	[450 °C, 500 °C, 550 °C]	Spur Gear	[G_{A450}, G_{A500}, G_{A550}]	24.00	4.4	4.86
B	[450 °C, 500 °C, 550 °C]	Rectangular	[R_{450}, R_{500}, R_{550}]	27.00		11.22
C	[500 °C]	Spur Gear	[G_{B500}]	11.40		2.16

A minimum temperature of 450 ^{o}C was used because using billet temperature lower than that could result in a poor quality of extrudate. Experiment in Set A was designed to investigate the resulting weld strength on the complex extruded profile. Set B experiment investigated the model's accuracy on the simple geometry subjected to different temperature range. Experiment in Set C was carried out to investigate the possibility of extrusion with extremely low extrusion ratio on the complex geometry. By varying the temperature, extrusion ratio and geometry, all the corresponding deformation parameters will respond in real time accordingly. The physical appearance

of each extrudate just after the hot extrusion process is given in Figure 6-6. A closer examination on the spur gear profile as shown in Figure 6-6 (c) reveals that an extrusion with an extremely low extrusion ratio (ER = 2.16) fails to produce a satisfactory result. The whole extrudate structure was distorted due to insufficient induced plastic work. Thus, it was excluded for further investigation.

(a) (b) (c)

Figure 6-6: Condition of extrudates after hot extrusion through the dies of: (a) spur gear geometry (ER = 4.86), (b) rectangular geometry (ER = 11.22), (c) large spur gear geometry (ER = 2.16)

6.7.4 Evaluating the Bond Strength

The tensile tests were performed to determine the experimental weld strengths before comparison with the predicted strengths can be done. The tensile tests were conducted at 298 °K (room temperature), with a crosshead speed of 0.05 mm/sec, and detailed procedure is briefed in Section 3.2. Long continuous small spur gear and rectangular profiles, as shown in Figure 6-7 (a) and (b), were cut to 100 mm length. The gear profiles were turned while the rectangular profiles were milled to the dimensions according ASTM-E8 M sub-size [105] and when pulled, the welded areas experienced

only a tensile force. The crosshead of the tensile machine was properly aligned to ensure failure occurs in tension mode with minimal samples' rotation. Approximately two-third of each sample's grip area were clamped to the machine. Results from the tensile tests could be distorted and invalid if slippage took place. Then, the top crosshead moved vertically upwards after the machine switched on. The top crosshead displacement was moving continuously until the sample failed. The cross section within the gage length was taken as a nominal bonded area. Analysis of the failure mode on each sample was made using Scanning Electron Microscope (SEM) images while the weld lines assessment were carried out to identify the quality of bonding. Figure 6-7 (c) shows a large spur gear profile that was sliced to small length and polished. It can be easily seen that many defectives gear teeth have been produced after the extrusion process. This indicates that the extrusion ratio of lower than 4 was not suitable to produce a complex-shape extruded profile, similar to suggestion by Chiba et al. [12].

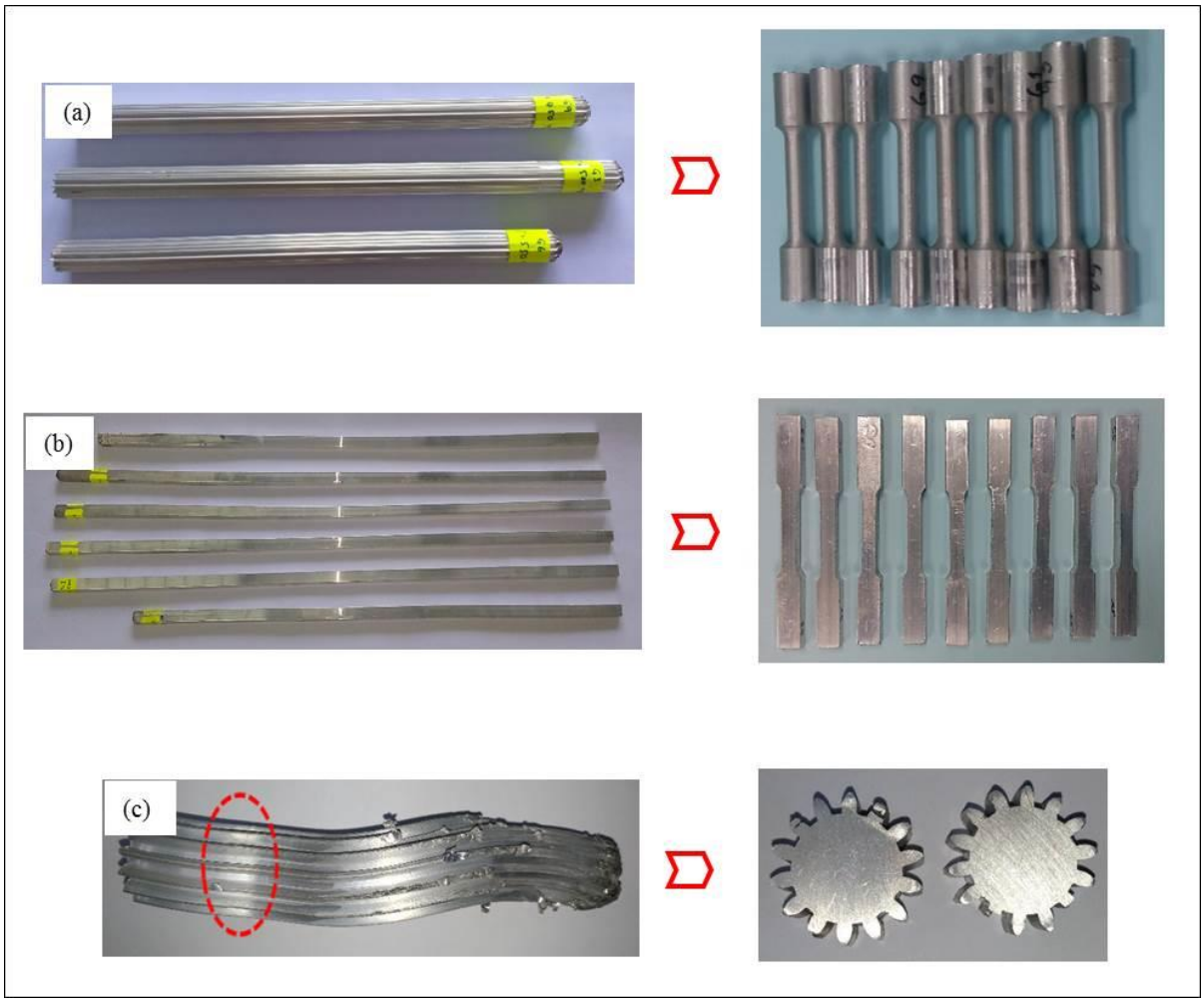

Figure 6-7: Extruded profiles converted to tensile samples (a) Spur gear (*ER* = 4.86) cut to cylindrical dog-bone, (b) rectangular shape (*ER* = 11.22) cut to plate dog-bone; (c) extruded profile of large spur gear (*ER* = 2.16) cut to gear shape

6.7.5 Setup for Finite Element Simulation

In order to predict the weld strength via the deduced model, the deformation-related variables such as strain, normal contact stress, shear stress, and flow stress experienced during the weld creation must be established. This was realised by carrying out finite element simulations for each physical experiment. The deformation variables used to calculate the predicted weld strength in Section 6.8 were retrieved during the steady

stage only. It is postulated that a stable process reveals a maximum effective stress in each experiment. Finite element simulations were conducted using Deform 3D v11.0, implementing as an implicit time integration analysis. Each aluminium billet was modelled as a 3D plastic material and meshed using an approximately 200,000 3D tetrahedral elements with one point integration.

Adaptive meshing was used to accommodate large strains and also to avoid an excessive element distortion during simulation. All tools were set as a rigid body, and setup for the finite element model is given in Figure 6-8. The aluminium material was assumed to follow a von Mises material with isotropic hardening. All flow stress curves used for simulation were retrieved from Deform 3D library and ref. [109]. The flow curves in general corresponded to the Eq. (3-15) in Section 3.5.2. Since friction affects the simulation accuracy, an appropriate coefficient of friction between billet-container and die's bearing surface-extrudate must be applied so that the finite element analysis accurately simulate the deformations. The rough surface that commonly encountered on the chip-based billet generates a very high friction between the billet and container when both are in contact. Details of the simulation settings are given in Table 6-5.

Table 6-5: Parameters setting for 3D finite element simulations

Parameter	Value/Type
Billet material	AA6061
Ram, container, & die materials	H-13 tool steel (set as rigid body)
Element type	3D Tetrahedral, 1 point integration
Billet temperature	450°C, 500°C, 550°C
Tools temperature	300°C
Heat transfer coefficient	5 (N/sec/mm/°C)
Ram speed	4.4 mm/s
Friction (billet/container)	Shear type, μ = 0.95 (Adhesion was considered between billet and container since no lubricant was applied)
Friction coefficient (bearing)	Shear type, μ = 0.85 (Minimum lubricant was applied at entrance of bearing land)

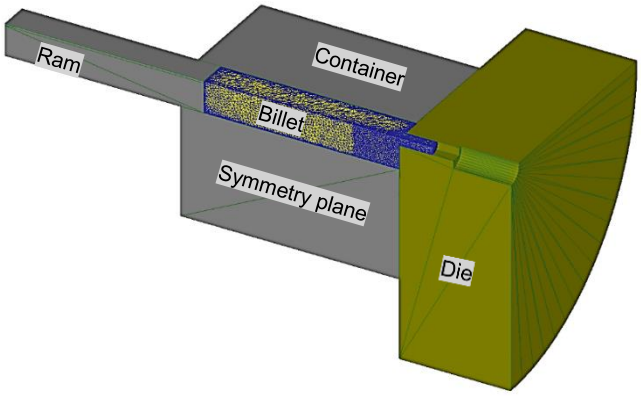

Figure 6-8: Finite element model for aluminum alloy extrusion, simulated as symmetric plane

6.7.5.1 Stages in Hot Extrusion Process

Figure 6-9 shows progression of hot extrusion process simulated through the Deform 3D software. The initial load increases rapidly in the beginning as the billet upsets to fit the container. The pressure increases further to cause a long displacement within the upsetting stage, then rose sharply during the unsteady extrusion stage. In this stage, the heterogeneous structure is formed with dislocation and subgrain density accumulated progressively in the die region. Finally, it reaches the peak pressure region during the steady extrusion stage.

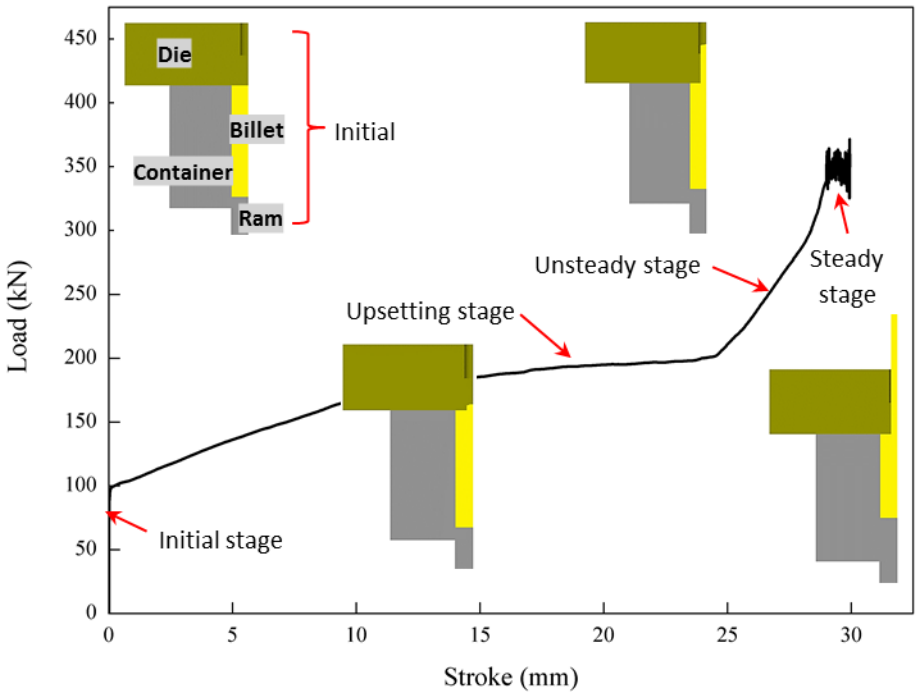

Figure 6-9: Hot extrusion stages (Temperature = 500°C; Die = rectangular geometry)

6.7.5.2 Accuracy Checking of Simulations

Prior to retrieval of the deformation variables, several checks were performed to confirm the accuracy of the simulations. By comparing the results of load versus stroke curves as given in Figure 6-10 between the simulated and experimental results, final validation of the simulations was made. Two curves of load against stroke were plotted over different profile geometries for extrusion at 500°C. As can be seen in Figure 6-10, the simulated and experimental results are in agreement within a maximum error of 6 – 15 %. The experimental value was slightly larger than the simulated value, which could be explained by the two main sources of error: the temperature drop and friction conditions. Throughout all experiments, the billets experienced a temperature drop during the evacuation process from furnace into container, prior to extrusion. On top of that, the die that on contact with the body of the extrusion machine dissipates heat too, thus the temperature drop is getting worse. Meanwhile the FE simulations performed in each case were assumed in an isothermal. Therefore, the coefficient of interfacial heat transfer between the container, die and billet can be only accurately determined by simulations rather than experiments. The flow stress is inversely proportional to the temperature. As the temperature dropped, the resulting flow stress and extrusion force increased, leading to the fundamental reason of load data deviations between the experimental and simulation.

Moreover, the coefficients of friction in the FE simulations were taken 0.85 for die and billet, while 0.95 for billet and container. A very thin lubricant was applied at the die entrance to reduce a poor bonding quality. Applying an excessive lubricant covering on a large surface area of chips greatly hamper bonding between them. The absolute

friction between the billet and container could be higher than the value set in simulation. A rough surface in nature encountered on the chip-based billet (see Table 3-4) could generate a stick-slip condition. A larger friction coefficient increases the friction force, leading to the main discrepancy between the experimental and simulated extrusion force.

The validity of the simulation results were also examined qualitatively by comparing the profile fronts obtained from the experiments and simulations as shown in Figure 6-11. The experimental profile fronts were measured by Dino-Lite Digital Microscope. Although the profile front geometry was not included during the tensile test due to very poor welding quality encountered in each experiment and was excluded during the numerical simulations (because in the state of unsteady stage), but it can be observed that the sizes and shapes of the both extruded profile fronts are in good agreement with the experimental results. Therefore, according to both results in Figure 6-11, the accuracy of the numerical simulation results have been justified to be further used in subsequent analyses.

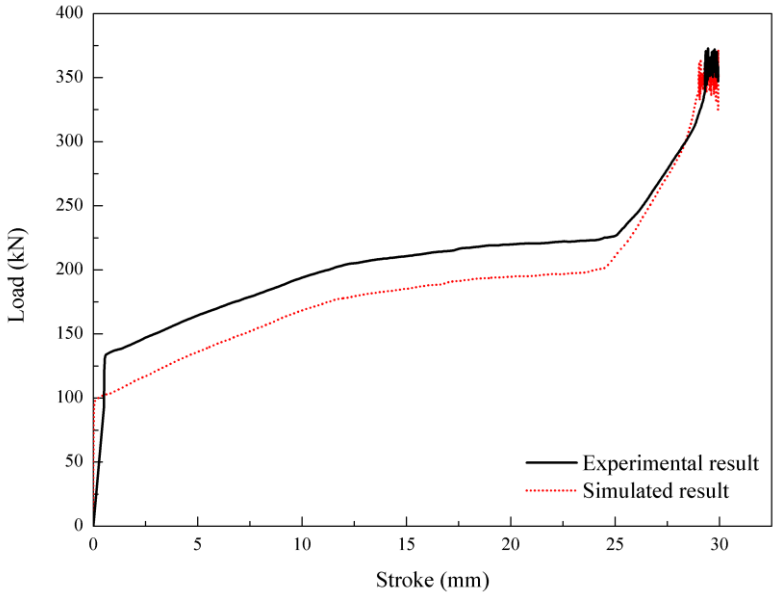

(a)

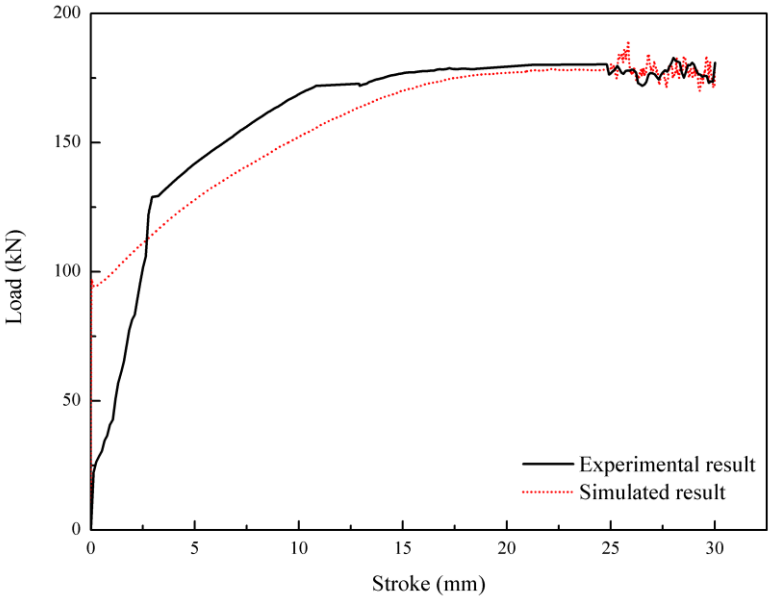

(b)

Figure 6-10: Simulated and experimental load vs. stroke curves for extrusion performed at 500°C: (a) Rectangular die, (b) Spur gear die

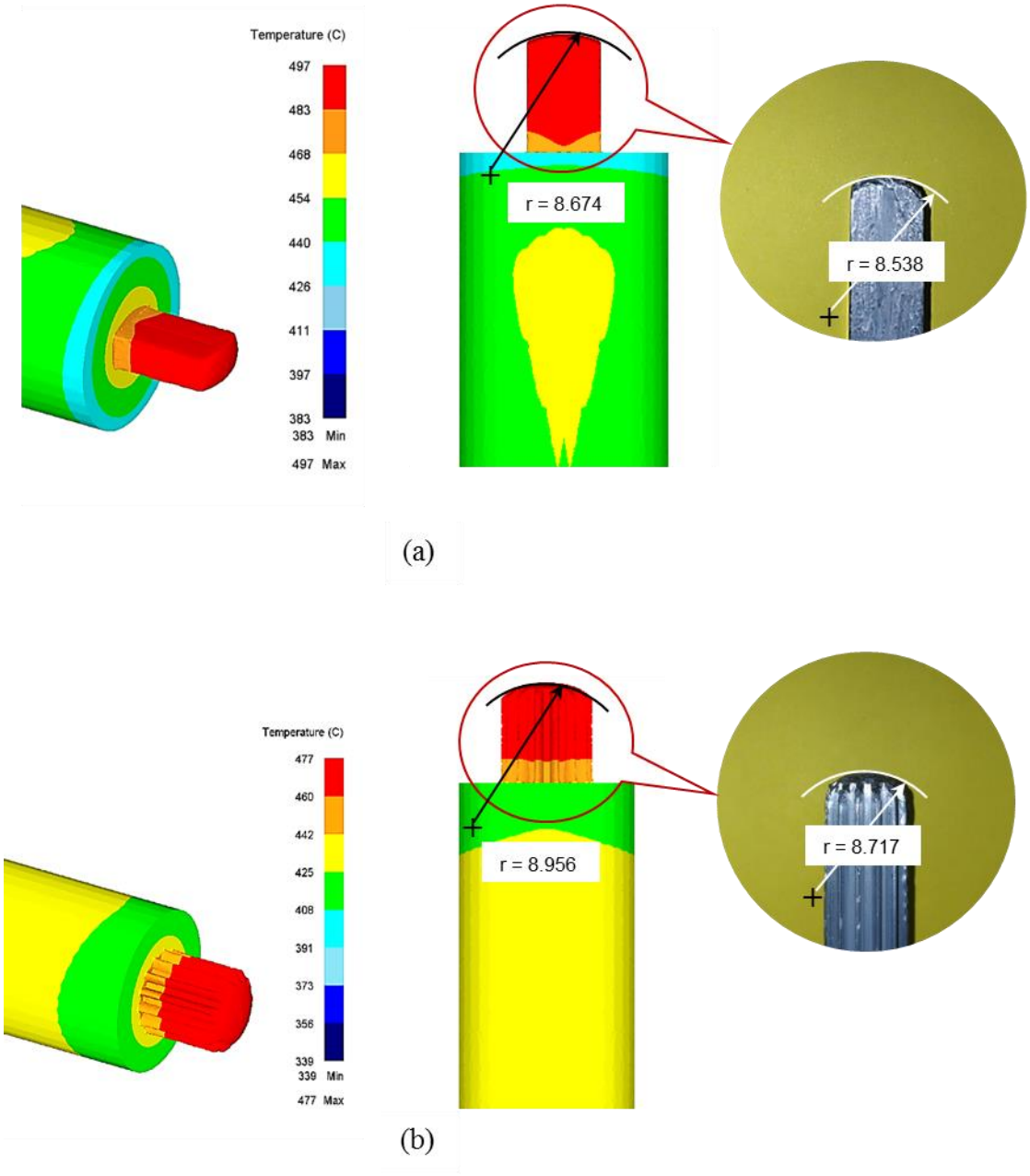

Figure 6-11: Comparison of profile fronts obtained from the experiments and simulations for different profile geometry, extruded at 500°C (all unit in mm): (a) rectangular geometry and (b) spur gear geometry

6.8 Results

This section presents the results of the experimental tensile tests on solid-state welds created under the various temperature settings. The measured tensile bond strengths are compared with those predicted by the newly developed model, Eq. (6-22).Table 6-6 presents the parameters used in the new model with their definitions. The new model predicts solid-state weld strengths as a function of temperature on different extruded profiles.

Table 6-6: Parameters used to predict the tensile strength

Symbol	Parameter						Definition
	G_{A450}	G_{A500}	G_{A550}	R_{450}	R_{500}	R_{550}	
$*Y$ (MPa)	69.540	62.639	54.087	32.270	28.757	26.069	Aluminium flow stress
$*\sigma_n$ (MPa)	87.458	91.879	115.552	42.831	56.069	52.503	Normal contact stress
$*\tau_{app}^2$ (MPa)	290041.783	111462.797	13831.254	37656.840	4317.255	2990.047	Shear stress
$*Ry$ (N)	1018.716	947.281	817.203	732.983	627.726	586.068	Total force in Y direction
$*Fy$ (N)	1008.478	937.761	808.990	669.616	573.459	535.402	Component of force in direction parallel to shear area (Y direction)
v	0.439	0.439	0.439	0.439	0.439	0.439	Fraction of the final contact area without a protective oxide layer
p_{ex} (MPa)	63.487	57.187	49.380	29.461	26.254	23.800	Pressure required to micro-extrude the substrate aluminium through the cracks
σ_0 (MPa)	130	130	130	130	130	130	Nominal strength of the bulk aluminium (σ_0), AA6061-O
TS_{rd} (MPa)	4.449	10.728	13.012	4.719	11.378	13.801	Tensile bond strength recovery

							due to diffusion mechanism
A_{shear} (m^2)	0.001873	0.002809	0.006879	0.003451	0.008728	0.009791	Area of shear generated on billet, near to die entrance
θ (°)	8.13	8.13	8.13	24	24	24	Angle of force component in Y direction
η				0.121			Fraction of surface oxidized by the entrapped air
[b] r (μm)				2.422			Square root of asperity height of chips
[b] ψ (°)				0.11			Asperity inclination angle
T (K)				298			Room temperature
[a]σ_{oxide} (MPa)				≈ 260			Tensile strength of oxide fragments
k (MPa)				≈ 37			Aluminium shear flow stress
[a] t_c (nm)				≈ 10			Thickness of oxide fragments
λ (nm)				≈ 140			Length of oxide fragments
ε				1			Engineering strain
σ_{TS} (MPa)	174.252	200.018	206.696	163.786	178.618	181.021	Predicted tensile bond strength
TS_{exp} (MPa)	[157.888, 151.491, 154.599]	[181.101, 182.405, 177.361]	[188.205, 177.968, 176.789]	[150.378, 144.149, 129.676]	[138.486, 150.538, 131.453]	[145.18, 156.113, 130.051]	Experimental tensile strength
Error (%)	10 - 15	9 - 13	9 - 17	8 - 26	18 - 36	15 - 39	Comparison between predicted and actual strength

Note: The parameters with symbol '' were retrieved from the finite element simulations*
: [a]Strength of oxide and thickness were taken from refs. [127] and [128]
: [b]Roughness parameters were measured using a confocal imaging profiler

Figure 6-12 presents the experimental and predicted tensile strengths for temperatures ranging from 450 °C to 550 °C. The results show that the tensile bond strength are very sensitive to temperature, with the strength increased to maximum 19 % for the gear geometry and 11 % for the rectangular geometry, from 450 °C to 550 °C of extrusion temperature . The model predicts fairly accurate the strength recovery of the extrudates from chips and gives a satisfactory agreement with the experimental results. Nevertheless, it overestimates with higher degree of errors for tensile strength of the rectangular geometry, extruded at 500 °C and 550 °C, respectively. The majority of gear profiles revealed a slightly higher tensile strength compared to rectangular profiles. These correspond to higher flow stress, normal contact stress, shear stress and total force generated during the hot extrusion process as given in Table 6-6. According to Cooper and Allwood [80], the threshold strain decreases with an increase in normal contact stress, temperature, or shear stress, and hence leading to the strength enhancement of any welds. While higher shear stresses at the chips' interface causing the length of oxide fragments stretches further to expose more virgin metal which contributes to better weld bonds.

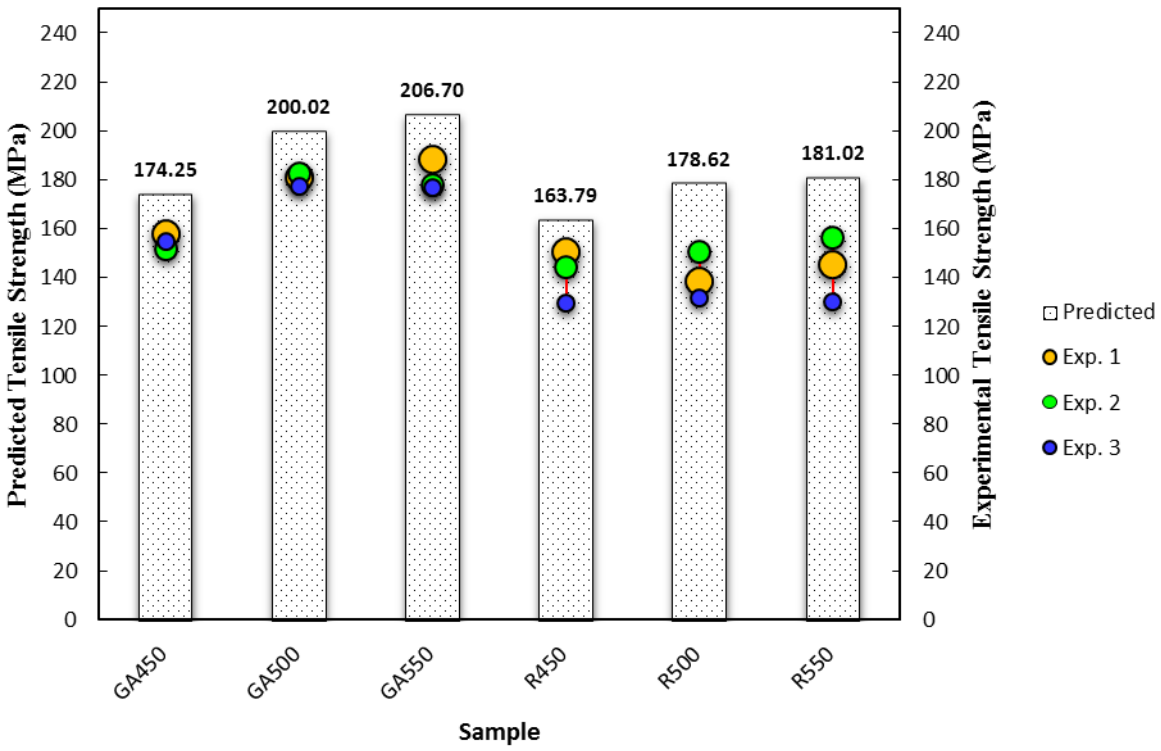

Figure 6-12: Tensile bond strength of between prediction and experiment, subjected to various process temperatures and die geometry

6.8.1 Stress-strain Relationship

The influence of extrusion temperature and die geometry on the tensile strength of extruded profiles was analysed by plotting true stress versus true strain curves from the results of uniaxial tensile tests and presented in Figure 6-13 (a). It can be clearly seen that the tensile strengths vary slightly for different die geometry and temperature. The variation range of the tensile strengths for gear extrudates is 150 - 190 MPa, and the variation range of the tensile strengths for rectangular extrudates is only 130 - 160 MPa. However, the maximum strains before breaking obviously revealed that the rectangular geometry is superior to the gear geometry which ranges from 37 - 39 % compared to 26 – 32 %, respectively. The ductility of the extrudates are increased with the increase

of extrusion ratio. The extrudates with the higher extrusion ratio always exhibit a better ductility than those extruded with the lower extrusion ratio for a given similar temperature.

Figure 6-13 (b) shows fracture morphologies of each sample for rectangular and gear profiles after the tensile test, examined by SEM. Macroscopic observations show some of the samples exhibit cleavage plane mixed with the small equiaxed dimples. Samples shown in Figure 6-13 (b) for rectangular profile consistently exhibit predominant ductile characteristics with small conical equiaxed dimples and without cleavage. Also, samples of gear profile, extruded at 500 °C and 550 °C revealed brittle and ductile fracture mechanisms consisting of microvoids and cleavage fracture. The brittle mechanism fracture could be the main reason of ductility inferior as compared to rectangular profile samples. It was postulated that the shape of the dimples on fracture surface was determined by the level of induced stress [129]. Furthermore, Den Bakkera et al. [130] show that in the solid-state bonding, the degree of atomic bonding on the coalesced interfaces of weld seams on fracture surfaces determines the size and depth of the emerged dimples which also responsible for the ductility of the extruded profiles.

The higher strength recovery on the gear geometry profiles in this study could be attributed to the presence of large and deep dimples on each sample as seen in Figure 6-14, implies that the atomic bonding among the chips is excellent. Besides, the level of induced normal stress and shear stress are also higher than that of rectangular geometry profiles, as given in Table 6-6. According to Shen et al. [131], a large and deep dimple represents a strong atomic bonding and superior ductility while vice versa for a small and shallow dimple. On the other hand, if appearance of the cleavage plane

is apparently visible in any fracture surfaces, this shows a sign of brittle fracture. The observed samples of G_{A500} and G_{A550} yield a scatted cleavage plane throughout the fracture surfaces. Therefore, it can be concluded that the G_{A500} and G_{A550} samples experienced a lower ductility when compared to samples R_{450}, R_{500} and R_{550}. The size and shape of dimples in all samples for the rectangular geometry, shown in Figure 6-14, are slightly smaller than that of gear geometry samples with non-existent of cleavage observed. Therefore, this condition could be used to describe the reason of superior ductility encountered in all rectangular geometry profiles.

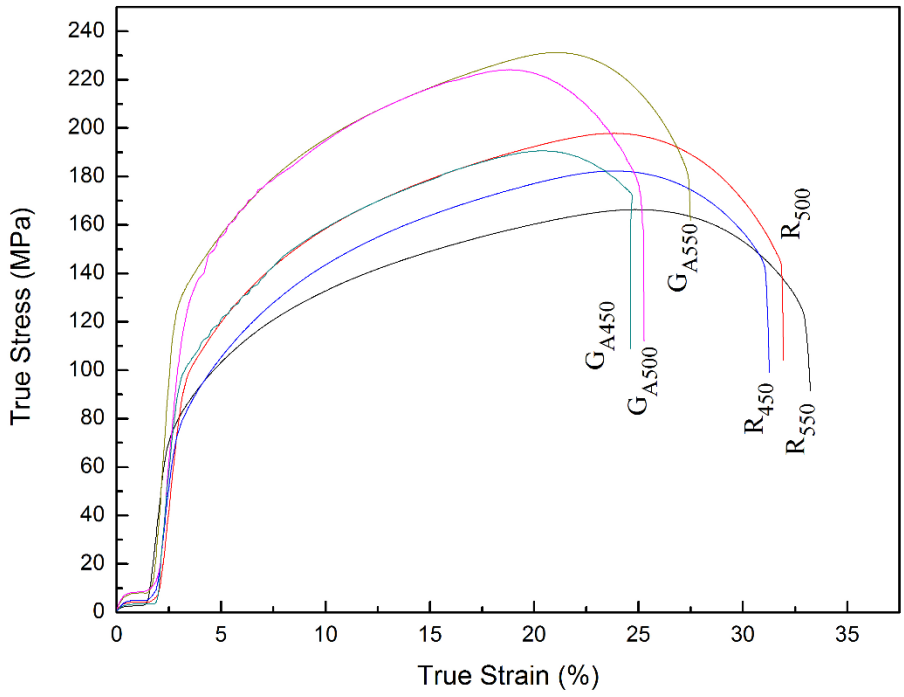

(a)

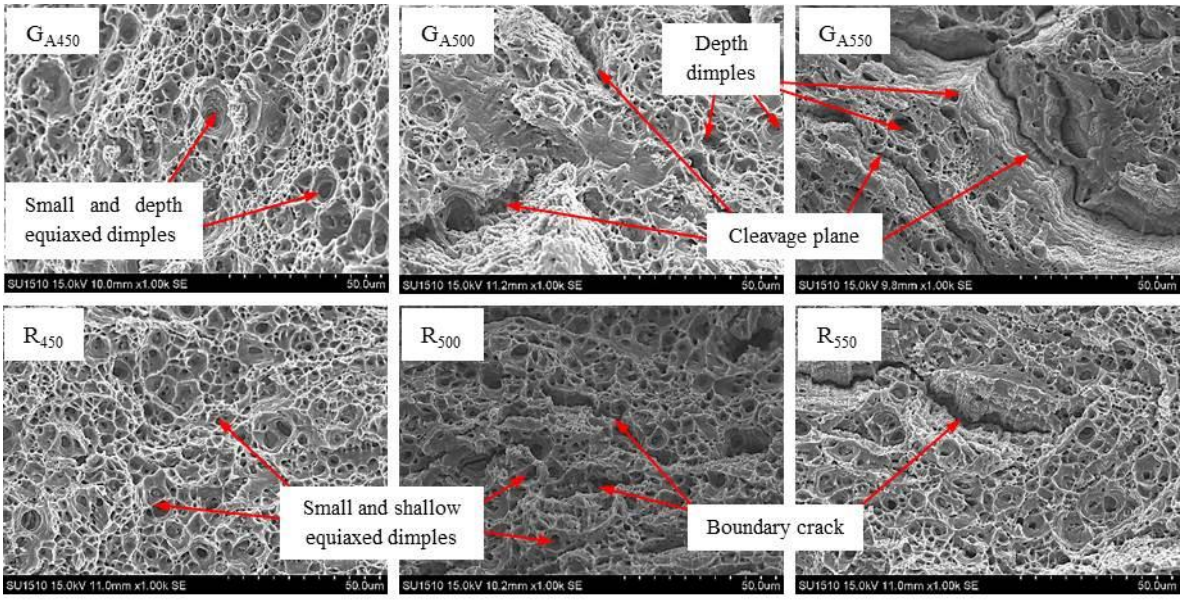

(b)

Figure 6-13: (a) True stress vs. true strain of each tensile sample; (b) Fracture surface of each sample examined by SEM (x 1.00k magnification)

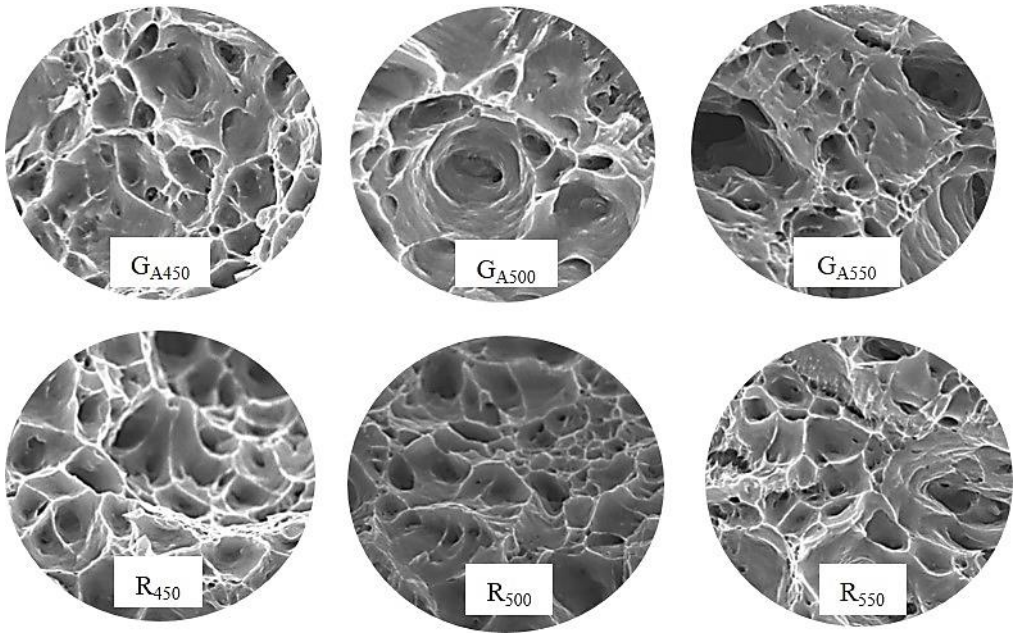

Figure 6-14: Morphologies of the fracture surface on each sample, examined by SEM (x 2.00k magnification)

6.8.2 Microstructural Evolution

The analysis of microstructural evolution becomes important in the investigation of the welding mechanism in hot extrusion of the recycled chips. The remaining butt end with approximately 22 mm length from the extruded profiles were cut for the microstructure analysis. This discarded butt was then taken out from the container and sectioned for microstructure analysis. Method of sample preparation for microstructure examination is clearly described in Section 3.4. Figure 6-15 shows the microstructure images of butt end with important observed regions are marked for sample extruded at 500 °C through the gear geometry die, captured by LOM. Furthermore, Figure 6-17 shows the butt ends of other samples sectioned to examine the element contents of the selected spots. As can be clearly seen in Figure 6-15 (Image C), the boundaries of the compressed chips

at the container side are visible in white colour. The emergence of shear plane in the vicinity of the dead metal zone is represented in Image B and D. The grain boundaries of the un-deformed extrudate are collapsed, and pinned together within the deformation zone before its shape is permanently altered. Most of the grains experienced recrystallization and grain growth within the deformation zone under the effects of normal forces, shearing forces and temperatures. As can be seen in Images B and D (Figure 6-15), as soon as the billet approaches the deformation zone, the chip grain boundaries were gradually elongated before completely being transformed into long continuous chip boundaries with noticeable fine weld lines. This is due to the fact that many oxide layers are broken down to form fine oxide fragments as shown in Image F (top) of Figure 6-15. It is believed that the oxide layers are completely collapsed and their original positions are rearranged upon leaving the shear plane. The fragmented oxide layers are distributed evenly within the extruded structure and many weld lines exist as a result of good chip welds.

The SEM image in Figure 6-15 (E) has proven that the compressed chips at the upsetting stage still contained larger oxide strings, apparently between the adjacent of each chip boundary. The existent oxide strings are a sign of not welded aluminum layers [41]. One can postulate that the metallurgical bonding of chips is very poor before entering the shearing zone. The conditions of oxide layers between chips within the shearing zone are in the state of continuously broken down and porosities are vanishing which can be determined by the SEM-EDS analysis. The evolution of oxide layers and porosities can be seen by comparing the SEM micrographs in Figure 6-15 (E) and Figure 6-15 (F) in which the porosities after extrusion did not exist. The results of EDS

analysis as given in Table 6-7 consistently revealed higher oxygen content by weight percentage in Region C (billet region) instead of Region A (extrudate region) of each sample. Even inspection on the oxygen content by EDS which covers a wider area for Region A compared to smaller area of Region C as depicted in Figure 6-16 (a and b), the resulting oxygen element is still low in Region A. This confirmed that Region C has high oxygen density, applicable on the billet just before its passes the shearing zone. This can be further supported by the bar charts presented in Figure 6-16 (d and e) where the oxygen element is substantially reduced after the extrusion. The level of oxide contamination before and after extrusion has a considerable effect and that can describe the level of mechanical strength enhancement.

Higher shear force, acting along the shear area in the case of extrusion through the gear geometry die results in an improved breaking down of the oxide layers into small fragments, and hence homogeneously distributing them. The homogeneous distribution of the oxide fragments permits more virgin-to-virgin metal be on contact to promote a better welding. The presence of oxide layers within the chip boundaries are found impinging the grain growth caused by the diffusion and induced normal pressure in the die bearing (see the magnified Image F in Figure 6-15). Humphreys and Hatherly [132] also observed and discussed this phenomenon in their findings. The shear force breaks the oxide layers to small fragments and promotes contact in between metal-to-metal to establish, allowing some grains to grow over the region of collapsed oxide layers and some restricted from growing by the finely broken oxide particles that took place between the newly formed grain boundaries.

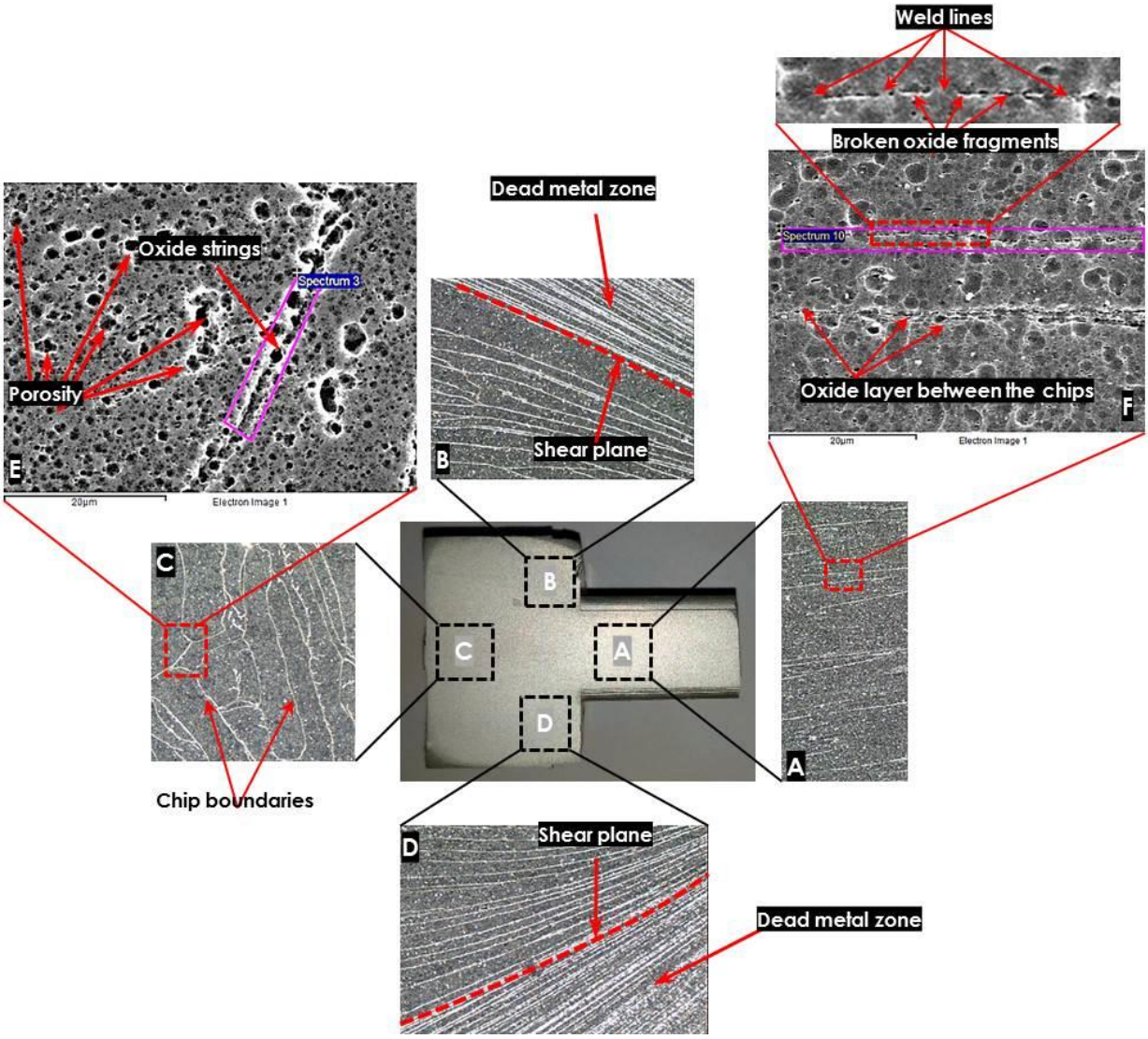

Figure 6-15: Images from different spots of the discarded butt end from gear geometry profile, extruded at 500 °C (Sample G_{A500})

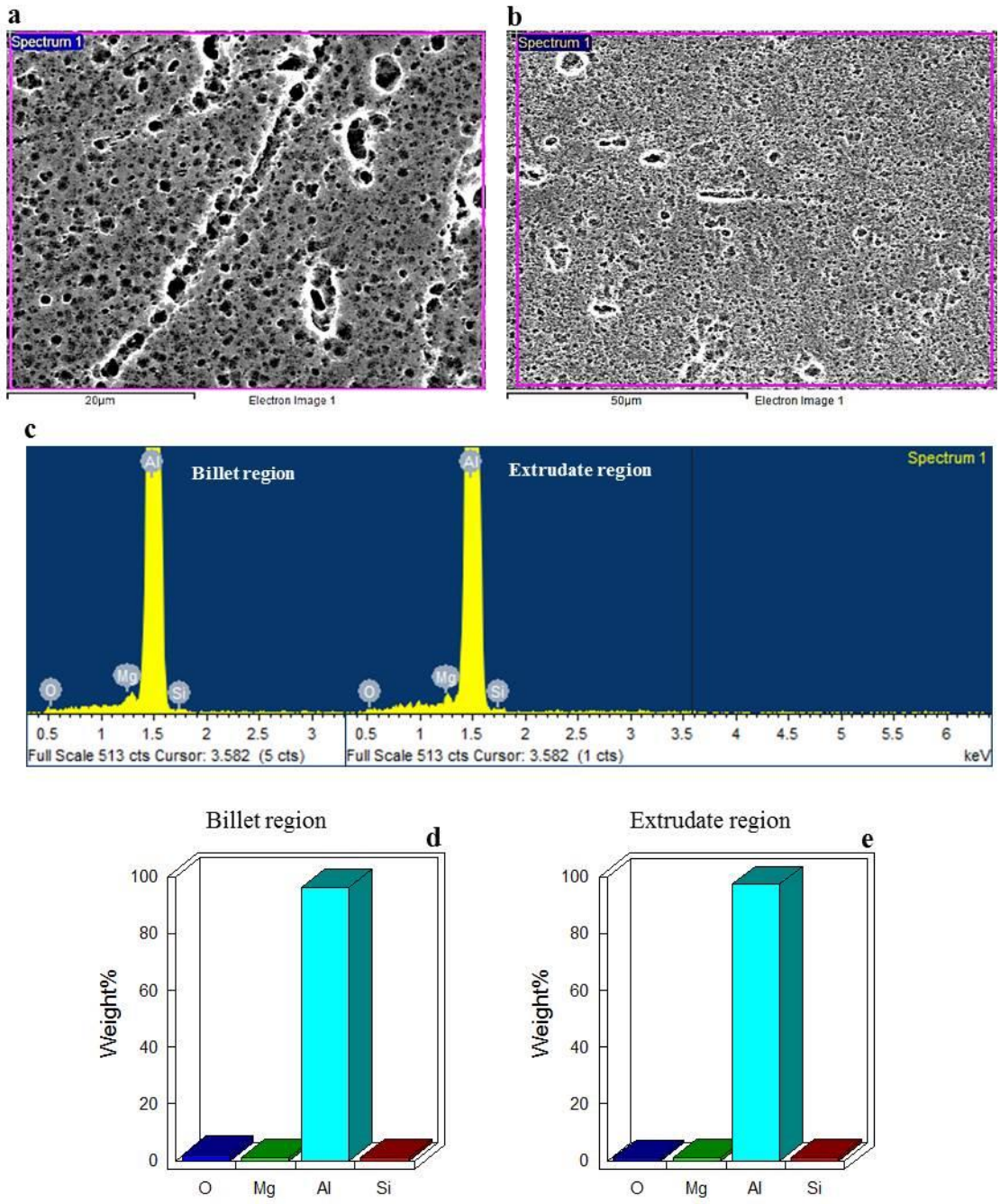

Figure 6-16: SEM micrographs of the butt end for sample GA500 (a) billet section (area in image C, Figure 6-15), (b) extrudate section (area in image A, Figure 6-15 (c) the distribution of oxygen on the selected spots and (d and e) weight % of elements on the billet and extrudate regions

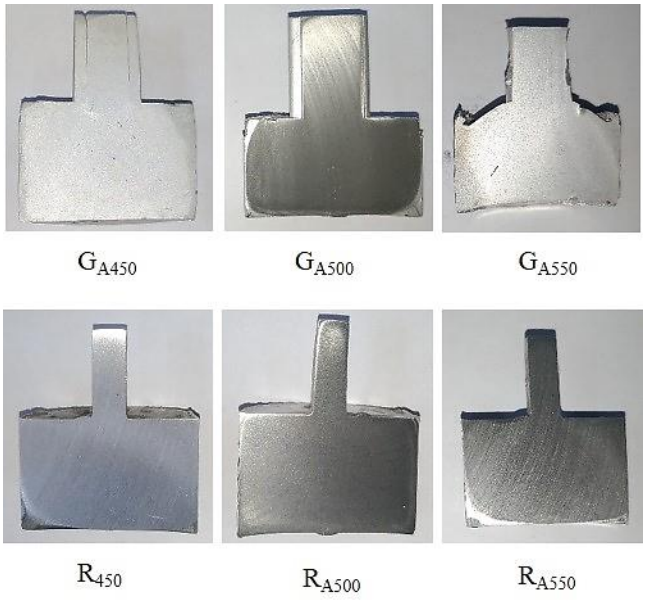

Figure 6-17: Sectioned butt ends of other samples for SEM-EDS analysis

Table 6-7: The distribution of oxygen for the scanned spots as shown in Figure 6-15 (A) and (C) of all samples (average data of 3 scanned spots)

Sample Notation	**Temperature (°C)**	**Die Geometry**	**Oxygen Element (by Weight %)**	
			Region C	**Region A**
G_{A450}	450 °C	Spur Gear	2.00	1.62
G_{A500}	500 °C		2.10	0.89
G_{A550}	550 °C		2.20	1.30
R_{450}	450 °C	Rectangular	1.22	0.88
R_{500}	500 °C		2.89	2.29
R_{550}	550 °C		2.54	2.27

6.8.3 Discussion

The proposed model is fairly accurate in predicting tensile strengths as shown by results in Table 6-6. The final tensile bond strength equation, σ_{TS} integrates the model that was initially derived through the thin film theory and diffusion theory. The authors [80] who built the weld strength model on the basis of film theory and evaluated by the corresponding shear strength of the bonded AA1050 sheets have successfully proved that the developed model followed the film theory of bonding.

They compared the micrograph obtained in their study (Figure 6-18 (a)) with the TEM micrograph obtained by Barlow et al. [121] (Figure 6-18 (b)) and postulated that the resulting regions of good bonding are likely to resemble those found by authors in [121]. Despite the observed fragment lengths obtained by authors in [121] covering a wider area, the magnitude is of the same order as predicted by Eq. (6-7) which is within 140 nm. This proves that the proposed model with the assumed mechanisms (as in the thin film theory of bonding) is valid.

The SEM micrographs shown in Figure 6-19 (a) and (b) also revealed similar patterns where the islands of oxide fragments can easily be seen distributed along the welded interface. It proved the validity of the thin film theory of bonding mechanisms applied in the case of hot extrusion of chips. At higher extrusion temperature of 500 °C as shown in Figure 6-19 (a), the broken oxide fragments mostly exhibit size smaller than 300 nm length, and the oxide fragments end is difficult to identify due to their finer morphology, even at higher magnification than that of Figure 6-18 (a). While at lower extrusion temperature of 450 °C as depicted in Figure 6-19 (b), the oxide fragments are

broken to the size less than 500 nm. According to the film theory of bonding, the emergence of cracks along the stretched weld line interface are could be either due to the oxide fragments or due to the failure of establishing close contact in between the surfaces in these regions during bonding.

The weld strength model built by Cooper and Allwood [80] underestimates the weld strengths for temperatures 423 °K and 473 °K. The model predicted the weld strengths in better accuracy for temperature lower than 423 °K as shown in Figure 6-20 and most likely at higher temperatures, the model underestimated the influence of strain-rate. These findings implied that the diffusion significantly affects the bonding process. This led to the development of diffusion-strengthening model, to encompass the effect of temperature on the tensile bond strength recovery. It is found in [80], over the higher temperatures of 423 °K and 473 °K , the average shear strength was dropped between 25 % – 35 % due to an increase in the strain-rate. In this study, the tensile bond strength model overestimated tensile strengths of sample R_{500} and R_{550}, both extruded at higher temperatures as shown in Table 6-6. This could be also due to the effect of strain-rate on the extruded profiles in which the time contact between billet and die is reduced. Diffusion relies on time as given in Eq. (6-20) and as the contact time is reduced due to the massive material flow at higher rate, the diffusional transport matter is minimised thus affecting the final weld strengths. Moreover, an estimation method that was used to calculate the formed undefined shearing area on the butt end contributes to an error in the calculations. The diffusion theory can explain high temperature solid-state bonding, while the film theory of bonding can be best describing the solid-state bonding at low temperature.

The model presented in this work is built on the basis of Cooper and Allwood [80] work. The authors in [80] using the film theory of bonding mechanisms tested the model by flat rolling experiment. The current model is more comprehensive in predicting the strength of solid-state chip welds because the effect of diffusion phenomenon was included. Nevertheless, it is applied in different contact of application, thus the accuracy of both models cannot be compared. The proposed model is used to predict the weld strength of solid-state chip welds and evaluated through the tensile strength test while model in [80] is used to predict the weld strength of solid-state bonding of aluminium sheets and evaluated via the shear strength test. The validity of the shear strength model in [80] is evaluated by decoupling the strain, strain-rate, normal contact stress, temperature and shear stress while the new model is unable to decouple all those parameters due to the complexity of hot extrusion process. Several parameters such as temperature, extrusion ratio and die design were varied in the current experiments. Variables such as normal stress, shear stress and flow stress corresponded to the temperature and extrusion speed settings, and only can be determined via the FE simulation work in the case of extrusion process.

The model in Eq. (6-22) is particularly useful to predict the weld bonds quality of the solid-state recycled aluminium chips via the hot extrusion process. It can be further applied in hot forging process for direct aluminium recycling. Although the solid-state recycling through the hot extrusion offers a tremendous improvement in terms of energy consumption and environmental conservation, not all operating variables related to die design, extrusion ratio and operating regimes can be completely understood from purely experimental work. Therefore, to completely understand the influential

variables, an analytical model that allows prediction of the weld strength recovery of directly recycled materials is required. This important to ensure that the recycled product meets the expected strength and functioned satisfactorily during its useful service life. After the reliability of the deduced model has been tested under several conditions, the model was found to provide some underlying accuracy. However, the degree of relative accuracy is varies for different part geometries.

Based on the experimental findings, the gear profile shows greater strength when compared to the rectangular profile even though the extrusion ratio of rectangular profile is more than twice of the gear. Many postulated that good quality bonding of direct recycled chips is closely related to high extrusion ratio [23, 60, 61]. However, this principle does not work on the gear profile. It could be the broken oxide layers are more efficient on the gear profiles due to higher shearing forces generated in shearing zone leading to distribution of homogeneous oxide particles (Refer to results in Table 6-6). Moreover, the increase in normal stress in the die during steady state extrusion compared to effective stress resulted in an improved welding of the chips. Finer and an intricate tooth shape on the gear die creates a flow resistance and therefore generates large back pressure. To overcome the back pressure, more forces are drawn and subsequently increase the shear stress in the shearing zone, breaking more oxide layers to facilitate the welding of virgin metals. An excessive back flow in extrusion of gear profiles delayed contact time between die and chips, thus diffusion was prolonged to create sound weld bonds. Large plastic deformation generated due to large pressure and shearing action also helps to improve surface diffusion on the bonded interfaces of chips.

As the process temperature increases, the diffusion mechanisms are found increased as demonstrated by the results in Table 6-6. It is known that aluminium and its oxides are mutually insoluble [93], therefore, diffusion is likely to take place if contact between virgin-to-virgin metal that is absent from the oxide layers is established. Since the oxide particles are very hard and give hurdles to bonding, the fragmentation of the oxide particles to extremely fine would be desirable in the solid-state recycling. The strength recovery due to diffusion mechanism in the solid-state recycling can be best explained by the theory of diffusion mechanism of the void closure. According to Derby and Wallach [133], there are two sources of surface diffusion in the diffusion mechanism of the void closure, mainly from surface and interface modes. The surface source diffusion is driven by the difference of surface free energy by means of surface diffusion and volume diffusion that occurs when the adjacent atoms on the surface of void are transmitted from the regions of larger curvatures to those with smaller curvatures. While, the interface source diffusion is driven by the chemical potential gradient by means of surface diffusion and volume diffusion, triggered when the adjacent atoms on the contact interface are transmitted to the void necks [134]. The surface source diffusion furthermore would not results in the change of void volume, but instead only results in the change of atom distributions on the void surface as postulated by Ma et al. [135].

Therefore, under the diffusion mechanism, the porosity reduction of the extruded profile as depicted in Figure 6-15 (F) is the manifestation of the void closure and the magnitude reduction of the volume of voids is determined directly by the interface source diffusion. With the higher temperature setting, the activation energy of diffusion

is reduced, and more atoms are transferred to the void necks. The presence of high pressure helps to reduce the distance travelled by the atoms hence led to the massive atoms departure which directly improved the weld bonds. Other studies on void closure due to diffusion mechanism action, some researchers advocated to quantitatively predict the volume evolution of void through the geometrical models, and some proposed the mathematical models of void closure [136, 137]. It is found that the previously developed void closure models are complex and a lot of assumptions made on the shape of void reduce the model's accuracy. Thus the models are impractical to make use in the solid-state recycling context. As reported by Cooper and Allwood [123], the atomic diffusion is obviously influenced by the factors of temperature, time and material. Therefore, the formulated model in Eq. (6-20) has successfully described the domain of the diffusion mechanism being studied as one of the most influential variables that contribute to the strength recovery of the solid-state recycled aluminium.

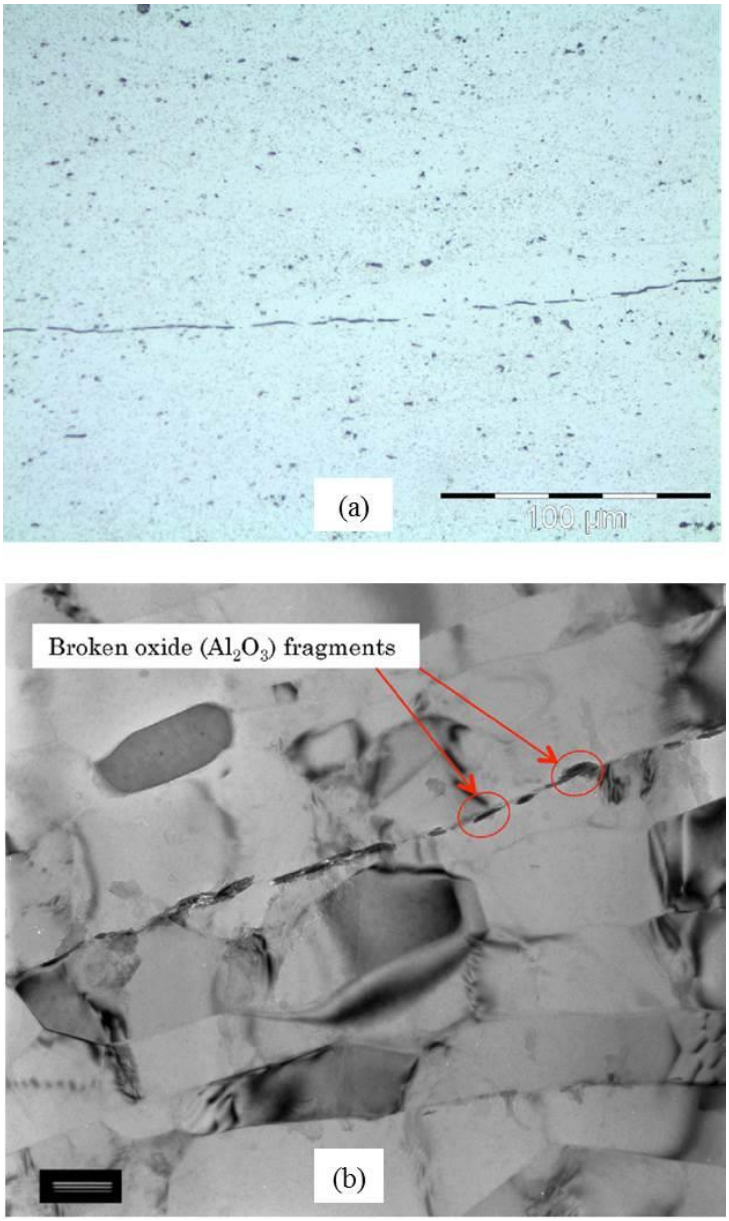

Figure 6-18: (a) Cross-section of welded interface created at 423 K (σ_n = 110 MPa, ε = 0.8) [80] and (b) TEM micrograph showing dispersion of Al_2O_3 fragments in a matrix of roll bonded AA1050 aluminium foil (Barlow et al. [121]). Scale bar is 0.2 μm. (Rolling direction ↔)

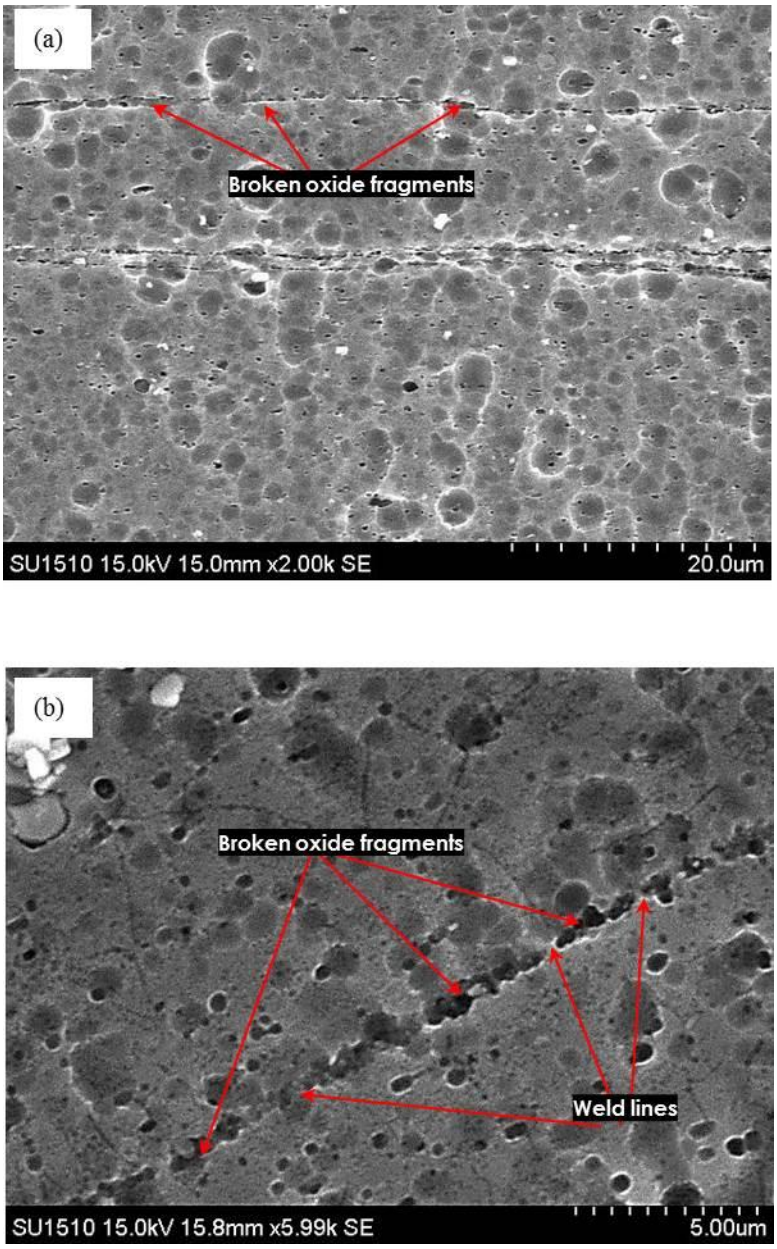

Figure 6-19: Welded interface at sectioned butt end (a) sample G_{A500} (Temperature = 500 °C) and (b) sample R_{450} (Temperature = 400 °C)

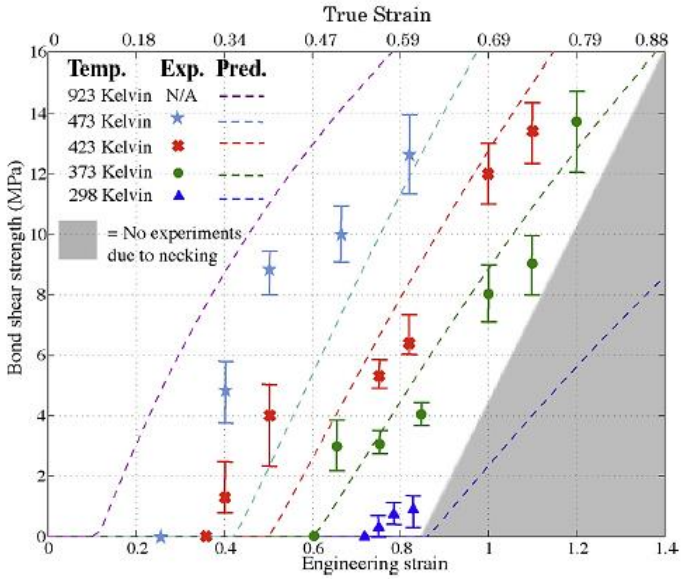

Figure 6-20: Effect of temperature on the shear bond strength (Conditions: Normal contact stress = 110 MPa, strain-rate = 0.03 s−1, interfacial shear stress = 0 MPa)

6.9 Conclusions

This chapter presents a detailed analytical study devoted to the modeling of a weld strength prediction of solid-state recycled aluminium chips through the hot extrusion operation. The governing equation of diffusion-strengthening mechanism is derived and integrated with the weld strength model deduced by the previous researchers [80]. All relevant deformation variables in the weld bond formation are thoroughly considered by the previously developed model. The adoption of the Fick's second law and an Arrhenius type of relationship provides a novel mathematical formulation to effectively quantify the diffusion-strengthening effect. While the Fick's second law was used to describe the fundamental relationship of tensile bond strength recovery with the process time, an Arrhenius relationship was used to correlate the tensile bond strength recovery rate with the activation energy and temperature. For validation purpose, a series of experiments have been conducted on the gear and rectangular extruded

profiles. The current model predicts the tensile bond strength recovery of gear profile within the errors of 9 % to 17 %, while for the rectangular profile geometry, the errors are within 8 % to 39 %. The calculated error percentage on the rectangular profile is slightly higher, and the main reasons could be due to the effects of strain-rate and inaccuracy in the shear area estimation. The developed model provides important guidelines to engineers when considering the solid-state recycling which allows them to correctly combine the deformation parameters with the extrusion ratio (reflected directly by the die design) that can result in an optimum weld strength recovery with the least trial.

CHAPTER 7 : HEAT TREATMENT

7.1 Heat Treatment

Producing alloys/composites by direct recycling usually yields a material performance that is slightly lower than the secondary production by remelting. It is important to know whether the chips that have been machined from bulk alloy could be heat treated to enhance its properties to be equivalent or comparable with higher alloy grade within the same class. For instance, it is interesting to know whether the chips from AA6061-T4 bulk aluminium (solution heat-treated and naturally aged) used in direct recycling can be heat treated to reach AA6061-T6 condition (solution heat-treated and artificially aged) or not. This possibility can only be revealed by conducting the heat treatment process on the chip-based extrudate. The heat treatment is used to enhance the properties of metallic materials and the desirable properties can be obtained through the microstructure changes.

The purpose of this study was to investigate the potential of enhancing the chip-based extruded gears made of AA6061-T4 (stock material used to produce chips) mechanical property to T6 performance. To the best of the author knowledge, there are no specific studies on this aspect previously reported. Optimising both solution and aging heat treatment to such alloys could reveal better secondary material performance. The heat treatment allows the alloys to be strengthened by the precipitation hardening mechanisms [138, 139]. As key process in this study, the T6 solution heat treatment and artificial aging were implemented over the chip-based extruded gears. The effect

of different aging time was studied to reveal its influences on the direct recycled AA6061-T4 alloy.

7.2 Procedure of Heat Treatment

After the extruded profiles in the form of gear (extruded from gear A) left the die, they were allowed to cool down for couple of hours before they were cut and ground to the length of 10 mm. Then, during solution heat treatment, the sample was heated to 530°C for 120 minutes to dissolve all alloying elements (single phase formed) before rapidly quenched into cold water at 100˚C/s (quenching rate) to achieve fast cooling. Distinct artificial aging times were implemented as a consideration of two important issues related to heat treatment which is the selection of temperature and the duration of aging treatment. Both are dependent on its previous chemical composition and heat treatment history [140, 141]. The entire parameters used in the heat treatment of gear profiles are given in Table 7-1. The temperature applied as a function of time for the heat treatment is shown systematically in Figure 7-1.

Table 7-1: Parameters of heat treatment at T6 condition

Parameter	Notation	Unit	Setting
Extrusion Temperature	T	ºC	450, 500, 550
Aging temperature	T_a	ºC	175
Aging time	t_a	minutes	240, 480
Temperature of solution heat treatment	T_{SHT}	ºC	530
Duration of solution heat treatment	t_{SHT}	minutes	120
Quenching rate	$(dT/dt)_q$	$^{\circ}Cs^{-1}$	100

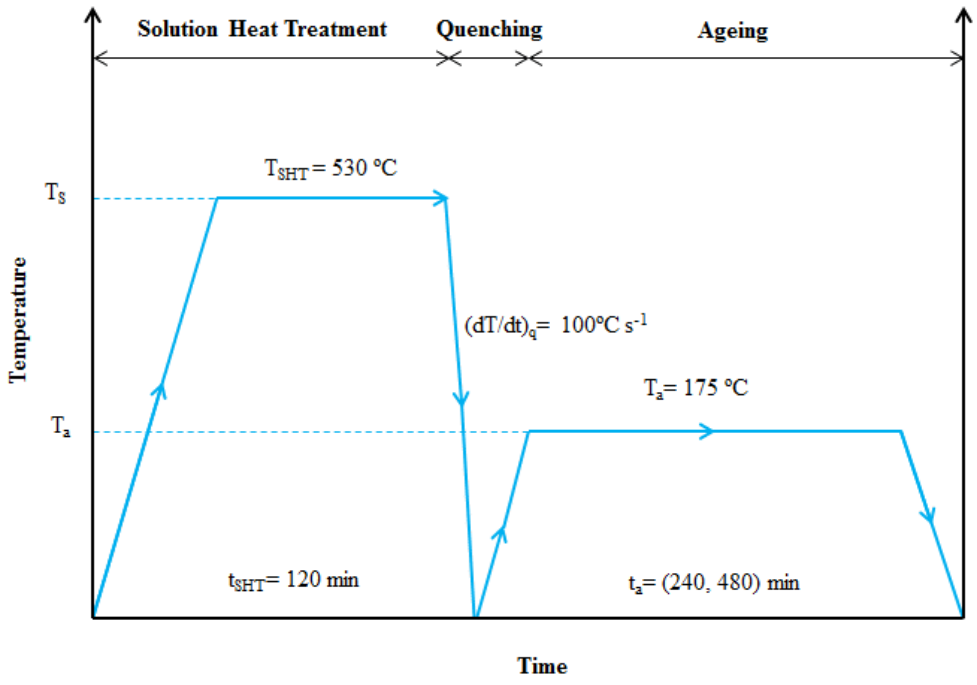

Figure 7-1: Temperature diagram of heat treatment flow over time

The hardness test is usually used to estimate the mechanical strength of metallic materials where greater hardness value shows the better ability of material to resist from permanent deformation. Samples for microhardness (MH) test as shown in Figure 7-2

were prepared according to method described in Section 3.4, except etching was skipped. The microhardness test was performed using Vickers Hardness tester (Shimadzu HMV-2TE) by forcing a square-based pyramidal diamond indenter, having face angles of 136º at 2.942 N. The duration of the applied load was 10 seconds, involving 10 randomly distributed indentations on each sample. The sequence of the heat treatment implementation after the hot extrusion has been carried out is shown in Figure 7-3.

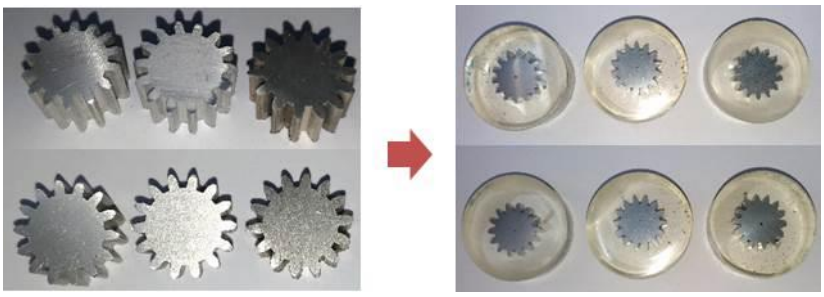

Figure 7-2: Prepared samples for microhardness measurement

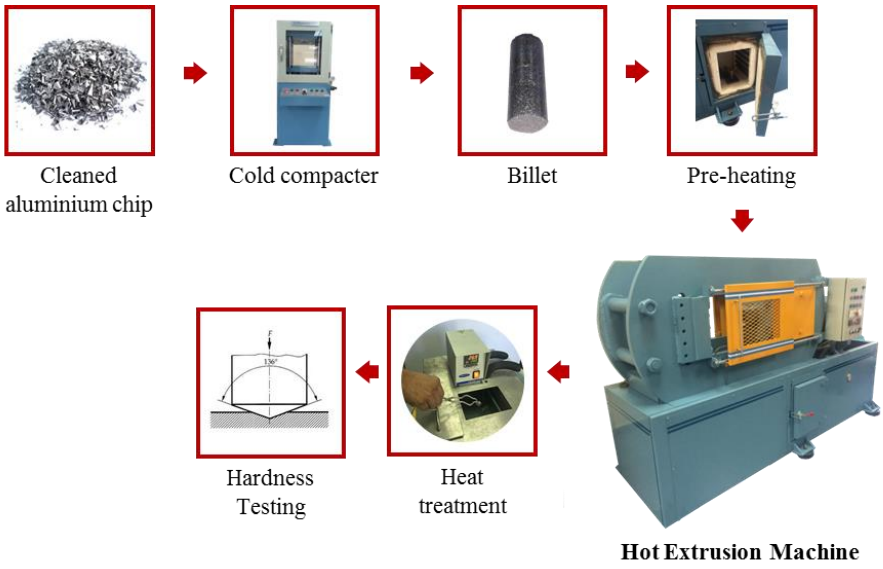

Figure 7-3: Process flow of T6 condition-heat treatment after gear extrusion

7.3 Results and Discussion

The overall results of microhardness measurement on the extruded gear profiles after the heat treatment are given in Table 7-2 and categorized according to extrusion temperature. As can be seen in Figure 7-4 the microhardness of the extruded gears depends on the extrusion temperature and aging time. The factor of aging time has considerably more influence over the microhardness than the extrusion temperature. Significant increase in hardness can be seen taking place in shorter aging time of 4 hours and the hardness increased between 80% - 110% for all samples regardless of the extrusion temperature while at aged time of 480 minutes, the hardness is enhanced to only between 50% - 70%, all are compared to hardness of non-heat treated gears. There has been a slight increase in hardness over the extrusion temperature and this indicates that the extrusion temperature has a minor influence on the hardness. The effect of extrusion temperature is linearly proportional to the measured hardness in all samples observed. The highest hardness of gear (105.66 HV) is obtained at maximum extrusion temperature of 550°C with 4 hours aging time. The heat treatment has a positive effect on the hardness of gears that produced from AA6061-T4 stock material for chips. Also, no significant difference, in terms of the microhardness values as taken throughout the indented points as shown in Figure 7-5 for both samples aged at 240 minutes and 480 minutes, indicates that the samples are equally homogenized.

Table 7-2: Results of microhardness measurement

Sample category	Extrusion temperature, T (°C)	Microhardness (HV)		
		Non-heat treated	Heat treated	
			Aging time, t_a (min)	
			240	480
A	450	48.96	99.68	81.89
B	500	52.81	102.62	86.48
C	550	57.83	105.66	90.64

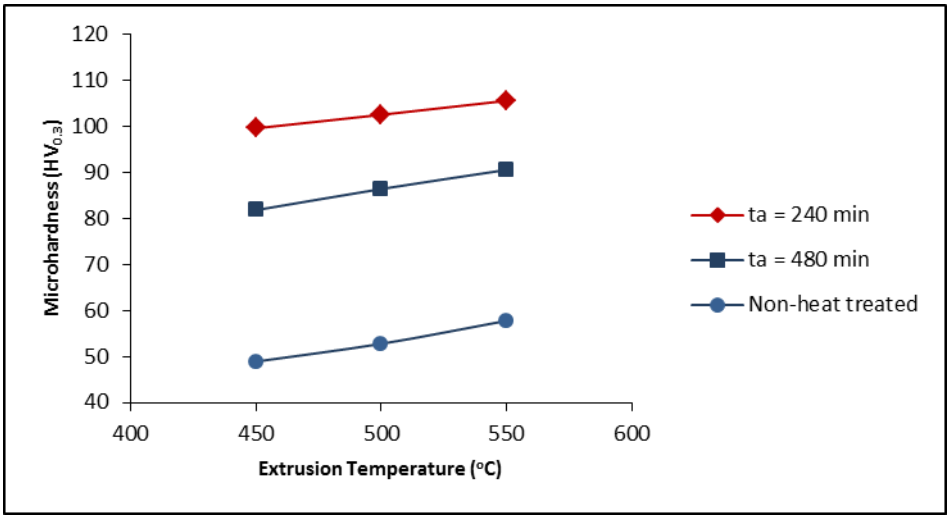

Figure 7-4: Microhardness values at different extrusion temperatures and aging times

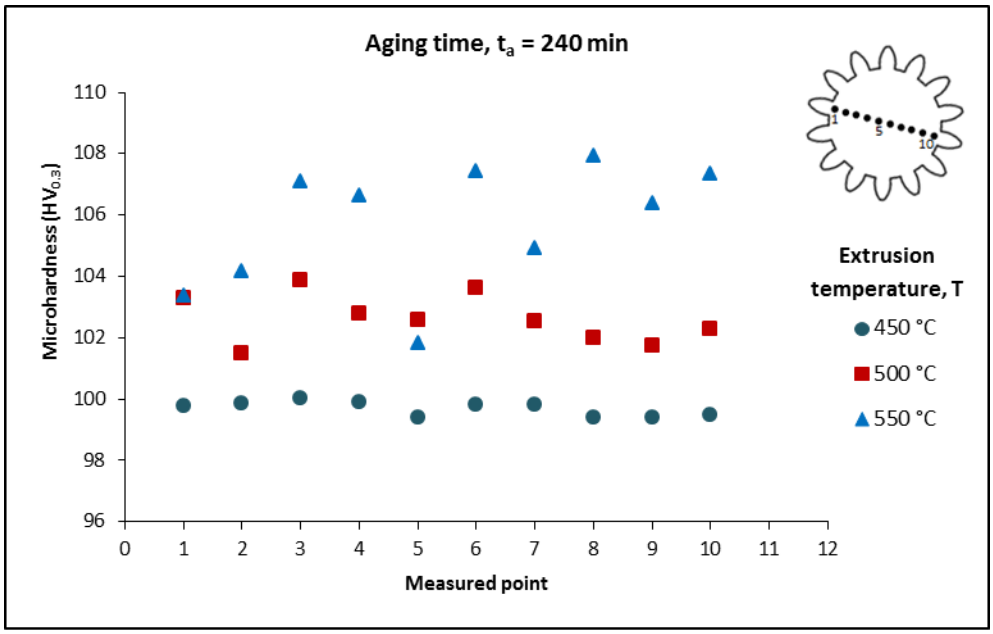

(a)

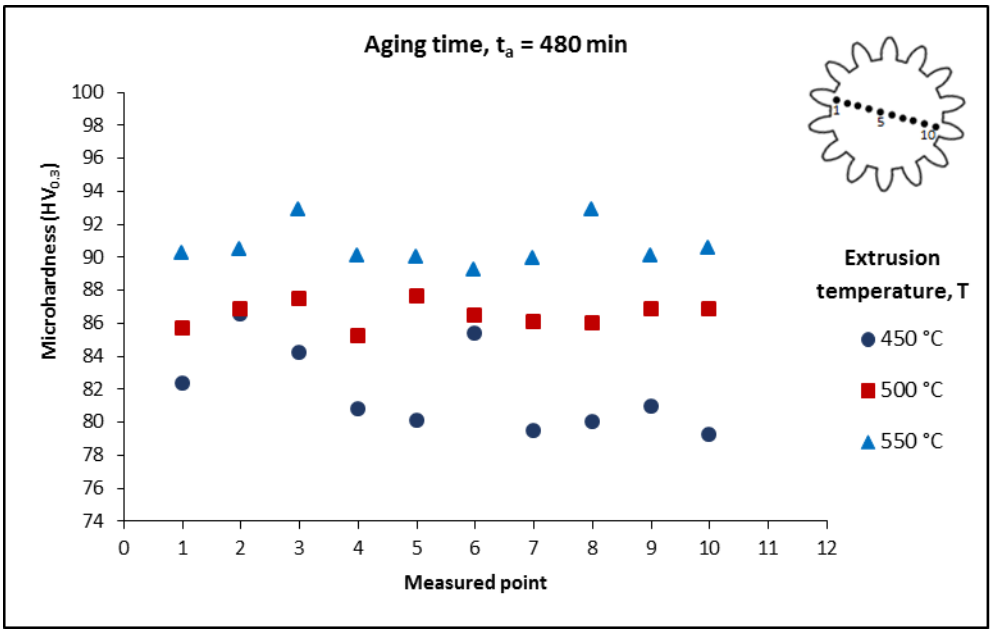

(b)

Figure 7-5: Microhardness measured at multiple points along the gear's cross section (a) 240 minutes aging time, (b) 480 minutes aging time

The effect of T6 solution heat treatment and aging time on the initial condition of chips from as-received AA6061-T4 alloy was further analysed by the XRD method as reported in Figure 7-6. Several reference patterns using FCC Al (JCPDS # 03-065-2869), FCC $Al_{0.7}Fe_3Si_{0.3}$ (JCPDS # 00-045-1204) and BCC $Fe_{0.95}Mn_{0.05}$ (JCPDS # 01-071-8287) were assigned for peaks detection in all spectra reported. Since the largest measured pattern was β-AlFeSi in all samples, the discussion is focused on the β-AlFeSi as shown on top legend in Figure 7-6. As can be seen in Figure 7-6, the non-heat treated sample showed evidences of peak broadening due to the presence of smaller grains. Using Scherrer estimation method yielded a grain size of 23.63 nm β-AlFeSi for this non-heat treated sample. In contrast, samples aged at 4 hours and 8 hours showed no evidences of peak broadening, thus suggesting that the presence of larger grains of β-AlFeSi are observed by XRD. The grains measured for both samples aged at 4 hours and 8 hours revealed 102.01 nm and 66.33 nm, respectively. These results are corresponding to the microhardness measurement for both samples where sample with larger grains tend to have higher hardness. Besides, the intensity of β-AlFeSi detected in XRD spectra reported in Table 7-3 for sample aged at 4 hours proves that sample with the highest intensity of β-AlFeSi resulted in superior hardness compared to sample with lower intensity (sample aged at 8 hours and non-heat treated sample).

The microhardness of the samples with the higher content of secondary-phase particles such as AlFeSi in the heat treated AA6061 aluminum samples is higher than that of non-heat treated samples. As shown in Table 7-3, more secondary-phase particles are present in the gear aged at 240 minutes compared to those found in the gear aged at 480 minutes. This resulted in the respective sample with the highest microhardness. The

distribution of rigid secondary-phase particles in each sample is assumed homogenous. This can be seen through visual comparison of hardness distributions as shown in Figure 7-5 (a) and (b) where the hardness at center and tooth regions differs little, consistent in many points apparently. The secondary-phase particles were examined via X-ray diffraction. These particles are substantially hard, which explains the observed changes of other properties of composites after heat treatment.

It is shown that the heat treatment on the directly recycled material from low performance alloy (T4 condition) can be enhanced to reach to T6 alloy performance. The new finding provides an idea on repetitive recycling potential of chip-based finished product that is used in the direct recycling. As-received AA6061-T4 and AA6061-T6 aluminium have hardness approximately equivalent to 74 HV and 111 HV [142]. While direct recycled AA6061-T4 aluminium without the heat treatment resulted in hardness equivalent to 57.83 HV, extruded at 550 °C. It shows that the hardness of the direct recycled aluminium is inferior by 16.17 HV as compared with the as-received AA6061-T4. After the heat treatment at T6 condition has been carried out, the hardness is increased from 57.83 HV to 105.66 HV with 240 minutes aging time. Comparing with the as-received AA6061-T6, the heat treated sample was just inferior by 5.34 HV. An optimum mechanical properties is possible to achieve by proper controlling the aging time because this factor is found as the major influence over the hardness results. It can be inferred that the solid-state recycled aluminium can reach to T6 condition from the stock material of AA6061-T4 bulk aluminium. This would allow a repetitive solid-state recycling on the chips and the resulting product shows a promising quality to consumers.

In this study, the strengthening mechanisms during the heat treatment were caused by the solid solution and precipitation of solid phase. During solution heat treatment, the corresponding materials experienced high temperature that led to impurity atoms to dissolve into solid solution which impose lattice strains surrounding the host atoms. Subsequently, the emerging lattice strain field interactions between dislocations and the impurity atoms restricted the dislocation movement which in turn improved the strength [143]. Furthermore, the precipitation hardening is achieved by reheating immediately the solution heat treated samples at 175 °C for 4 and 8 hours. At this stage, the solute atoms diffuse to form small precipitates. A secondary-phase of intermetallic precipitation (solute rich particles) emerges in the matrix contributes to strength enhancement, hardness and other mechanical properties improvement [138, 140]. These secondary-phases are metastable and therefore transformed into equilibrium phase with an appropriate aging time. As the aging time and the temperature increase, the density of Guinier–Preston zones expand accordingly [144]. Hence, the increase in degree of irregularity of the lattices causes an increase in the mechanical properties. Nevertheless, proceeding aging time to 480 minutes has caused the microhardness to decrease linearly. The main reason could be due to the formation of different precipitates that has a disruptive influence in hardness and a common attribute of over aged alloy as reported by many other researchers [145-149].

The maximum hardness exhibited was 105.66 HV at 240 minutes of aging time and at extrusion temperature of 550 °C, considered as the peak-aged. An increase in hardness could be due to diffusion assisted mechanism, grain growth and also by the hindrance of dislocation due to impurity of foreign atoms (emergence of second phase

intermetallic particles), since that the material quenched from 530 °C (solution heat treatment) will contain a large vacancy concentration [145]. Variations in the microhardness could be explained by the differences in microstructure, density of dislocation, strain distribution and types of second phase intermetallic particles in the respective samples. Deformation at higher temperature allows greater recovery and recrystallization than those at lower temperature, subsequently the hardness of the gear extruded at 550 °C is higher than that of the gear extruded at 450 °C.

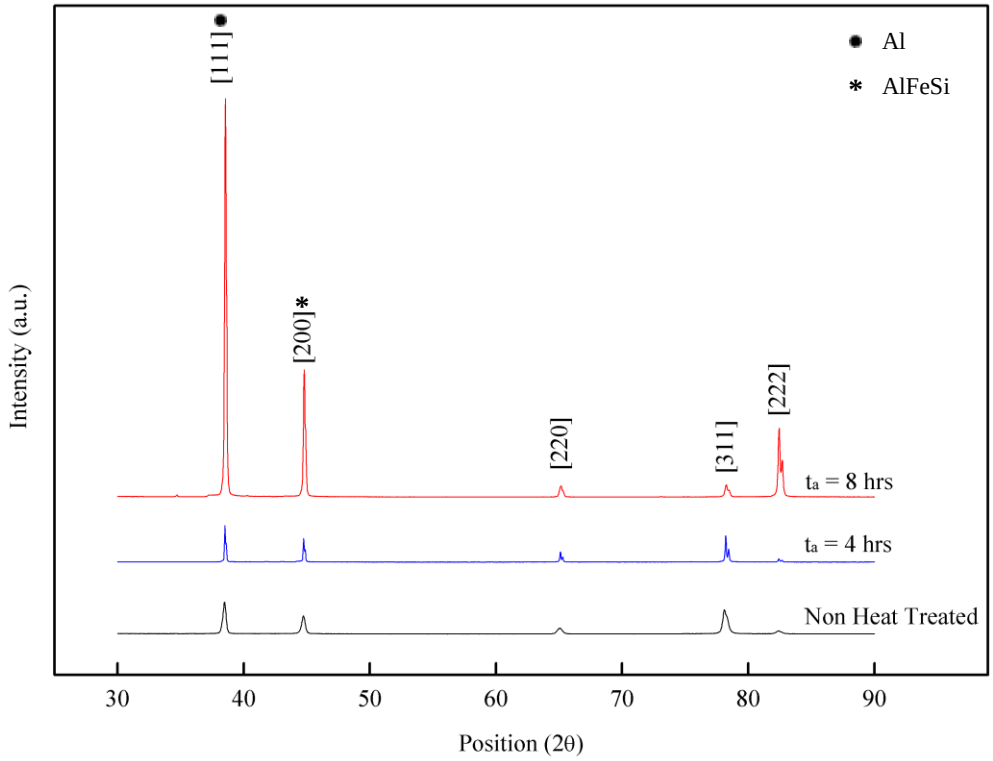

Figure 7-6: Results of XRD analyses on non-heat treated and heat treated samples at 550°C extrusion temperature

Table 7-3: XRD data of selected samples

Sample	Extrusion Temperature, T (°C)	Aging time, t_a (hrs)	β-AlFeSi	
			Crystallite Size (nm) [200]	Intensity (%) [200]
Non-heat treated	550	NIL	23.63	33.6
Heat-treated		4	102.01	66.2
Heat-treated		8	66.33	56.4

7.5 Conclusions

The heat treatment process on AA6061-T4 aluminium has been carried out successfully in this study. The dominant factor influencing the hardness is aging time, more significant than the extrusion temperature. The maximum hardness obtained was 105.66 HV with 240 minutes aging time considered as the peak-aged. Achieving such a peak point was assisted by the diffusion mechanism within the matrix aluminium. An excessive vacancy present as the material leaves the quenching process allows the impurity atoms to interfere the atom dislocation which resulted in an improved hardness. While over aging was encountered when the aging time was scheduled more than 240 minutes. This might due to the coalescence of the precipitates into larger particles, resulted in fewer obstacles to the movement of dislocation. Higher extrusion temperature was found to improve the chip bonding, which could be caused by the inter-particle diffusion transport matter. Higher ductility, often associated with the higher billet temperature, generates more strains in hot extrusion process, and intensifies the diffusivity between the aluminium chips.

CHAPTER 8 : CONCLUSIONS AND FUTURE WORK

This chapter presents a summary of major findings and novel contributions in the area of solid-state recycling via the hot extrusion process. The recommendations for future work are also included for potential improvement in the proposed technique. This would justify the technological feasibility in the practical aspect of its implementation.

8.1 Concluding Remarks

There are several conclusions can be drawn from this study as summarized below:

8.1.1 The Effects of Preheating Time and Temperature

Study on the aspect of optimum billet temperature and preheating duration led to the findings that both factors have significant effect on the mechanical properties of the chip-based extrudate. In order to obtain sufficient tensile strength for practical application, in case where the extrusion ratio is lower than or equal 11.22, the use of operating temperature of more than 400°C is emphasized. The maximum strength of the current recycled material can reach 98 % of the strength of as-cast material (AA6061-T6). Although the recovery tensile strength never quite develop into full-fledged, post-processing such as heat treatment could further enhance mechanical performance of the recycled materials. Furthermore, for any recycled materials which

could not regain their strength to maximum, several other applications such as frames for window, partition, door and etc. that do not require full strength and ductility, can be produced by the proposed recycling technique.

Under the severe strain condition, homogeneity of the billet structure seems to increase notably as the preheating time was extended to two hours with extrusion temperature held at high setting. Also, an improved inter-particle chip diffusion as a result of temperature increase had further maximised the mechanical strength and ductility of the extrudates. The results of the finite element simulation confirmed that the damage-free extrudates can be obtained at higher temperatures. On top of that, when the temperature kept at sufficiently high level, the flow stress and extrusion force of material decrease which in turn led to the energy-saving process. It is found that the Normalized Cockroft and Latham damage criterion in finite element simulation is useful in predicting the cracks and warpage emergence. Using predictive approach of foreseeing the crack and warpage formations, significant time and cost can be reduced in comparison with the experimental trial and error approach. Also, public confidence in process reliability of the solid-state recycled product relies towards how efficient the method in saving the money and other related resources.

8.1.2 The Influence of Surface Topography on the Weld Strength

Study on the influence of surface topography over the weld strength through the hot forging operation provides a fundamental understanding of the oxidation effect caused by the entrapped air. The severity of the oxidation is mainly affected by the surface

roughness of aluminium chip/sheet and the temperature at which the process is performed. Higher surface roughness would normally entrap more air (indirectly oxygen) and hinders the bonding of chips. In the condition where the intimate contact of less than 10 atomic spacings (≈ 2.9 nm) achieved between the chip boundaries, an inter-atomic force becomes stronger to attract atoms to form joints. It is found that if the effect of asperity height were merely to be considered (without the presence of temperature and pressure), it does affect the weld strength. High thermal energy and pressure are required to reduce the effect of asperity height (larger asperity height would aggravate the oxidation by entrapping more oxygen). With more heat, the strain increases proportionally to the heat. This causes chips to be continuously stretched, exceeding the threshold strain for weld formation. The heat also promotes interface diffusion which enables an excessive departure of atoms to the void necks that finally reduced the porosity and improved the weld bonds. The pressure plays its role to reduce the distance travelled by the atoms to permit more migration of atoms, thus improved the surface and interface diffusions.

8.1.3 The Weld Strength Prediction Model

A new model for the weld strength prediction in solid-state recycling via the hot extrusion process is successfully developed. This model includes both the tensile bond strength recovery due to diffusion and deformation variables (initially developed by Cooper and Allwood [80]). The diffusion-strengthening model is derived through the diffusion theory of Fick's second law and an Arrhenius relationship while the tensile

bond strength model is developed through the theory of thin film bonding. Some important relationships between the deformation variables, extrusion ratio and die geometry over the resulting weld strength have been deduced from the current research work and is summarized as follows:

(1) High heat is required on the aluminium interface to soften it and allow further stretching of chips until the threshold strain is exceeded to form welds;
(2) The flow stress is inversely proportional to the temperature. As the temperature dropped, the corresponding flow stress increases resulting in an increase of extrusion force;
(3) When the normal contact stress in the die's bearing area or shear stress in the shearing zone increases, it decreases the threshold strain to enhance the weld strength;
(4) Magnitude of normal contact stress higher than the yield strength is necessary to create a sound bonding because this condition is likely to increase the real contact area of chips and to encourage more micro-extruding of chips between an island of broken oxides;
(5) At higher temperatures on the rectangular extruded profile, an increase in strain-rate as a result of massive metal flow resulted in lower tensile bond strength;
(6) The weld strength recovery due to diffusion mechanism is very sensitive to temperature and time contact between the die and billet. For instance, for a bond created between 450 °C - 500 °C with the rectangular die geometry (having a die length equal to 27 mm), the corresponding tensile bond strengths increase from 4.791 MPa to 13.801 MPa higher than the gear die geometry (die length equal to 24

mm) which only increased from 4.449 MPa to 13.012 MPa. Theoretically, the longer the die length, the contact time between die and billet is delayed to promote a better diffusion bonding.

8.1.4 The Heat Treatment on Solid-state Recycled Materials

The heat treatment on the recycled aluminium AA6061-T4 at T6 condition has been carried out successfully and the hardness was greatly improved from 57.83 HV to 105.66 HV (240 minutes aging time). The maximum obtainable hardness of the heat treated sample just differ by 5.34 HV with as-received AA6061-T6 sample. The main mechanisms that help to improve the hardness property are solid solution and precipitation of solid phase. During the solid solution heat treatment, the impurity atoms dissolve into solid solution to impose lattice strains on the host atoms while in the precipitation of solid phase, the emergence of secondary-phase of intermetallic precipitations contributed to the mechanical properties improvement. Aging time is the most influential factor on the hardness and therefore, must be controlled properly. The novel achievement obtained in this heat treatment process provides a great opportunity in the area of solid-state aluminium recycling where it is proved that the directly recycled materials can be heat treated repetitively. Therefore, the materials can be used over and over again during their useful service life.

8.2 Research Contributions

(1) There are no any specific studies devoted to investigate the minimum preheating temperature and preheating time in homogenization treatment that used to further minimise the energy consumption in solid-state recycling, as summarised in Table 2-2. The homogenization related variables were selected without a concrete justification by a numerous researchers. Although one of the advantages of recycling in the solid-state can be noticed from its reduction of using the intensive energy for remelting, prolong preheating chip-based billet at high temperature to establish a sufficient weld bond will continue to waste the energy. A literature survey shows there is no specific study carried out to investigate the minimum preheating time for billet's homogenization and minimum temperature that should be applied for extrusion in relatively low extrusion ratio which can result in an acceptable chip-based extrudate quality. Proper guidelines on preheating time and temperature have been suggested for billet's homogenization in hot extrusion of chips which will optimise the energy consumption.

(2) Study on the influence of surface topography over the resulting weld strength of chips provides a useful guideline to engineers who will be implementing the solid-state recycling. With a given specified strength, they can regulate the process variables such as temperature and normal pressure to combat the effect of oxidation, which is aggravated by the severity of the entrapped air of within the chip surfaces.

(3) In this study, a novel tensile bond strength model which includes the effect of diffusion mechanism, has been established and is very useful in predicting the quality of the weld bonds formation. The current model is more comprehensive, enables the weld quality to be anticipated through the calculated tensile strength value. This indeed eliminates the physical tensile test, hence can save a lot of time and money. Furthermore, the deduced model can be further applied to predict the weld quality of other processes such as in hot press forging of direct aluminium recycling. Another advantage of this model can offer is that, an acceptable prediction over the weld quality of multiple die designs combined with different operating regimes can be achieved. This will notify the engineers whether the selected settings are feasible or vice versa.

(4) The heat treatment conducted in this work has proved that the directly recycled material from low performance alloy (stock at T4 condition) can be enhanced to reach T6 alloy grade. These new findings provide an idea on repetitive recycling potential of chip-based finished product for sustainable manufacturing agenda.

8.3 Recommendations for Future Work

The findings reported in the present study show some interesting potential for future improvement. Further research work in this area could rationalise the technological feasibility of the proposed recycling method for practical implementation. A number of aspects can be further explored for future development in this area. There are as follows:

(i) Further work can be undertaken to directly predict the weld strength of solid-state recycled materials via the numerical simulation. A user-subroutine program can be embedded to an existing finite element package for this purpose. This enables the software to directly compute the tensile strength value in real time. Therefore, the weld quality of chips can be quickly inspected by this way.

(ii) Further improvement can be done in numerical simulation of damage evolution of chip-based billet during the extrusion process. This can be realised by developing a new damage criterion which considers both the effects of diffusion and other deformation variables simultaneously. Therefore, the optimum quality can be easily obtained.

(iii) Current experimental work only covered aluminum alloy AA6061 as a recycled material. Development of diffusion-strengthening model can be further extended to other materials to observe its accuracy and consistency in predicting the weld strength that caused by the diffusion mechanism. The experiments can cover a wide variety of chip types, temperature range, pressure range, multiple consolidation processes and various process time interval.

(iv) The final tensile bond strength model can be further applied to predict various other profiles including, but not limited to, L shape, T shape, C channel, profile for frame,

corner shape, hollow profile and etc. to thoroughly evaluate the model's accuracy. This would further reveal any inaccuracies or misleading fundamentals applied during the model development. By doing so, a necessary adjustment can be done to allow the model to be more adaptable on a wide variety of process range.

APPENDIX A: A FLAT-FACE DIE WITH RECTANGULAR GEOMETRY

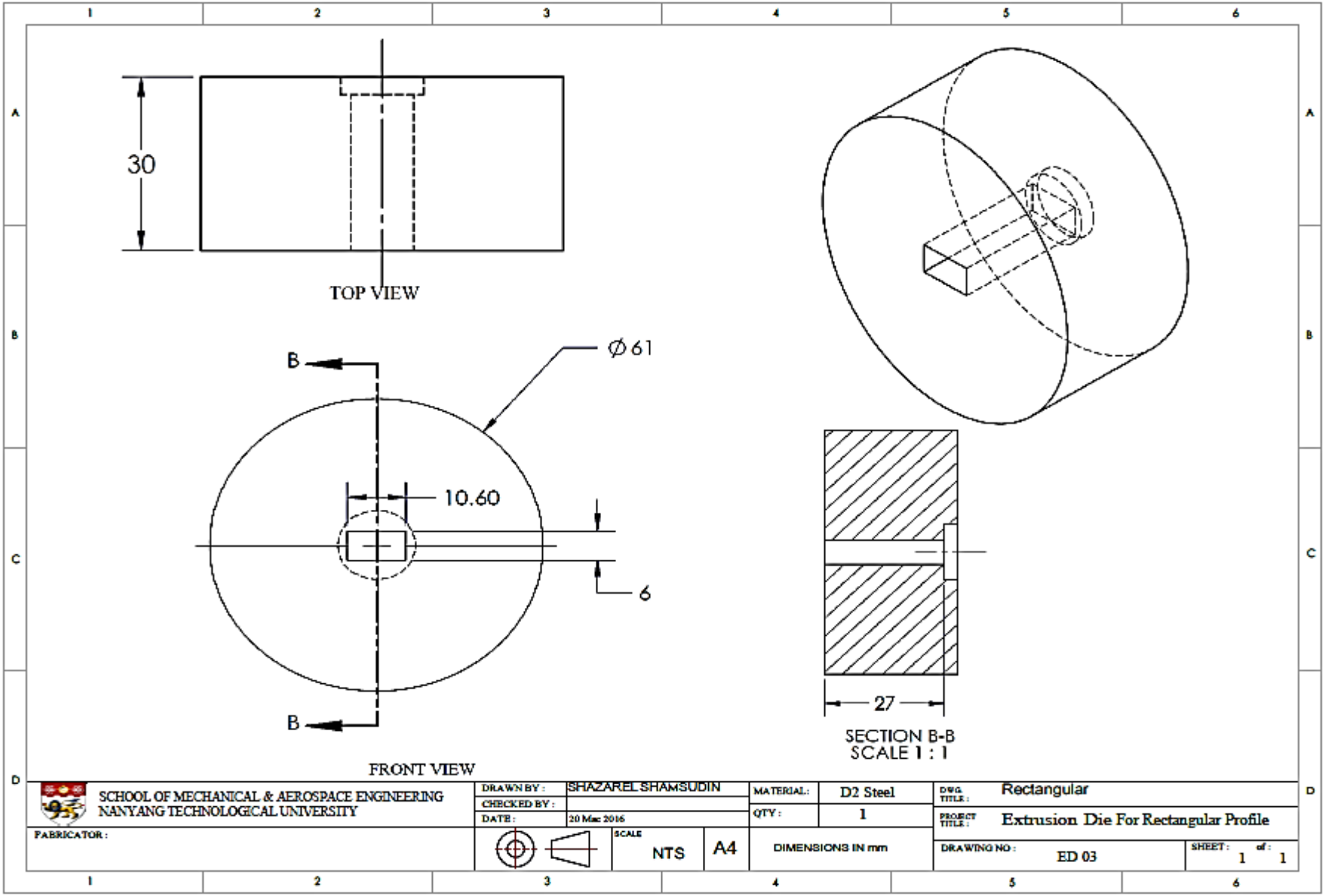

APPENDIX B: A FLAT-FACE DIE WITH SPUR GEAR GEOMETRY (ER: 11.22)

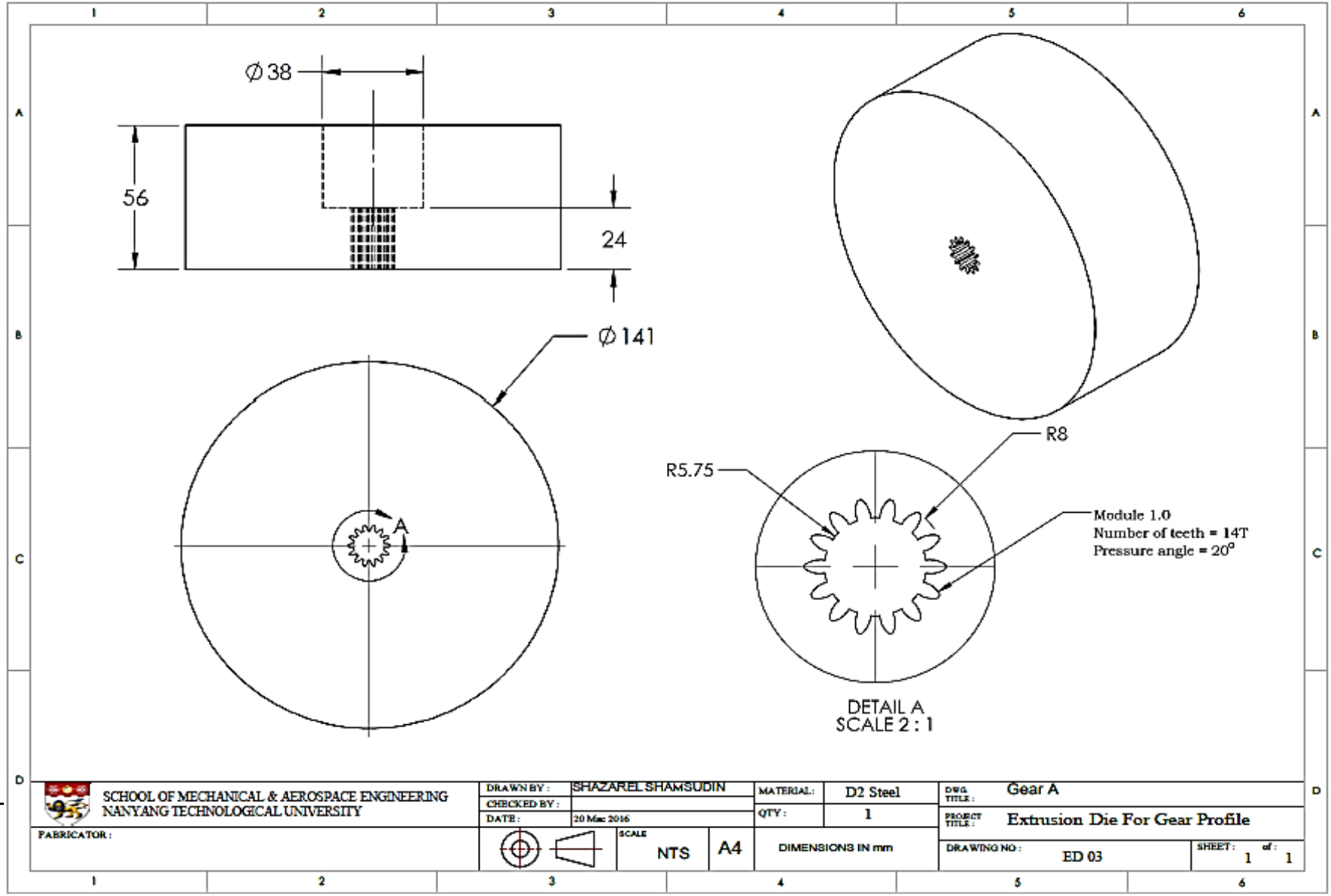

APPENDIX C: A FLAT-FACE DIE WITH SPUR GEAR GEOMETRY (ER: 2.16)

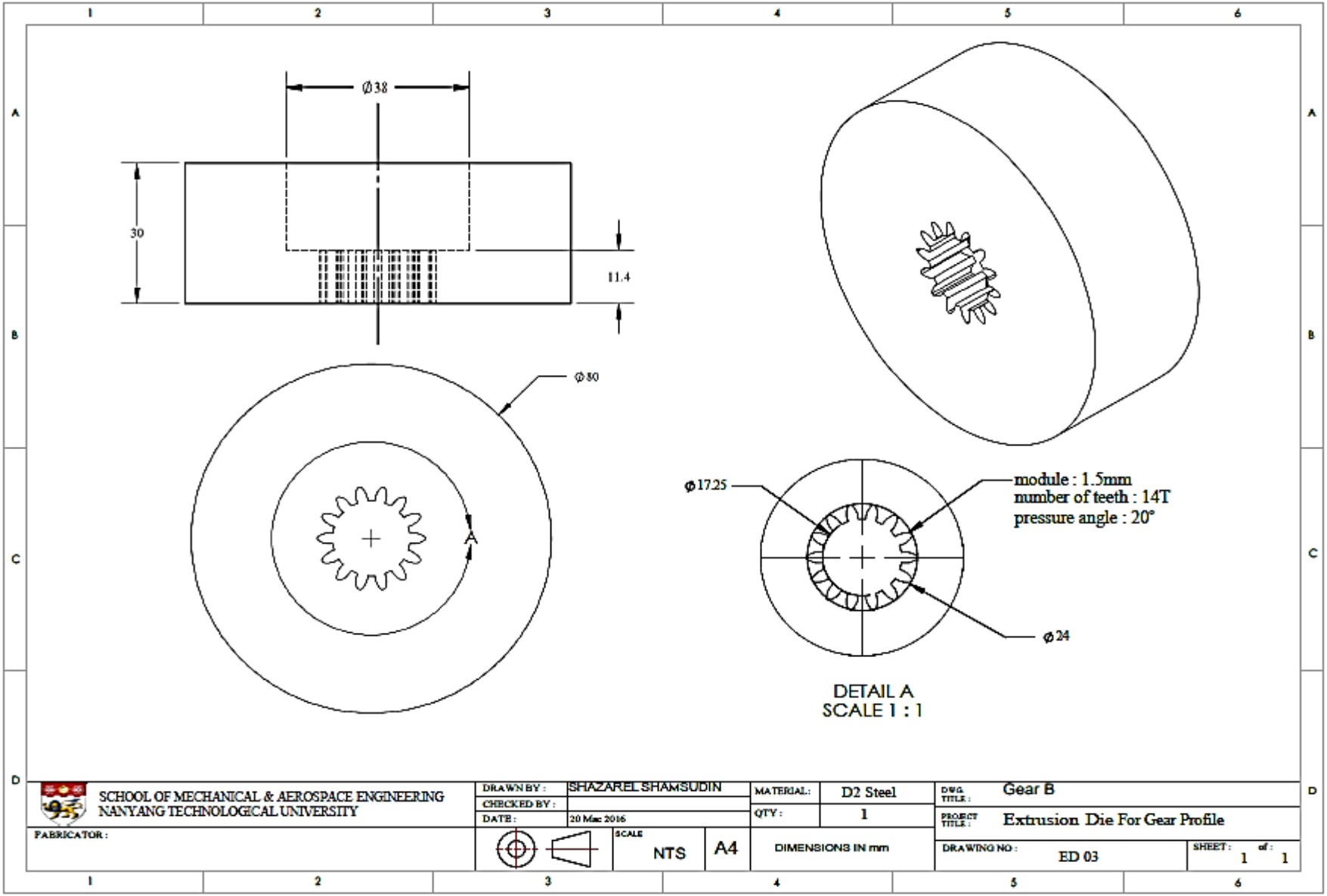

APPENDIX D: DERIVATION OF THE OXIDIZED SURFACE FRACTION

This appendix details out derivation of the surface fraction that will be oxidized by the entrapped air between the asperity heights of chips and given by the symbol, η.

Calculation of η

It is suggested that the real contact geometry between two aluminium surfaces comprises of an appropriate imaginary rough surface rather than a flat surface [120] as illustrated in Figure D-1. Here, the roughness characteristics are assumed to have equivalent root mean square of the asperity heights (r_{eq}), and the asperity inclination angle (ψ_{eq}) which take the values of $\sqrt{2\mathrm{r}}$ and $\sqrt{2\psi}$ respectively as shown in Figure D-1. Now the estimation of the entrapped air volume is done in a single 'valley' (per unit depth). Taking the volume of oxygen is 21% of the total entrapped air volume, therefore:

$$Volume_{O_2} = 0.21 \times \sqrt{3} r_{eq} \times \frac{\sqrt{3} r_{eq}}{\tan(\psi_{eq})} \quad \text{(D-1)}$$

Since that an approximately one mole of gas molecules contained in 22.41 (0.0224 m^3) of volume at standard pressure and temperature, therefore, the number of O_2 moles in this volume is given by the following equation:

$$Moles_{O_2} = \frac{Volume_{O_2}}{0.0224} \times \frac{298}{T} \quad \text{(D-2)}$$

Bonding is inhibited with an oxide layer minimum of 2.9 nm thick (equivalent to ten aluminium atom spacings) [93]. When the molar mass of Al_2O_3 = 0.102 kg mol^{-1}, and its density = 4000 kg m^{-3}, therefore ≈ 1.7 × 10^{-4} moles of O_2 are needed to oxidize a 1 m^2 surface to a depth of 2.9 nm (ten aluminium atom spacings). The following equation correlates area of the 'valley floor' (per unit depth) from one peak to the next.

$$Area = 2 \times \frac{\sqrt{3} r_{eq}}{\sin(\psi_{eq})} \quad \text{(D-3)}$$

Thus, the resulting moles of O_2 to complete the oxidation on this surface:

$$Moles_{Complete\ Oxidation} = (1.7 \times 10^{-4}) \times 2 \times \frac{\sqrt{3} r_{eq}}{\sin(\psi_{eq})} \quad \text{(D-4)}$$

The fraction of the surface that can be oxidized is therefore given by the following equation:

$$\eta = \frac{Moles_{O_2}}{Moles_{complete\ oxidation}} = 50{,}000 \times r_{eq} \times \cos(\psi_{eq}) \times \frac{298}{T} \quad \text{(D-5)}$$

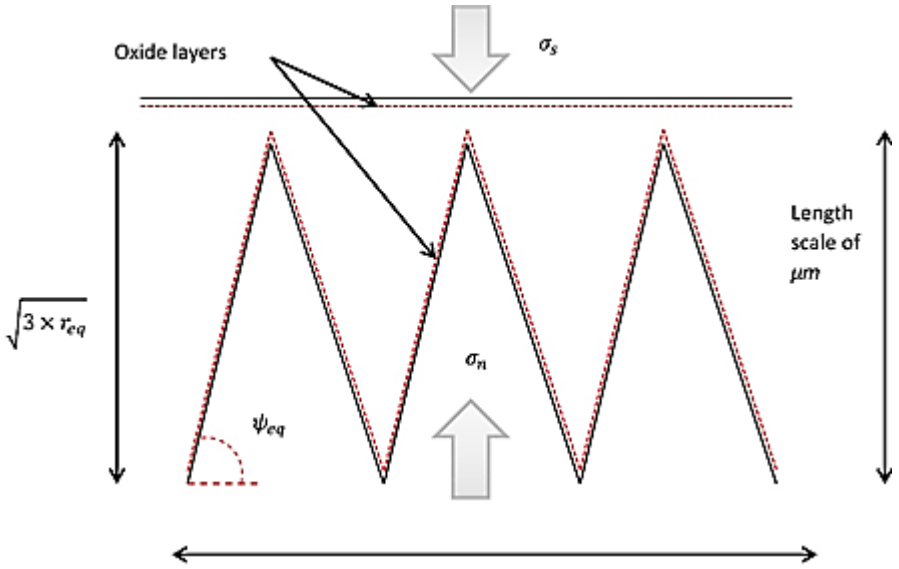

Figure D-1: Simplified contact geometry of between chips' interface (Adapted from [120])

APPENDIX E: DERIVATION OF ASPECT RATIO OF THE OXIDE FRAGMENTS

This appendix details out derivation of the aspect ratio of the oxide fragments. Bonding will be initiated if exposed aluminium on both sides of the interface are overlapped. For simplification, an assumption is made that the substrate aluminium exposed on one side is always adjacent to the substrate aluminium exposed on the other side and both are completely overlapped.

Equilibrium Analyses on Oxide Fragments

The scenario where the oxides are not broken together is demonstrated in Figure E-1. In this circumstances, the top oxide restraints the separation of the bottom oxide, thus reducing the tensile stress experienced in the bottom oxide, and thereby making it less likely to crack in the beginning. In the scenario of the oxides cracking together, assuming the adjacent oxide is free from frictional restraint, a greater amount of tensile stress will be developed in the oxides causing them to crack. In this study, it is assumed that the adjacent oxides crack together, causing an exposed aluminium substrate to completely overlapping. The moment aluminium is stretched, its oxide is cracked and substrate aluminium begins to flow into the cracks. The oxide cracking occurs continuously until the tensile stress within the oxide is less than the tensile strength of oxide. By considering the force equilibrium on an oxide fragment as illustrated in Figure E-2, therefore the aspect ratio of the oxide fragments can now be calculated. The ξ_A and ξ_B are the distances between the trailing and leading end of the oxide fragment and the neutral point of the friction hill on the oxide fragment. Force equilibrium on

horizontal direction implies $\xi_A = \xi_B = (\lambda / 2)$. The maximum tensile stress, σ_m, shown in Figure E-3 is given by $(\lambda k / 2t_c)$, occurs at the neutral point of the oxide. The following equation therefore gives an aspect ratio of the resulting oxide fragment.

$$\left(\frac{\lambda}{t_c}\right)_{no\ shear} = \frac{2\sigma_{oxide}}{k} \qquad \text{(E- 1)}$$

With the present of a shear stress at the interface, the forces acting on the oxide are as illustrated in Figure E-3. From horizontal force equilibrium:

$$\xi_A\left(k + \tau_{app}\right) = \xi_B\left(k - \tau_{app}\right) \qquad \text{(E- 2)}$$

Since $\xi_A + \xi_B = \lambda$, the location of neutral point is at:

$$\xi_A = \frac{\lambda}{2}\left(1 - \frac{\tau_{app}}{k}\right) \qquad \text{(E- 3)}$$

Subsequently, the maximum tensile stress in the sample is:

$$\sigma_m = \frac{\lambda k}{2t_c}\left(1 - \frac{{\tau_{app}}^2}{k^2}\right) \qquad \text{(E- 4)}$$

Thus, the aspect ratio of the oxide fragments finally takes the following form:

$$\left(\frac{\lambda}{t_c}\right)_{shear} = \frac{2\sigma_{oxide}}{k} \times \left(1 - \frac{{\tau_{app}}^2}{k^2}\right)^{-1} \qquad \text{(E- 5)}$$

All illustrations presented in Figure E-1, E-2 and E-3 are adapted from [80].

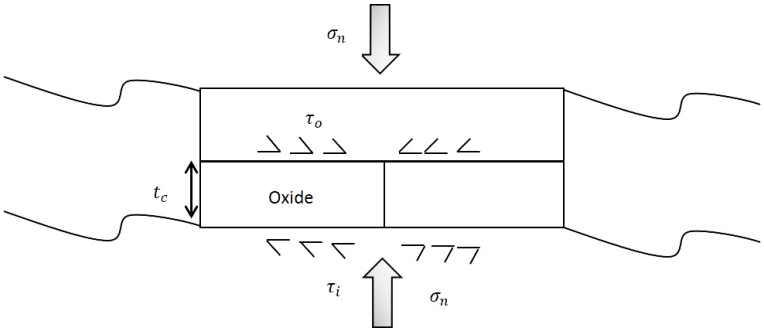

Figure E-1: Condition in which adjacent oxides do not crack together.

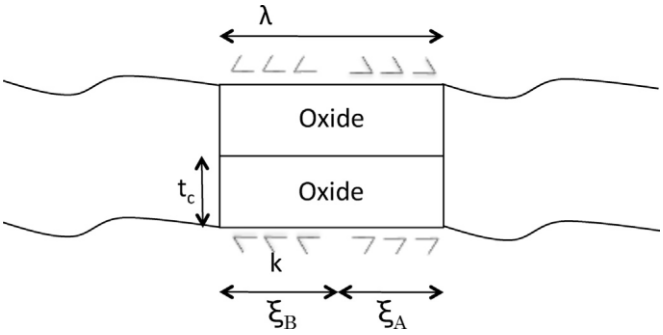

Figure E-2: Forces acting on oxide fragments

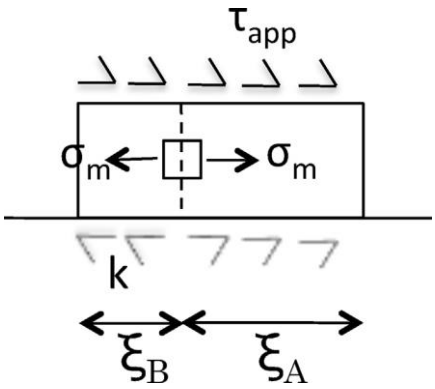

Figure E-3: Force equilibrium on fragment with interfacial shear stress, τ_{app}

APPENDIX F: FLOW STRESS ROUTINE IN DEFORM 3D SIMULATION

The tabular format is the most versatile format in that it can represent any material where flow stress can be given as a function of strain, strain rate, and temperature:

$$\sigma = f\ (\varepsilon, \dot{\varepsilon}, T) \tag{F-1}$$

Where,
σ = Flow stress
ε = Strain
$\dot{\varepsilon}$ = Strain-rate
T = Temperature

```
      IMPLICIT REAL*8 (A-H,O-Z), INTEGER*4 (I-N)
C ****   USER DEFINED VARIABLES ****
      CHARACTER*80 IUSRVL
      COMMON /IUSR/ IUSRVL(10)
C     TO READ DATA (10 RESERVED LINES)
C       READ(IUSRVL(LINE NUMBER),*) DATA1,DATA2,DATA3...
C     TO WRITE DATA (10 RESERVED LINES)
C       WRITE(IUSRVL(LINE NUMBER),*) NEWDATA1, NEWDATA2, NEWDATA3 ...
C      THIS ROUTINE IS USED TO DEMONSTRATE THE IMPLEMENTATION OF
C      MATERIAL ROUTINE.  ALL THE REAL VARIABLES SHOULD BE DOUBLE
C      PRECISION. THE DEFINITION OF ARGUMENTS ARE DESCRIBED AS FOLLOWS:
C     INPUT :
C      TEPS    =  EFFECTIVE STRAIN
C      EFEPS   =  EFFECTIVE STRAIN RATE
C      TEMP    =  TEMPERATURE
C     OUTPUT :
C      YS      =  FLOW STRESS
C      YPS     =  DERIVATIVE OF FLOW STRESS W.R.T. TEPS
C      FIP     =  DERIVATIVE OF FLOW STRESS W.R.T. EFEPS
C
      COMMON /ELMCOM/ RZE(2,4),URZE(2,4),STSE(6),EPSE(6),EFEPSE,EFSTSE,
     +            TEPSE,RDTYE,TEMPE(4),DTMPE(4),DAMAGE,
     +            USRE1(1500),USRE2(1500),
     +            USRNE(1500,4),NODEE(4),KELE,KELEL,KGROUP
C     EXAMPLE :
C       PEM = STRAIN_RATE SENSITIVITY INDEX
C       YS = MATERIAL_CONSTANT * (STRAIN)**PEN* (STRAIN_RATE)**PEM
C       PEN = STRAIN SENSITIVITY INDEX
C       FIP = MATERIAL_CONSTANT * PEM * (STRAIN_RATE)**(PEM-1.)
C       YPS = 0.
C    STRAIN CAN COME FROM ONE OF THE THREE SOURCES
C     (1) FROM THE INPUT ARGUMENT "TEPS"
C     (2) FROM THE ELEMENT COMMON BLOCK "TEPSE"
C     (3) FROM THE USER DEFINED STATE VARIABLES (SEE THE ROUTINE "USRST1")
C     THE FOLLOWING EXAMPLE IS WRITTEN BASED ON THE USED DEFINED STATE
C     VARIABLE
      IF (STRAIN.LE.0.) STRAIN = 1.E-5
      EFEPS=EFEPSE
      PEN = 0.15
      PEM = 0.1
      YS0= 1.0
      YS = 10. * STRAIN**PEN* (EFEPS)**PEM+YS0
      FIP = 10. * STRAIN**PEN* PEM * (EFEPS)**(PEM-1.)
      YPS = 10. * PEN * STRAIN**(PEN-1.) * (EFEPS)**PEM
      IF(STRAIN.EQ.1.E-5) YPS=0.0

      RETURN
      END
C*************************************************************
```

REFERENCES

1. *History of Aluminum*. 2017; Available from: http://www.aluminum.org/aluminum-advantage/history-aluminum.
2. Das, S.K. and Yin, W., *The worldwide aluminum economy: The current state of the industry.* JOM, 2007. 59(11): p. 57-63.
3. *Mineral Commodity Summaries 2006*. 2006, Washington, DC, U.S: U.S. Geological Survey.
4. Bray, E.L., *2005 Minerals Yearbook Aluminum*. 2006, Washington, DC, U.S: Geological Survey.
5. *The Aluminum Statistical Review for 2008*. 2009, Arlington, VA, U.S: The Aluminum Association, Inc.
6. Lazzaro, G. and Atzori, C., *Recycling of aluminum trimmings by conform process.* Minerals, Metals & Materials SOC(TMS), Warrendale, PA,(USA). 1991: p. 1379-1384.
7. Gronostajski, J., Marciniak, H., and Matuszak, A., *New methods of aluminium and aluminium-alloy chips recycling.* Journal of Materials Processing Technology, 2000. 106(1-3): p. 34-39.
8. Gronostajski, J.Z., Marciniak, H., and Matuszak, A., *Production of composites on the base of AlCu4 alloy chips.* Journal of Materials Processing Technology, 1996. 60(1–4): p. 719-722.
9. Gronostajski, J., Chmura, W., and Gronostajski, Z., *Bearing materials obtained by recycling of aluminium and aluminium bronze chips.* Journal of Materials Processing Technology, 2002. 125–126(0): p. 483-490.
10. Misiolek, W.Z., et al., *High quality extrudates from aluminum chips by new billet compaction and deformation routes.* CIRP Annals - Manufacturing Technology, 2012. 61(1): p. 239-242.
11. Haase, M., Ben Khalifa, N., Tekkaya, A.E., and Misiolek, W.Z., *Improving mechanical properties of chip-based aluminum extrudates by integrated extrusion and equal channel angular pressing (iECAP).* Materials Science and Engineering: A, 2012. 539(0): p. 194-204.
12. Chiba, R., Nakamura, T., and Kuroda, M., *Solid-state recycling of aluminium alloy swarf through cold profile extrusion and cold rolling.* Journal of Materials Processing Technology, 2011. 211(11): p. 1878-1887.
13. Chiba, R. and Yoshimura, M., *Solid-state recycling of aluminium alloy swarf into c-channel by hot extrusion.* Journal of Manufacturing Processes, 2015. 17(0): p. 1-8.
14. Güley, V., Khalifa, N.B., and Tekkaya, A.E., *Direct recycling of 1050 aluminum alloy scrap material mixed with 6060 aluminum alloy chips by hot extrusion.* International Journal of Material Forming, 2010. 3(1): p. 853-856.

15. Ingarao, G., Di Lorenzo, R., and Micari, F., *Sustainability issues in sheet metal forming processes: an overview*. Journal of Cleaner Production, 2011. 19(4): p. 337-347.

16. Schwarz, H., *Aluminum production and energy*. Encyclopedia of energy, 2004: p. 81-95.

17. Macintosh, W.H., *Induction furnaces for melting secondary aluminium.* Conservation & Recycling, 1983. 6(1): p. 41-48.

18. Butterwick, L. and Smith, G., *Aluminium recovery from consumer waste-I. Technology review.* Conservation & recycling, 1986. 9(3): p. 281-292.

19. Stern, M., *Method for treating aluminum or aluminum alloy scrap*. 1945, Google Patents.

20. Tekkaya, A.E., et al., *Hot profile extrusion of AA-6060 aluminum chips.* Journal of Materials Processing Technology, 2009. 209(7): p. 3343-3350.

21. Bertram, M., Buxmann, K., and Furrer, P., *Analysis of greenhouse gas emissions related to aluminium transport applications.* The International Journal of Life Cycle Assessment, 2009. 14(1): p. 62-69.

22. Gronostajski, J. and Matuszak, A., *The recycling of metals by plastic deformation: an example of recycling of aluminium and its alloys chips.* Journal of Materials Processing Technology, 1999. 92-93(0): p. 35-41.

23. Fogagnolo, J.B., Ruiz-Navas, E.M., Simon, M.A., and Martinez, M.A., *Recycling of aluminium alloy and aluminium matrix composite chips by pressing and hot extrusion.* Journal of Materials Processing Technology, 2003. 143-144(0): p. 792-795.

24. Samuel, M., *A new technique for recycling aluminium scrap.* Journal of Materials Processing Technology, 2003. 135(1): p. 117-124.

25. Cui, J., Kvithyld, A., and Roven, H., *Degreasing of Aluminium Turnings and Implications for Solid-State Recycling*. 2010, Minerals, Metals and Materials Society/AIME, 420 Commonwealth Dr., P. O. Box 430 Warrendale PA 15086 USA.

26. Cui, J., Werenskiold, J.C., and Roven, H.J. *New approaches for recycling of aluminum scraps*. in *TMS Annual Meeting*. 2009.

27. Gronostajski, J., Matuszak, A., Marciniak, H., and Samuel, M., *Aluminium base composites for high temperature application.* Inżynieria Materiałowa, 1998. 19: p. 750-735.

28. Cui, J. and Roven, H.J., *Recycling of automotive aluminum.* Transactions of Nonferrous Metals Society of China, 2010. 20(11): p. 2057-2063.

29. Chmura, W. and Gronostajski, Z., *Bearing materials obtained by diffusion bonding of aluminium and aluminium bronze chips.* Archives of Civil and Mechanical Engineering, 2007. 7(2): p. 53-66.

30. Jianqing, J., Aibing, M., Huanan, L., and Rongsheng, T., *The wear properties of an alumina-aluminosilicate fibre hybrid reinforced Al-Si alloy in a lubricated condition.* Wear, 1994. 171(1): p. 163-168.

31. Pathak, J., Karimi, D., and Tiwari, S., *Room temperature wear characteristics of Al-Si-Cd bearing alloys.* Wear, 1993. 170(1): p. 109-117.

32. Torabian, H., Pathak, J., and Tiwari, S., *Wear characteristics of Al-Si alloys.* Wear, 1994. 172(1): p. 49-58.

33. Samuel, M., Gronostajski, J., and Matuszak, A., *Mechanical properties and industrial application of aluminium base composites.* Proc of II Int. Sem. Zagadnienia Transferu Nowoczesnych Technologii Obróbki Plastycznej, Wrocław, 1996: p. 107-124.

34. Gronostajski, J.Z., Kaczmar, J.W., Marciniak, H., and Matuszak, A., *Production of composites from Al and AlMg2 alloy chips.* Journal of Materials Processing Technology, 1998. 77(1–3): p. 37-41.

35. Gronostajski, J.Z., Marciniak, H., Matuszak, A., and Samuel, M., *Aluminium-ferro-chromium composites produced by recycling of chips.* Journal of Materials Processing Technology, 2001. 119(1): p. 251-256.

36. Chmura, W. and Gronostajski, Z., *Bearing composites made from aluminium and aluminium bronze chips.* Journal of Materials Processing Technology, 2006. 178(1–3): p. 188-193.

37. Schikorra, M., Pantke, K., Tekkaya, A.E., and Biermann, D. *Re-use of AA6060, AA6082, and AA7075 aluminum turning chips by hot extrusion*. in *9th International Conference on Technology of Plasticity, ICTP 2008*. 2008. Hanrimwon Publishing Co., 206-3 Ojang-dong, Jung-gu, Seoul, 100-310, Korea, Republic of.

38. Sherafat, Z., Paydar, M.H., and Ebrahimi, R., *Fabrication of Al7075/Al, two phase material, by recycling Al7075 alloy chips using powder metallurgy route.* Journal of Alloys and Compounds, 2009. 487(1–2): p. 395-399.

39. Sherafat, Z., Paydar, M.H., Ebrahimi, R., and Sohrabi, S., *Mechanical properties and deformation behavior of Al/Al7075, two-phase material.* Journal of Alloys and Compounds, 2010. 502(1): p. 123-126.

40. Haase, M. and Tekkaya, A.E., *Cold extrusion of hot extruded aluminum chips.* Journal of Materials Processing Technology, 2015. 217(0): p. 356-367.

41. Güley, V., et al., *Effect of die design on the welding quality during solid state recycling of AA6060 chips by hot extrusion.* Materials Science and Engineering: A, 2013. 574(0): p. 163-175.

42. Haase, M. and Tekkaya, A.E., *Recycling of Aluminum Chips by Hot Extrusion with Subsequent Cold Extrusion.* Procedia Engineering, 2014. 81(0): p. 652-657.

43. Paydar, M., et al., *Equal channel angular pressing–forward extrusion (ECAP–FE) consolidation of Al particles.* Materials & Design, 2009. 30(3): p. 429-432.

44. Tang, W. and Reynolds, A.P., *Production of wire via friction extrusion of aluminum alloy machining chips.* Journal of Materials Processing Technology, 2010. 210(15): p. 2231-2237.

45. Song, L., Yuan, Y., and Yin, Z., *Microstructural Evolution in Cu-Mg Alloy Processed by Conform.* 2013.

46. Suzuki, K., et al., *Recycling of 6061 aluminum alloy cutting chips using hot extrusion and hot rolling.* Materials Science Forum, 2007. 544: p. 443-446.

47. Allwood, J., Huang, Y., and Barlow, C. *Recycling scrap aluminium by cold-bonding*. in *8th International Conference on Technology of Plasticity*. 2005. Verona.

48. Orlov, D., et al., *Improvement of mechanical properties of magnesium alloy ZK60 by integrated extrusion and equal channel angular pressing.* Acta Materialia, 2011. 59(1): p. 375-385.

49. Chino, Y., et al., *Tensile properties and blow forming of 5083 aluminum alloy recycled by solid-state recycling.* Materials transactions, 2004. 45(8): p. 2509-2515.

50. Mani, B. and Paydar, M., *Application of forward extrusion-equal channel angular pressing (FE-ECAP) in fabrication of aluminum metal matrix composites.* Journal of Alloys and Compounds, 2010. 492(1): p. 116-121.

51. Ying, T., Zheng, M.-Y., Hu, X.-S., and Wu, K., *Recycling of AZ91 Mg alloy through consolidation of machined chips by extrusion and ECAP.* Transactions of Nonferrous Metals Society of China, 2010. 20: p. s604-s607.

52. Luo, P., et al., *Analysis of microstructure and strengthening in pure titanium recycled from machining chips by equal channel angular pressing using electron backscatter diffraction.* Materials Science and Engineering: A, 2012. 538: p. 252-258.

53. Kondoh, K., Luangvaranunt, T., and Aizawa, T., *Solid-state recycle processing for magnesium alloy waste via direct hot forging.* Materials transactions, 2002. 43(3): p. 322-325.

54. Aizawa, T., Luangvaranunt, T., and Kondoh, K., *Solid state recycling of recyclable aluminum wastes with in-process microstructure control.* Materials Transactions, 2002. 43(3): p. 315-321.

55. Yusuf, N.K., Lajis, M.A., Daud, M.I., and Noh, M.Z., *Effect of Operating Temperature on Direct Recycling Aluminium Chips (AA6061) in Hot Press Forging Process.* Applied Mechanics and Materials, 2013. 315: p. 728-732.

56. Lajis, M.A., Khamis, S.S., and Yusuf, N.K., *Optimization of Hot Press Forging Parameters in Direct Recycling of Aluminium Chip (AA 6061).* Key Engineering Materials, 2014. 622: p. 223-230.

57. Suzuki, K., Shigematsu, I., Imai, T., and Saito, N., *Influences of chip characteristics and extrusion conditions on the properties of a 6061 aluminum alloy recycled from cutting chips.* Japan Institute of Light Metals 2005. 55(9): p. 395-399.

58. Peng, T., et al., *Microstructure and high tensile strength of Mg–10Gd–2Y–0.5Zr alloy by solid-state recycling.* Materials Science and Engineering: A, 2010. 528(2): p. 715-720.

59. Jahedi, M., et al., *Deformation rate effect on the microstructure and mechanical properties of Al–SiC p composites consolidated by hot extrusion.* Materials Science and Engineering: A, 2012. 556: p. 23-30.

60. Hu, M.-L., Ji, Z.-s., and Chen, X.-y., *Effect of extrusion ratio on microstructure and mechanical properties of AZ91D magnesium alloy recycled from scraps by hot extrusion.* Transactions of Nonferrous Metals Society of China, 2010. 20(6): p. 987-991.

61. Güley, V., Khalifa, N.B., and Tekkaya, A.E. *The Effect of Extrusion Ratio and Material Flow on the Mechanical Properties of Aluminum Profiles Solid State Recycled from 6060 Aluminum Alloy Chips*. in *The 14th International ESAFORM Conference on Material Forming*. 2011. American Institute of Physics.

62. Wu, S., Ji, Z., and Zhang, T., *Microstructure and mechanical properties of AZ31B magnesium alloy recycled by solid-state process from different size chips.* Journal of Materials Processing Technology, 2009. 209(12–13): p. 5319-5324.

63. Chmura, W. and Gronostajski, J., *Mechanical and tribological properties of aluminium-base composites produced by the recycling of chips.* Journal of Materials Processing Technology, 2000. 106(1): p. 23-27.

64. Gronostajski, J., Chmura, W., and Gronostajski, Z., *Phases created during diffusion bonding of aluminium and aluminium bronze chips.* Journal of Achievements in Materials and Manufacturing Engineering, 2006. 19(1): p. 32-37.

65. Samuel, M., *Reinforcement of recycled aluminum-alloy scrap with Saffil ceramic fibers.* Journal of Materials Processing Technology, 2003. 142(2): p. 295-306.

66. Mindivan, H., Cimenoglu, H., and Kayali, E.S. *Production of the composite from 6082 Al alloy chips and fly ash particles by hot pressing*. in *TMS Annual Meeting*. 2009.

67. Sugiyama, S., Mera, T., and Yanagimoto, J., *Recycling of minute metal scraps by semisolid processing: Manufacturing of design materials.* Transactions of Nonferrous Metals Society of China, 2010. 20(9): p. 1567-1571.

68. Guluzade, R., Avcı, A., Turan Demirci, M., and Faruk Erkendirci, Ö., *Fracture toughness of recycled AISI 1040 steel chip reinforced AlMg1SiCu aluminum chip composites.* Materials & Design, 2013. 52(0): p. 345-352.

69. Hu, M.-l., et al., *Solid-state recycling of AZ91D magnesium alloy chips.* Transactions of Nonferrous Metals Society of China, 2012. 22, Supplement 1(0): p. s68-s73.

70. Chino, Y., Hoshika, T., and Mabuchi, M., *Mechanical and corrosion properties of AZ31 magnesium alloy repeatedly recycled by hot extrusion.* Materials transactions, 2006. 47(4): p. 1040-1046.

71. Chino, Y., et al., *Mechanical properties of Mg-Al-Ca alloy recycled by solid-state recycling.* Materials transactions, 2005. 46(12): p. 2592-2595.

72. Hu, M., Ji, Z., Chen, X., and Zhang, Z., *Effect of chip size on mechanical property and microstructure of AZ91D magnesium alloy prepared by solid state recycling.* Materials Characterization, 2008. 59(4): p. 385-389.

73. Gronostajski, Z., *The deformation processing map for control of microstructure in CuAl9. 2Fe3 aluminium bronze.* Journal of Materials Processing Technology, 2002. 125: p. 119-124.

74. Zhao, Z.-d., et al., *Microstructure and mechanical properties of Mg-Zn-Y-Zr alloy prepared by solid state recycling.* Transactions of Nonferrous Metals Society of China, 2011. 21(2): p. 265-271.

75. Donati, L., Tomesani, L., *The prediction of seam welds quality in aluminum extrusion.* Journal of Materials Processing Technology, 2004. 153–154(0): p. 366-373.

76. Bay, N., *Mechanisms producing metallic bonds in cold welding.* WELDING J., 1983. 62(5): p. 137.

77. Plata, M. and Piwnik, J. *Theoretical and experimental analysis of seam weld formation in hot extrusion of aluminum alloys*. in *Proceedings Of International Aluminum Extrusion Technology Seminar*, 2000.

78. Valberg, H., *Extrusion welding in aluminium extrusion.* International Journal of Materials and Product Technology, 2002. 17(7): p. 497-556.

79. Ceretti, E., Fratini L., Gagliardi F., Giardini C., *A new approach to study material bonding in extrusion porthole dies.* CIRP Annals - Manufacturing Technology 2009. 58: p. 259-262.

80. Cooper, D.R. and Allwood, J.M., *The influence of deformation conditions in solid-state aluminium welding processes on the resulting weld strength.* Journal of Materials Processing Technology, 2014. 214(11): p. 2576-2592.

81. Hambli, R., *Statistical damage analysis of extrusion processes using finite element method and neural networks simulation.* Finite Elements in Analysis and Design, 2009. 45(10): p. 640-649.

82. Hambli, R. and Reszka, M., *Fracture criteria identification using an inverse technique method and blanking experiment.* International Journal of Mechanical Sciences, 2002. 44(7): p. 1349-1361.

83. Rice, J.R. and Tracey, D.M., *On the ductile enlargement of voids in triaxial stress fields∗.* Journal of the Mechanics and Physics of Solids, 1969. 17(3): p. 201-217.

84. Hartley, P., Pillinger, I., and Sturgess, C.E., *Numerical modelling of material deformation processes: research, development and applications*. 2012: Springer Science & Business Media.

85. Cockcroft, M.G. and Latham, D.J., *A simple criterion of fracture for ductile metals*. 1966.

86. Clift, S.E., Hartley, P., Sturgess, C., and Rowe, G., *Fracture prediction in plastic deformation processes.* International Journal of Mechanical Sciences, 1990. 32(1): p. 1-17.

87. Ghosh, A.K., *A criterion for ductile fracture in sheets under biaxial loading.* Metallurgical Transactions A, 1976. 7(4): p. 523-533.

88. Atkins, A., *Surfaces produced by guillotining.* Philosophical magazine A, 1981. 43(3): p. 627-641.

89. Atkins, A., *Possible explanation for unexpected departures in hydrostatic tension-fracture strain relations.* Metal Science, 1981. 15(2): p. 81-83.

90. Oyane, M., Sato, T., Okimoto, K., and Shima, S., *Criteria for ductile fracture and their applications.* Journal of Mechanical Working Technology, 1980. 4(1): p. 65-81.

91. Ayada, M. *Central bursting in extrusion of inhomogeneous materials*. in *Proceedings of 2nd International Conference on Technology for Plasticity, Stuttgart, 1987*. 1987.

92. Smith, W.F. and Hashemi, J., *Foundations of materials science and engineering*. 2011: McGraw-Hill.

93. Tylecote, R.F., *Solid Phase Welding of Metals*. 1968, London: Edward Arnold (Publishers) Ltd. .

94. Kazakov, N.F., *Diffusion bonding of materials*. 2013: Elsevier.

95. Conrad, H. and Rice, L., *The cohesion of previously fractured FCC metals in ultrahigh vacuum.* Metallurgical Transactions, 1970. 1(11): p. 3019-3029.

96. Rabinowicz, E., *Friction and wear of materials.* 1965.

97. Semenov, A., *The phenomenon of seizure and its investigation.* Wear, 1961. 4(1): p. 1-9.

98. Parks, J.M., *Recrystallization welding.* Welding J, 1953. 32(5): p. 209s-222s.

99. Zhang, W.B., Niels *State of the Art in Cold Welding*. in *Invited paper, JOM-/, 7th Int. Conf. on the Joining of Materials*. 1995. Elsinore, Denmark.

100. Pendrous, R., Bramley, A., and Pollard, G., *Cold roll and indent vvelding of some metals.* Metals Technology, 1984. 11(1): p. 280-289.

101. Davis, J.R., *Gear materials, properties, and manufacture*. 2005: ASM International.

102. *ASTM B221M − 13, Standard Specification Aluminum and Aluminum-Alloy Extruded Bars, Rods, Wire, Profiles, and Tubes (Metric), ASTM International*. West Conshohocken, PA, 2013.

103. *ASTM G131-96, Standard Practice for Cleaning of Materials and Components by Ultrasonic Techniques, ASTM International* West Conshohocken, PA, 2016.

104. Montgomery, D.C., *Design and analysis of experiments*. 2008: John Wiley & Sons.

105. *ASTM E8 / E8M-16a, Standard Test Methods for Tension Testing of Metallic Materials, ASTM International*. West Conshohocken, PA, 2004.

106. *ASTM E112-13, Standard Test Methods for Determining Average Grain Size, ASTM International* West Conshohocken, PA, 2013.

107. Chen, D.-C., You, C.-S., and Gao, F.-Y., *Analysis and Experiment of 7075 Aluminum Alloy Tensile Test.* Procedia Engineering, 2014. 81: p. 1252-1258.

108. Kim, H., Yamanaka, M., and Altan, T., *Prediction of ductile fracture in cold forging by FE simulations. Engineering Research Center for the Net Shape Manufacturing*. 1994, Report No. ERC/NSM-94-42.

109. Prasad, Y., Rao, K., and Sasidhar, S., *Hot working guide: a compendium of processing maps*. 2015: ASM international.

110. An American National Standard, *Standard Test Methods for Tension Testing of Metallic Materials [Metric]*, in *Designation: E 8M -04*. 2004.

111. Lela, B., Krolo, J., and Jozić, S., *Mathematical modeling of solid-state recycling of aluminum chips.* The International Journal of Advanced Manufacturing Technology, 2016: p. 1-9.

112. Chino, Y., et al., *Blow forming of Mg alloy recycled by solid-state recycling.* Materials Transactions, 2004. 45(2): p. 361-364.

113. Gronostajski, J.Z., Kaczmar, J.W., Marciniak, H., and Matuszak, A., *Direct recycling of aluminium chips into extruded products.* Journal of Materials Processing Technology, 1997. 64(1-3): p. 149-156.

114. Bhushan, B., *Surface roughness analysis and measurement techniques*, in *Modern Tribology Handbook, Two Volume Set*. 2000, CRC press. p. 74-144.

115. Inglesfield, J., *Adhesion between Al slabs and mechanical properties.* Journal of Physics F: Metal Physics, 1976. 6(5): p. 687.

116. Wu, H.-Y., et al., *Effect of heat treatment on the microstructure and mechanical properties of the consolidated Mg alloy AZ91D machined chips.* Journal of Materials Processing Technology, 2009. 209(8): p. 4194-4200.

117. Hosford, W. and Caddell, R., *Metal forming: metallurgy and mechanics*. 2007, Cambridge University Press, Cambridge.

118. Nicholas, M., *Material aspects of ceramic-ceramic and ceramic-metal bonding*, in *Advanced Joining Technologies*. 1990, Springer. p. 160-171.

119. Sherwood, W. and Milner, D., *The effect of vacuum machining on the cold welding of some metals.* J Inst Metals, 1969. 97(1): p. 1-5.

120. O'callaghan, P. and Probert, S., *Prediction and measurement of true areas of contact between solids.* Wear, 1987. 120(1): p. 29-49.

121. Barlow, C., Nielsen, P., and Hansen, N., *Multilayer roll bonded aluminium foil: processing, microstructure and flow stress.* Acta Materialia, 2004. 52(13): p. 3967-3972.

122. Hill, R., *The mathematical theory of plasticity*. Vol. 11. 1998: Oxford university press.

123. Cooper, D.R. and Allwood, J.M., *Influence of Diffusion Mechanisms in Aluminium Solid-state Welding Processes.* Procedia Engineering, 2014. 81(0): p. 2147-2152.

124. Roshan, M.R., Mirzaei, M., and Jenabali Jahromi, S.A., *Microstructural characteristics and tensile properties of nano-composite Al 2014/4 wt.% Al2O3 produced from machining chips.* Journal of Alloys and Compounds, 2013. 569(0): p. 111-117.

125. Callister, W.D. and Rethwisch, D.G., *Materials science and engineering*. Vol. 5. 2011: John Wiley & Sons NY.

126. Borg, R.J. and Dienes, G.J., *An introduction to solid state diffusion*. 2012: Elsevier.

127. Alexander, W. and Shackelford, J., *Materials Science and Engineering Handbook*, in *CRC*. 2000. p. 406.

128. Vargel, C., *Corrosion of aluminium*. 2004: Elsevier. 626.

129. Li, H., Fu, M., Lu, J., and Yang, H., *Ductile fracture: experiments and computations.* International journal of plasticity, 2011. 27(2): p. 147-180.

130. Den Bakker, A., Werkhoven, R., Sillekens, W., and Katgerman, L., *The origin of weld seam defects related to metal flow in the hot extrusion of aluminium alloys EN AW-6060 and EN AW-6082.* Journal of Materials Processing Technology, 2014. 214(11): p. 2349-2358.

131. Shen, Z., et al., *Microstructure and mechanical properties of friction spot welded 6061-T4 aluminum alloy.* Materials & Design (1980-2015), 2014. 54: p. 766-778.

132. Humphreys, F.J. and Hatherly, M., *Recrystallization and related annealing phenomena*. 2012: Elsevier.

133. Derby, B. and Wallach, E., *Theoretical model for diffusion bonding.* Metal Science, 1982. 16(1): p. 49-56.

134. Yu, J., Zhao, G., and Chen, L., *Analysis of longitudinal weld seam defects and investigation of solid-state bonding criteria in porthole die extrusion process of aluminum alloy profiles.* Journal of Materials Processing Technology, 2016. 237: p. 31-47.

135. Ma, R., Li, M., Li, H., and Yu, W., *Modeling of void closure in diffusion bonding process based on dynamic conditions.* Science China Technological Sciences, 2012: p. 1-12.

136. Hill, A. and Wallach, E., *Modelling solid-state diffusion bonding.* Acta Metallurgica, 1989. 37(9): p. 2425-2437.

137. Orhan, N., Aksoy, M., and Eroglu, M., *A new model for diffusion bonding and its application to duplex alloys.* Materials Science and Engineering: A, 1999. 271(1): p. 458-468.

138. Forcellese, A. and Gabrielli, F., *Warm forging of aluminium alloys: a new approach for time compression of the forging sequence.* International Journal of Machine Tools and Manufacture, 2000. 40(9): p. 1285-1297.

139. Tanner, D. and Robinson, J., *Reducing residual stress in 2014 aluminium alloy die forgings.* Materials & Design, 2008. 29(7): p. 1489-1496.

140. Meng, C., *Effect of preheating condition on strength of AA6060 Aluminium Alloy for extrusion*. 2010, Auckland University of Technology.

141. Pezda, J., *The effect of the T6 heat treatment on hardness and microstructure of the EN AC-AlSi12CuNiMg alloy.* Metalurgija, 2014. 53(1): p. 63-66.

142. *ASTM E140-12be, Standard Hardness Conversion Tables for Metals Relationship Among Brinell Hardness, Vickers Hardness, Rockwell Hardness, Superficial Hardness, Knoop Hardness, Scleroscope Hardness, and Leeb Hardness1, ASTM International* West Conshohocken, PA, 2013.

143. Garrett, R., Lin, J., and Dean, T., *An investigation of the effects of solution heat treatment on mechanical properties for AA 6xxx alloys: experimentation and modelling.* International Journal of Plasticity, 2005. 21(8): p. 1640-1657.

144. Siddiqui, R.A., Abdullah, H.A., and Al-Belushi, K.R., *Influence of aging parameters on the mechanical properties of 6063 aluminium alloy.* Journal of Materials Processing Technology, 2000. 102(1): p. 234-240.

145. Demir, H. and Gündüz, S., *The effects of aging on machinability of 6061 aluminium alloy.* Materials & Design, 2009. 30(5): p. 1480-1483.

146. Ozturk, F., et al., *Influence of aging treatment on mechanical properties of 6061 aluminum alloy.* Materials & Design, 2010. 31(2): p. 972-975.

147. Mirzakhani, B. and Mansourinejad, M., *Tensile properties of AA6061 in different designated precipitation hardening and cold working.* Procedia engineering, 2011. 10: p. 136-140.

148. Masoud, I., Mansour, T.A., and Al Jarrah, J., *Effect of heat treatment on the microstructure and hardening properties of 6061 aluminum alloy.* J. Appl. Sci. Res, 2012. 10: p. 5106-5113.

149. Risanti, D., Yin, M., del Castillo, P.R.D., and van der Zwaag, S., *A systematic study of the effect of interrupted ageing conditions on the strength and toughness development of AA6061*. Materials Science and Engineering: A, 2009. 523(1): p. 99-111.

LIST OF PUBLICATIONS

Journal:

[1] Shamsudin, S., Lajis, M. A., & Zhong, Z. W. (2016). Solid-state recycling of light metals: A review. Journal of Advances in Mechanical Engineering, 8(8), 1-23. ***(ISI Indexed)***

[2] Shamsudin, S., Zhong, Z., Ab Rahim, S., & Lajis, M. (2016). The influence of temperature and preheating time in extrudate quality of solid-state recycled aluminum. The International Journal of Advanced Manufacturing Technology, 1-13. ***(ISI Indexed)***

[3] Shamsudin, S., Lajis M. A., Zhong, Z. W., Ahmad A., & Wagiman, A. (2017). Weld Strength in Solid-State Recycling of Aluminium Chips. Journal of Material Science and Engineering Technology. ***(ISI Indexed)***

Conference:

[1] Shamsudin, S., Lajis, M. A., & Zhong, Z. W. (2016). Evolutionary in Solid-state Recycling Techniques of Aluminium: A review. Procedia CIRP, 40, 256-261. ***(EI Compendex and Scopus Indexed)***

[2] Lajis M. A., Ahmad A., Yusuf, N.K., Yusuf, Shamsudin, S., & Zhong, Z. W. Parametric Optimisation of Heat Treated Recycling Aluminium (AA6061) by Response Surface Methodology. The 3rd International Conference on Green Design and Manufacture. 2017. Krabi, Thailand. ***(Scopus Indexed)***